An Investigation into the Effect of Carbon and Niobium on Microstructure Development during Reheating of Steel

by

Omar Khalid

Thesis submitted for the degree of Doctor of Philosophy

Department of Materials Science and Engineering

The University of Sheffield

February 2017

Dedicated to my parents

Khalid Mahmood & Naheed Khalid

I. Abstract

Thermo-mechanical rolling processes can be divided into three stages, reheating, rolling, and cooling. An important parameter in obtaining a sound microstructure with good mechanical properties is to start with a uniform austenite structure. It is of paramount importance that the prior austenite grain size is kept small and as uniform as possible during the reheating stage.

There has been a considerable amount of work done on the prior austenite grain size and its effects on the mechanical properties of the steel. However there is a gap in the literature, when the niobium content is less than 0.02 wt. % in low, medium or high carbon steels. There is also a gap when it comes to the effect of varying carbon on the prior austenite grain size. Research on the effect of carbon and niobium on the austenite grain growth during different reheating temperatures, varying hold times at different reheating temperatures, and varying reheating rates is insufficient. The outputs from this thesis will be used to increase the accuracy of predictions for the austenite grain size during different reheating temperatures using empirical models, and to gain knowledge on the T_{GC} (Grain coarsening temperature) with respect to each composition.

In this work a detailed study of the effect of temperature, hold time and reheat rate on both the prior austenite grain size microstructure and precipitation evolution, of microalloyed steels in the as reheated condition is investigated. Five different carbon steels (0.08 wt. %, 0.2 wt. %, 0.4 wt. %, 0.6 wt. %, and 0.8 wt. %) each consisting of a plain C-Mn composition (with no niobium element addition) and three different niobium concentrations (0.005 wt. %, 0.01 wt. %, and 0.02 wt. %) were investigated. The reheat temperatures ranged from 950°C to 1250°C in 50°C increments, after which the specimens were held for an hour and then quenched in ice water. The average prior austenite grain size was determined using ASTM E112 as a function of reheat temperature, hold time and reheat rate, Standard deviation analysis has been used to measure the bimodal distribuation of the grain size. Second phase particles were analysed using TEM (transmission electron microscopy).

Results from this investigation indicate, that the niobium increases the formation of pearlite in the as received material. The micro hardness tests indicate that in the low carbon (0.08 wt. %) steel the ferrite phase and pearlite is not affected by the niobium wt. % as the hardness values remain constant with increasing niobium. However a decrease in ferrite grain size is observed with increasing niobium. Hardness increases with an increase in niobium content for medium carbon (0.4 wt. %) steel and for high carbon (0.8 wt. %) steel.

Reheating temperature results indicate that with an increase in carbon content for plain C-Mn steel there is a decrease in the average prior austenite grain size. Similar trends of decreasing austenite grain size can be seen in all the range of carbon contents

microalloyed with niobium. The standard deviation results have shown that the amount of niobium addition in the steel determines the T_{GC}. It has also been shown that as the carbon content increases so does the T_{GC} , the temperature at which the abnormal grain growth starts to occur.

During different hold times and for different carbon contents at a reheat temperature of 1050°C and 1150°C it was indicated that in plain C-Mn steel, the prior austenite grain growth was linear as a function of increasing time. When niobium is present in the specimen at 1050°C the growth trend is logarithmic. As the reheat temperature is raised to 1150°C the growth trend for plain C-Mn and 0.005 wt. % Nb steel are linear with increasing time. Both the 0.01 wt. % Nb and 0.02 wt. % Nb steels experience a logarithmic growth trend. Standard deviation analysis was used to measure the bimodality of the prior austenite grains and showed that other than hold time, reheat temperature also plays a major part in normal/abnormal grain structure together with the wt. % of Nb.

It was found that the time exponent *n* values are higher for 1150°C and lower for 1050°C. This is because of the reduction in solute drag which is attributable to the Zener pinning imposed by NbC particles at grain boundaries. The *n* value decreases dramatically for 0.8wt% carbon steel for the same niobium content. At the higher temperature of 1150°C the *n* value remains relatively constant for all the carbon contents. However for the 0.8 wt. % carbon steel there is a decrease in the *n* value for the 0.01 and 0.02 wt. % Nb microalloyed steels.

The effect of reheating rate on the decrease in the prior austenite grain size was more prominent for heating rates of 2.5°C s^{-1} and 5°C s^{-1} at lower temperatures of 1000°C. When the heating rate was 15°C s^{-1} the decrease in the prior austenite grain size was not as significant. The effect of precipitates indicated that with increasing heating rate the precipitation number density decreases, the average precipitate size decreases and the precipitates are much finer at higher heating rates.

II. Acknowledgements

Bismillāhi r-raḥmāni r-raḥīm

In the Name of Allah, the Most Beneficent, the Most Merciful.

The Holy Prophet of Allah Muhammad (S.A.W.) has said: *Attainment of knowledge is a must for every Muslim and to Seek knowledge from the Cradle to the Grave.*

All thanks to Almighty Allah (God) for giving me the ability and strength to accomplish this work. I would not be in this position if Allah did not place my wife Parveen (Puneet) Khalid, aka (Round Round) by my side since I decided to come back to studying.

I would like to express my special appreciation and thanks to my supervisor, Dr. Richard Thackray. My PhD has been an amazing experience and I thank Richard wholeheartedly for his tremendous academic support, whose guidance, and constructive comments are valuable, not only during this Thesis but also during the MEng Program.

Similar, profound gratitude goes to Dr. Eric J Palmiere, for his constant faith in my lab work, and for being so dedicated to his role as my secondary supervisor. I am hugely appreciative to both my supervisors, who have been truly dedicated mentors, for not only encouraging my research but for allowing me to grow as a researcher. I would also like to thank my lecturers who taught me during my undergraduate years.

I would like to thank the technical members of the University who have been kind enough to extend their help at various phases of this research, whenever I approached them, and I do herby acknowledge all of them. I thank Dean Haylock, Kyle Arnold and Michael Bell, for their support during my experimental work. I would also like to thank Peng Zeng and Sheryl for training me on TEM and SEM. I would like to acknowledge the financial support given by the Engineering and Physical Sciences Research Council (EPSRC).

Of course no acknowledgements would be complete without giving thanks to my parents. I am extremely grateful to my father, Khalid Mahmood who has always been an idol of mine, and hopefully with this PhD I can become one step closer to becoming like him. Now dad you can now stop saying “If only you had studied further.” My mother, Naheed Khalid, for her prayers, encouragement and helping me at every stage of my personal and academic life, teaching me to study hard and to give priority in my life to the quest for knowledge, and longed to see this achievement come true.

I would also like to give sincere gratitude to my mother-in-law, Surjit Deol, for always praying for me, who also longed to see this achievement come true, and most importantly my father-in-law, Jaswinder Deol for allowing me to marry his daughter, therefore obtaining this PhD (a full circle) .

I also wish to extend thanks to the rest of my family for their encouraging words of support (Nazam, Tania, Ali, Hassan, Rajneet, Romessa, and Zara).

Finally, I know if my grandparents were with me today, they would be very proud.

Contents

LIST OF FIGURES

LIST OF TABLES

LIST OF FIGURES IN APPENDIX

LIST OF TABLES IN APPENDIX

1. Introduction

Niobium is a transition metal with a body centered cubic crystal structure, which is used as an microalloying element in the steel industry, as well as numerous uses in other industries; namely nuclear, aerospace and superconducting magnets.

It is a well-established that a uniform and fine distribution of ferrite grains result in high toughness coupled with high strength, and that these mechanical properties are strongly influenced by microalloying elements such as vanadium (V), titanium (Ti) and of course niobium (Nb). These may be added to steel singularly or in a combination. The effects of these alloying additions are strongly influenced by the thermal or thermo-mechanical processing schedule [1] therefore affecting the evolution of the final ferrite grain structure and any precipitate population. The slabs produced by continuous casting are reheated prior to rolling, this is done so that it reduces the inhomogeneity of the cast structure, and dissolves the majority of the microalloy precipitates, so that they are available to precipitate at a later time for grain boundary pinning. To achieve the maximum grain refinement it is a common practice to have a two or three stage controlled rolling (plastic deformation) step after reheating [1, 2, 3].

Niobium (Nb) is known to be the most effective alloying element for grain refinement during rolling as it pins the grain boundaries during reheating [4]. The influence of niobium can be understood by the way it controls the grain coarsening temperatures (T_{GC}) of the austenite grains during reheating. The T_{GC} is defined as the temperature above which abnormal grain growth occurs, and is controlled by the stability of the second phase particles in austenite. Since reheating of the billet or slabs represents the first step prior to deformation of any sort, it is important to accurately obtain the correct value of T_{GC}. This is so that a bimodal austenite grain structure (a non-uniform grain size) is not present in the initial stage prior to deformation, because once formed it is difficult to remove during deformation [5]. If a bimodal grain structure is formed it is important to correct it (make it uniform as possible) prior to the deformation stage.

The influence of precipitates on the grain growth evolution in steel microstructures is well established, in that the presence of precipitates provides the pinning effect needed to inhibit the grain growth process at certain temperatures. However the pinning force of the second phase particles decreases with elevated temperatures and longer annealing time as a result of dissolution or coarsening of the precipitates.

The great influence that microalloying elements have on the properties of steel in terms of the microstructure obtained during the processing can lead to an improvement in the properties at a lower cost. The amount of carbon in the steel also makes a

difference to what the end product will be. Low carbon steels have typical uses in automobile body panels, and wire products. Medium carbon steels (0.4 to 0.6 wt. %) are used in rails, railway wheels and rail axles, whereas high carbon steels (0.8 wt. %) steels are used for spring material, high strength wires and wrenches.

The principal aim of this project is to study the microstructural and precipitate evolution as a function of different reheating temperatures T_{RHT}, different annealing times and reheating rates for both plain C-Mn steel and steel microalloyed with niobium, in particular to understand the effect of niobium content on the characterization of the prior austenite grains.

1.1 Scope and Objective of the Thesis

As will be described in the literature review, thermo-mechanical rolling processes can be divided into the following stages, reheating, rolling, and cooling. A great amount of physical metallurgy is related to these stages, which in turn influences the microstructure and subsequently the mechanical properties of the end product. It is of paramount importance that the prior austenite grain size is kept as small as possible during the reheating stage as shown in Figure 1-1, which shows the typical thermomechanical processing route of HSLA steels with the metallurgical mechanisms taking place during these processes. Niobium is a very important alloying element and its addition to steel is considered for three main reasons to give the following effects: first it can restrain the growth of austenite grains during reheating, second it also inhibits recrystallization of the austenitic phase prior to the α/γ transformation which is achieved through strain induced precipitation of NbC and thirdly precipitation hardening by NbC in the low temperature transformation product. Therefore controlled rolling and controlled cooling technology is a very effective way to increase the strength and toughness of steels containing niobium [6, 7, 8, 9].

There has been a considerable amount of work done on the prior austenite grain size and its effects on the mechanical properties of the steel. However there is a gap in the literature when the niobium content is less than 0.02 wt. % in low, medium and high carbon steels. Also there is little previous research on the effect of carbon additions whilst keeping all other elements constant. Therefore it could be said that research on the effect of carbon and low additions of niobium (below < 0.02 wt. %) on the austenite grain growth during different reheating temperatures, varying hold times at different reheating temperatures, varying reheating rates and different cooling rates is insufficient.

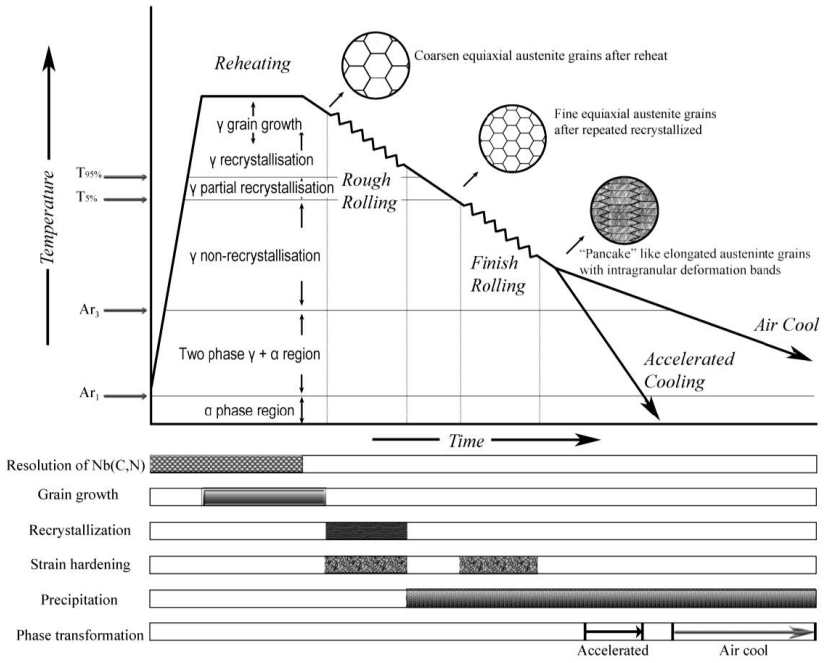

Figure 1-1: Illustration of the stages of thermomechanical processing and metallurgical mechanisms taking place during these processes [10].

A detailed list of the primary aims of this work is provided below.

1. To understand the effects of reducing the niobium content in the steel below 0.02 wt. %, (Plain C-Mn, 0.005 wt. %, 0.01 wt. % and 0.02 wt. % Nb). This is aimed at obtaining a better understanding of the effect of niobium and carbon content on austenite grain size and the abnormal grain growth temperatures, as these niobium contents have not been investigated previously.

2. Study isothermal grain growth of austenite in hypoeutectoid and hypereutectoid plain carbon steels with varying niobium content for different holding times at different reheating temperatures. This is to investigate the kinetics of austenite growth with respect to different carbon content.

3. Investigating the combined effect of varying niobium content and varying the continuous reheating rate for low carbon (0.08 wt. %) steel.

4. Characterization of the kinetics of NbC precipitation during different holding times at different reheating temperatures.

2. Literature Review

In this research, microstructure analysis has been carried out during reheating of plain C-Mn steel and C-Mn-Nb steel at different isothermal heating temperatures, hold times and at different heating rates.

The focus of this literature review is to build the necessary foundations to obtain an in depth understanding of the role of physical metallurgy for the experimental work, and the role of microalloying elements and their effect on the austenite grain refinement during the initial reheating stage and subsequent thermo mechanical processing.

2.1 Microalloyed Steel

Microalloyed steel is a term which was first applied to HSLA (High Strength Low Alloy) steels which contained niobium (Nb), vanadium (V), titanium (Ti), molybdenum (Mo), chromium (Cr), boron (B) either singly or in combination. They are used to facilitate precipitation hardening and/or microstructural grain refinement. The effectiveness of these microalloying elements is strongly dictated by the thermal and/or thermo-mechanical treatments the steel product undergoes.

2.1.1. General Overview

Microalloy additions in steel have been instrumental in the successful development of new steel products with enhanced property combinations. Microalloyed steels are not new, they have been present for the past 40 years. Microalloying technology developed for the production of flat products (plates, strips and line pipe) during the 1960's and 1970's has been applied to long products such as engineering bars, and forgings, since the 1980's [11]. In 1921 in Germany, small titanium additions to steel were exploited and the results showed improvements in strength [12].

Microalloying enables high strength parts to be produced in the as-forged condition without the need for a subsequent procedure of reheating, quenching and tempering; hence saving vast amounts of energy. Therefore the applications of microalloyed steels have been extended. Extensive use of microalloyed steel sheets in the automotive industry and flat rolled steels for pipeline plate products, with microalloy additions of less than several hundredths of a wt % [13] are a common practice in these industries.

Microalloying elements include niobium (Nb), vanadium (V), titanium (Ti), tantalum (Ta), chromium (Cr), molybdenum (Mo) and other alloying elements. These alloying elements dissolve at the high temperatures and serve two main purposes which are; precipitate strengthening during the cooling process in the formation of carbide, nitride

or carbonnitrides and grain refinement. If the process is combined with the temperature control, solution treatment or thermal mechanical processing a significant advantage in the steel mechanical properties can be achieved by this precipitation hardening.

Steels which require both high strength and toughness as a combination; this can only be achieved by refining or the reduction of the ferritic grain size. These steels are processed either by a controlled rolling procedure or by an accelerated cooling practice.

The purpose of controlled rolling is to obtain a fine-grained ferrite (α) in the final product as shown in Figure 2-1, and relies on the progressive refining of the austenite grain size by recrystallization between, or within, rolling passes. When the steels are rolled at high temperature around 1150°C in the austenite (γ) region , recrystallization quickly happens after plastic deformation (rolling) denoted by (a) and (b). The grain refinement of the γ region by recrystallization is effective to obtain fine-grained α eventually, since the grain boundaries of γ act as preferential nucleation sites of α. However, the refinement of the austenite γ region is limited as at high temperatures grain growth quickly occurs.

When rolling is carried out at lower temperatures, unrecrystallized γ can be obtained which is much more preferable than the recrystallized γ because the dislocation substructure acts as in-grain nucleation sites for α due to the deformation which is occurring at the lower temperature as the grain growth does not occur denoted by (c) and (d).

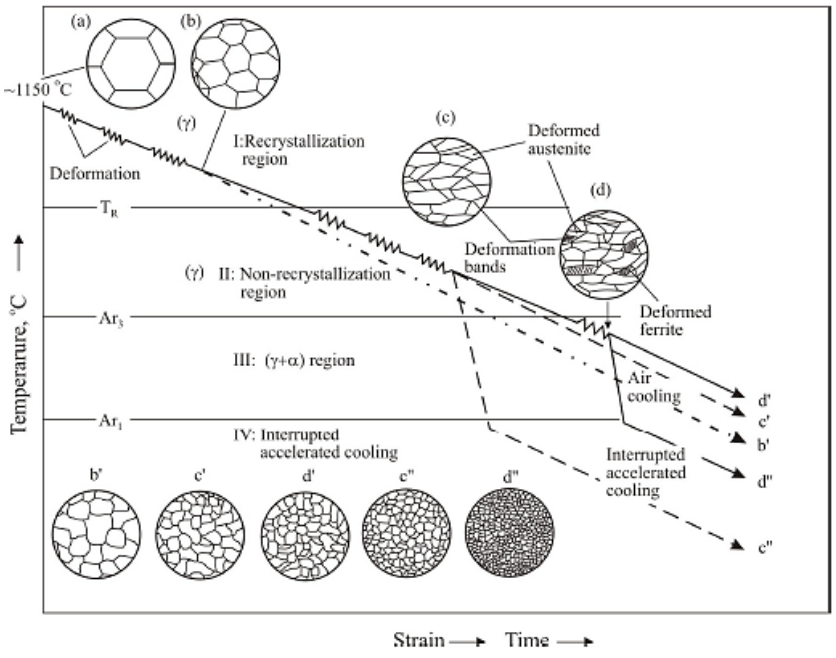

Figure 2-1:Schematic diagram of the microstructure evolution during the controlled rolling [14]

2.2 Strengthening Mechanisms in Microalloyed Steels

Microstructure evolution of polycrystalline materials (e.g. metals, ceramics) during reheating is very important, because of the average grain size and grain size distribution, which are directly related to the grain coarsening process. Hence the final grain size is a consequence of the initial austenite grain size therefore having an important role in the fracture toughness and the mechanical strength of steel. There are various ways of contributing to the yield strength of the steels e.g. matrix strengthening[1] (σ_m), solid solution strengthening (σ_{ss}), dislocation strengthening (σ_{dis}), precipitation strengthening (σ_{ppt}) and grain refinement strengthening (σ_d). The relationship between the matrix microstructure and the yield strength can be summarised

$$\sigma_y = \sigma_{ss} + \sigma_{dis} + \sigma_{ppt} + \sigma_m + \sigma_d \tag{2-1}$$

Much research has been done showing that ferrite grain size refinement can simultaneously improve steel strength and toughness, on the other hand, all the other strengthening mechanisms to some extent cause a decrease in the steel toughness whilst increasing strength as shown in Figure 2-2.

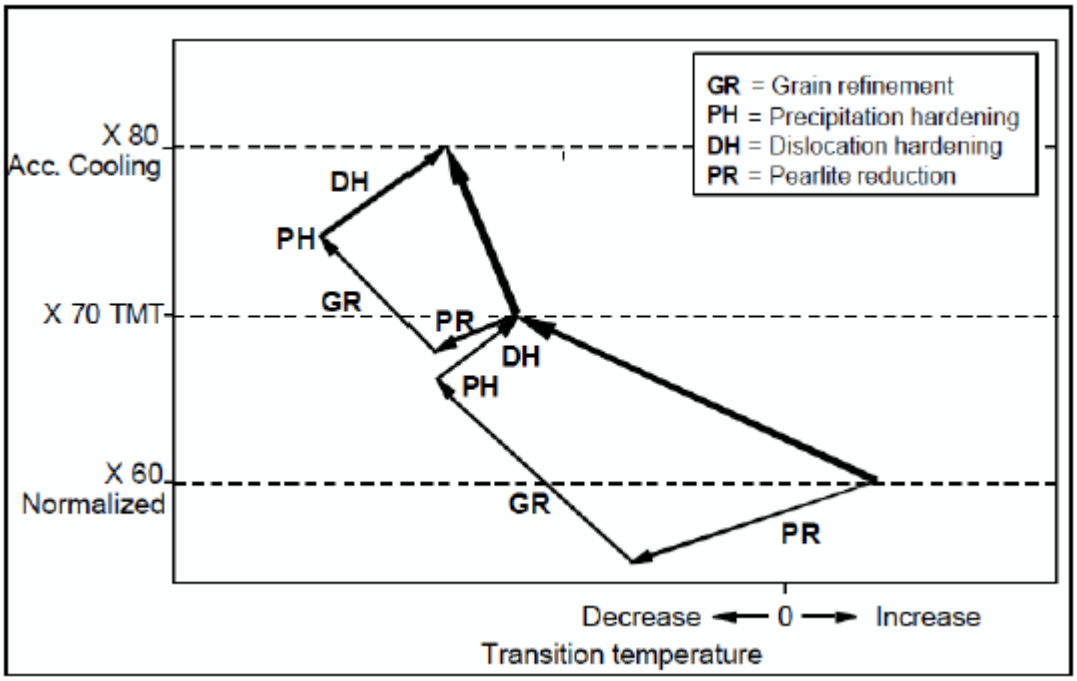

Figure 2-2: The microstructural effects for increasing the strength and toughness in microalloyed steels [15].

[1] Matrix strength is the base strength of steel.

2.2.1. Grain Size Refinement

The Hall-Petch Equation (2-2) shown below gives a relationship between mechanical properties (e.g. yield stress) and grain size [16]. The relation predicts that as the grain size in polycrystalline metal decreases the yield strength increases. The Hall-Petch relationship is based on the concept that during the movement of dislocations through the polycrystalline metal, the grain boundaries act as barriers to impede the dislocation movements. The yield strength is higher in fine grained polycrystalline material as opposed to large grained polycrystalline material; this is because the reduced grain size gives a greater total grain boundary area to impede dislocation movement, therefore increasing the strength and toughness of the steel.

$$\sigma_y = \sigma_i + kD^{-\frac{1}{2}} \tag{2-2}$$

Where:

σ_y = the yield stress
σ_i = the "friction stress," representing the overall resistance of the crystal lattice to dislocation movement.
k is the "locking parameter," which measures the relative hardening contribution of the grain boundaries.
D is the grain diameter.

It can be seen from Figure 2-3 where the y-axis is yield strength and the x-axis is 0.2 % proof strength that the contribution to yield strength from grain refinement is 60% ~ 70% of the overall strengthening methods mentioned earlier. Therefore, it can be concluded that the predominant method for the improvement in the strength and toughness is through grain refinement technology, as the remaining strengthening methods only increase the proof strength of the material and not the ductility.

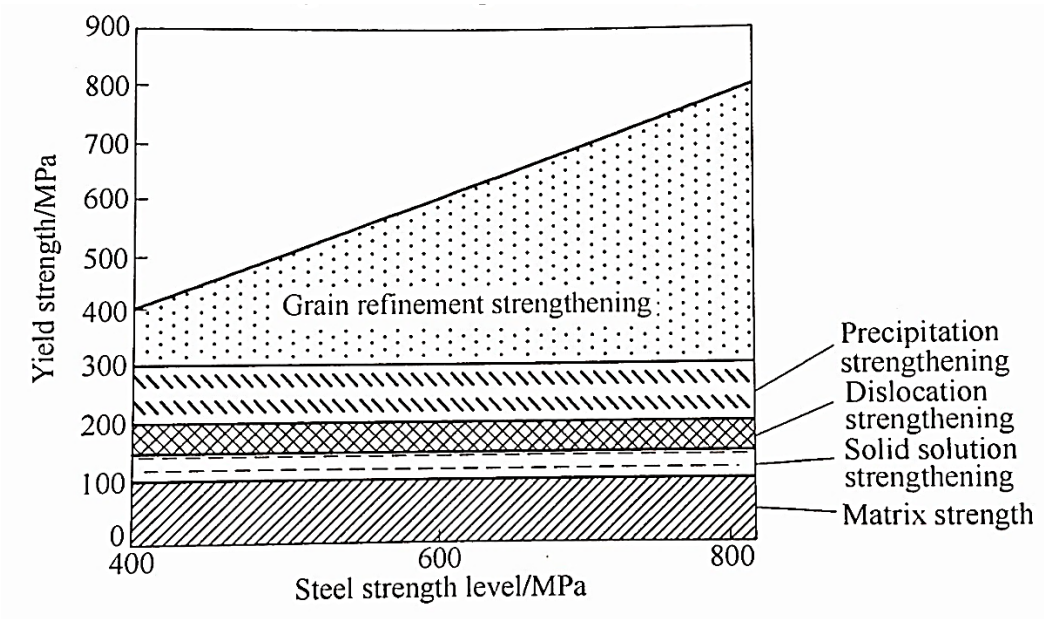

Figure 2-3: Scheme of various strengthening effects [17]

It is clear that the role of grain size is an important factor in determining mechanical properties in steel and therefore it is important to understand the grain coarsening process as a first step towards achieving the desired microstructure, as the initial stage of any deformation process is reheating the slab or billet.

2.2.2. Solid Solution Strengthening

Solid solution strengthening is achieved by adding solute atoms into the solvent crystal lattice matrix; which in turn generally produces a stronger alloy as to when composed of the same pure metal. The strengthening occurs due to the matrix lattice becoming elastically distorted by the solute atoms; these solute atoms have a concentration in the vicinity of dislocations, thereby leading to reduced mobility of the dislocations and hence increasing the stress needed to move dislocations again [18]. There are two types of solid solution strengthening; one being substitutional solid solution where the solute atoms are of similar size in comparison to solvent atoms in the lattice and occupy these lattice points, the second is interstitial solid solution. This is where the solute atoms are much smaller than the solvent lattice atoms. Depending on the size of the solute atoms the range of the effect of the solid solution strengthening is determined by the difference in the size between the solute and the solvent atoms. The Hume-Rothery rule states that for substitutional solid solution formation to be favorable, the difference of the atomic radius of the solute element should be no more than 15% of the solvent atomic lattice matrix (Fe, host phase); if the difference between them is greater the 15% the extent of solid solubility is restricted to less than 1% [16]. However, on the other hand for interstitial solid solutions, the interstitial elements e.g.

carbon, nitrogen, oxygen, hydrogen, and boron should be smaller than the solvent atomic lattice matrix as they would occupy the interstitial positions.

2.2.3. Precipitation Strengthening

Precipitation strengthening is another important strengthening mechanism in HSLA steels. The presence of second phase carbide particles in the Iron (Fe) matrix can significantly obstruct the dislocation movement and therefore increase the strength of the alloys. Based on the stability of the precipitates (second phase particles) the strengthening could be achieved at higher temperatures. There are two different mechanisms within precipitation strengthening; precipitation hardening and dispersion strengthening.

2.2.4. Work hardening or Dislocation Strengthening

Dislocations are a very important mechanism in strengthening HSLA steels, if the dislocations can move with relatively ease throughout the crystal structure, it means that the material does not provide any resistance intrinsically to the movement of the dislocations and therefore the steel becomes less strong. Creating dislocations in the material can obstruct the dislocations themselves [19]. Therefore plastic deformation at lower temperatures introduces new dislocations in the metals, leading to increased dislocation density, the movement of the dislocations become more difficult due to interfering effects of other dislocations.

2.3 Niobium and Niobium alloys

Niobium (Nb) was discovered in the 18th century by an English chemist Charles Hatchett, however the element itself was discovered by John Winthrop who was a rock collector and a scientist and he named the new element columbite. It was his grandson who sent the element to the British Museum to be displayed and analysed; it was then that Hatchett attempted to analyse the ore. In 1802, Hatchett published the results into his investigation of the unknown ore in the Philosophical Transactions of the Royal Society of London (An Analysis of a Mineral Substance from North America, Containing a Metal Hitherto Unknown) where he concluded that the element was unknown and called the new element “Columbium” [20]. Unbeknown to Hatchett there were two elements in the columbium (which is known as niobium) and tantalum. The benefits of using niobium as a microalloying element were known since the late 1930s, [21] however the first commercially produced niobium microalloyed steel was in the form of hot strip which was produced by National Steel in the United States of America

for flat products and also forgings. In 1972 researchers at Thyssen Germany developed low cost non heat-treated steels for automobile crankshafts [22].

According to the 2011 British Geological Survey (BGS) [23] the element niobium is a high supply risk. Figure 2-4 represents the world production of niobium. The BGS report is based on three factors; production concentration (when the commodity is concentrated in a few countries), reserve base distribution (It is important to assess where elements might be sourced in the future, nearly 87 per cent of the world's reserve base of niobium is found in Brazil) and governance indicators (political stability of a producing country and what impact it may have upon the supply of mineral commodities).

During the past 35 years there have been several events which have seen the use of niobium as an alloying addition increase. In 1978 due to the shortage and the price escalation of Molybdenum (Mo), the steel industry replied with the removal of Mo from the composition used for API X70 steel grades and a niobium (Nb) – chromium (Cr) design composition was introduced with thermo mechanical controlled processing (TMCP). A similar incidence occurred in 1988/89 when the price of Vanadium (V) increased to $50/kilo, this led the steel industry to eliminate vanadium (V) from many steel compositions and use molybdenum (Mo) and chromium (Cr) with TMCP as a substitute. The most recent event took place in 2005 – 2008 when there was a huge increase in the price for vanadium (V) ($85/kilo) and Mo ($75/kilo) again; this forced the steel industry to redevelop niobium (Nb) – chromium (Cr) type steels [24].

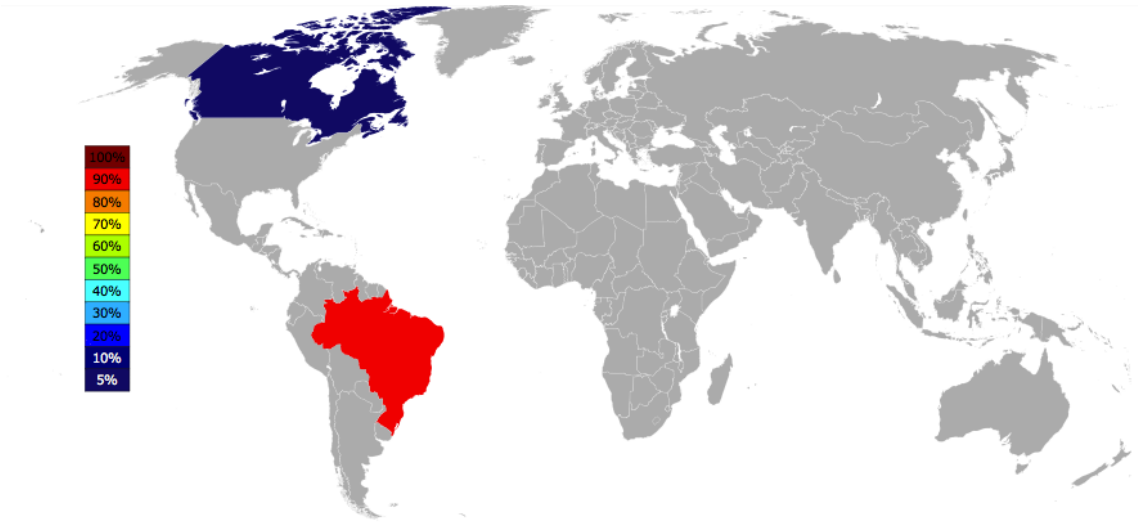

Figure 2-4: World niobium production [25].

2.3.1. Extraction

Even though discovered in 1801, the first successful commercial production of ferroniobium did not occur until 1965 by Companhia Brasileira de Metalurgia e Mineracao (CBMM) in Brazil [26].

There are four stages in the production of high purity niobium; (1) extraction of Nb_2O_5 (niobium pentoxide) from niobium ores through leaching or chlorination/distillation, (2) reduction of Nb_2O_5 by carbothermic or aluminothermic processing to form metallic powder or sponge, (3) a consolidation process to form electrodes through sintering or re-melting, and finally (4) using an electron beam to re-melt and refine [27, 26].

Ferro-niobium which contains 60 – 70 % of niobium is the main product that is used in the steel industry; this is a large scale production operation which is achieved by aluminothermic reaction with a mixture of iron oxide and niobium oxide. The end product is aluminium oxide and ferroniobium.

2.3.2. General Metallurgy

Niobium (Nb) is a ductile transition metal with a large atomic radius of 41, transition metals are characterized by the atomic structure of the element, where the outer shell contains electrons whilst the inner shell is not completely filled. Transition metals are the only elements with an unfilled inner shell. Niobium has a relatively high melting point of 2465 ± 8 degrees centigrade. At high temperatures it reacts with carbon, nitrogen, sulphur and oxygen, therefore when being processed should be placed in a protective atmosphere [27].

The increase in production and development of niobium and its alloys comes from the steel industry, due to it being an effective microalloying element by combining with carbon and nitrogen in steel to form niobium carbides, nitrides and carbonitrides. The majority of niobium (an estimated 90.2%) is used in the form of ferroniobium form in applications for high strength low alloy steel (HSLA), stainless steel, and heat resistant steels due to its high melting point. The principal markets for the 90.2% ferroniobium are; automotive industry, heavy engineering and infrastructure, petrochemical sector, power plants and the oil and gas industry. Super-alloys, superconductors and functional ceramics take 3.0 %, 3.4 % and 3.4 % respectively [28].

2.3.3. Crystallography

Niobium in the pure form has a body centred cubic (bcc) crystal lattice structure with a coordination number of 8 and a lattice constant a = 0.3294 nm [27], because it is a

cubic crystal system all the three axis are at right angles and of equal lengths, $\alpha = \beta = \gamma = 90^{o}$, $a = b = c$.

2.3.4. Effect of Niobium in HSLA Steel

As discussed previously niobium is a very important alloying element and its addition to steel is considered for three main reasons to give the following effects: first it can restrain the growth of austenite grains during reheating, second it also inhibits recrystallization of the austenitic phase prior to the α/γ transformation which is achieved through strain induced precipitation of NbC and thirdly precipitation hardening by NbC in the low temperature transformation product. Therefore controlled rolling and controlled cooling technology is a very effective way to increase the strength and toughness of steels containing niobium. At present the content of niobium is usually higher than 0.02 wt. % in the niobium alloyed steels because when combined with carbon and nitrogen, it can form precipitates in the steel [29]. Over the past two decades niobium has become the first choice for HSLA products, since it increases the strength predominately via grain refinement; as shown in Figure 2-5, the amount of niobium content needed to obtain the same strength increase as steel with titanium is much lower.

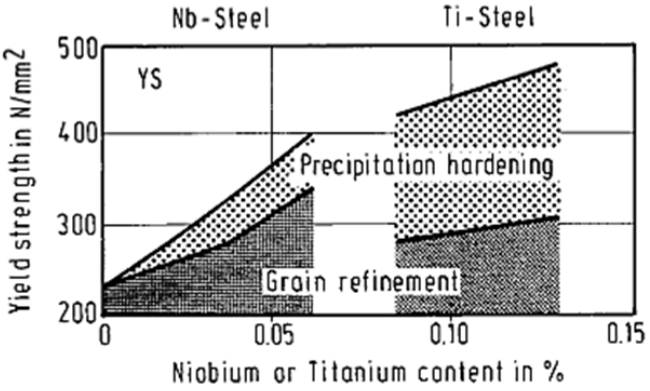

Figure 2-5: Strengthening mechanism in micro alloyed HSLA sheet: (Left Nb Steel and Right Ti Steel) [30].

Work carried out by Meuser et al., [31] investigated the optimization of process parameters using a large mill scale trial of a 35 mm plate of API X80 steel grade. It was concluded that at cooling rates between 10 and 15 K/s (kelvin) an almost complete bainitic microsturcture is obtained, the work also stated that the Charpy impact toughness as well as the strength of the heavy plate material can be influenced by the slab reheating temperature. As the temperature of the slab increases more niobium would be in solution which would positively affect the yield and tensile strength. Figure 2-6 indicates that the lowering of the carbon equivalent value over the last 2 decades in

the X80 grade improves the weldability of the steel. Due to the decrease in the carbon content this aids the solubility of niobium carbides (NbC). As a result of the decrease of the carbon content there has been an increase in strength in steel grades and larger amounts of microalloying additions to steel have become necessary; this trend is shown in Figure 2-7.

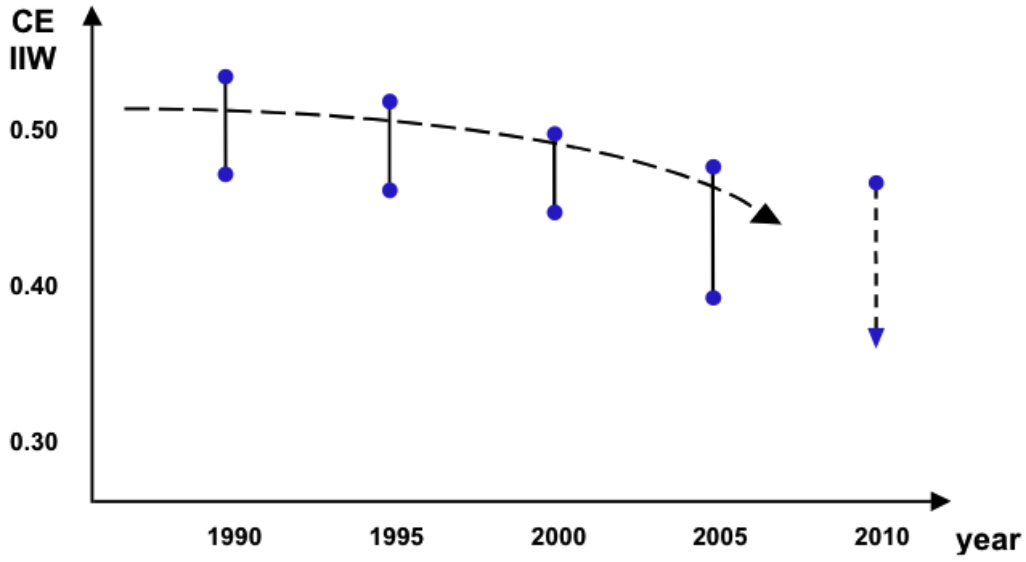

Figure 2-6: The diagram shows the decrease in the Carbon Equivalent due to the change in chemistry the development of modern microalloyed steels [31]. IIW= International Institute of Welding.

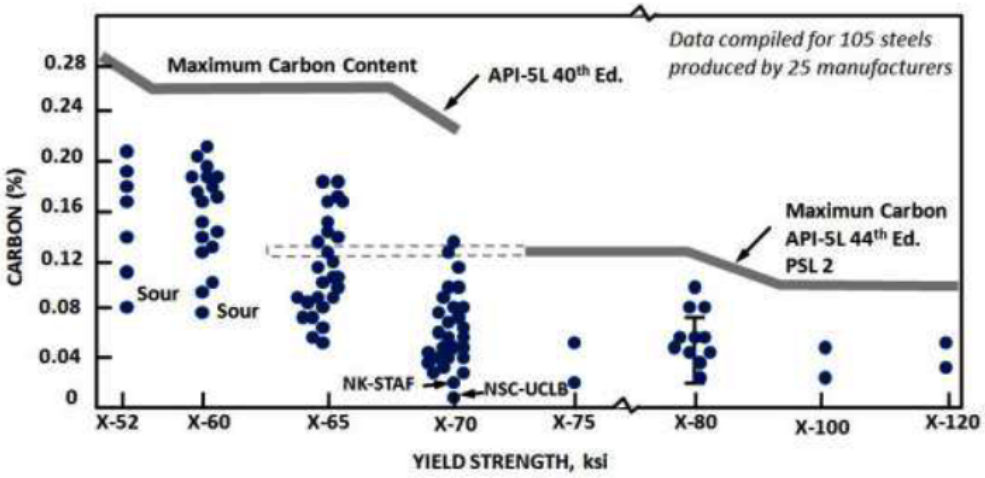

Figure 2-7: Relationship between the carbon content and yield strength for high strength grade steels [24].

During the initial hot rolling process deformation is often carried out above $0.6T_m$ (T_m is the melting temperature) [32]. As deformation proceeds a dynamic restoration

process occurs; which includes dynamic recovery and recrystallization. Dynamic recovery occurs during deformation at high temperatures, unlike static recovery which occurs after deformation. The difference between static and dynamic recovery is that during dynamic recovery, stored energy continues to be introduced even as it decreases via the recovery process. Dynamic recrystallization once again is a process which occurs during deformation where nucleation and grain growth occur during deformation, rather than afterwards as in static recrystallization. The mechanisms are different for both of the restoration processes, and take into account the material chemistry and microstructure parameters of the material.

The recrystallization behaviour during hot deformation is an important phenomenon which contributes to the homogenization and refinement of the end microstructure and the effects of Nb are well known on the retardation of recrystallization; by the way of solute drag effect and pinning of induced precipitates, such as Nb(C, N). This leads to more strain being accumulated therefore providing abundant nucleation locations for new grains to grow and therefore refinement of the microstructure as a result. The ferrite grains nucleate on sites of austenite grain boundaries and intergranular defects, such as deformation bands which are introduced during the plastic deformation process. Many studies have been conducted on the recrystallization behaviour of Nb bearing steels [33, 34, 35].

A study carried out by Niu, et al., [34] investigated the behavior of dynamic recrystallisation (DRX) in high grade API X80 and X100 pipeline steels with different niobium concenterations. This investigation was carried out by through a single pass compression experiment using a Gleeble 1500 thermomechanical simulator. The Poliak-Jones (P-J) method [36] was used to calculate the critical strain and the deformation activation energy of DRX was determined using the stress-strain data during experiment. The chemical compositions for the two pipeline steels are given in Table 2-1, and the experimental procedure is given in [34].

Table 2-1: Chemical composition of API X80 and X100 (wt. %).

Steel	C	Si	Mn	P	S	Nb	Ti	Others
X80	0.05	0.18	1.75	0.007	0.0010	0.095	0.015	Mo, Ni
X100	0.06	0.20	1.85	0.007	0.0010	0.08	0.015	Cu, Al

The results have shown that X80 pipeline steel has a higher peak strain and stress value in comparison to that of the X100 pipeline steel as shown in Figure 2-8 (Left). The balance between work hardening and the softening effect of recrystallization is represented by the peaks of the strain-stress curve; therefore it suggests that the increase of Nb content in X80 is able to retard the DRX behaviour. The results of kinetics of

DRX are also shown in Figure 2-8 (Right) where f_{dyn} is the recrystallization fraction; here it can be observed that with the increase in Nb concentration the DRX process gets inhibited.

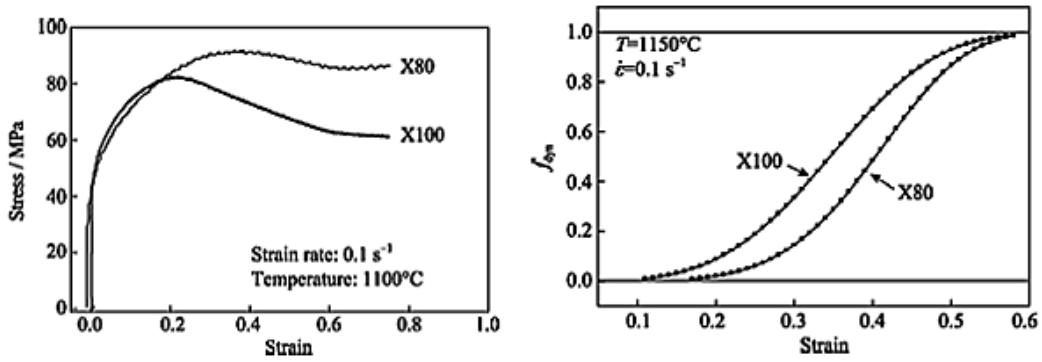

Figure 2-8: True strain-stress curve for X80 and X100 pipeline steel, (Conditions) T = 1100 °C and $\dot{\varepsilon}$ = 0.1 s^{-1} (Left) and Kinetic curves of DRX (Conditions) T = 1150 °C and $\dot{\varepsilon}$ = 0.1 s^{-1} (Right)

The Johnson-Mehl-Avrami (JMA) formula shown by Equation (2-3) is always used to express the kinetics of DRX, where *n* is a numerical exponent which is independent of temperature and can vary in value from 1 to 4, and *k* on the other hand shown in Equation (2-4), is sensitive to temperature as it depends on nucleation rate N and growth rate G, therefore both are constants related to the material.

$$f = 1 - exp(-kt^n) \tag{2-3}$$

$$K = \frac{\pi N G^3}{3} \tag{2-4}$$

A Johnson-Mehl-Avrami plot is useful to determine the progress of precipitation providing an overall picture of the precipitation process in terms of volume fraction transformation as a function of time.

Since the DRX is a continuous deformation process during hot rolling, it is widely described in the form represented in Figure 2-8 (Right), recrystallization fraction against the ε. The influence of Nb on the recrystallization can be in separated into three interdependent categories given below:

First being the solute drag effect, in which dissolved Nb atoms decrease the drift mobility of the grain boundary which in turn retards the recrystallization. The influence of solutes and particles on drift mobility was recognized as early as 1949 [37, 38].

It can be seen in Figure 2-9 (a) that with the increase in the Nb concentration the drift mobility of grain boundaries decreases dramatically, at the same time the deformation

activation energy increases with the increase in Nb as shown in Figure 2-9 (b) by Niu, et al., [34]. The combination of decreased mobility and increased deformation activation energy leads to the critical strain for DRX, therefore refining the austenite grains after recrystallization.

Second, a high density of deformation induced precipitate are to retard the nucleation of recrystallization [39]. This is because during thermo mechanical processing of the microalloyed steels precipitation is strain induced and occurs mostly on dislocations in the deformed regions.

The third is grain boundary pinning by second phase particles which retards the growth of the recrystallized grains. Zener, [40] made the first attempt to explain the theory in which he indicated that the energy of the grain boundary would be lowered when a particle would be present in the vicinity of a grain boundary.

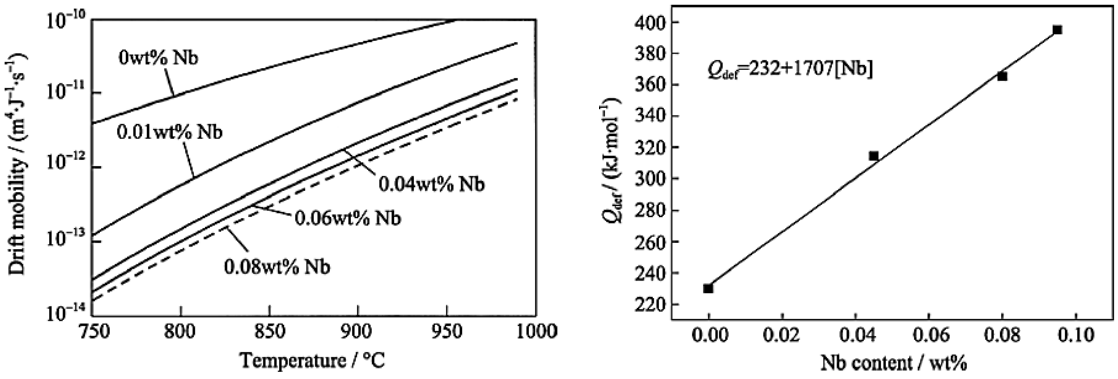

(a) (b)

Figure 2-9: (a) shows the relationship between the dissolved Nb concentration, temperature °C and drift mobility and (b) this graph represents the relationship between the (Q_{def}) deformation activation energy and the Nb content.

Niu, et al., [34] indicated in his work that the relationshoip between Q_{def} and Nb concentation can be estimated as Q_{def} = 232 + 1707 x [Nb] (KJ/mol). Q_{def} is the activation energy associated with the deformation energy which is often used in the expression for the Zener-Holloman parameter. It is an important physical parameter which gives an indication of the deformation difficulty degree in plasticity deformation theory [41].

A torsion test to study the effcets of precipitation was developed by Le Bon, et al., [42]. The experiment was performed using cylinders (6 mm dia. X 50 mm long) of steel samples with and without Nb during and after deformation over a wide extent of temperatures, strains and strain rates. The chemistry of the steel is given in Table 2-2. The amount of Nb precipitated in the austenite was estimated from the loss of secondary hardening potential of the steel on tempering (600°C, 1h).

Table 2-2: Chemical composition of the Nb-steel and Nb-free steel (wt. %)

	C	Mn	Si	S	P	Al	N	Nb
Nb free	0.17	1.36	0.36	0.012	0.027	0.029	0.009	-
Nb	0.17	1.35	0.31	0.021	0.014	0.017	0.011	0.040

The left hand side of Figure 2-10 indicates the hardness (y-axis) and temperature in °C (x-axis). The results show that as dissolution of Nb carbonitrides occurs the hardness increases. The hardness values peak after reheating at around 1250°C for Nb bearing steel, with the results being in reasonable agreement with chemical analysis of extracted precipitates. The right hand size of the figure indicates the hardness on the (y-axis) and time in seconds (x-axis), where rev stands for revolutions per minute. Table 2-3 indicates the relation between the number of revolutions (*N*), the shear strain at the periphery of the torsion sample (γ), and the reduction of the plate (ρ,%) for Figure 2-10. The strain input is relevant because with increased amount of strain the start time for precipitation decreases as would be shown later on in Figure 2-10. The precipitations in the unstrained condition proceeded very slowly; after a solution treatment at 1260 ° and isothermal holding at 900 °C. As shown in Figure 2-10, at least 300 to 1000 seconds are required before an increase in hardness is shown. The interval of time required for the development was long, the rate was also slow, when compared to increasing the amount of deformation, both incubation times and reaction period decreased. The distribution of the particle size for the un-deformed sample after isothermal holding revealed a mean size in the range of 1000-3000 Å in contrast to the strain-induced precipitation sample which revealed a mean size in the range of 30-40 Å.

Table 2-3: Number of revolutions (N), the rational shear strain (γ) and reduction of thickness of plate (ρ,%).

N	1	2	3	4	5	6	7	8	9	10	15
γ	0.38	0.75	1.13	1.50	1.90	2.30	2.6	3.0	3.4	3.8	5.7
ρ, %	17	32	43	53	62	67	73	78	82	85	95

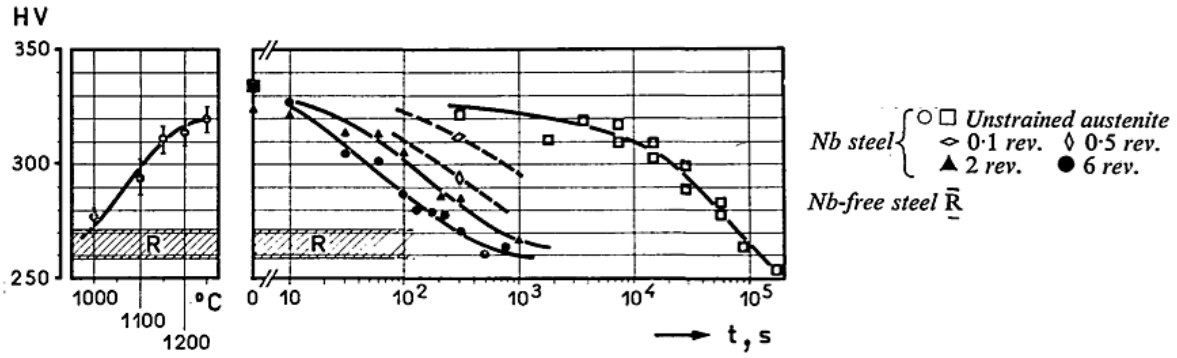

Figure 2-10: Unstrained austenite and deformed austenite in Nb bearing steels [42]

The larger the deformation at a given temperature the faster the static recrystallization occurs, the fastest kinetic measurements were obtained after the largest deformation compatible with the absence of dynamic recrystallization. Nb bearing and Nb-free steel deformed at a temperature of 900°C. The Nb-free steel is completely recrystallized after 3s and the Nb bearing steel starts to recrystallize after 10 s and is completed before 1000 seconds which is shown in Figure 2-11. The recrystallization rate after 10 s is slow since both precipitation and recrystallization occurs simultaneously. As the holding time is increased to >2 s, there is an acceleration in static recrystallization. The kinetics were fitted to a Johnson-Mehl-Avrami form equation which is shown in an earlier study Equation (2-3).

According to Le Bon, et al., [42], at a temperature of 900°C, the exponent n in Equation (2-3) depends on the holding time, these are given in Table 2-4 and represent the n for different holding times, this shows the complexity of recrystallization when precipitation and recrystallization occur simultaneously.

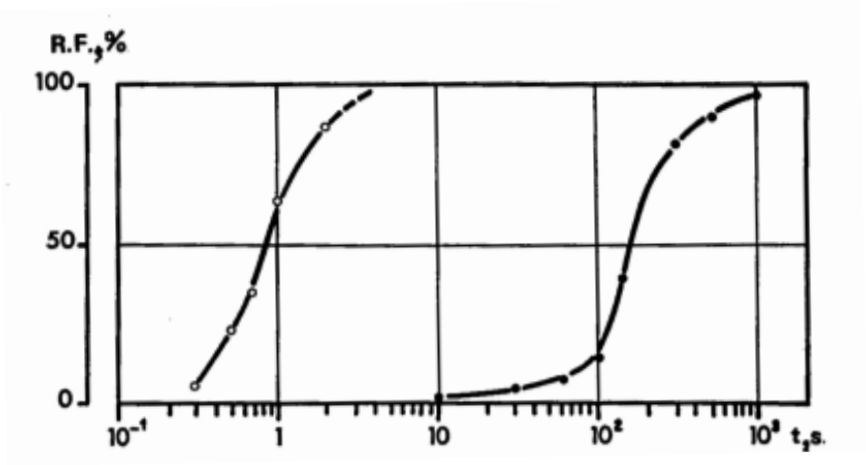

Figure 2-11: Diagram representing the static recrystallization kinetics of austenite after the largest deformation compatible with the absence of dynamic recrystallization. (White circles plain C-Mn steel, Black circles Nb steel).

Table 2-4: Values of exponent n for different holding times.

Holding time Ranges (Seconds)	n
$10 - 10^2$	~ 1
$10^2 - 3x10^2$	3 - 4
$3x10^2 - 10^3$	~ 1

A recrystallization/time/temperature (RTT) curve is shown in Figure 2-12, when comparing, Nb bearing steel and Nb-free steel. The curve for Nb bearing steel, moves to longer recrystallization times and kinked at a temperature of around 900°C. The data from the RTT curves made it clear that no constant n value could be obtained if precipitation occurs; this is because no unique Johnson-Mehl-Avrami form of the equation can be fitted with the isothermal recrystallization curve.

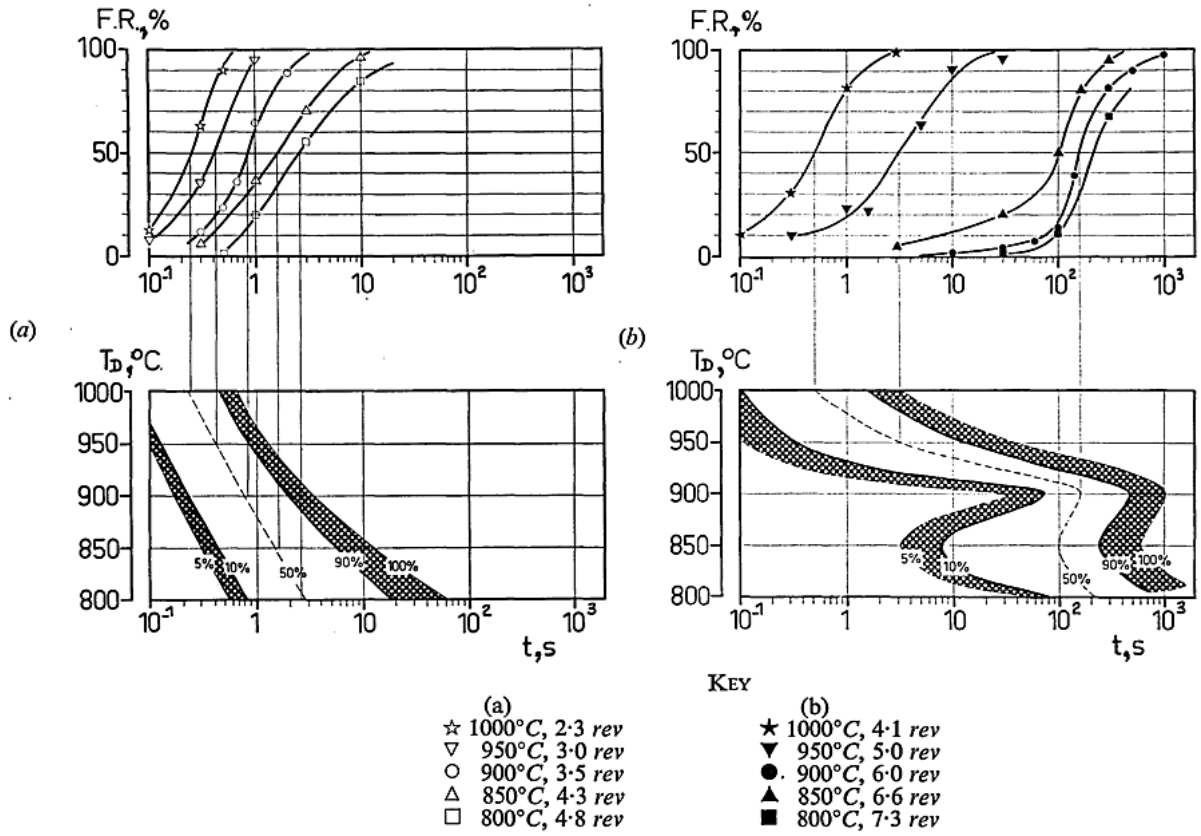

Figure 2-12: Shows the recrystallization kinetics and recrystallization/time/temperature (RTT) diagram for (a) Nb-free (b) Nb steel

A study conducted by Yu, et al., [29], compares two steel samples; one with 0.013% niobium and the other without niobium. The chemical composition is shown below in Table 2-5.

Table 2-5: Chemical composition of Steel A and Steel B [29].

Composition	C	Si	Mn	Cr	Mo	Nb	P	S
Steel A	0.040	0.20	0.72	0.41	0.42	-	0.008	0.0102
Steel B	0.041	0.21	0.70	0.40	0.41	0.013	0.007	0.0085

The results obtained by Yu, et al., [29] in this study found that under the same conditions, there was an increase in strength of Nb steel B of on average 55 MPa than that of Nb free steel A. There was also a difference in the ferrite grain size in steel B, which was 1.4μm smaller than that of steel A on average.

Based on the precipitation hardening theory [43] of microalloying, Nb can form very small Nb(C, N) particles with the carbon and nitrogen atoms in steel, which can inhibit recrystallization and the growth of austenite grains. Furthermore the Nb(C, N) can also precipitate from deformed austenite and ferrite.

The results of the study found that the amount of niobium in steel B was not sufficient for precipitation as there was no Nb(C, N) found in steel B therefore concluding that the niobium still dissolves in the matrix. The state of niobium in solution or in precipitation has a significant effect on the recrystallization, grain growth, and the γ/α transformation of austenite [44]. A study by Jian-chun et al., [44] measured the kinetics of isothermal transformation of austenite to ferrite in steels containing different niobium content under deformed and un-deformed conditions. The study found that the influence of niobium on the transformation behavior depends on the thermo-mechanical history of the steel.

2.4 Effect of Alloying Elements

The role of the alloying elements is important in any steel composition; from the level of carbon to the additional alloying elements that control the initial and final structure giving it the mechanical properties required. Hosseini et al., [45] suggested that to achieve the required microstructure and the mechanical properties good metallurgical knowledge of the different processing parameters involved including the chemical composition of the steel is required.

The microlloying elements play a role in four major ways:

- Control of austenite grain coarsening by pinning the grain boundaries,
- Precipitation strengthening
- Solid solution strengthening and
- Increasing the hardenability.

2.4.1. Carbon (C)

In high strength low alloy (HSLA) steels, carbon is a strength controlling element and plays a critical role in forming carbide precipitates or finely dispersed precipitates in the ferrite matrix which are important for precipitation strengthening and grain refinement in steels. These precipitates form by combining with microalloying elements such as titanium (Ti), molybdenum (Mo), vanadium (V), tantalum (Ta), chromium (Cr) and niobium (Nb). As the wt. % of carbon increases, this also affects the amount of alloying elements able to dissolve in solution during the reheating stage at higher temperatures therefore making it difficult to precipitate during rolling [13]. Weldability of the steel is another issue in relation to the amount of carbon concentration; quantities lower than 0.25 wt. % does not create weldability or formability issues [46]. Figure 2-13 shows the ductile to brittle transition graph which indicates that the effect of increasing carbon can be seen to decrease the absorbed energy in a charpy V-notch test. Therefore a lower carbon content gives more of a ductile fracture then a higher carbon content which gives a brittle fracture. This increase in strength is caused by a solid solution strengthening effect by the carbon atoms in the Fe matrix. As deformation proceeds the moving dislocations interact with the carbon atoms and these impede the movement of the dislocations and increase strength.

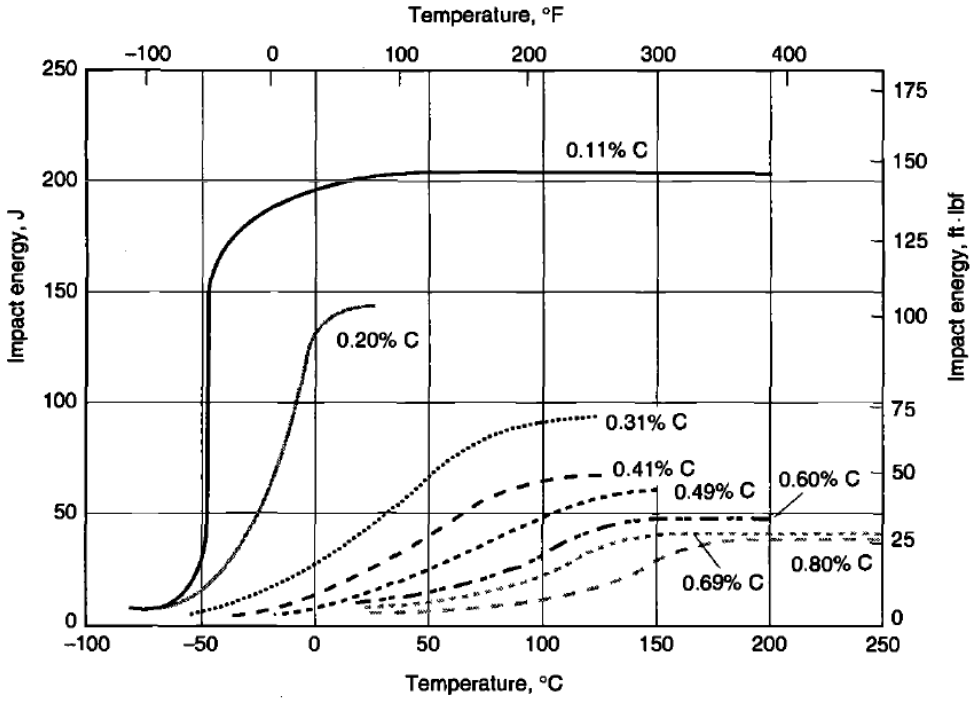

Figure 2-13: Effect of carbon content in ferrite-pearlite steels on Charpy V-notch transition temperature and shelf energy [47].

2.5 Microstructure

The microstructure in steel is a critical factor that controls the strength and toughness of steel. Control of the microstructure is brought about by the following; the composition, heat treatment, and hot or cold deformation [48]. The typical microstructure of high strength low alloy (HSLA) steels generally consist of ferrite-pearlite aggregate. Typical HSLA steels can have yield strengths of around 320MPa and an ultimate tensile strength of 440MPa [49].

1. The composition controls the phases present and their morphology and proportions through transformation characteristics.

2. Heat treatment affects the size, distribution and proportion of the phases present, including second phase particles. It also controls the grain size, dislocation structure, defect structure and composition of the phases by non-equilibrium or equilibrium partitioning.

3. Mechanical processing of the steel e.g., hot rolling or cold rolling. The effects induced by the deformation process influences many of the features listed above. The deformation process also has a critical effect on the crystallographic textures developed.

There are two solid-state transformations experienced in pure iron upon heating from room temperature; it has a stable ferrite α, body-centred cubic (BCC) structure to a temperature of 910°C (the A_3 point), at this point it transforms from the ferrite structure, to a austenite γ, face-centred cubic (FCC) structure. At 1390°C it transforms back to a ferrite δ structure[2] and stays stable until the melting point is reached at 1538°C [50]. Almost all steels rely on this transformation to obtain the desired microstructure, but in the reverse order starting from elevated temperatures in the austenite phase region.

The presence of solutes, such as carbon, manganese, silicon molybdenum, nickel, vanadium, chromium and niobium can greatly affect the transformation temperatures; for example increasing the carbon content, lowers the second solid-state transformation temperature from 910°C to 723°C.

The rate of cooling from elevated temperatures is another factor which controls the transformation temperature.

[2] There is no difference between α-ferrite or δ-ferrite crystal structure, high temperature ferrite is labelled as δ-ferrite.

Figure 2-14 shows the Fe – C phase diagram indicating the different phases which form as a function of temperature and carbon concentration.

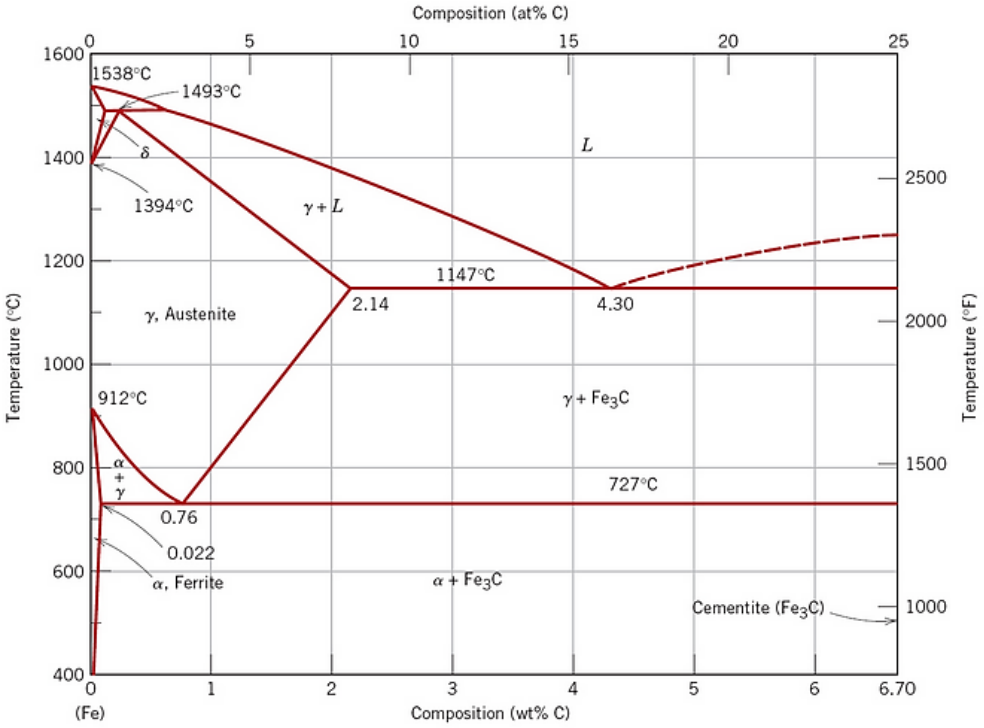

Figure 2-14: Fe-C binary diagram showing phase stability of austenite, ferrite and cementite [51].

2.6 Phase Transformation in Steel

As emphasised previously, the mechanical properties and the performance of a steel product, depend on its microstructure characteristics. There are five major transformation products which occur during the decomposition of austenite; allotriomorphic ferrite α, Widmanstätten ferrite α_W, pearlite *P*, bainite α_B and martensite α′. These phases are all categorised by the change in their crystal structure due to the atomic movement.

Microstructure evolution in steels is generally if not always a heterogeneous transformation as opposed to homogenous. There are three mechanisms by which the crystal structure changes are achieved during heterogeneous transformation [52]: (1) growth control by heat transport e.g., solidification, (2) thermally activated growth, for example the formation of pearlite from austenite and (3) athermal (independent of temperature) growth through glissile interface, for example the formation of martensite from austenite which is a diffusionless transformation.

2.7 Microstructure Evolution during Reheating

As the first step in most if not all industrial heat treatments is heating the steel in the austenitic range, this process is known as austenitization. It is challenging to characterize the austenitic microstructure of the final steel product as opposed to characterizing the austenite decomposition microstructure; regardless, there is a significant body of work available on the formation of austenite during reheating in the literature [53, 54, 55, 56, 57]. However with recent advancements in complex high strength steels such as dual phases, quenched and partitioned (Q & P) and Transformation Induced Plasticity (TRIP) steels, there has been a renewed interest in studying austenite formation. All the high strength steels have an essential processing stage involving partial austenitization, which is intentionally employed during heat treating of these steels; this is called intercritical annealing (heating between the lower and upper critical temperatures for particular steels) and is mostly used for manufacturing of automotive applications. The microstructure evolution in the heat affected zone of welds also attracts further interest in the formation of austenite. Other than austenite formation for which nucleation and growth in pure iron occurs rapidly [58], the starting microstructures from which austenite formation has been investigated includes pearlitic, hypo-eutectoid, and hyper-eutectoid steel microstructures, cold rolled (CR) [56, 55] and hot rolled (HR) ferrite-pearlite microstructures [57], ferritic matrix with spheroidized carbides [55] structure and an initial starting martensitic structure.

2.8 Grain Growth in Metals and Alloys during Reheating

Grain growth is a process by which the smaller grains are reduced in size by the expanding larger grains, this leads to a decrease in the total grain boundary area in the polycrystalline material as it is heated to higher temperatures. The driving force for this process is to reduce the overall grain boundary energy in the polycrystalline material. There are two types of modes for grain growth: normal grain growth (continuous) and abnormal grain growth (discontinuous).

Burke & Turnbull [59], summarised the principal mechanism for grain growth in 6 points, these are presented below:

i. Grain growth occurs by grain boundary migration and not by coalescence of the neighbouring grains.

ii. Grain boundary migration is a discontinuous process, for example the grain boundary migration rate for any particular boundary movement is not

constant in subsequent heating periods; and even the grain boundary migration direction could change.

iii. A given grain may be growing into a neighbouring grain on one side whilst simultaneously being consumed by a neighbouring grain on another side.

iv. The rate of the consumption of the grains by its neighbouring grains is frequently more rapid just as the grain is about to disappear.

v. A curved grain boundary usually migrates towards its centre of curvature as this reduces the area of the boundary and hence the energy associated with it.

vi. Grains included by angles of > 120° will grow until the stable angle of 120° are achieved and grains included by angles of < 120° will be consumed.

2.8.1. Normal Grain Growth (Continuous Grain Growth)

Normal grain growth is where the microstructure coarsens uniformly and is classified as a continuous process; it normally takes place in plain Carbon – Manganese (C-Mn) steel without any alloying elements and generally normal grain growth can be defined as having four main attributes as noted by Kurtz & Carpay [60]:

1. Uniform appearance, the grains have a relatively small range of grain sizes and shapes, there is a continuance of a uniformly-sized grain structure.

2. Scaling, changing the magnification is not enough to make the grains appear similar at various times.

3. Log-normality, the distributions of both grain size and topological parameters (e.g. the number of grain faces) can be well fitted by a log-normal distribution; hence the Gaussian distribution can be used to estimate the number of grain faces or grain diameter.

4. Stability, there is no change in the crystal structure and it remains stable against any irregularities during grain growth.

2.8.2. Abnormal Grain Growth (Discontinuous Grain Growth)

Terms such as grain coarsening, discontinuous grain growth, exaggerated grain growth and secondary recrystallization have all been used as alternative names for abnormal grain growth. In normal grain growth the spread of the grain size in the structure remains uniform, where as in abnormal grain growth process, a non-uniform spread of the grain size is observed; this is a result of several grains growing more rapidly compared to others.

Cahn, [61] has summarized the general characteristics of abnormal grain growth in the following 7 points:

1. The large grains which form during abnormal grain growth are not freshly nucleated; they are merely particular grains of the initial microstructure which have become enlarged.

2. Abnormal grain growth is sluggish in the initial stages of the process; as there is a significant incubation period before the abnormal grain growth gets under way.

3. The factors which determine the choice of which grains are to undergo abnormal grain growth, the mechanisms by which the early stages of growth occur are the least understood parts of the process. It is generally agreed that for the grains which are going to develop into abnormal grains (i.e. the secondary grains to be) should be significantly larger than the average grain size of the initial structure (i.e. primary grains). Secondly, they must have orientations which should appreciably diverge from the main microstructure.

4. In order for grain growth to occur in an abnormal manner, something must inhibit normal uniform grain growth, it is only when the normal grain growth is slow that the larger grains can grow.

5. When the process of abnormal grain growth has been completed, any orientation texture within the final microstructure, is usually different from the texture which was present in the initial microstructure at the start of the process.

6. For any particular metal there is usually a well-defined minimum temperature which much be exceeded for the abnormal grain growth process to occur, this is usually referred are the grain coarsening temperature.

7. The driving force for abnormal grain growth is similar to that for normal grain growth, i.e. the reduction of total grain boundary area and energy within the microstructure. However under certain circumstances, the behaviour of abnormal grain growth could be affected by the surface energy of the metal.

Hillert M. [62] postulated that for abnormal grain growth to occur and to be present in the final state of the material, the material in the initial stages should have a grain distribution with few grains having a grain size of more than 1.8 times the average grain size of the overall microstructure. This theory has been questioned and shown to be incorrect by Srolovitz et al., [63] and Thompson et al., [64] as they have indicated that there should be another factor other than the grain size over their neighbouring grains in order to grow abnormally. Gladman, [65] has suggested in his work that three conditions are required simultaneously for abnormal grain growth to occur; these are three conditions are:

- The size of the largest grain must be greater than 1.5 times that of the average grain size in the microstructure.
- Grains of overall average size must be stagnated or pinned, and
- A wider initial log-normal of the grain size should be present.

Computer simulation to explain the initial nucleation stage for the abnormal grain growth process has been done by Novikov, [66] In his work he concludes that large grains with high mobility boundaries are small in number and they are surrounded by stagnated low mobility smaller grains; therefore allowing the larger grains to keep growing.

2.8.3. Grain Coarsening Temperature (T_{GC})

The grain coarsening temperature is extremely important as it controls the initial uniform equiaxed austenite size and distribution; since the reheating of steel slabs is the initial stage to any subsequent deformation. The grain coarsening temperature is indicated by the temperature above which abnormal (discontinuous) grain growth or secondary recrystallization becomes prevalent in the structure. Cuddy et al., [67] reported that the grain coarsening temperature lies below the solution temperature of the second phase particles; this is because the second phase particles dissolve and/or grow to the extent that the pinning of the second phase particles falls below a critical value. The influence of the microalloying elements on the grain coarsening temperature and prior austenite grain size during reheating are shown in Figure 2-15 (a) which shows

that Ti or TiN is very effective to suppress austenite grain coarsening even above the normal reheating temperature range, and Nb or Nb (C, N) can prohibit austenite grain coarsening roughly below 1150°C. Figure 2-15 (b), indicates that normal grain growth takes place in plain C-Mn steel specimens in which the prior austenite grains grow in a continuous manner and with a gradual increase in the grain size. As opposed to plain C-Mn steel, abnormal grain growth is observed for the remaining microalloyed (V, Al and Nb) steels at certain temperatures (1000°C for vanadium, ~1100°C for aluminium and ~1150°C for niobium steel specimens depending on the concentration).

The grain coarsening temperature is usually determined by an experimental method of heating a series of specimens in the desired temperature range between 900°C to 1300°C or higher in increments of 50°C or 100°C. It is then held at each temperature for 30 or 60 minutes, than quenched into water or iced water as this would help obtain a full martensitic microstructure. Palmiere, et al., [68] investigated 5 steel compositions, one plain C-Mn steel and the other 4 with varying amounts of niobium. The study indicated that prior austenite grains in plain C-Mn steel are indicative of normal grain coarsening with a consistent normal distribution and the grain size increases systematically with increasing temperature. The grain coarsening temperature was also found to increase with increasing niobium content. Figure 2-16 illustrates the evolution of the prior austenite grains as a function of different reheat temperatures for 0.048 wt. % Nb steel; as it can be seen, the grain coarsening temperature is at 1100°C for this specific microalloyed steel specimen. This abnormal grain growth is caused by the decrease in stability and solubility of the precipitates which pin the grain boundaries.

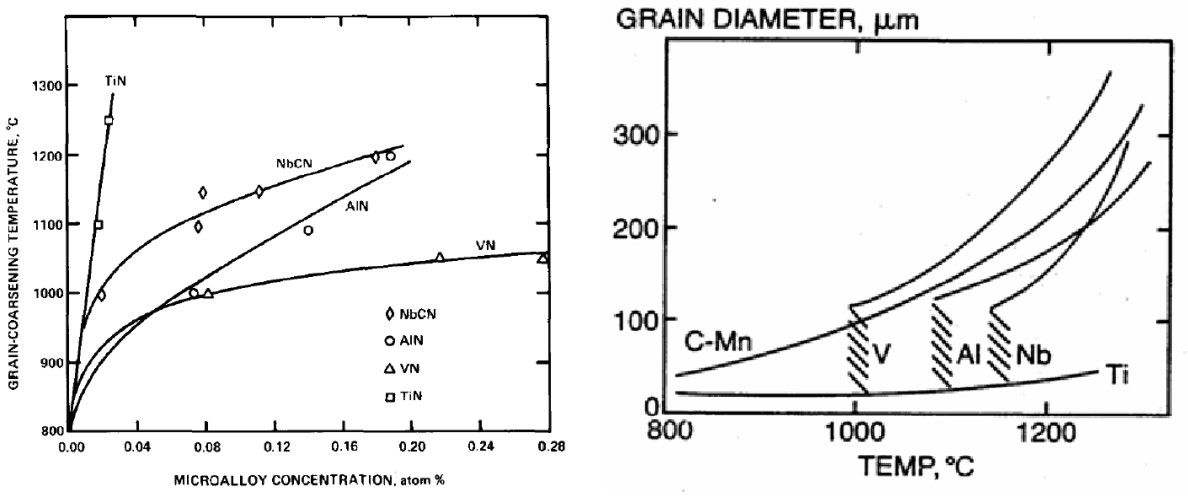

(a) (b)

Figure 2-15: (a) Increase in the grain coarsening temperature of four types of microalloyed steels with increasing microalloy concentrations [67], and (b) austenite grain growth as a function of different microalloying elements [69].

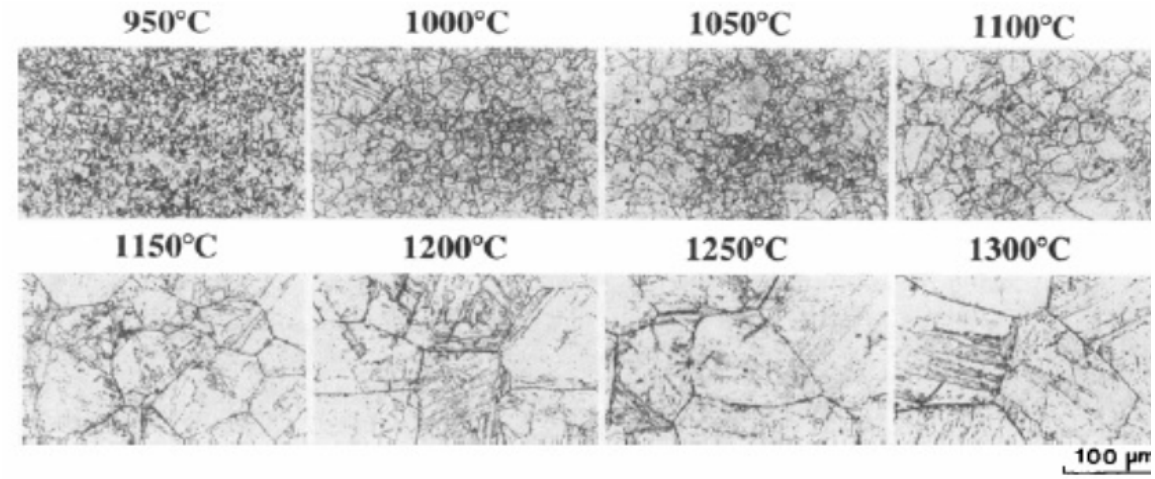

Figure 2-16: Evolution of the prior austenite grains in a Nb (niobium) microalloyed steel after reheating isothermally at different temperatures for 30 minutes and water quenching [68].

The effects of having the reheating temperature close to the grain coarsening temperature leads to a mixed prior austenite grain size of normal and abnormal distributions in the structure; this mixed austenite grain structure cannot be removed even by repeated deformation, recrystallization, or phase transformation [70, 5]. This mixed grain structure has also been found to have inferior mechanical properties [71].

A model has been proposed by Gladman, [72] and Gladman, et al., [73] which predicted the grain coarsening temperature and is given in Equation (2-5). It calculates the critical effective size of the precipitate to pin the motion of prior austenite grain boundaries which is given by r_{crit}. R_0 is the average radius of the austenite grains, f is the volume fraction of the precipitates and Z is the heterogeneity factor which is given by the ratio of the radii of coarsening and average pinned austenite grains. It has been observed that the value of Z = 1.5 for Nb microalloyed steels [74, 73]. According to Equation (2-5), the prior austenite grains will no longer be suppressed and abnormal grain coarsening will commence if the size of the second phase particles are above the r_{crit}.

$$r_{crit} = \frac{6R_0 f}{\pi}\left(\frac{3}{2} - \frac{2}{Z}\right)^{-1} \tag{2-5}$$

Cuddy, et al., [67] in their work reported a linear relationship which is given in Equation (2-6), where a linear increase is observed for the grain coarsening temperature (T_{GC}), with the calculated temperature for complete dissolution of the microalloying precipitates (T_{DISS}) and A and B are constants of the corresponding precipitates.

$$T_{GC} = A + BT_{DISS} \tag{2-6}$$

Palmiere, et al., [68] has also developed a relationship predicting the grain coarsening temperature (T_{GC}) of the austenite grains and the dissolution temperature (T_{DISS}) of precipitates this is shown in Equation (2-7).

$$T_{GC} = T_{DISS} - 125°C \tag{2-7}$$

To summarise, if the reheating temperature is too low compared to the grain coarsening temperature, the microalloying precipitates are not available for precipitation hardening or/and precipitation strengthening further down the processing route. When the reheating temperature is close to that of the grain coarsening temperature, a mixed initial austenite grain size is produced. Lastly, if the reheating temperature is too high the precipitates dissolve and/or become too large to significantly pin the austenite grain boundaries, this leads to very coarse large prior austenite grains due to the lack of inhibition to grain growth, hence it would require higher amounts of deformation to reduce the initial austenite grain size by recrystallization.

2.9 Grain Growth Law

The initial empirical equation for normal grain growth kinetics for isothermal temperatures was first proposed by Beck et al., [75] and is expressed in Equation (2-8).

$$D = A_1 \cdot t^n \tag{2-8}$$

where D, is the average grain size (μm), t is the time at the austenitisation temperature, A_1 is a material constant which depends on the metal composition and n is the time exponent which depends on the temperature and the composition but both are independent of grain size. Equation (2-8) can derived by assuming the following, that rate of grain growth of the prior austenite grains $\left(\frac{dD}{dt}\right)$ is proportional to grain boundary per unit volume of the material (k), which is proportional to the inverse of instantaneous grain diameter $\left(\frac{1}{D}\right)$. This is given in Equation (2-9), and integrating this equation leads to Equation (2-10).

$$\frac{dD}{dt} = k \cdot \left(\frac{1}{D}\right) \tag{2-9}$$

$$\therefore D^2 = k \cdot t + c \tag{2-10}$$

$$D^2 - D_0^2 = A_1 t \tag{2-11}$$

Assuming D_0^2, is the initial austenite grain size at the start of the annealing process (t = 0) gives Equation (2-11); however the initial grain size is sometimes neglected as it is smaller than that after coarsening [76]. This assumption is justified as the initial austenite grain size would be a function of temperature; as the austenite grain would be nucleated from the ferrite and cementite mixture during the heating process.

Taking the natural logarithm of Equation (2-8) to give Equation (2-12)

$$\ln D = n \ln t + \ln A_1 \tag{2-12}$$

Thus a plot of $[\ln D]$ versus $[\ln t]$ gives a straight line where the n (time exponent) as the gradient and A_1(material constant) as the y-intercept can be obtained.

2.9.1. Grain Growth Exponent "*n*"

The exponent "*n*" is the time exponent for grain growth and its values are theoretically expected to be 0.5 or 2 when taken as $\left(\frac{1}{n}\right)$ where *n* is 0.5. In this review the "*n*" value would be taken as the reciprocal $\left(\frac{1}{n}\right)$.

Beck, et al., [75] has shown that the time exponent in a high purity aluminium material was found to increase as a function of temperature and become closer to the theoretical value of 0.5 close to the melting point. Figure 2-17 illustrates a collection of *n* values for a number of different materials summarised by Higgins, [77]; an interesting point to note is that the experimental values of *n* are rarely found to be 0.5, never the less there is a general trend in which the "*n*" value increases with temperature. More recently, Yao et al., [78] for Nb-V-Ti microalloyed steel have also shown that the *n* value can increase with temperature until 1000°C after which it remains relatively constant at around 0.28 ± 0.02.

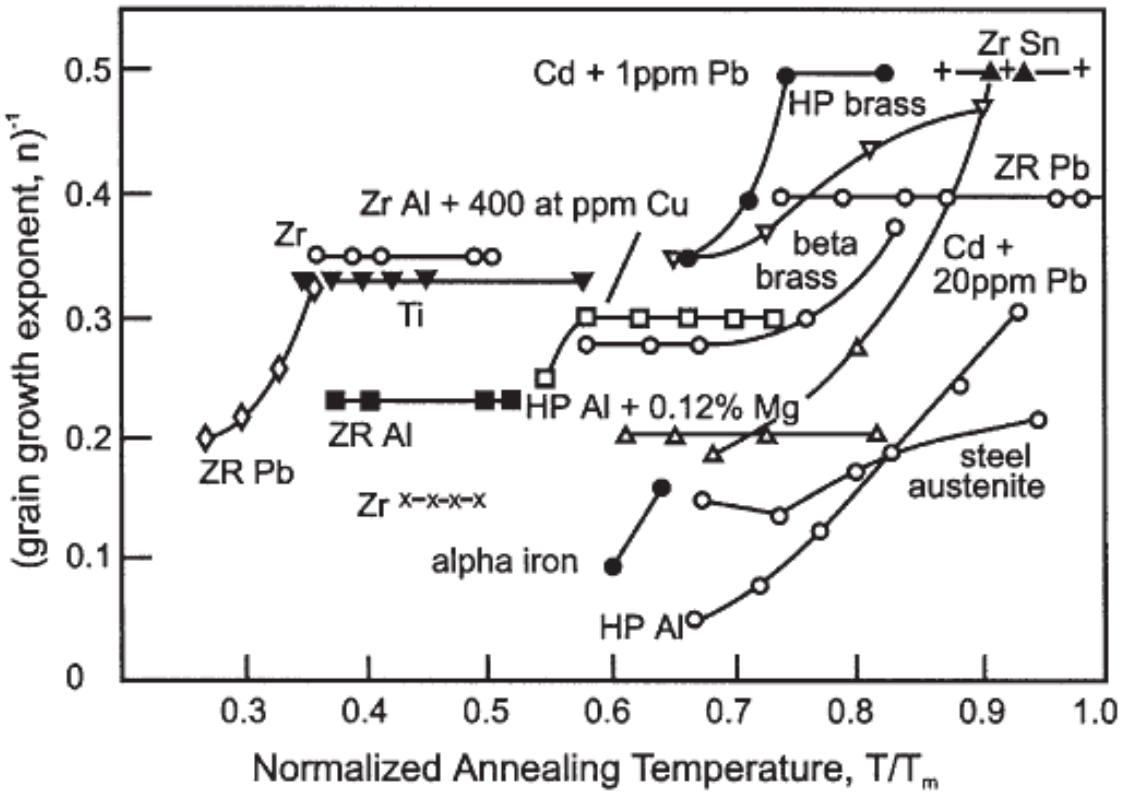

Figure 2-17: Temperature dependence of the time exponent in isothermal grain growth [77].

Burke, et al., [59] and Higgins, [77] have discussed reasons why the *n* value is below the theoretical value of 0.5 also more recently Humphreys & Hatherly, [79]. In this work they suggested that the main reasons for *n* to be lower than the theoretical value of 0.5 are related to the following:

1. Assuming that austenite grain growth is independent of holding time is incorrect as grain growth rate decreases as the grains grow larger.

2. Due to the solute drag effect on the grain boundaries and therefore the rate at which austenite grains grow may not be proportional to the driving force.

3. The initial and the changing grain size distribution during austenite grain growth can affect the measured grain growth kinetics.

Mizera et al., [80] have analysed the *n* values for normal and abnormal grain growth and indicated that the *n* value increases at the abnormal grain growth temperature. More recently, Sinha et al., [81] investigated the time exponent value for normal and abnormal grain growth characteristics, in which the results indicated that the *n* value for

normal grain growth are between 0.4 to 0.44 for the temperature range of 1173 to 1323 Kelvin, (900°C to 1050°C) and for abnormal grain growth are 0.90 to 2.0 for the temperature range of 1173 to 1223 Kelvin (900°C to 950°C).

2.10 Activation Energy

As the grain growth is a diffusion controlled process, the activation energy for the transfer of atoms across a grain boundary is reported to be half of that of self-diffusion. The activation energy for iron diffusion in austenite is 286 $kJmol^{-1}$ therefore the expected activation energy for grain boundary diffusion should be 173 $kJmol^{-1}$. Austenite grain growth kinetics have been modelled using the classic isothermal grain growth relationship given by Sellars & Whiteman, (1979) [3] shown in Equation (2-13). This is referred as the Sellars model and a variant of this is shown in Equation (2-14) and referred to as the Anelli model [82].

$$D^n - D_0^n = A_2 \cdot \exp \cdot \left(\frac{-Q}{RT}\right) \cdot t \tag{2-13}$$

$$D - D_0 = A_3 \cdot \exp \cdot \left(\frac{-Q}{RT}\right) \cdot t^n \tag{2-14}$$

Where D_0 and D are the initial and final grain size (μm) respectively, n is the time exponent, A_2 and A_3 are material constants, R is the universal gas constant (8.31 J $mol^{-1}K^{-1}$), t is the time at the austenitisation temperature T in Kelvin (K) and Q is the activation energy for boundary motion (grain growth).

A wide range of activation energy for austenite grain growth in steels is reported by many studies. These have been compiled in

Table 2-6, along with the material constant parameters A, and grain growth exponent n.

There is a lack of explanation in the past, but one possibility is that there is a non-linear relationship between the driving force and boundary velocity.

Table 2-6: Summary of models describing austenite grain growth in steel.

Steel Type	Model	N	A	Q (kJmol^{-1})	Ref
Rolling C-Mn	$D^n - D_0^n = A_2 \cdot \exp \cdot \left(\frac{-Q}{RT}\right) \cdot t$	10 10	3.87 x 10^{32} 5.02 x 10^{53}	400.0 for Temp > 1000°C 914.0 for Temp < 1000°C	[3]
Forged Waspaloy disc	``	3	2 x 10^{26}	595.0	[83]
C – Mn	``	7	1.45 x 10^{27}	400	
C – Mn – V	``	10	2.60 x 10^{28}	437	[84]
C – Mn – Ti	``	4.5	4.10 x 10^{23}	435	
GCr15	``	2.77	3.12 x 10^{19}	458	[85]
Microalloyed	``	5	1.60 x 10^{32}	716.9	[86]
Medium C – Mn – Nb	``	2.5	1.03 x 10^{16}	397.7	[76]
C – Mn	``	4.1	1.72 x 10^{21}	$352.2 + 21.8x_C + 19.9x_{Mn} + 7.2x_{Cr} + 7.4x_{Ni}$	[87]
A36 (fine grains)	``	3.4	5.46 x 10^{54}	1291	
A36 (coarse grains)	``	8.2	1.51 x 10^{47}	840	[88]
A36	``	14.9	1.94 x 10^{68}	1089	
API X65	``	3	1.2 x 10^{6}	107	[89]
API X70	``	3	1.1 x 10^{6}	120	
Nb – V – Ti	``	3.6	1.79 x 10^{30}	693.2	[78]
EQ70 (transverse)	``	14.3	4.87 x 10^{41}	597.88	[90]
EQ70 (longitudinal)	``	16.7	2.91 x 10^{47}	673.5	

C – Mn – Nb	``	9.7	1.7×10^{34}	463	[91]
Low C – M	``	2	4.27×10^{12}	66	[92]
C – Mn – V	$D = A_3 \cdot \exp \cdot \left(\frac{-Q}{RT}\right) \cdot t^n$	0.068 0.127	3.3×10^5 7.16×10^8	115 for Temp < 1000°C 195 for Temp ≥ 1000°C	[93]
Low Carbon	``	0.18	9.1×10^6	126	
High (0.71) Carbon	``	0.19	7.9×10^4	69	[82]
High (0.85) Carbon	``	0.12	4.1×10^7	141	
Low alloy	``	0.211	76.71×10^3	$89.1 + 3.6x_C + 1.2x_{Ni} + 1.4x_{Cr} + 4.0x_{Mo}$	[94]
300M	``	0.17	4.04×10^6	132	[95]

2.11 Solute Drag

The solute drag effect, is associated with dissolved Nb atoms which decrease the drift mobility of the grain boundary which in turn retards the austenite grain growth. The influence of solutes and particles on drift mobility was recognized as early as 1949 [37, 38]. According to the solute drag theory, the solute atoms diffuse and segregate to the grain boundaries to reduce the internal stresses, and therefore exert drag forces on the moving grain boundaries [6, 7, 8, 9]. Figure 2-18 shows that the solute drag effect increases rapidly with increasing boundary velocity until a critical point is reached (vertical dotted line). At this point the grain boundary migration is solute dependent and is referred to as low velocity. However, as the boundary velocity exceeds the critical point the magnitude of the effect of the solute segregation at the moving boundaries is reduced [96].

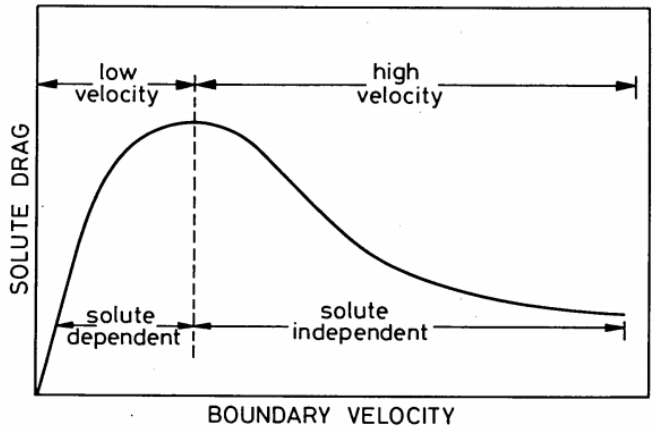

Figure 2-18: Solute drag vs change from low velocity to high velocity behavior of grain boundaries [96].

2.12 Heating Rate

2.12.1. Prior Austenite Grain

The effect of heating rate on the formation of austenite has been known to increase the austenite transformation start and finishing temperatures; Ac_1[3] and Ac_3[4] [58, 97, 98]. Previous studies on heating rate have been shown to not have any effect on the prior austenite grains, with some showing an increase and others indicating that there is

[3] The Ac_1 temperature is at which the austenite transformation begins to form on heating.
[4] The Ac_3 temperature is at which the ferrite to austenite transformation is completed upon heating.

a decrease in the prior austenite grain size. Grossmann, [99] has shown that for 0.17 wt. % carbon steel the heating rate of $0.1°C\,s^{-1}$ (slow heating), $2°C\,s^{-1}$ (moderate rate of heating) and $3.1°C\,s^{-1}$ have no effect on the austenite grain growth when heating to a temperature of 925°C.

Rosenberg & Digges [100] analysed 0.5 wt. % to 1.12 wt. % Carbon steel at the following heating rates; with the highest heating rate being 750 Fahrenheit min^{-1} ($6.65°C\,s^{-1}$) and 940 Fahrenheit min^{-1} ($8.41°C\,s^{-1}$) and the lowest being 9 Fahrenheit min^{-1} ($0.2°C\,s^{-1}$). The temperatures the specimens were heated to were 1475 Fahrenheit (801°C), 1500 Fahrenheit (815°C) and 1800 Fahrenheit (982°C). The results indicated that prior austenite grain size tended to increase with the increase in heating rate.

Sheard & Nutting, [96] investigated varying heating rates on a high purity Fe-C alloy with 0.47 wt. % C. The results indicate that heating the material to 795°C at $15min^{-1}$ ($0.25°C\,s^{-1}$) decrease the prior austenite grain size of the material, however the opposite is observed when the reheating temperature is raised to 875°C at a higher reheating rate of $26min^{-1}$ ($0.4°C\,s^{-1}$); where the prior austenite grain sizes increased. Figure 2-19 shows the prior austenite grain size evolution as a function of different reheating temperature and heating rates (min^{-1}).

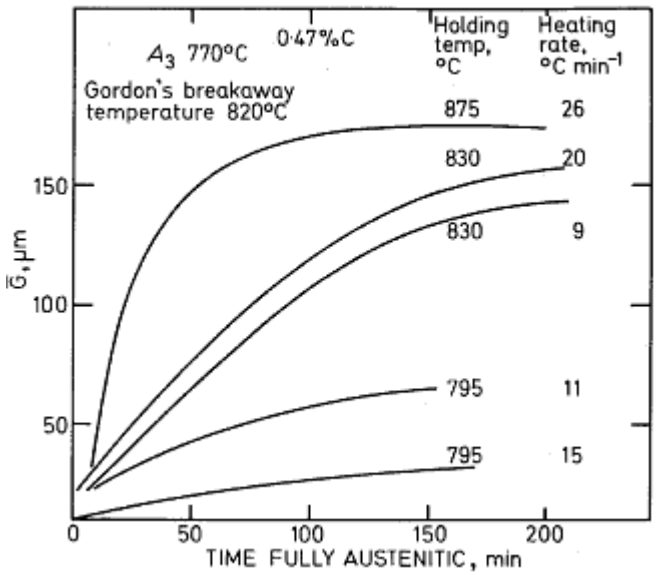

Figure 2-19: The average grain size [96].

A recent study by Danon, et al., [101], looked at heterogeneous austenite grain growth for a martensite to austenite transformation for different heating rates varying between $0.083°C\,s^{-1}$ to $100°C\,s^{-1}$, combined with different austenitization temperatures ranging from 1010°C to 1135°C. Danon, et al., in this study has shown that prior austenite grain size does not change much and remains relatively constant

with increasing reheating rate to 1010°C, however when the austenitization temperature is at 1135°C the prior austenite grain size decreases considerably with increasing heating rate, this is shown in Figure 2-20. Danon, et al., has also shown that the varying heating rate has different effects on the overall microstructure of being either homogenous or heterogeneous; when the austenitization temperature was 1010°C the microstructure was homogenous until 50°C s^{-1}, and after this heating rate there were a few isolated coarse prior austenite grains. At a higher austenitization temperature of 1050°C it was shown that the heterogeneous microstructure is obtained at lower heating rates of 5°C s^{-1} and higher; however when the austenitization temperatures were at 1135°C the overall microstructure was homogenous at any reheat rate.

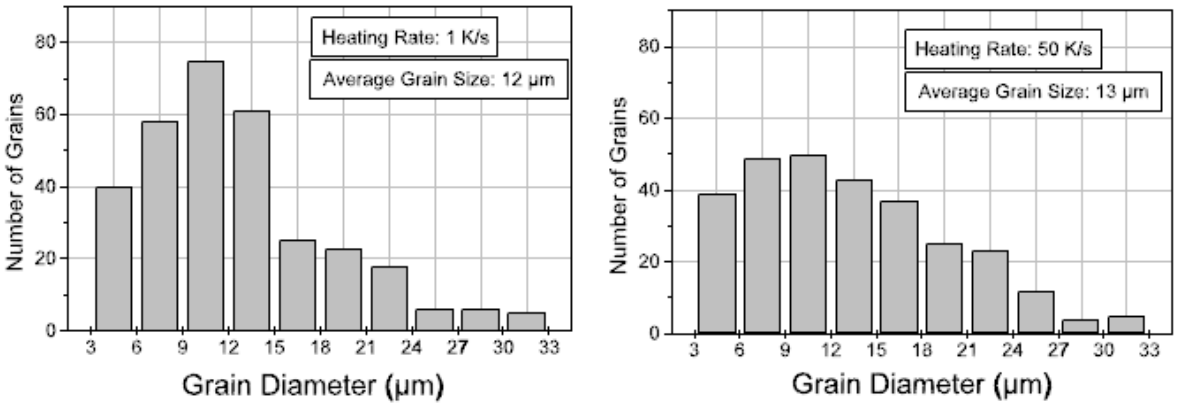

Austenitization temperature 1010°C

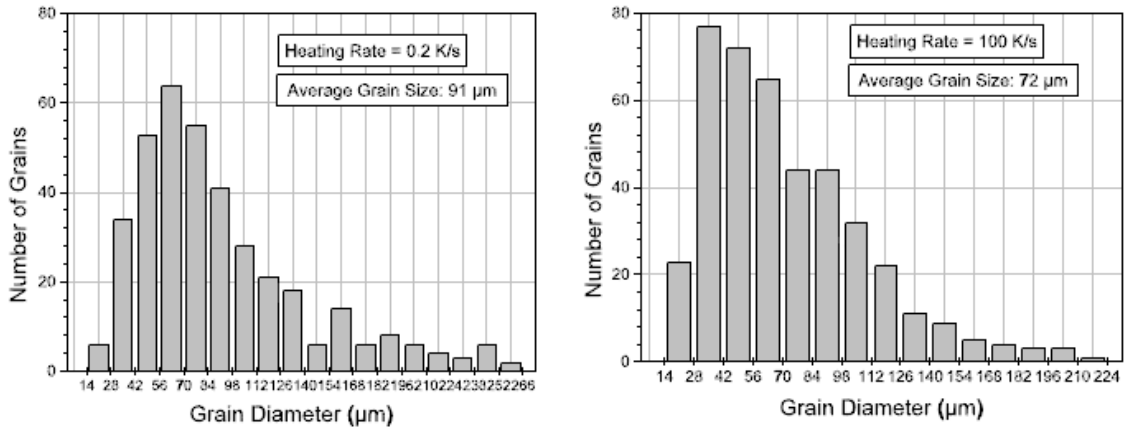

Austenitization temperature 1135°C

Figure 2-20: Prior Austenite grain size distribution at two different austenitization temperatures of 1010°C and 1135°C for low and high heating rates [101].

Martin et al., [102] investigated the effect of 3 different heating rates (0.05°C s^{-1}, 0.5°C s^{-1}, and 5°C s^{-1}) for different austenitization temperatures ranging from 910°C to 1250°C in ~50°C increments. The work has shown that the prior austenite grain size decreases with increasing reheating rate; the results obtained can be seen in Figure 2-21

which shows the effect of three different heating rates for the varying austenitization temperatures for a niobium (Nb) microalloyed steel; the chemical composition for the steel is shown in Table 2-7. At lower temperatures of 950°C and 1000°C the prior austenite grain size does not vary much with increasing heating rate, however at a higher temperature of 1100°C onwards the difference of the prior austenite grain size becomes much more noticeable; similar findings were presented by Danon, et al., [101]. The author also reported that as the heating rate increases, so does the grain coarsening temperature. It should be noted that this is for a niobium microalloyed steel where niobium carbides present in the steel pin the grain boundaries [1]. Plain C-Mn steel without any microalloying elements would not show the same characteristics.

Table 2-7: Chemical composition [wt. %]

C	Mn	Si	S	P	Nb	Cu	Cr	Ni	Mo	Al	N
0.11	1.47	0.27	0.013	0.015	0.031	0.011	0.03	0.03	0.006	0.039	0.0051

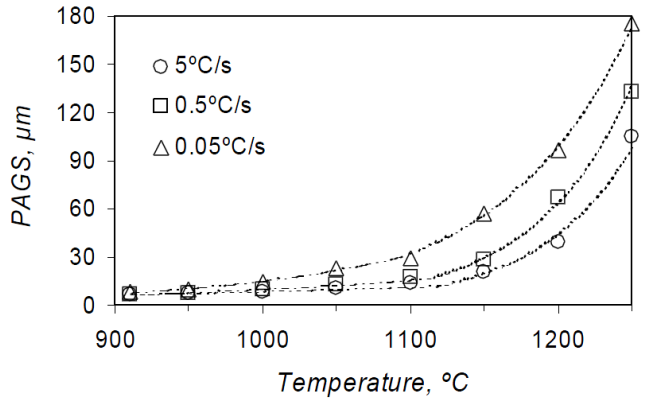

Figure 2-21: The graph represents the evolution of the prior austenite grain size for three different heating rates at different austenitization temperature [102].

Banerjee et al., [97] investigated the nonisothermal heating effects on the prior austenite grain growth kinetics for microalloyed steel and have shown similar results of decreasing the prior austenite grain size with increasing heating rate. Banerjee, et al., used a heating rate from low as 10°C s^{-1} to 1000°C s^{-1}, the austenitization temperatures used were 950°C, 1150°C and 1350°C. Change in the decrease of prior austenite grain size, as a function of heating rate decreases at higher heating rates. The results presented are similar to Danon, et al., [101] whereas at lower temperature the change in the prior austenite grain size does not change much with increasing heating rate.

2.12.2. Precipitate Size and Density

Studies have been performed to investigate the effect of precipitates during continuous heating at different heating rates and it has been shown to have an effect on the precipitation size and on the precipitate density [101, 102, 103, 104, 105, 97, 88]. As mentioned in the earlier sections niobium carbides act to pin prior austenite grain boundaries from moving and hinder their growth. Militzer et al., [88] found that austenitizing Al-killed plain carbon steel at a heating rate of $300°C\,min^{-1}$ produced larger prior austenite grains then when the heating rate was $6000°C\,min^{-1}$ with the austenitization temperature being 1100°C. The larger grains at the lower heating rate was attributed to the dissolution of AlN on heating, leading to dispersion of the precipitates unable to pin the grain boundaries. Alogab K. A et al., [105] have shown that the heating rate to the austenitization temperatures of 1050°C has a strong influence on the number density of the precipitates and the average precipitate size; an increase in heating rate from $20°C\,min^{-1}$ ($0.3°C\,s^{-1}$) to $145°C\,min^{-1}$($2.4°C\,s^{-1}$) resulted in an increase in the average precipitate size and an decrease in the number density of the precipitates.

2.13 Methods Detect Niobium Precipitate in Austenite

The knowledge of precipitation data is vital in steels; this is because they have a direct effect on the mechanical properties by controlling the grain sizes. Therefore the extent to which alloying elements such as Nb, Ti and V can be maintained in solid solution in austenite is dictated by the appropriate solubility product. This holds great importance in thermo mechanical controlled processing; as it has been shown that the solubility product varies with temperature therefore generating retarding forces under controlled conditions. Carbon when combined with niobium form a number of carbides, the one of interest in high strength low alloy steel is the cubic niobium monocarbide. This carbide precipitates in austenite and is a nonstoichiometric compound which can be represented as NbC_x, where the x varies from 0.75 to 0.98 [106]. The solubility of NbC in the austenite phase has been studied in numerous investigations, a paper written by Nordberg & Aronsson, [107], prudently reviews and summarises 13 independent investigations which examines the solubility products associated NbN, NbC, NbC_x, and NbC_xN_y. The solubility product Equation (2-15) is below for niobium carbides, NbC,

$$Log[Nb\ wt.\%][C\ wt.\%] = A - \frac{B}{T} \tag{2-15}$$

There are several different techniques to detect Nb(C, N) precipitates in austenite and obtain the solubility product of niobium carbide, nitrides and carbonitride in austenite. Each technique has advantages, there are however limitations and the use of assumptions with the different methods, which leads to differences between the solubility products obtained. The most common methods are listed below:

1. Transmission Electron Microscope
2. Thermodynamic calculations
3. Chemical or Electrolytic Separation of the precipitates
4. Electrical Resistivity Testing
5. Hardness Testing
6. Statistical treatment of existing solubility products

The following sections summarize each technique with the advantages and disadvantages.

2.13.1. Transmission Electron Microscope (TEM)

The most frequently used technique to detect precipitates is probably the transmission electron microscope (TEM). This is because the technique is highly sensitive in observing small precipitates which are present at the onset of the precipitation process; as well as the growth and coarsening kinetics, the technique also provides composition information and crystallographic information of the particles.

There are however a few drawbacks to this technique; the major one being sampling error as the prepared specimen only represents a comparatively small area of the bulk material under examination. The other drawback being the time it takes to prepare the samples which need to be examined; two types of techniques are used to prepare the samples for the observation of particles, carbon extraction replicas and thin foil. Preparing thin foils, although harder to prepare then the carbon extractive replicas, allows analysis of particles less than 2nm in size whereas with carbon extractive replicas it is difficult to extract particles smaller than 2 to 3nm [108].

2.13.2. Thermodynamic Calculations

During thermodynamic calculations the interaction between different elements is often neglected, leading to an assumption that the activity coefficient is unity. However work done by Sharma et al., [106], and more recently by Balasubramanian et al., [109], have achieved a more realistic solubility product by a nonunity activity coefficient. This is by incorporating the Wagner interaction parameter during the calcuation which takes into

account the effects of the alloying elements on the solubility of niobium carbonitride, Nb(CN), in austenite.

2.13.3. Chemical or Electrolytic Separation of the precipitate

The technique of chemical isolation and separation of the precipitates has advantages in that it can extract large amounts of precipitates in a short time [110] in terms of volume fraction measurements, also giving the best accuracy of the composition and structure of the particles making it useful to researchers [111]. Nonetheless it has limitations, the problems in this technique arises in regards to very fine precipitates which may not be included in the analysis and also that the exact composition of the precipitates may have disagreements as this may be due to the nitrogen content that is in the low carbon steel (0.05 wt. %) [107].

2.13.4. Hardness Testing

The hardness technique for obtaining a solubility product is questionable as it is based on the assumption that an increase in the amount of niobium content would increase the hardness proportionally, assuming that niobium dissolved in austenite during the reheating stage at high temperatures which would subsequently precipitate in ferrite as Nb(CN) during cooling.

However as this does occur, it is not necessary that all the carbon and nitrogen has to be associated with the precipitates. There are other factors which affect the hardness which make it difficult to separate the hardness from precipitates from other mechanism such as grain size, dislocation strengthening and solid solution strengthening. Therefore the drawback of this method is that there is an uncertainty of the actual volume fraction of the precipitates which affects the hardness rather than other factors.

2.13.5. Statistical treatment of existing solubility products

The size of the precipitate and its effect on the solubility product is neglected in all the methods above, thermodynamics indicate that larger particles are not as soluble as small particles, therefore the methods mentioned above may predict the solubility product for the precipitates to be more stable then would be expected.

2.13.6. Overview on the methods

Descriptions above regarding the different methods to identify niobium carbide precipitation indicate that there is no one single method which has advantage over another; for this particular investigation the transmission electron microscope (TEM) method would be used with the carbon extractive replicas from the point of view of

time. The morphology and density can also be analysed from the carbon extractive replicas which is an important section of this research.

2.14 Prior Austenite Grain Boundary Etching

Etching is basically a controlled corrosion process resulting from electrolytic action between surfaces of different potential [112]. When studying characterization of microstructure evolution in the austenite region, carbon steel and high strength low alloy steels, rely on ice water quenching to preserve the original austenite grain boundaries. The revealing of prior austenite grain boundaries are important because the end properties of heat treated steels are influenced by grain size produced during heating in the austenite region. There are many methods which are used to review the prior austenite grain boundaries in a steel sample. The method used commonly is chemical etching, however there are other methods such as oxidation etching and thermal etching. All three of these etching techniques will be discussed.

2.14.1. Chemical Etching

Saturated aqueous picric acid solution is most commonly used to reveal prior-austenite grains because it produces a slow, uniform dissolution of the ferrite lamella with the cathodic cementite in relief, but suppresses ferrite grain boundaries.

Nonetheless, it is difficult to reveal the prior-austenite grain boundaries because no one single etchant is used for all samples. To obtain a successful etch there should be a chemical attack on the boundaries but not on the matrix. Tempering the specimen can aid in improving etch response without affecting the grain size; as it is a well-known phenomenon that impurities (e.g. P, Sn, Sb, and As) segregate to prior austenite grain boundaries [113, 114] when held for long periods from 1 to 100 hours, in the temperature range of 350ºC – 600ºC [115, 116]. The study of segregation of impurity elements to grain boundaries has been studied using auger electron spectroscopy to investigate the cause of temper embrittlement.

Barraclough [117] in 1973, reviewed the use of different etching soluations to outline the prior austenite grain boundaries in 0.42 wt. % Carbon steel with a martensitic microstructure obtained by quenching. Specimens were etched in the quenched state and after tempering at different temperatures for different durations. Barraclough concluded that to produce a consistently sufficent delineation of the prior-austenite grain boundaries, tempering for two hours at a temperature of 625°C, then furnace cool to 550°C and a hold for 72 hours with finally water quenching was needed. He also concluded that the picric acid solution works best when heated to 85°C. A similar method was employed by Mahajan, et al., [118] in which the samples were etched in

boiling water saturated with picric acid. In both the cases the solutions were based on saturated aqueous picric acid plus a wetting agent[5] [119], the wetting agent generally utilised is sodium alkyl sulphonate "Teepol"[6]. Nelson, [120] evaluated the effect of five wetting agents for the delineation of the prior-austenite grain boundaries using saturated aqueous picric acid; the wetting agents experimented with were zephiran chloride, Tergitol p-28, Triton X-100, Aerosol-22, and sodium tridecylbenzene sulfonate. Nelson found four different responses by evaluating the effect of increasing the concentration of the wetting agents: 1) A maximum limit is obsevered where a noticeable sharp improvement occurs, however over this limit higher concentrations of the wetting agent do not produce an effect. 2) There is a slight gradual improvement with increasing the concentration of the wetting agent, however above the maximum limit higher concentrations are detrimental. 3) The wetting agents have little or no value. 4) The wetting agent is counterproductive in any concentration or damaging with increasing the concentration.

2.14.2. Oxidation Etching

This technique reveals the prior-austenite grain boundaries by relying on the fact that oxidation accumulation preferentially occurs along the grain boundaries or by grain boundary decarburization (reduction of carbon) [112]. This method required the steel specimen to be slightly polished prior to placing it in an electrically heated furnace with an oxidizing atmosphere; so that oxidation can occur on the required side, the polished side should be facing upwards. Once the sample is placed in the furnace at the required temperature for the desired hold time at that temperature the sample is water quenched to form a martensitic structure. Careful removal of the oxide layer must be performed during the grinding and polishing stage, as excessive grinding would remove the affected layers of oxide.

The drawback of this method is that at high austenitization temperatures the bulk diffusion rate is too high to preferentially oxidize the grain boundaries; however at temperatures below 1038 ºC [121], the grain boundary diffusion permits selective oxidation as it predominates.

2.14.3. Thermal Etching

The thermal etching method consists of heating a steel sample which has been finely pre-polished with a 1µm diamond paste and placed in an inert atmosphere or a vacuum with a pressure of at least 1 Pa or higher to avoid oxidation [122, 123] to the

[5] A wetting agent is used to change the surface energy of a liquid or solid surface and influence interfacial interactions (modifying etch behaviour).

[6] Sodium alkyl sulphonate is known as Teepol in the United Kingdom.

austenitization temperature and then cooling it down to room temperature. The prior austenite grain boundaries are shown by grooves which decorate them, these grooves at the grain boundaries are formed by matter transport and surface tension effects. The rate at which the specimens are cooled from there austenitization temperature has an effect on the grooves which decorate the prior austenite boundaries. When the cooling rate is too slow ghost traces of the groves occur, this leads to differences between the inner and outer grain size, therefore leading to false measurements of the prior austenite grain size. Also during slow cooling from high temperatures (>1200°C), an austenite grain can continue its growth therefore complicating the accuracy of the prior austenite grain boundaries [123].

2.14.4. Other methods

A direct method to observe the prior austenite grain boundaries at high temperatures is by a high temperature microscope [124].

Another method used by many researchers to reveal the prior austenite grain boundary is by the precipitation of ferrite, cementite, and fine pearlite [112, 125]. Vander Voort, [112] has reported that when successfully employed it is a reliable method for austenite grain size measurements, the drawback of this is that considerable experimentation would be required before obtaining reliable results. However in this work this technique would not be possible due to the high carbon (0.8 wt. % having an all pearlite structure).

2.14.5. Overview on the methods

The etching methods stated above, all have their advantages and disadvantages. As the temperatures used in this work would be as low as 950°C and as high as 1250°C and certain compositions would consist of a wholly pearlite microstructure, the best etching technique for this work would be chemical etching.

3. Experimental Work

One of the main objectives within the current work is to investigate the evolution of the prior austenite grain growth microstructure. The grain growth reheat temperature study was carried out on five different carbon chemistries with varying Nb contents. The heat treatment temperature ranges were between 950°C to 1250°C and for different hold times for two temperatures of 1050°C and 1150°C. The steels were produced and supplied by TATA UK.

3.1 Material Chemistry

The investigation was carried out on five different carbon chemistries, low (0.08 wt. % C and 0.2 wt. % C), medium (0.4 wt. % C and 0.6 wt. % C) and high (0.8 wt. % C). These Silicon-killed laboratory steels had been rough rolled into 50mm thick plates. The detailed composition of each of these steel specimens used is provided in Table 3-1 for 0.08 wt. % C, Table 3-2 for 0.2 wt. % C, Table 3-3 for 0.4 wt. % C, Table 3-4 for 0.6 wt. % C and Table 3-5 for 0.8 wt. % C. The compositions have been kept as identical as possible for all the specimens so that only the effect of niobium carbide is studied, hence aluminium was not used as a deoxidizer as it forms aluminium-nitride (AlN) precipitation, and silicon was used instead.

Table 3-1: Chemical composition of 0.08 wt. % Carbon steel specimens.

Initial	C, wt. %	Mn, wt. %	Si, wt. %	S, wt. %	P, wt. %	Nb, wt. %
VS 522(1A)	0.086	0.98	0.20	0.003	0.01	0
VS 522(1B)	0.085	1.00	0.19	0.003	0.01	0.005
VS 522(2A)	0.078	0.98	0.17	0.003	0.01	0.01
VS 522(2B)	0.080	0.98	0.18	0.003	0.01	0.02

Table 3-2: Chemical composition of 0.2 wt. % Carbon steel specimens.

Initial	C, wt. %	Mn, wt. %	Si, wt. %	S, wt. %	P, wt. %	Nb, wt. %
VS 539(7A)	0.2	1.03	0.19	0.008	0.018	0
VS 539(7B)	0.2	1.03	0.19	0.007	0.018	0.005
VS 539(8A)	0.2	1.01	0.19	0.007	0.015	0.01
VS 539(8B)	0.2	1.01	0.19	0.007	0.015	0.02

Table 3-3: Chemical composition of 0.38 wt. % Carbon steel specimens.

Initial	C, wt. %	Mn, wt. %	Si, wt. %	S, wt. %	P, wt. %	Nb, wt. %
VS 539(9A)	0.38	1.00	0.20	0.003	0.018	0
VS 539(9B)	0.38	0.98	0.20	0.007	0.018	0.005
VS 540(0A)	0.39	1.00	0.20	0.008	0.016	0.01
VS 540(0B)	0.38	1.00	0.20	0.007	0.016	0.02

Table 3-4: Chemical composition of 0.6 wt. % Carbon steel specimens.

Initial	C, wt. %	Mn, wt. %	Si, wt. %	S, wt. %	P, wt. %	Nb, wt. %
VS 540(1A)	0.60	1.0	0.20	0.010	0.15	0
VS 540(1B)	0.60	1.0	0.20	0.007	0.15	0.005
VS 543(7A)	0.59	1.0	0.19	0.007	0.12	0.01
VS 543(7B)	0.60	1.0	0.20	0.007	0.13	0.02

Table 3-5: Chemical composition of 0.8 wt. % Carbon steel specimens.

Initial	C, wt. %	Mn, wt. %	Si, wt. %	S, wt. %	P, wt. %	Nb, wt. %
VS 522(3A)	0.79	0.98	0.21	0.003	0.01	0.005
VS 522(3B)	0.79	0.99	0.21	0.003	0.01	0
VS 522(4A)	0.80	0.96	0.20	0.003	0.01	0.01
VS 522(4B)	0.80	0.96	0.20	0.003	0.01	0.02

3.2 Material Processing

The initial received steel bars for the present research were ingots which were cast in a vacuum induction furnace; the ingots were reheated to 1200°C for 1 hour and hot rolled at 1100 °C to 50mm thick plates and air cooled.

The specimens were machined into cubes of 10mm by 10mm by 10mm from the rough rolled steel plates. In total 140 cubes were machined from each of the five different carbon contents for the reheating experiment work. The dimensions of the cubes were chosen so that during heating of the cubes a uniform temperature is provided throughout the material and when quenching in ice water a sufficient cooling rate is obtained giving a full martensitic transformation.

3.3 Reheat Temperature Work

A tube furnace filled with argon gas was used for this reheating temperature study. A tube furnace was used as shown in (Figure 3-1) as it is much more accurate in maintaining the temperature at a constant with (deviation ±3°C). Thermocouples were used to measure the temperature range in the centre hot zone within the tube furnace.

Figure 3-1: Tube furnace used for the heat treatments e.g. reheat temperature and isothermal hold times.

The lowest temperature was set at 950ºC; this temperature was used as the lowest temperature because according to JMatPro predictions the austenite phase field starts at this temperature, whereas the highest temperature employed was 1250ºC. This was to ensure that the NbC precipitates could dissolve into solution as much as possible for the low carbon to high carbon steel specimens. The temperature was increased in 50°C increments within the range of 950°C to 1250°C; for all five different carbon content steels.

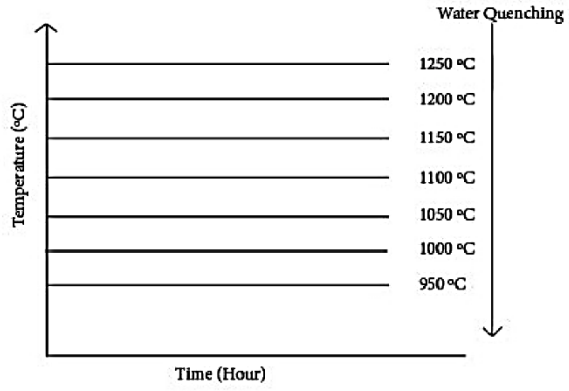

Figure 3-2: Above is an illustration of the reheating temperature and quenching process used for the three carbon steels with varying niobium concentration to examine the microstructural evolution.

The cube samples were inserted in to the furnace once the desired reheat temperature was reached; the specimens were austenitized for 1 hour to permit full austenitization. Following reheating, the specimens were immediately quenched in an ice water bath; an illustration of the process is shown in Figure 3-2. The specimens were then prepared for optical micrographic techniques to analyse the microstructural changes which are attend at different reheating temperatures. Carbon replicas would also be made to measure the amount of dissolved Nb.

3.4 Isothermal Hold Time

The isothermal hold time experiments were carried out in an identical tube furnace to which the reheating temperature experimental work was done. This was to further keep the temperature profiles identical with ±3°C error in the temperature range. These experiments were also carried out under a argon atmosphere, two temperature ranges were chosen 1050°C and 1150°C and the specimens were held for 1, 3 and 6 hours at each temperature.

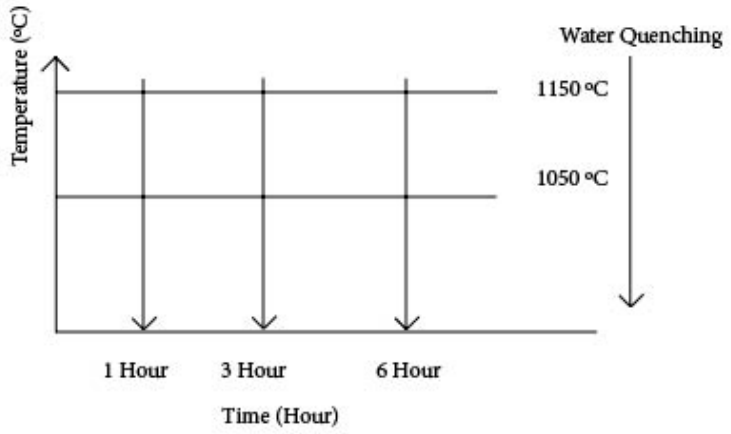

Figure 3-3: Above is an illustration of the reheating temperature and quenching process used for the three carbon steels with varying niobium concentration to examine the microstructural evolution.

3.5 Reheat Rate Work

The reheat rate experimental work was carried out on low carbon steel the composition of which is given in Table 3-1. It was carried out by using a SERVOTEST TMC machine shown in Figure 3-4 to simulate different reheating rates of 2.5°C s^{-1},

5°C s^{-1} and 15°C s^{-1} to the austenitization temperature of 1000°C and 1100°C, and repeating the work again but with a 5 minute hold.

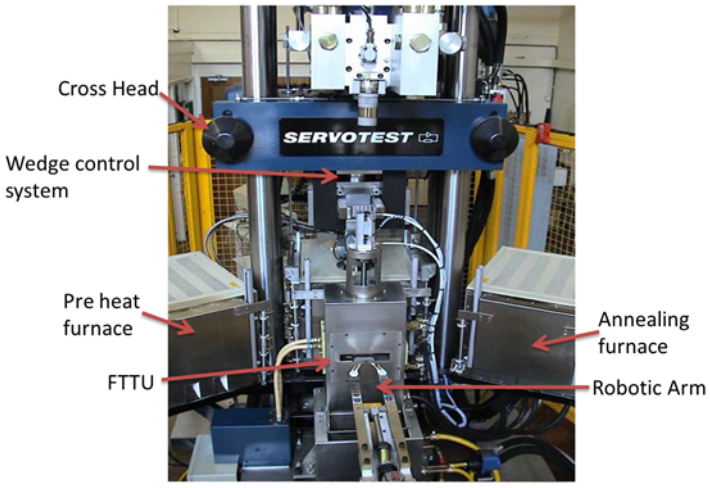

Figure 3-4: The key components of the SERVOTEST TMC machine are indicated.

Figure 3-5 illustrates the experimental profile which was performed. The first stage of the reheat work was done by reheating the specimens at different reheating rates of (2.5°C s^{-1}, 5°C s^{-1} and 15°C s^{-1}) to 1000°C and water quenching. The same procedure was repeated when reheating to 1000°C but this time the specimens were held at 1000°C for 5 minutes and then water quenched; this was also repeated for a higher temperature of 1100°C. During the reheating rate experiment a thermocouple was placed in the AXI specimens to monitor the reheating rate of the specimens as shown in Figure 3-6.

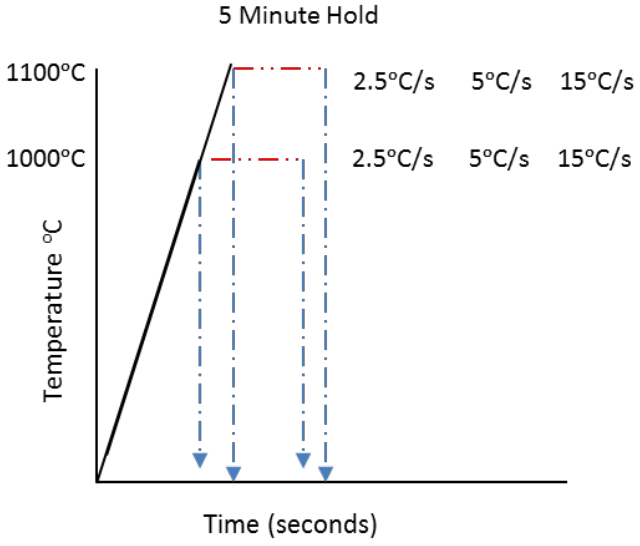

Figure 3-5: Illustration of the reheating rate experimental work.

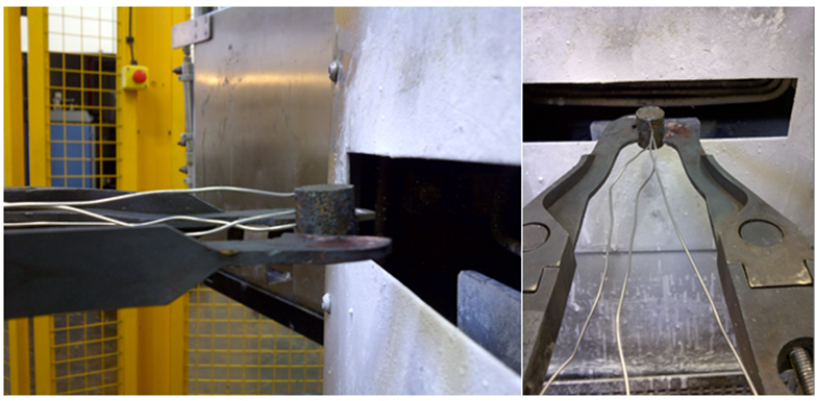

Figure 3-6: Shown here is the AXI specimen being helped by the robotic arms into the FTTU unit, with three thermocouples attached to the specimen. This is to obtain a temperature distribution throughout the specimen.

3.6 Hardness Testing

The hardness tests were performed on a variety of as received material; low, medium and high steel compositions with varying niobium content. The specimen preparation were similar to that of optical microscopy and scanning electron microscopy, the etchant used was 2 % Nital which helped to show the ferrite and pearlite microstructures. A Struers Durascan 70 hardness tester, fitted with a diamond, square based pyramid, Vickers indenter was used.

Two different loads were used for the indentations, 25g and 1000g for a dwell time of 15 seconds. A total of 20 indentations were made after which an average value was taken.

3.7 Atomic Force Microscopy (AFM)

The development of the new etching technique which is discussed later on uses the AFM technique to analyses the roughness of the etched surface and the depth of the prior austenite grain boundaries from locations where the grain boundaries are clearly visible. A Dimension 3100 atomic force microscope machine was used to analyse the surface of the specimen of the surface area analysis was $30\mu m^2$ in a tapping mode, scanning rate of 0.500 Hz and sample/line 512. The initial specimen preparation is identical to that in Section 3.8.3 and the etching procedure is explained later on.

3.8 Microstructure Analysis

Microscopic techniques have been used to principally investigate the as received and prior austenite grain microstructure. The microscopy techniques carried out in this study include: light optical microscopy (LOM) (Nikon Eclipse LV150), scanning electron microscopy (SEM) (IFE Inspect F) and transmission electron microscopy (TEM) (FEI Tecnai T20); with the exception of transmission electron microscopy (TEM), sample preparation for all other microscopic techniques was essentially identical.

3.8.1. Scanning Electron Microscopy (SEM)

For the As received material, FEI Inspect F SEM microscope with an operating voltage of 10 and 20kV and using a spot size[7] ranging between 2 to 3 in order to get a better resolution of the features. The images taken in the Inspect F SEM had magnifications ranging from 1000x to 30000x. The SEM analysis was only performed on the As-received material.

3.8.2. Transmission Electron Microscopy (TEM)

The precipitate analysis was done using the FEI Tecnai T20 TEM on carbon extraction replicas placed on the copper grids. From each specimen 2 carbon replicas were analysed with images taken from random places from each of the replicas. The FEI Tecnia T20 was operated with an accelerating voltage of 200kV. Further, the chemical analysis of the precipitates was carried out using an Oxford instruments energy dispersive X-ray spectroscopy (EDX) detector (Oxford Instruments, Oxford, UK) with was fitted with the microscope.

3.8.3. Sample Preparation for LOM and SEM

The heat treatment samples and reheating rate temperature samples were mounted in Bakelite before grinding and polishing. Grinding and polishing was carried out on a Buehler AutoMet 250, grinding was done on several grits of SiC papers, starting from P120, P240, P400, P800 and P1200 (European standard) to obtain a scratch free surface with no disparities. After each grinding stage the specimens were rinsed. After the last grinding stage the sample was rinsed and the samples were than polished using 6μm, 3μm and 1μm polishing solutions once again washing the specimen prior to polishing with the next solution. The specimens were then ready to be etched to reveal the microstructure desired. These were then stored in a desiccator, ready for optical microscopy and/or SEM analysis.

[7] The spot size is a cross sectional diameter that the cone of the beam makes on the surface of the sample. The units of the spot size are arbitrary units.

3.8.4. Sample Preparation for Carbon extraction replicas

The identical sample preparation was used for LOM and SEM as explained earlier but the specimens for whom precipitation analysis was required were lightly etched with 2% Nital solution for 5 seconds prior to carbon coating the specimens.

Carbon coating on the specimen was done using a carbon coater unit (Speedivac carbon coater). After the specimen was coated with a carbon film under high vacuum, the surface of the specimen coated with the thin carbon film was cut in to approximately 2mm square grids, the next step was to paint the remaining areas of the Bakelite with varnish where there was no metal specimen. This ensured that the only the carbon coating on the metal surface reacted when submerging the specimen into 10% nital[8] solution until bubbles started to form on the surface. Once the bubbles started to form below the carbon coating, the specimens were then removed from the 10% nital solution and placed in methanol until the 2mm layers start to peel off. The carbon replicas were then fished out of the methanol using 400 mesh copper grids and stored for analysis on the TEM.

3.9 Quantitative Metallography

3.9.1. Phase quantification

The volume fraction of pearlite phase was measured using ImageJ which is a freeware image analysis software. After importing the light optical micrograph of the as received material into ImageJ, a threshold is applied to differentiate between the pearlite phase and the ferrite phase, this was done to calculate the amount of each phase present in the microstructure. This was done on the As-Received material with a ferrite-pearlite microstructure. The average value was obtained from a total of 10 light optical micrographs.

3.9.2. Prior Austenite Grains

The main objective of this work is to look at the effect of different reheating temperature, hold times and reheating rates on prior austenite grains. The prior austenite grain size was measured on OminMet, a software using the linear intercept method as outlined in ASTM E112 [126] as shown in Figure 3-7. In short, the method consisted of drawing lines over the microstructure, of equal distance so that no line is passing the same grain twice to ensure correct results. By measuring the number of intersections made with the grain boundaries, the mean intercept length was determined. Since the

[8] Solution made of 10 mL of nitric acid in 90 mL of ethanol.

prior austenite grains were equiaxed the average prior austenite grain size was obtained. This technique was performed on at a fixed 50 fields of view per sample. These various images of each sample were used for measuring grain sizes for accuracy; the heterogeneity near the abnormal grain coarsening temperature was measured with the Standard deviation values which also enabled the 95 % confidence limit to be calculated.

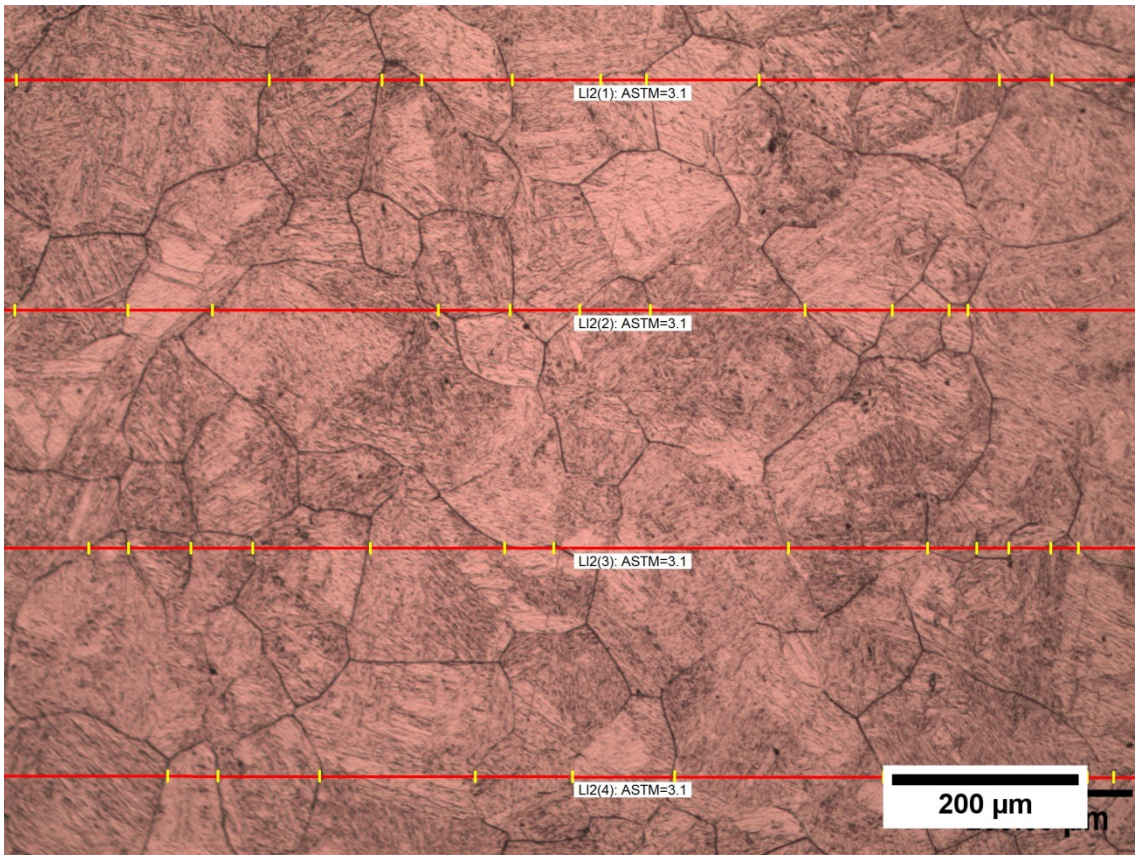

Figure 3-7: Austenite grain size measurements using the OmniMet software.

3.9.3. Precipitation Size and Distribution

ImageJ analysis software was used to analyse the precipitate size and distribution, by calibrating the software with the scale bar on the TEM micrograph. The TEM images were taken from random areas from within the carbon extraction replicas in order to get a reasonable representation of the precipitates. The number density was made by manually counting the precipitates and dividing by the surface area. Energy Dispersive X-ray Spectroscopy (EDX) was used to identify the precipitates. The TEM analysis was confined to the steels with the highest amount of Nb content.

3.10 Statistical Analysis

The calculation of the mean of a set of results can be used in order to determine the mean of a population. An error term may be utilised in order to provide a range of values in which results are expected to lie; this range is referred to as an interval. The error term, and hence the width of an interval, for a set of results is dependant on:

(i) Sample size, n – larger sample sizes give smaller intervals.
(ii) Variability of the measurement (given by standard deviation) – the larger the standard deviation, the greater the interval width.
(iii) The level of confidence required for the population mean – the greater the confidence required, the greater the interval width [127].

3.10.1. Population and Sample Properties

The mean and standard deviation of a population and a sample taken from the population are related. The mean and standard deviation of a population are denoted μ and σ respectively whilst the mean and standard deviation of a sample of the population are denoted *s* and $\bar{x}$ respectively. The means and standard deviations of the population and the sample can be related in the following way:

$$\bar{x} = \mu \tag{3.1}$$

$$s = \frac{\sigma}{\sqrt{n}} \tag{3.2}$$

where *n* is the size of the sample.

3.10.2. Confidence Interval for Small Samples

For a small sample size where $n \leq 30$ a confidence interval for the data can be calculated using the following equation:

$$\bar{x} \pm \frac{ts}{\sqrt{n}} \tag{3.3}$$

where *t* is a value obtained from statistical tables. The value of *t* required depends on two factors:

(i) The confidence level required – this determines the α value to look up in the appropriate statistical table. For example, for a 95% confidence level:

$$\alpha = \frac{1-0.95}{2} = 0.025 \tag{3.4}$$

(ii) The sample size, n, which determines the degrees of freedom, $\upsilon = n - 1$, to look up in the statistical table [127].

For a large sample size where $n \geq 30$ a 95% confidence interval for the data can be calculated using the following equation.

$$\bar{x} \pm 1.96 \frac{s}{\sqrt{n}} \tag{3.5}$$

The Statistical software IBM SPSS Statistic V22.0 Software (IBM, 2013) was used to statistically analyse and determine possible significant differences in the precipitate data set in Chapter 7.

Exploratory data analysis was conducted prior to carrying out statistical analysis to determine whether parametric assumptions had been met. The assumption of normality is a pre-requisite for statistical tests. This was examined through tests for normality, mean, and standard deviation for each precipitate size along with graphical analysis with the use of histograms, box plots and confidence intervals (error bars).

Statistical analysis was utilised to critically understand the data and any possible differences. A Shapiro-Wilk's test ($p < 0.05$) Shapiro & Wilk [128] and Razali & Wah, [129] and a visual inspection of their histograms, normal Q-Q plots and box blots showed that the precipitates were not normally distributed.

Shapiro-Wilk tests [128] were performed to assess the normality of the distribution, which is also a suitable test for large sample sizes [130]. This test provides a p value, and if the p value is greater than alpha level of 0.05, it accepts the null hypothesis that the data is normally distributed. However, within the data set of this research study the alpha level was found to be below p value of 0.05 for all data sets, thus rejecting the null hypothesis that the data was in fact not normally distributed [131]. Further to this, it is argued that additional tests should be applied to verify distribution of data; for example Field (2013) argues Shapiro-Wilk analysis in large sample size may create significant normal distribution in any data set, and therefore visual inspection of histograms and skewness and kurtosis measures should be used in conjunction with the Shapiro-Wilk test (Field, 2013).

For a detailed description of the theory behind some of the techniques used in this analysis, please refer to Appendix A.

4. Etching

4.1 Delineation of Prior Austenite Grain Boundaries

As described in the literature review, delineation of the prior austenite grains can be done by many techniques; the one used in this work is through the chemical etching process for high purity microalloyed steels. The results presented in this are achieved after numerous trial and error experiments in which various influential factors had to be changed e.g. etching temperature, time, wetting agent, hydrochloric acid content and how and when to clean the etchant layer of the specimen surface. Once the right conditions had been achieve a suitable technique was developed, which would bring out the prior austenite grain boundaries. Finally the mechanisms of the new etching technique were looked at in more detail using atomic force microscopy (AFM).

As the majority of this research is based on the prior austenite microstructure in high purity cast steels, it is important to get the etching technique right to minimise time taken to obtain a specimen which delineates the prior austenite grain boundaries and from which the grain size can be calculated.

4.2 Introduction

Etching is a controlled corrosion process resulting from electrolytic action between surfaces of different potential [112]. Previous investigations have used Sodium alkylate sulfonate (Teepol), however in those studies the steel was of a commercial composition and not the type used in this work which is laboratory cast low impurity steel.

The successful etching solution was produced by dissolving picric acid into 100ml of distilled water which was heated and maintained at 80°C, it is important to keep stirring the picric acid until the distilled water is completely saturated with picric, as this helps with the dissolution of the picric in water. However, the stirring also helps keep the solid dry picric crystals from forming on the sides of the glass beaker, as in its dry form, picric acid can be very explosive[9]. The second step is to add a few drops (4 drops) of hydrochloric (HCL) acid into the solution and then the wetting agents (1 gram). An important point to note is that the solution has been matured using 3 dummy specimens for 5 minutes each (15 minutes in total).

[9] The Material Safety Data Sheet Picric acid (MSDS) is in located in the Appendix B.

4.3 Sodium alkylate sulfonate (Teepol)

Using Teepol as a wetting agent, the results of all three different carbon contents are shown in Figure 4-1 from low carbon (0.08 wt. %), medium carbon (0.4 wt. %) and high carbon (0.8 wt. %) steels. All the specimens have been quenched in ice water from the given temperatures shown below the micrographs. All the starting microstructures were martensitic, it can be seen that it is difficult to distinguish between the prior austenite grain boundaries and the inner martensitic structure. Sodium alkylate sulfonate (Teepol) has proven to give poor results which do not outline the prior austenite grain boundaries; therefore making it extremely difficult to measure the prior austenite grain size for the specimen.

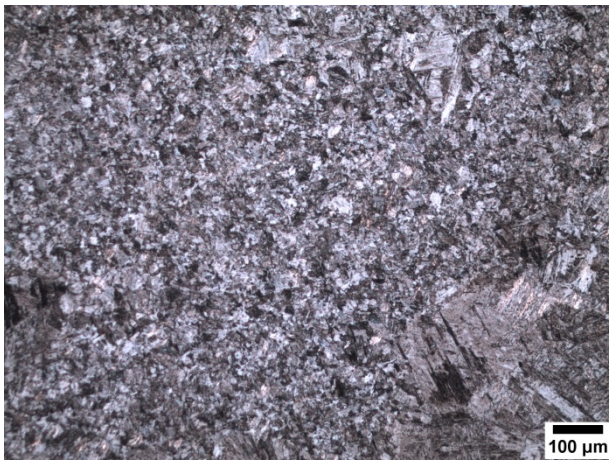

0.02 wt. % Nb 10x mag (1050°C)

0.02 wt. % Nb 10x mag (1150°C)

(a) Low Carbon (0.08 wt. %) Steel

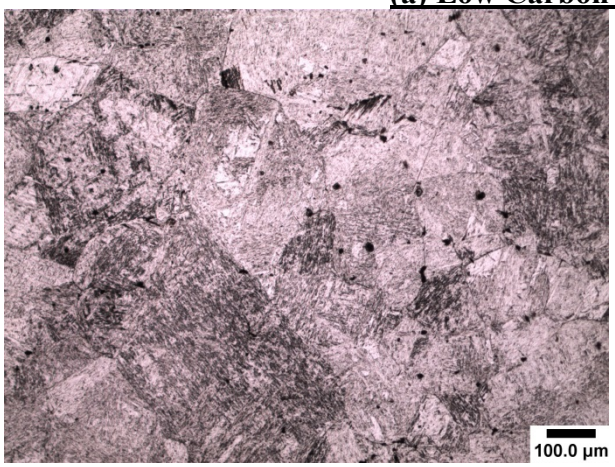

0.005 wt. % Nb (1100°C)

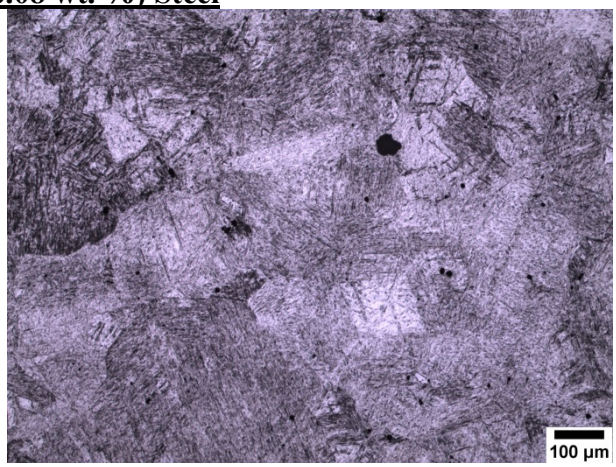

0.01 wt. % Nb (1150°C)

(b) Medium Carbon (0.4 wt. %) Steel

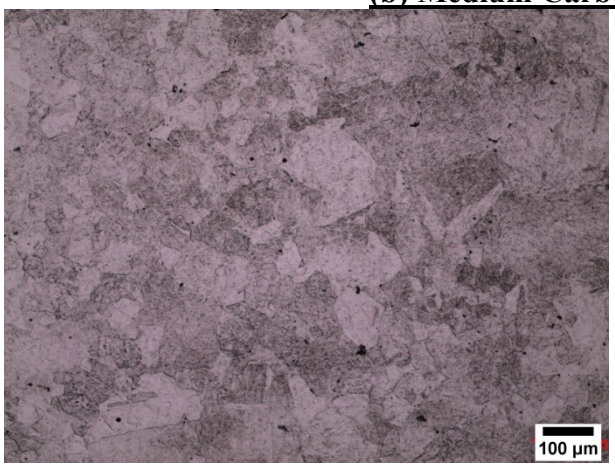

0.02 wt. % Nb 10x mag (1000°C)

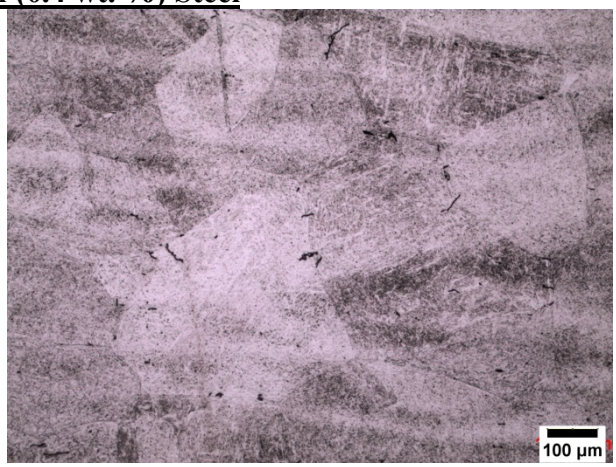

0.005 wt. % Nb 10x mag (1000°C)

(c) High Carbon (0.8 wt. %) Steel

Figure 4-1: Steel specimens etched with saturated picric acid with sodium alkylate sulfonate (Teepol) as a wetting agent

4.4 New Wetting Agent

The two new wetting agents used in this work have been proven to give excellent results and have proven to be the most effective wetting agents are **Sodium dodecyl sulfate (SDS)** and **Sodium dodecylbenzene sulfonate (SDBS),** the results of which can be seen in the micrographs presented in Figure 4-2. An important point to note is that Sodium dodecyl sulfate (SDS) is an effective wetting agent for low carbon steel (0.08 wt. %) and (0.2 wt. %) to medium carbon (0.4 wt. %) and (0.6 wt. %) steel specimens but this wetting agent did not show any prior austenite grain boundaries in the high carbon (0.8 wt. %) steel specimens. Sodium dodecylbenzene sulfonate (SDBS) was the most effective wetting agent for high carbon (0.8 wt. %) steel specimens as can be seen in Figure 4-2(c).

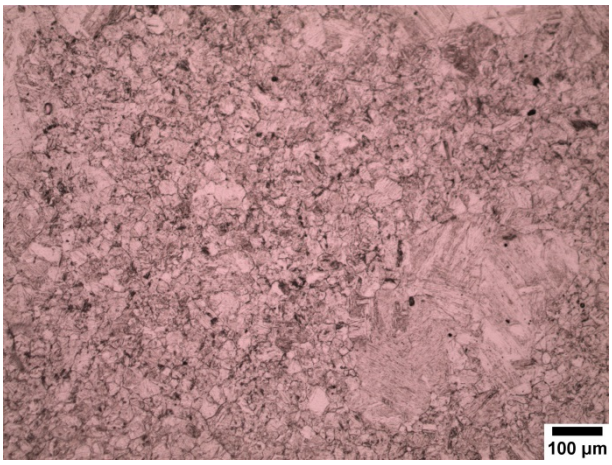

0.02 wt. % Nb 10x mag (1050°C)

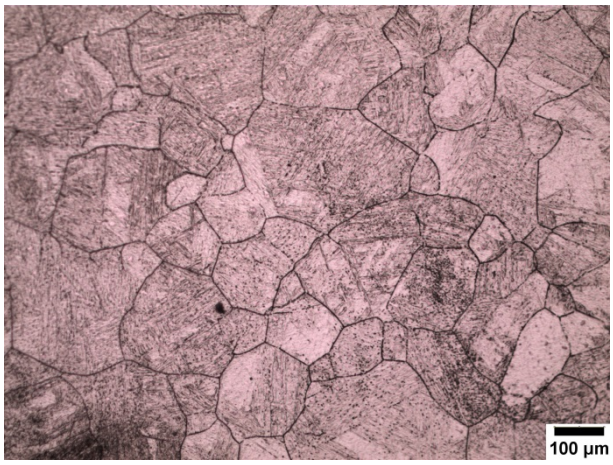

0.02 wt. % Nb 10x mag (1150°C)

(a) Low Carbon (0.08 wt. %) Steel

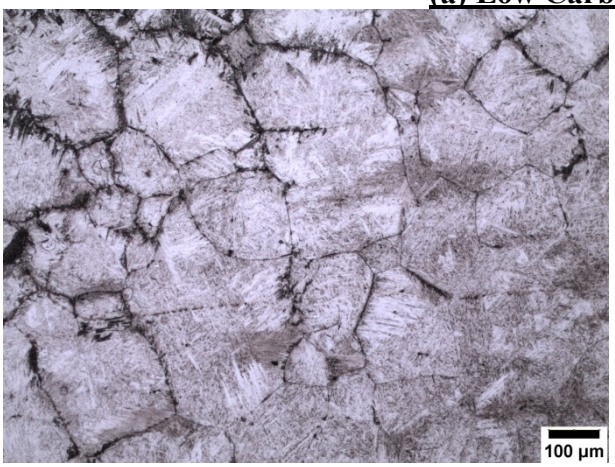

0.005 wt. % Nb (1100°C)

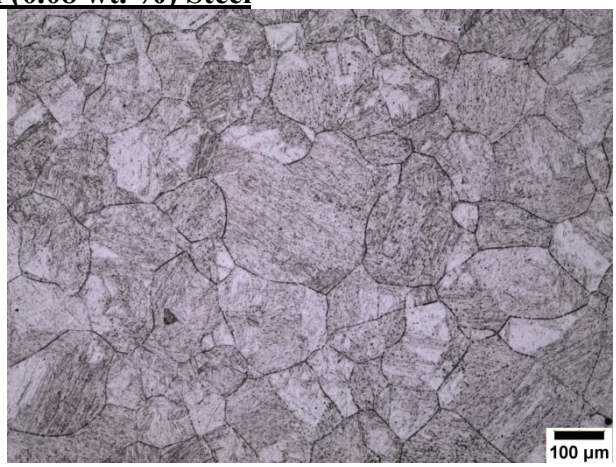

0.01 wt. % Nb (1150°C)

(b) Medium Carbon (0.4 wt. %) Steel

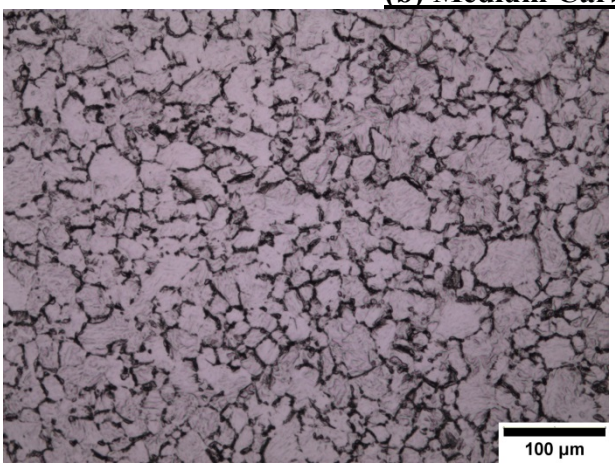

0.02 wt. % Nb 20x mag (1000°C)

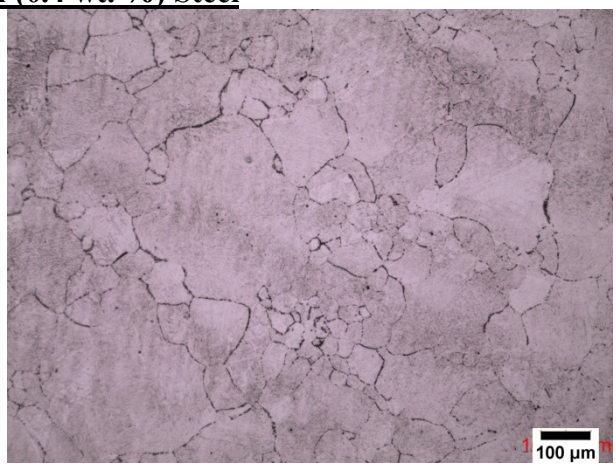

0.005 wt. % Nb 10x mag (1000°C)

(c) High Carbon (0.8 wt. %) Steel

Figure 4-2: Steel specimens etched with saturated picric acid with sodium dodecyl sulfate (SDS) as a wetting agent used for (a, and b) and sodium dodecylbenzene sulfonate for (c).

It is important to note that when etching the specimen submerged in the saturated picric solution it should be not be moved as this affects the etching layer[10] that forms on the specimen surface causing one size to be thicker and the other to be thinner. In Figure 4-3 (a) the black outline represents the area where the etching layer was thin and the red shaded area is where the etching layer would be thicker; as the grain boundaries are much more clearly defined. Figure 4-3 (b) shows the light optical micrograph of how the delineation of the prior austenite grain boundaries should be when the etching layer is evenly on the surface.

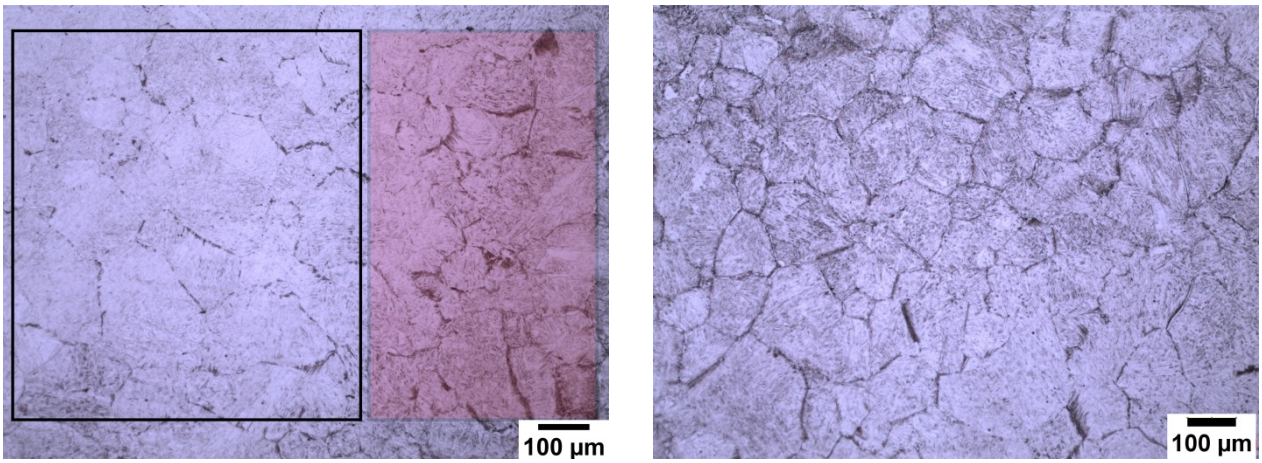

(a) (b)

Figure 4-3: Etching layer effect and etching time.

Prior to looking at the following results, it is important to note that for every time interval a fresh solution was made and the same specimen had been grinded and polished again to keep the experimental work as accurate as possible.

Figure 4-4 illustrates the effect of the etchant layer on the specimen with increasing time, submerged under saturated picric acid. It can be seen in the first row (Etching layer) that the etchant layer gets thicker with increasing time, second row (LOM, light optical microscope) shows the micrographs of the microstructure obtained for the amount of time the specimen was submerged in to the solution.

As shown in the micrographs when submerged for 30 seconds, the martensitic structure is revealed but no prior austenite grain boundaries can be seen. As the submerged time increases to 120 seconds the austenite grain boundaries start to be outlined, however the image is still not good enough to give reliable results. The best results have been obtained by submerging the specimen into the solution for 600 seconds, where a thick black etchant layer is formed on the steel surface; after removing

[10] As the steel specimen is submerged into the solution, the etchant starts to react with the surface of the specimen, which results in the formation of a protective etchant layer on the surface. This is what is referred to as the etching laying in this work. Etching is a controlled corrosion process resulting from electrolytic action between surfaces of different potential.

the thick etchant layer from the surface, somewhat clear prior austenite grain boundaries can be observed.

The third row (AFM, atomic force microscopy) indicated the topography of the surface at each time interval. The topographies have been taken from the bulk structure and the grain boundaries after etching from random locations. The results from the atomic force microscopy will be presented in the next section in more detail; however the topography image for 30 seconds can be seen to give a rough structure where no indication of prior austenite grain boundaries can be found. A thin groove of the prior austenite grain boundaries can be seen at 120 seconds in the AFM image of the topography (dark orange line in the middle). The best results are obtained at 600 seconds showing a deep grooved prior austenite grain boundary which is consistent with the dark prior austenite grain boundaries shown by the light micrograph images.

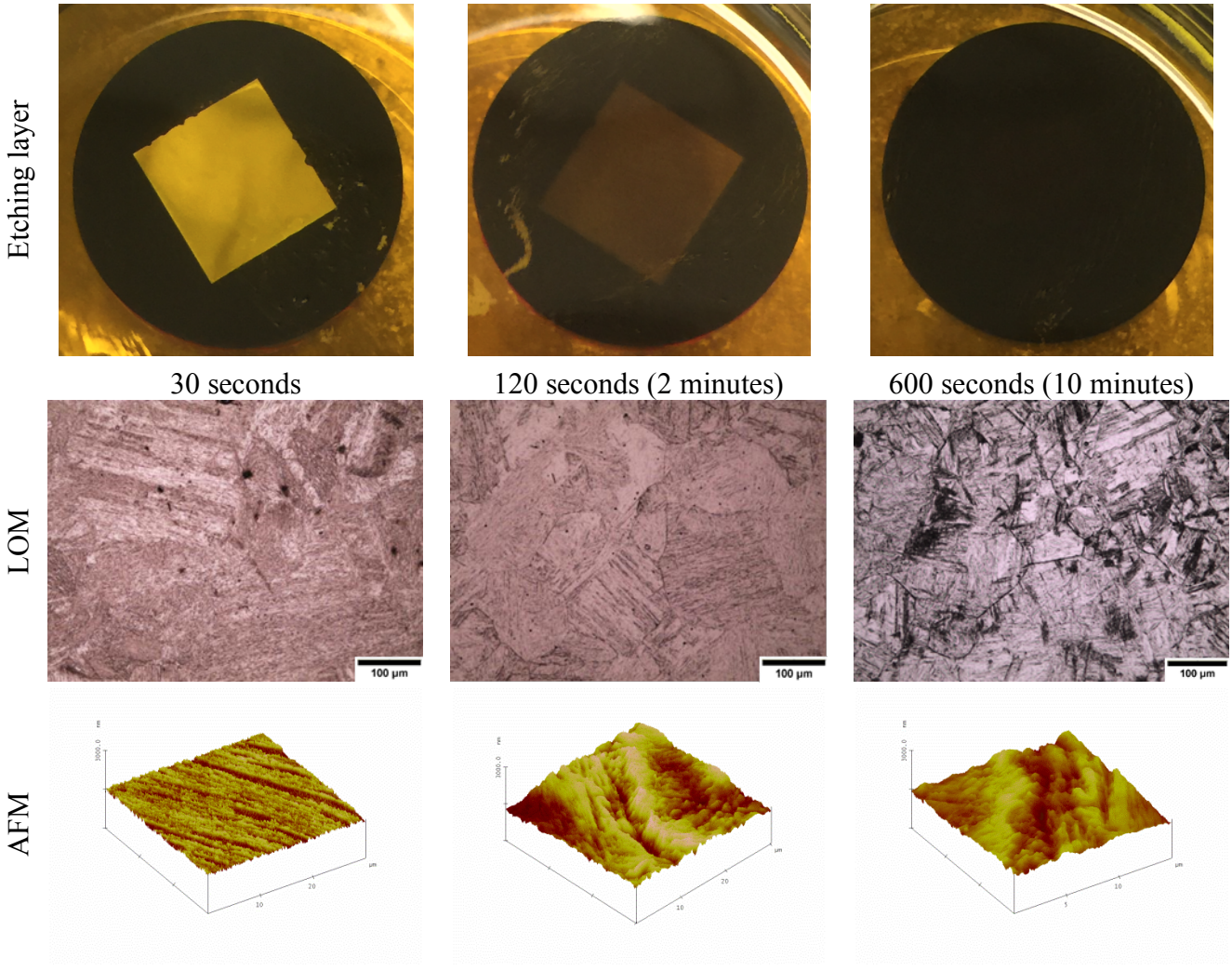

Figure 4-4: The effect of submerging specimen for different durations in saturated picric acid.

The results shown above give a clear indication that the formation of a dark thick etchant layer on the surface of the specimen is beneficial and can be part of the etching mechanism.

4.5 Atomic Force Microscopy (AFM)

Atomic force microscopy was used to obtain the topography of the surface of the steel specimen which has been etched using different wetting agents and at different times which in turn gives a thicker etchant layer. This is to understand the mechanisms of the etching process during the time taken to form an etchant layer and the effect of the thickness of the layer.

Figure 4-5 shows the light optical and atomic force micrographs of the surface roughness for the specimen etched as a function of the time the etchant solution has been in use. The graph illustrates data using a pH meter (Omega PHH-37) to measure the acidity of the etchant solution. The pH results indicate that the acidity of the etchant solution decreases with time when the specimens are being etched in the solution. The initial pH value of the etchant solution starts at 1.22 pH and this increases to 1.27 pH after the first specimen is submerged into the solution for 5 minutes. As the second specimen is submerged for an additional 5 minutes the pH of the solution further increases to 1.31 ph. Overall the pH of the solution increases to 1.36 for a total etching time of 19 minutes.

An interesting point to note is that the roughness of the specimen surface after being etched also decreases; comparing the light optical micrographs and the atomic force micrographs in Figure 4-5. The first specimen etched for 5 minutes has a mean surface roughness of 117.61 nm indicating that the etchant had attacked the martensitic inner structure and the prior austenite grain boundaries. This is confirmed by the light optical microscope images showing the inner microstructure of the prior austenite grains being etched. As a fresh identical specimen is held for an additional 5 minutes in the same solution the mean surface roughness decreases to 91.94 nm giving better results. However the best results were obtained when the solution was in use for a total of 15 minutes (matured solution), the mean surface roughness was 58.45 nm and a clear distinction can be made of the inner structure and the prior austenite grain boundaries.

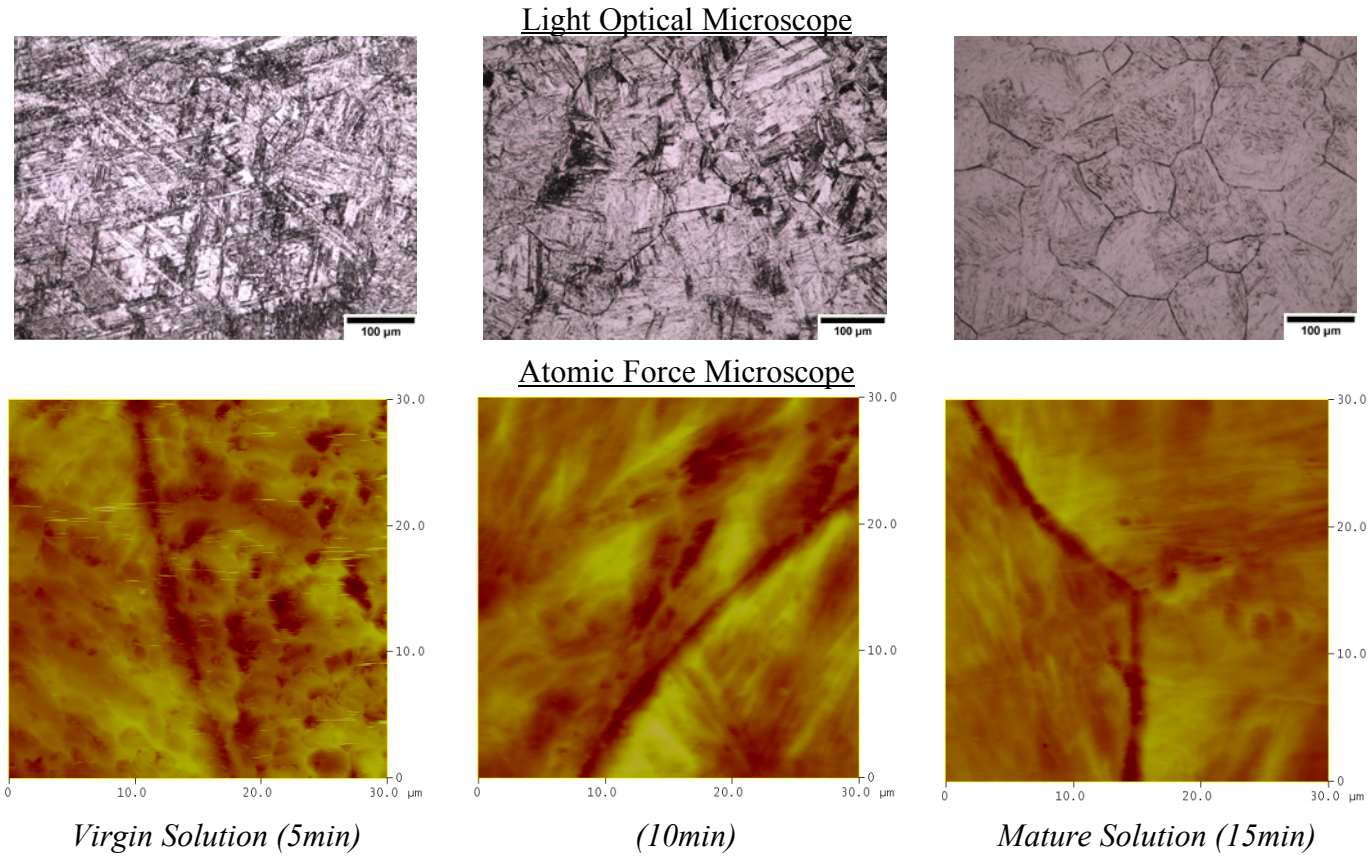

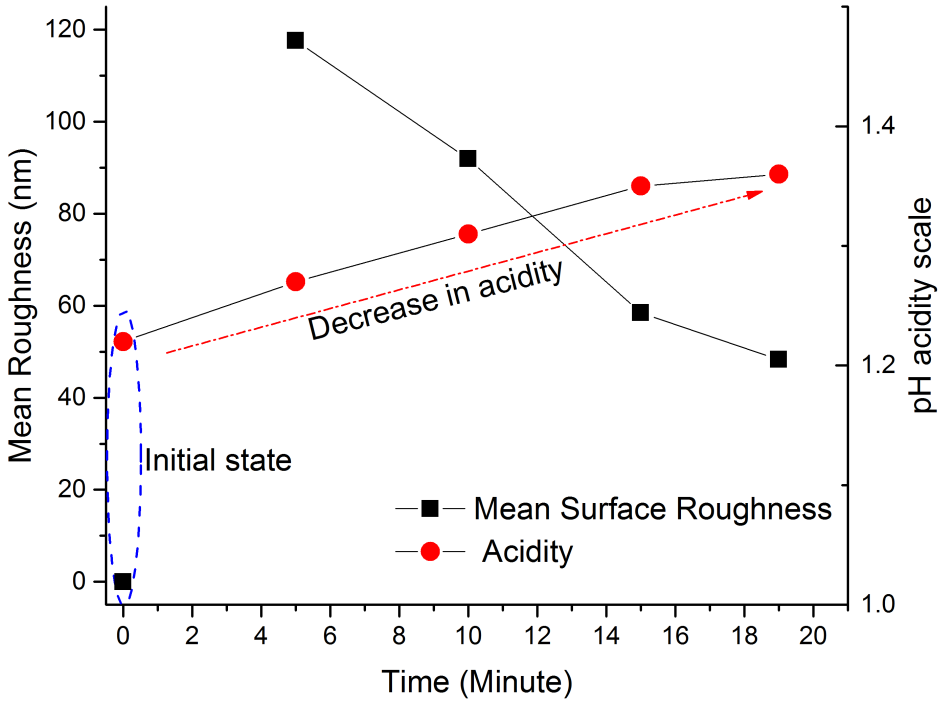

Figure 4-5: Specimen surface roughness versus time etchant solution in use and pH change.

Figure 4-6 (a) illustrates a surface profile analysis for a 30µm^2 area of the steel surface post etching, showing the martensitic inner structure (MIS) and the prior austenite grain boundaries (PAGB). It should be noted that the (PAGB) grooves are etched deeper than that of the (MIS); (b) shows the image of a triple junction point where three prior austenite grain boundaries meet, this image is obtained from the atomic force microscopy and corresponds to (a) clearly showing the MIS region and the PAGBs which are darker.

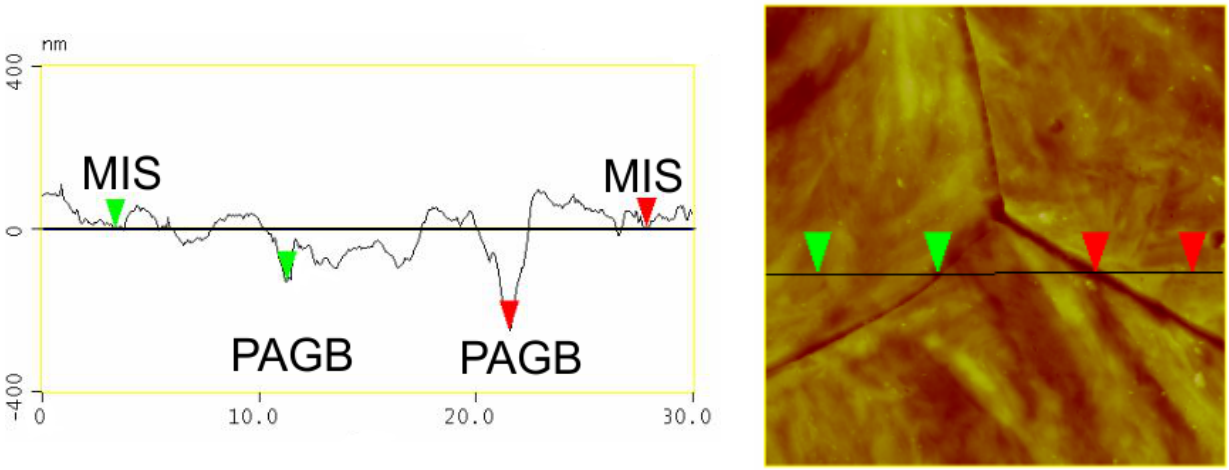

(a) (b)

Figure 4-6: Surface analysis shown in (a) and the two-dimensional image shown in (b).

Figure 4-7 illustrates a 3-dimensional image at a higher magnification analysing an area of 15µm^2 of the steel surface post etching and the prior austenite grain boundary groove can be seen in the centre and the martensitic inner structure on either side.

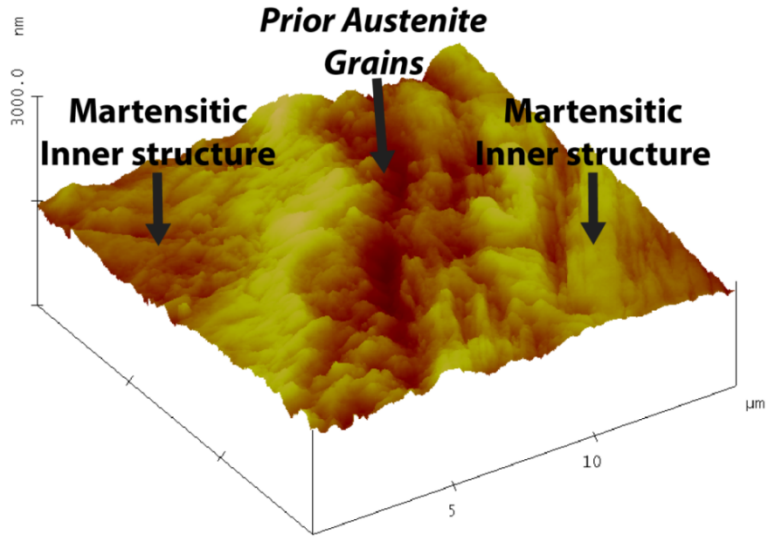

Figure 4-7: Etched surface image obtained by atomic force microscopy, showing the martensitic inner structure and the prior austenite grain boundaries.

The effect of using this etching technique is shown in more detail in Figure 4-8 (a) which shows the surface profile of the inner microstructure being close to the origin indicating that the etching technique used does not encourage the etching of the martensitic inner structure (MIS) but accelerates the etching of prior austenite grain boundary (PAGB) as shown in Figure 4-9 (a).

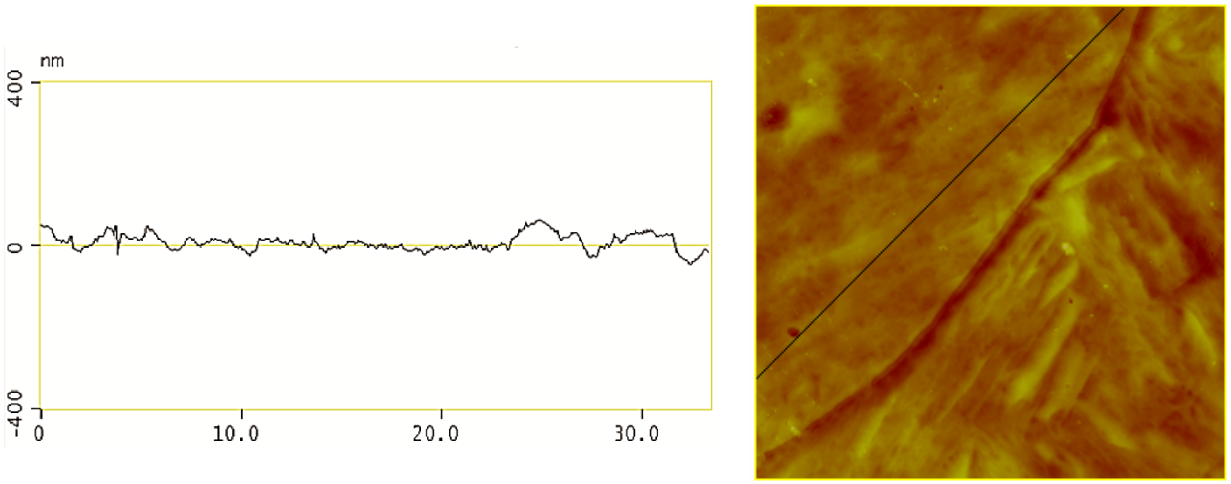

(a) (b)

Figure 4-8: Surface analysis of martensitic inner structure shown in (a) and the two-dimensional image shown in (b).

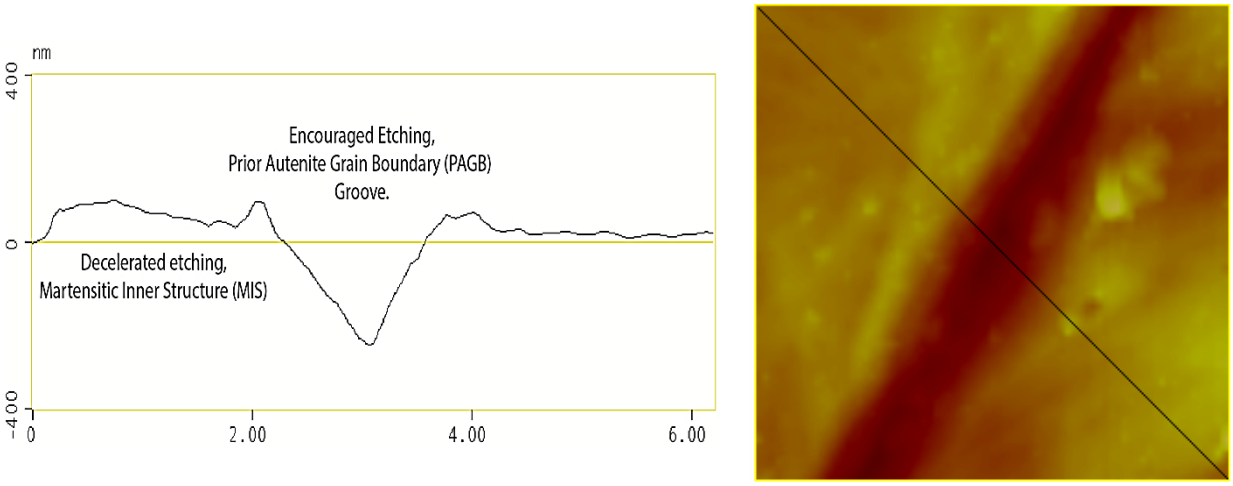

(a) (b)

Figure 4-9: Surface analysis of the prior austenite grain boundary shown in (a) and the two-dimensional image shown in (b).

4.6 Discussion of the Technique

Several different methods and techniques exist to reveal the prior austenite grain boundaries [112, 117, 132, 124, 125, 122, 123]. There are many influencing factors when it comes to etching prior austenite grain boundaries; such as wetting agent, hydrochloric concentration, solution concentration, temperature and the swabbing technique. The aqueous solution used is saturated with picric acid in distilled water as it was first used in 1955 and since then has become widely used in the delineation of prior austenite grain boundaries.

4.6.1. Effect of wetting agent

Wetting agents also known as surfactants or surface – active agents such as Teepol (sodium alkylsulfonate) are added in small amounts to the solution to change the surface energy of a liquid or solid surface and influence interfacial interactions (modifying etch behaviour). [119]. Nelson, [120] has reported that the concentration of the wetting agents give different responses to the etching. Voort, [119] has also reported the importance of wetting agents in the revealing of prior austenite grain boundaries. Many different wetting agents have been used by previous researchers to reveal the prior austenite grain boundaries and have shown to be effective with many different steel compositions [133, 134, 122, 117, 132] and different heat treatment conditions, e.g. as quenched, tempered or deformed. Sodium alkylate sulfonate (Teepol) is the most widely used wetting agent in saturated picric acid solution for the delineation of prior austenite grain boundaries.

Initially, sodium alkylate sulfonate (Teepol) was used as a wetting agent to etch the prior austenite grain boundaries from an initial martensitic structure quenched from 1050°C which can be seen in Figure 4-10; this wetting agent however proved to be unsatisfactory for high purity steels which were used in this work. As it can be seen from the micrograph, a few austenite grain boundaries were revealed (white arrows) but the grain size was difficult to determine as a lot of the internal martensitic structure was also revealed. This wetting agent was also proven to be insignificant in low carbon (0.08 wt. %) and high carbon (0.8 wt. %) steels as shown in Figure 4-1.

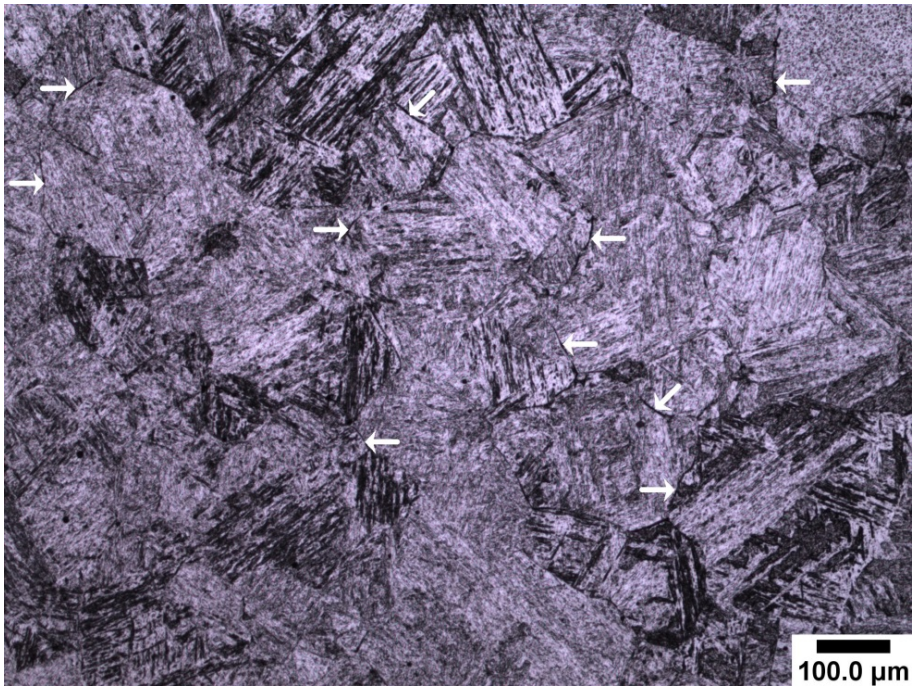

Figure 4-10: Optical light microscope micrograph showing prior austenite grain boundaries and internal structure, etched in saturated picric acid with Sodium alkylate sulfonate (teepol) (0.4 wt. %) carbon steel.

The new wetting agent used in this work to etch low carbon (0.08 wt. %) and (0.2 wt. %) all the way to medium carbon of (0.4 wt. %) and (0.6 wt. %) steels is sodium dodecyl sulfate (SDS). Sodium dodecylbenzene sulfonate (SDBS) has been proven to give significantly good results for high carbon (0.8 wt. %) steel as shown in Figure 4-2; as the etching of the martensitic inner structure (MIS) was retarded and etching of the prior austenite grain boundaries was promoted. A side by side comparison is shown for low carbon steel quenched in ice water from 1150°C in Figure 4-11 where the effect of the 2 wetting agents can clearly be seen. It is important to note that sodium dodecylbenzene sulfonate (SDBS) did not work for any other carbon steel concentrations in this work apart from high carbon (0.8 wt. %).

Wetting Agent

sodium alkylate sulfonate (Teepol) sodium dodecyl sulfate (SDS)

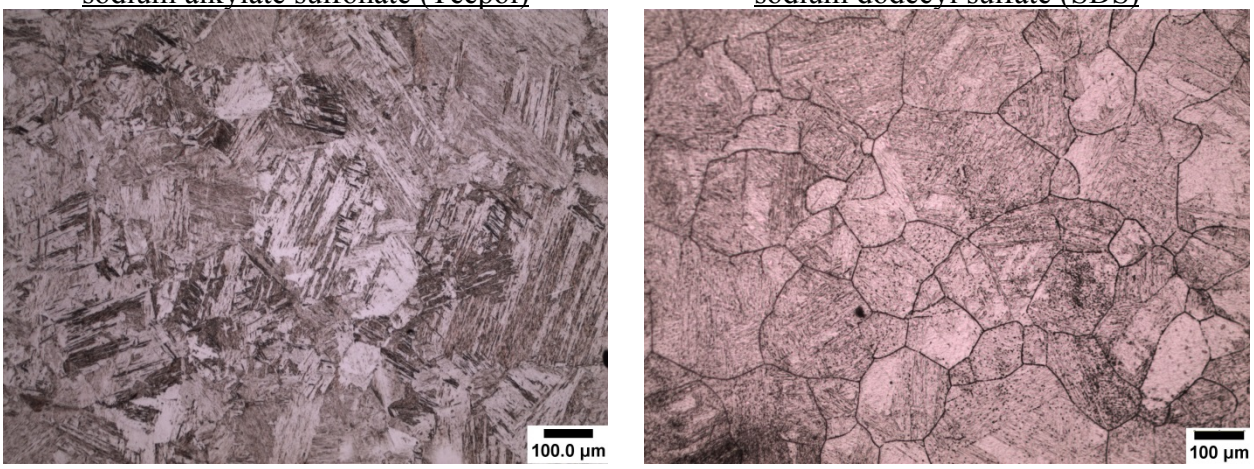

(a) Martensitic Inner structure revealed (b) Prior austenite grain boundaries revealed

Figure 4-11: Illustrates the effect of the wetting agent on low carbon (0.08 wt. %) steel with 0.02 wt. % Nb at 10x mag (1150°C).

It is known that the modification of the surface tension is achieved by adding surfactants to the etchant solution [119] and increasing the temperature, this further reduces the surface tension between the liquid etchant and specimen surface interface [135, 136]. The reduced surface tension energy by sodium dodecyl sulfate (SDS) with the temperature at 80 - 90°C provides good adhesion properties for a thick etchant layer to be formed on the steel specimen.

4.6.2. Effect of pH concentration

Previously done research has either investigated the chemistry of the etching solution [117, 122], or the temperature and time it has taken for the specimen to be etched revealing the prior austenite grain boundaries [132]. It is also known that the time needed for effective etching to occur could decrease with an increase in the temperature of the etching solution; the stability of the etching solution also changes with time due to the reactions occurring during etching [137]. The change in the concentration can be seen from the changes in the pH of the solution as the initial pH value prior to use was 1.22 which is acidic but becomes less acidic with use. It is known that etching of the grain boundaries is a controlled corrosive process between surface areas of different potential [136] and that an acidic solution increases the corrosion rate of steel. Therefore it is no surprise that the when the specimen is submerged in a virgin etching solution that the etchant attacks the whole microstructure as illustrated in Figure 4-5. The decrease in acidity of the etchant solution can be attributed to the decrease in the hydrogen ions during the reduction reaction. According to a simplified corrosion

reaction of steel in water, shown in Equation (4-1) - Equation (4-5), where *ads* represents *adsorbed* and implies that the reaction is occurring at the solid/liquid interface in a solid phase.

$$Fe + H_2O \rightarrow Fe(H_2O)_{(ads)} \quad (4\text{-}1)$$

$$Fe(H_2O)_{(ads)} \rightarrow Fe(OH^-)_{(ads)} + H^+ \quad (4\text{-}2)$$

$$Fe(OH^-)_{(ads)} \rightarrow Fe(OH)_{(ads)} + e^- \quad (4\text{-}3)$$

$$Fe(OH)_{(ads)} \rightarrow Fe(OH)^+ + e^- \quad (4\text{-}4)$$

$$Fe(OH)^+ + H^+ \rightarrow Fe^{2+} + H_2O \quad (4\text{-}5)$$

The five equations given above lead directly the anodic reaction shown by Equation (4-6).

$$Fe \rightarrow Fe^{2+} + 2e^- \quad (4\text{-}6)$$

The steel undergoes corrosion in acidic solutions which have a higher concentration of hydrogen (H^+) ions, the electrons that have been generated in Equation (4-6) combine with the Hydrogen (H^+) ions in a reduction reaction giving Equation (4-7) resulting in hydrogen gas (H_2). This in turn explains the decrease in acidity of the etching solution with use.

$$2H^+ + 2e^- \rightarrow H_2 \quad (4\text{-}7)$$

4.6.3. Effect of etchant layer

Barraclough [117] has indicated that removing of the etchant layer by swabbing with cotton during the etching process resulted in better outline of the prior austenite grain boundaries. The swabbing method used by Barraclough implies that the etching solution reacts with a fresh surface of the specimen and a thick etchant layer does not form on the specimen. This technique of continuously swabbing has been unsuccessful in this work. Shown in Figure 4-12 (a) and (b) is the identical specimen (a) has been swabbing continuously so that fresh etchant reacts with the surface, (b) has been swabbed after 4 minutes when a thick etchant layer had formed on the specimen. In this work the etchant layer on the specimen was kept still to form an even thick etchant layer on the

specimen; it has been shown in Figure 4-3 that moving the specimen can lead to an uneven etchant layer which does not give a uniform delineation of the prior austenite grain boundaries.

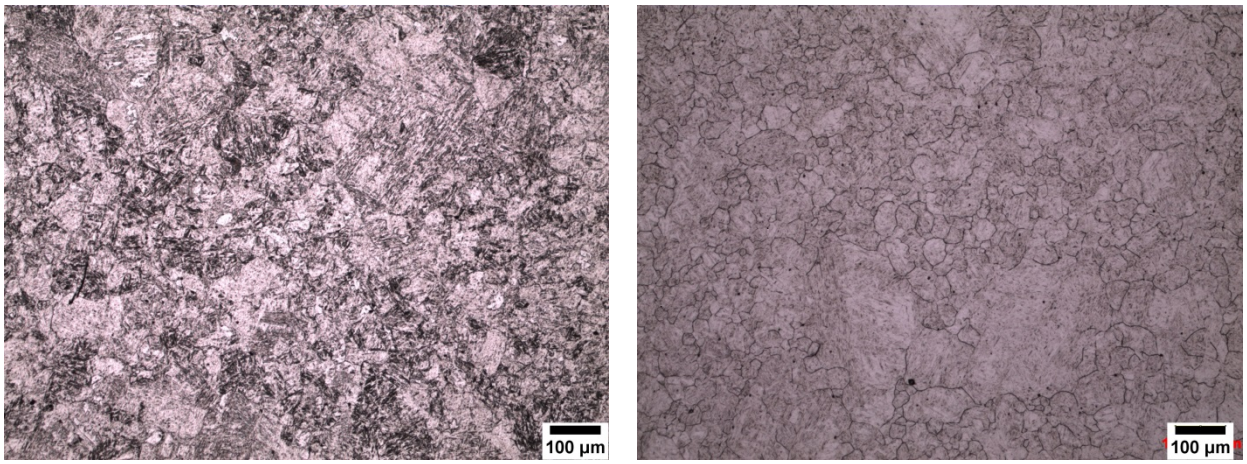

(a) (b)

Figure 4-12: (a) has been continuously swabbed during the etching process, and (b) has been swabbed once after the formation of the etchant layer.

4.6.4. Novel etching method

Picric acid mixed with distilled water results in a corrosive solution, therefore when the steel specimen is immersed in a corrosive solution the grain boundaries are highly susceptible to corrode.

It is known that the atoms of the metal surface are not homogenous. Some atoms are highly coordinated, as in close packed planes; some are arranged at the grain boundaries and others may be foreign solute atoms such as e.g. (Nb, P, Sn, Sb and As). These elements are known to segregate to the prior austenite grain [113, 114] and this results in a higher energy at the grain boundaries whereas the atoms lying within a relatively perfect close-packed structure have a lower energy [138]. Therefore the grain boundaries are more liable to corrosive attacks then the inner microstructure.

Figure 4-13 illustrates the surface of the steel after the specimen has developed a thick etching layer after etching for 2 – 4 minutes. The prior austenite grain boundary (PAGB) grooves can be seen where the selective grain boundary corrosion occurs and retarding the martensitic inner structure. As explained earlier this is due to the difference in the chemical potential of the martensitic inner structure (MIS) and the prior austenite grain boundaries (PAGB). The mechanisms of the etching process can be easily understood on the illustration. As the steel specimen is submerged into the solution the etchant starts to react with the surface of the specimen which results in the

formation of a protective etchant layer on the surface. The protective layer is a result of the corrosive reaction taking on the surface of the specimen. During the etching process the atoms are transferred from the anodic surface to the etching solution. This results in the formation of an insoluble metal compound which forms the layer [136]. The formation of this protective etchant layer on the surface is considered to be of vital importance in the etching process as it helps stop the fresh etching solution from reacting with the specimen surface, it further accelerates the anodic process [139] and allows the reacting etchant to keep reacting with the prior austenite grains.

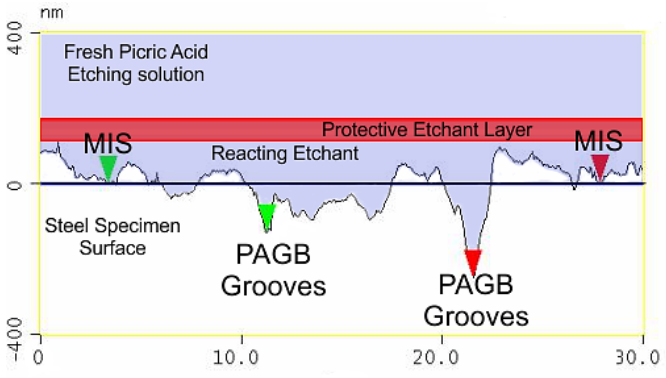

Figure 4-13: Illustration of the successful etching mechanism using atomic force microscope (AFM).

The unsuccessful etching mechanism can now be analysed in Figure 4-14 in which the specimen is swabbed with cotton to remove the etchant layer. This results in the picric acid attacking both the martensitic inner structure and the prior austenite grain boundaries. The importance of the etching layer during the etching process and its benefits have been explained earlier.

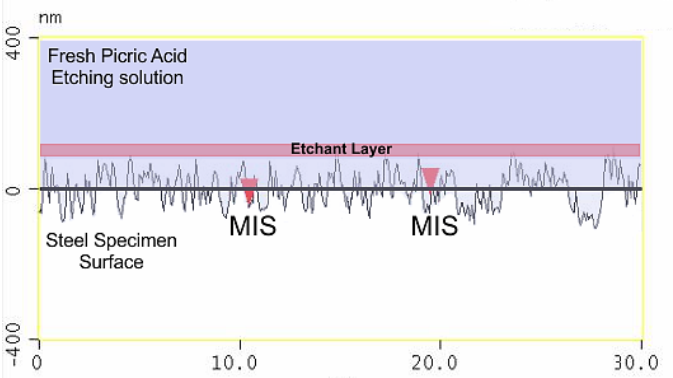

Figure 4-14: Illustration of the unsuccessful etching mechanism using atomic force microscopy (AFM).

Other influences which are important to consider during etching are the concentration of etchant solution, temperature, HCL concentration and the wetting agent used. The successful etching mechanism found in this work for high purity steel for low (0.08 wt. %) to high (0.8 wt. %) carbon steel worked very well to reveal the prior austenite grain boundary and restrict the etching of the martensitic inner structure.

In summary the successful etching solution was produced by dissolving picric acid into 100ml of distilled water which was heated and maintained at 80°C, until the distilled water is completely saturated with picric. The second step is to add 4 drops of hydrochloric (HCL) acid into the solution and then the wetting agents 1 gram of SDS (for every carbon composition from 0.08 wt. % C to 0.6 wt. % C) and 1 gram of SDBS for high carbon (0.8 wt. %). An important point to note is that the solution has been matured using 3 dummy specimens for 15 minutes prior to use.

5. Characterisation of As Received Material

5.1 Introduction

The as received microstructure of the initial material will be investigated in this chapter. The material had been characterized for all three carbon contents, 0.08 wt. %, 0.4 wt. % and 0.8 wt. % without niobium, only looking at the effect of carbon initially. The remaining compositions with varying niobium given in (Table 3-2 0.2 wt. % carbon and Table 3-4 0.6 wt. % carbon) have similar microstructure and have not been looked at in more detail in this study. The material examined in this chapter was received in the as rolled condition, it has been rough rolled at elevated temperatures of around 1100°C and air cooled.

5.2 Microstructure Characterization

Quantitative metallography analysis of the three carbon alloys in the as received condition includes area fractions of pearlite and the ferrite phase, and ferrite grain size. The specimens have been etched with 2% Nital.

It can be seen in Figure 5-1 (a, b, c, and d) that all alloys exhibited a ferrite-pearlite microstructure. The addition of niobium in 0.08 wt. % carbon does not make a noticeable difference in increasing the volume fraction of pearlite which is represented by the black regions and the ferrite is represented by the white regions as seen in Figure 5-1(a, b, c, d). The area fraction of pearlite has been analysed using image analysis software (OmniMet) from an average of 10 light micrograph images per composition.

The microstructure of the plan C-Mn and niobium microalloyed steels as illustrated in Figure 5-1 have predominantly blocky and polygonal ferrite morphology; very small islands of pearlites were also observed uniformly throughout the microstructure. The addition of Nb can be seen to have resulted in a decrease in the ferrite grain. The ferrite grain size was measured using the ASTM standard E 112 the results are given in Table 5-1.

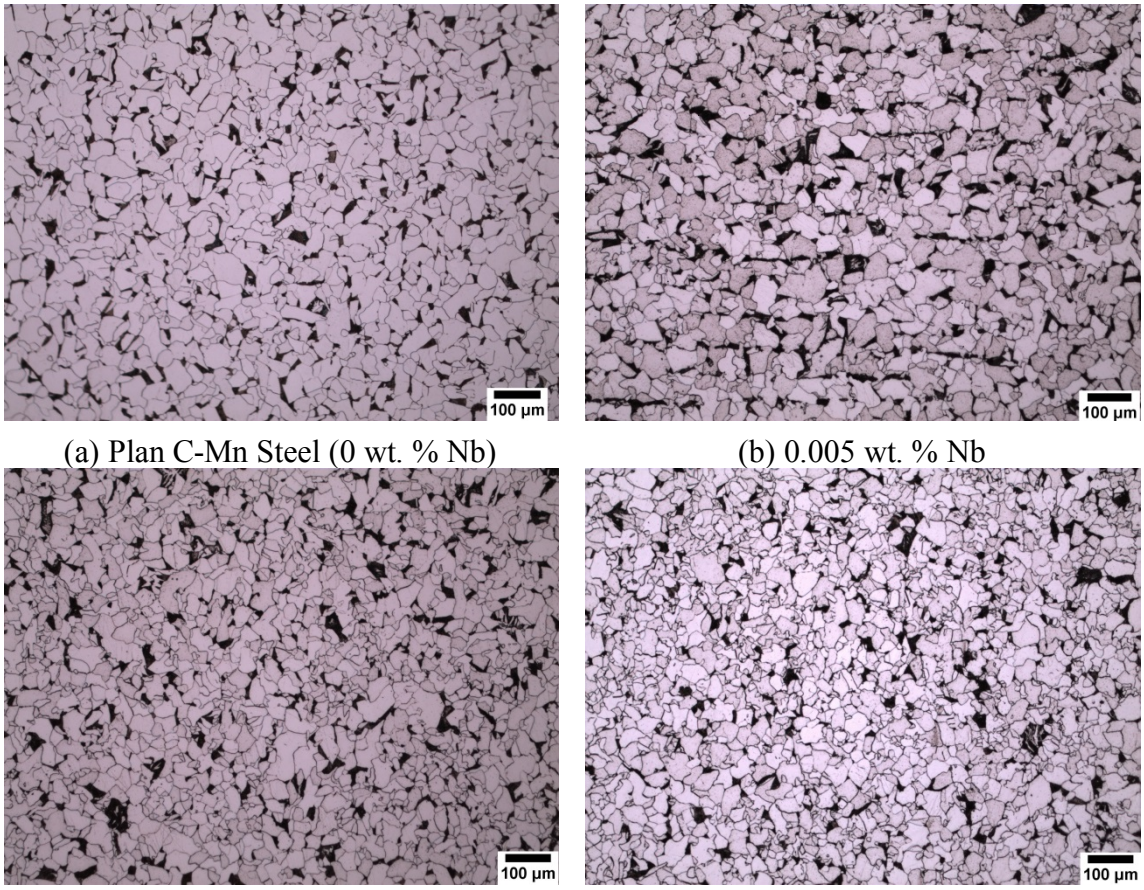

(a) Plan C-Mn Steel (0 wt. % Nb) (b) 0.005 wt. % Nb

(c) 0.01 wt. % Nb (d) 0.02 wt. % Nb

Figure 5-1: Light optical micrograph images of the as received 0.08 wt. % carbon steel. The black regions represent the pearlite region and white regions represent the ferrite phase. (Etched with 2% Nital).

Table 5-1: Ferrite grain size for 0.08 wt. % carbon steel

	Ferrite Grain Size, (µm)			
Temperature (°C)	Plain C-Mn	0.005 wt. % Nb	0.01 wt. % Nb	0.02 wt. % Nb
950	28.1 ± 1.6	26.7 ± 1.6	22.8 ± 1.3	20 ± 1.1

5.2.1.1. Volume fraction of pearlite

The volume fraction increase of pearlite for all three carbon contents with the respective niobium additions can be seen in Table 5-2. It can be seen that there is a slight increase in the volume fraction of pearlite for 0.08 and 0.4 wt. % carbon with increasing niobium content whereas for 0.8 wt. % carbon there is one major constituent which is pearlite. The micrographs for 0.08 wt. % carbon steel are shown in Figure 5-1.

Table 5-2: Volume fraction of pearlite, %, as a function of niobium content.

	Volume Fraction of Pearlite, %			
Carbon Content	Plain C-Mn	0.005 wt. % Nb	0.01 wt. % Nb	0.02 wt. % Nb
0.08	8.6 %	10.1 %	10.4 %	11.1 %
0.4	61.7 %	66.6 %	69.8 %	72.9 %
0.8	100 %	100 %	100 %	100 %

5.2.1.2. Scanning Electron Microscopy

A more detailed investigation of the C-Mn steel (without niobium) was done by using the scanning electron microscopic (SEM) technique because of the higher magnification which is not possible by the light optical microscope. The images in this chapter were taken using the FEI Inspect F operating between 10kV to 20kV and using a spot size ranging between 2 to 3. The micrographs shown in Figure 5-2(a) represents the pro-eutectoid ferrite and the pearlite structure. Figure 5-2(b) illustrates the pearlite structure at a higher magnification. In this micrograph the different ferrite and cementite phases can be observed separately. The SEM micrographs for 0.4 and 0.8 wt. carbon indicated similar results with the 0.8 wt. % carbon showing a whole pearlite structure.

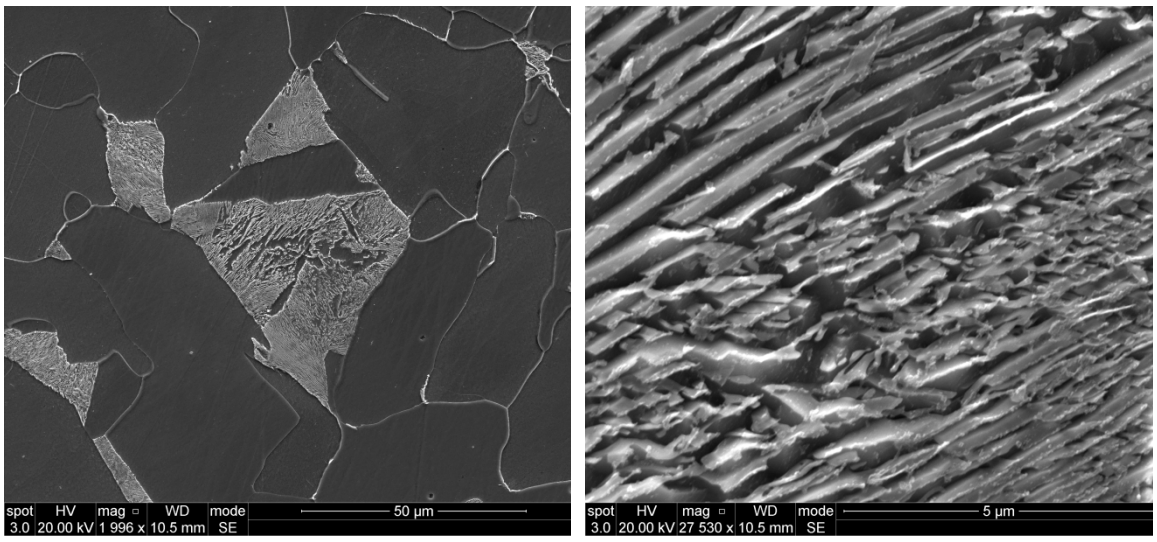

(a) Ferrite (Dark) and Pearlite (Light) (b) Pearlite morphology

Figure 5-2: Scanning Electron Micrographs images of as received 0.08 wt. % low carbon steel without niobium addition. Image (a) shows the ferrite (dark region) and pearlite (light region). (Etched with 2% Nital).

5.2.1.3. Hardness Testing

Two different loads were used for the micro (25g) and macro (1000g) hardness testing has been performed using a Vickers indenter with a square pyramid shape with a dewll time of 15 seconds the settings used for the hardness test are described in detail in (Experimental Work Chapter 3). A total of 20 indentations were made after which an average value was taken. Vickers hardness was performed to understand the effect of niobium micro alloy additions on the ferrite, pearlite and average hardness of the as received material microstructure. The error in the hardness values is calculated using the 95 % confidence limit mentioned in section 3.10.

The data for micro hardness for the three microalloyed steels can be seen in Table 5-3 that the variation in the micro hardness of the individual phases with increasing niobium content does not result in much of a hardness increase or decrease hence the micro hardness stays relatively constant for the 0.08 wt. % carbon steel. The hardness of the pearlite is indicated to be higher than the ferrite phase and is in the range of 248.5 ± 6.1 HV to 263.3 ± 3.5 HV with increasing niobium content showing no real change in hardness. The hardness of the ferrite phase is in the range of 121 ± 5.3 HV to 134.5 ± 7.9 HV once again showing not trend with increasing niobium content

For 0.4 wt. % carbon steel there is a variation in the micro hardness of the individual phases with increasing niobium content and that is that niobium does increase the hardness. The hardness of the pearlite is indicated to be higher than the ferrite phase and is in the range of 234.5 ± 13.16 HV to 250.33 ± 5.6 HV with increasing niobium content. The hardness of the ferrite phase is in the range of 141 ± 10.6 HV to 179.5 ± 13.4 HV.

As for the highest carbon content of 0.8 wt. % the data indicates that the hardness value without niobium is 288 ± 14 HV; the hardness keeps increasing with the addition of niobium from 0.005 wt. % (256.8 ± 28 HV), 0.01 wt. % (303.5 ± 25.25 HV) and 0.02 wt. % (310 ± 14.3 HV).

Table 5-3: Micro hardness for Ferrite and Pearlite.

		Micro Hardness, HV_{25g}			
		Plain C-Mn	0.005 wt. % Nb	0.01 wt. % Nb	0.02 wt. % Nb
0.08 Carbon	Ferrite	134.5 ± 7.9	121 ± 5.3	130.5 ± 6.4	128.5 ± 7.9
	Pearlite	248.5 ± 6.1	263.5 ± 3.5	257 ± 4.2	254 ± 4.38
0.4 Carbon	Ferrite	141 ± 10.6	158.5 ± 13.2	164 ± 2.2	179 ± 13.4
	Pearlite	234.5 ± 13.2	221 ± 10.5	241.5 ± 9.7	250.3 ± 5.6
0.8 Carbon	Pearlite	288 ± 14	256.8 ± 28	303.5 ± 25.3	310 ± 14.3

The macro hardness results are given in Table 5-4, it can be observed that there is a general trend of increasing hardness when the niobium content is increased in low carbon steel. The average hardness value without niobium is 136.8 ± 4.2 HV; the hardness keeps increasing with the addition of niobium from 0.005 wt. % (145.7 ± 4.8 HV), 0.01 wt. % (147.4 ± 5.69 HV) and 0.02 wt. % (150.4 ± 4.8 HV).

The results for 0.4 wt. % carbon also give a similar trend of increasing hardness when the niobium content is increased in medium carbon steel. The average hardness value without niobium is 188.5 ± 0.9 HV; the hardness keeps increasing with the addition of niobium from 0.005 wt. % (195.25 ± 2.24 HV), 0.01 wt. % (211.6 ± 1.87 HV) and 0.02 wt. % (213.75 ± 1.13 HV).

Finally for 0.8 wt. % carbon steel, hardness value without niobium is 274.6 ± 3.7 HV; the hardness keeps increasing with the addition of niobium from 0.005 wt. % (281.6 ± 10.6 HV), 0.01 wt. % (272.8 ± 9.73 HV) and 0.02 wt. % (291 ± 5.33 HV)

Table 5-4: Macro hardness for bulk material.

	Marco Hardness, HV_{1Kg}			
Carbon Content	Plain C-Mn	0.005 wt. % Nb	0.01 wt. % Nb	0.02 wt. % Nb
0.08	136.8 ± 4.2	145.7 ± 4.8	147.4 ± 5.7	150.4 ± 4.8
0.4	188.5 ± 1	195.25 ± 2.2	211.6 ± 1.9	213.8 ± 1.1
0.8	274.6 ± 3.7	281.6 ± 10.6	272.8 ± 9.7	291 ± 5.3

5.3 Short discussion on the effect of Nb on the Characterisation of the As Received Material

The results presented earlier, show a ferrite – pearlite microstructure for all the low carbon specimens (plain C – Mn and the microalloyed specimens). As the as received material was hot rolled at ~1100°C and then air cooled giving a ferrite – pearlite microstructure for the lower and medium carbon steel concentrations and a fully pearlite structure for high carbon steel (0.8 wt. % C).

5.3.1. Pearlite Volume Fraction

As the carbon content increases it is expected that the amount of pearlite would increase for 0.4 wt. % carbon and there would be a fully pearlitic microstructure for 0.8 wt. % C as shown in Figure 5-3 by the Fe – C phase diagram generated by Thermo-calc and with the SEM images taken by FEI Inspect F. This can be explained by a simple Fe – C phase diagram where the structure of the steel goes through a transformation from austenite to proeutectoid ferrite and austenite. Hillert M., [140] has gone into much more detail on the subject of the formation of pearlite, as this topic is not the scope of this research.

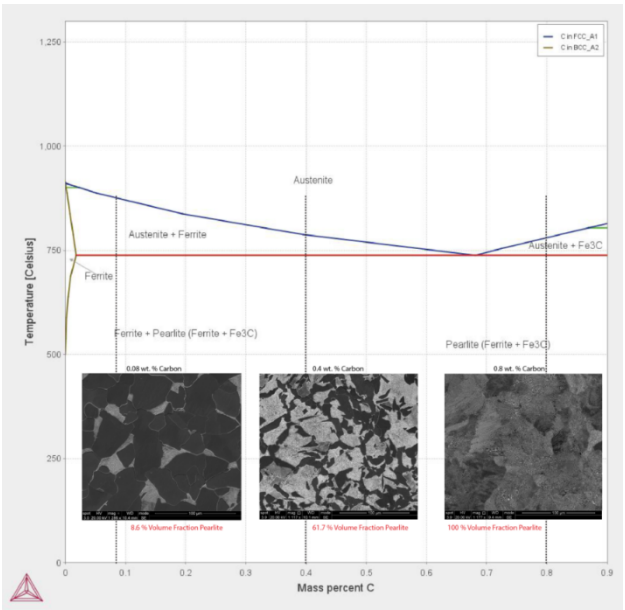

Figure 5-3: Plain Fe – C phase diagram, showing microstructure of 3 different carbon contents after normalising.

Increasing the Nb microalloying elements in low carbon steel (0.08 wt. % Carbon) decreases the ferrite grain size shown in Table 5-1 and increases the volume fraction of

pearlite which is also observed in 0.4 wt. % carbon and is shown in Table 5-2 similar findings are observed by Hui-jing et al., [141] which as shown that pearlite volume fraction increases with increasing niobium (Nb) and vanadium (V). This trend of increasing pearlite fraction with alloying elements is observed by many researchers [142, 141, 143]. Moor & Miller [143] have indicated that Nb additions accelerates the formation of pearlite colonies.

The increase in the volume fraction of pearlite with increasing Nb concentration could be attributed to the initial grain size prior to air cooling. It is known that Nb in solid solution decreases the grain boundary mobility by solute drag and decreases the transformation temperature [4]. Refinement of the prior austenite grains by NbC pinning the austenite grain boundaries occurs. Pearlite nucleation during transformation occurs exclusively at the austenite grain boundaries of which there are three types to consider: grain faces, edges and corners. A reduction in the prior austenite grain size would contribute to more nucleation sites because of the higher grain boundary area [144], as opposed to coarse grains which provide less nucleation sites for pearlite formation. The effect of prior austenite grain size has been shown to accelerate the rate of pearlite transformation indicating that the smaller the prior austenite grain size, the faster the kinetics for pearlite formation [145, 146].

5.3.2. Ferrite Grain Refinement

The decrease in the ferrite grain size in the low carbon steel (0.08 wt. %) can be explained based on the precipitation strengthening theory of microalloying elements. The ferrite grain refinement has been shown to be attributed to the Nb carbonitride precipitation in the austenite region. There are two types of transformation which lead to finer ferrite grains [147]. The first is that ferrite grains start to nucleate at the austenite grain boundaries, the Nb particles help the pinning of the prior austenite grains and inhibit austenite grain coarsening which leads to a smaller initial grain size [68] prior to hot deformation. Hence after deformation the fine recrystallized austenite grains can be transformed to even finer ferrite grains as more nucleation sites are available due to the increased grain boundary area of the austenite grains [148].

The second is when the austenite to ferrite transformation occurs at a lower temperature which is in the non-recrystallization region, where ferrite grains nucleate at the deformation bands [147]. This transformation mechanism does not contribute to the decrease in ferrite grain size in this work as the material was hot rolled in the region where recrystallization occurs, where grain growth is suppressed in the microalloyed specimens due to the precipitation pinning or solute drag effect [6, 149].

Hence the grain refinement is enhanced by the combined effect of increasing microalloying element (Nb) and hot deformation.

5.3.3. Precipitation Strengthening

The increase in Nb addition seems to have no precipitation strengthening effect on ferrite or in pearlite colonies in low carbon steel (0.08 wt. % Carbon) when air cooled from 1100°C as can be seen in Table 5-3. The hardness values for the ferrite grains obtained in the present work are in good agreement to those reported in literature by Kestenbach, without the presence of substructure hardening and/or precipitating particles [150]. Gray et al., [151] have also reported the loss of precipitation strengthening in ferrite due to the increased amount of precipitation of NbC in austenite during slower cooling rates.

Therefore, as there is no micro hardness increase observed in either pearlite or the ferrite phase with increasing Nb, this reconfirms that no precipitation strengthening is occurring in the matrix and that the precipitation process has taken place in austenite conditioning stage at 1100°C. In contrast, for macro hardness the values shown in Table 5-4 indicate a systematic increase in hardness with Nb concentration. It should be noted that the load used for macro hardness was HV_{1Kg} and that covered multiple ferrite grains, therefore the hardness increase could be attributed to the decrease in the ferrite grain size as shown in Figure 5-4. Similar findings have been reported by Qin et al., [152]. This trend contributes to the strengthening of the steel from the refinement of ferrite grain boundaries and follows the Hall-Patch relationship given by Equation (2-2) [16]. Similar results have been obtained by Hughes et al., [153] which show an increase in hardness with a decrease in grain size.

This increase in hardness is contributed to the grain refinement of ferrite grains where the boundaries act as obstacles, hindering the motion of dislocation which are caused by the plastic deformation during indentation [18, 43].

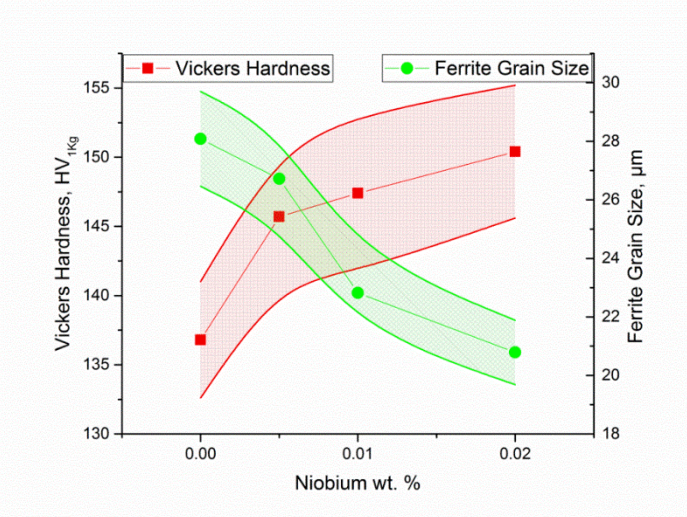

Figure 5-4: The effect of niobium on Vickers Hardness and Ferrite grain size in 0.08 wt. % Carbon.

Precipitation strengthening effects can be seen for the ferrite and pearlite microstructure for the medium carbon steel (0.4 wt. %) in Table 5-3. The hardness value of ferrite in plain C – Mn steel is 141 ± 10.6 $HV_{0.025g}$, similar to that of low carbon steel (0.08 wt. %) without any alloying elements which was 134.5 ± 7.9 $HV_{0.025g}$. The 10 $HV_{0.025g}$ increase can be explained by the higher amount of carbon content in medium (0.4 wt. %) carbon steel. There is a distinctive hardness increase for the ferrite grains with increasing niobium content. According to the equation given by Palmiere, et al., [68] the solubility temperature for 0.05 wt. % Nb is 1134.9°C and for 0.02 wt. % Nb is 1338.7°C. This implies not all of the NbC precipitates were in solution when the material was heated to 1200°C. The increase in the solubility temperature is expected as the NbC particles are much more stable in the medium carbon steel than in low carbon steel and therefore a higher temperature would be needed to dissolve them. According to the thermodynamic simulation performed on JMatPro, the predicted temperature range where dissolution of NbC starts is 1020°C – 1040°C (green rectangle) as shown in Figure 5-5 it implies that not all the NbC precipitates would be able to go in to solution at 1200°C.

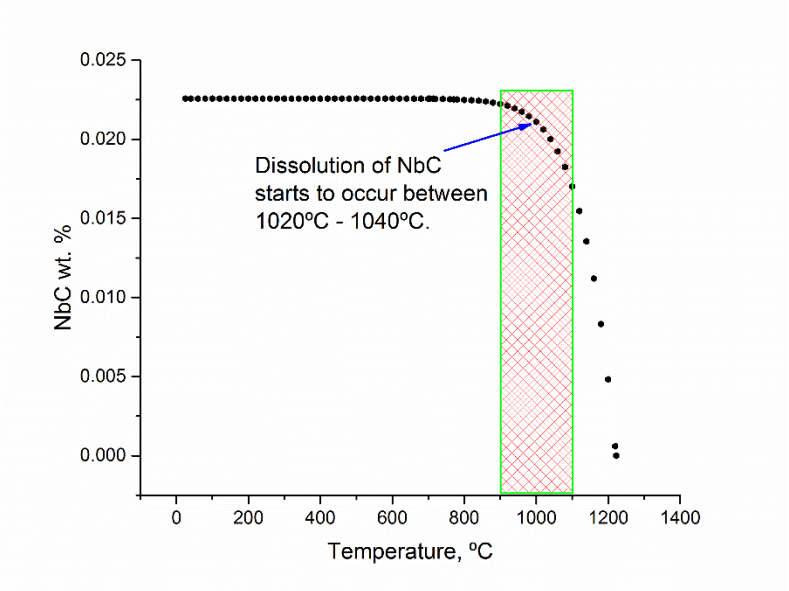

Figure 5-5: Dissolution kinetics of NbC predicted by JMatPro.

A review by DeArdo, et al., [4] shows that precipitates with face centered cubic crystal structure, do not fit well in the ferrite lattice which has a body centered cubic structure [4, 22]. The increment hardness increase in the ferrite grains with increasing Nb concentration is due to the lattice mismatch strains caused by the NbC precipitates and the ferrite lattice caused by Orowan – Ashby mechanisms [18, 154, 155, 1].

The hardness increase in pearlite with increasing Nb concentration for both medium (0.4 wt. %) and high (0.8 wt. %) carbon steels was observed. It is known that the decrease in the pearlite interlamellar spacing increase the strength of pearlite [18]. It has been shown by Moor, et al., [143] that Nb additions refine pearlite interlamellar spacing, which results in a hardness increase of the pearlite constituent. These results are similar to those observed in this work, therefore suggesting the pearlite interlamellar spacing refinement is the primary strengthening mechanism which contributes to the hardness increase observed in this work.

6. Reheat Temperature

As described in the literature review, thermo-mechanical rolling processes can be divided into the following stages, reheating, rough rolling, and table cooling; a great amount of physical metallurgy is related to these stages, which in turn influence the microstructure and subsequently the mechanical properties of the end product. It is of paramount importance that the austenite grain size is kept small as possible during the reheating stage; this work describes the effect of different reheat temperatures on the microstructure and the composition of the different carbon concentrations combined with microalloyed elements in the steel.

6.1 Introduction

The theory of grain growth evolution of a microstructure is well established; the grain growth process is a result of grain boundary motion driven by a reduction in their interfacial area energy as certain larger grains grow and consume their smaller neighbours [156] [157] [158]. This in turn leads to an increase in the average grain size. As grain growth is a thermally activated process at sufficiently high temperatures a polycrystalline material will evolve towards a single crystal given that there are no second phase particles impeding the grain boundary migration. The second phase particles are used as a method for grain growth control in microalloyed steel during the hot working process. The appropriate employment of the microalloying elements in high strength low alloy (HSLA) steels combined with thermo-mechanical processing; provides improvements in both toughness and strength.

The specimens have been etched with saturated picric acid with a wetting agent to reveal the prior austenite grain boundaries. The full details can be found in the Etching Chapter 4. The austenite grain size was measured using the intercept method ASTM standard E 112.

Standard deviation values generated when measuring the grain size using the ASTM standard E 112 are used to analyse when there is abnormal grain growth in the microstructure occurring at the different temperatures.

6.2 Solubility Limit

Obtaining knowledge of the solubility limit is important. Different solubility products obtained from literature are given in Table 6-1. In this work the temperature of total dissolution of second phase particles calculation has been done using

thermodynamic software called JMatPro 4.0 (Sente Software) in addition to using the solubility product equations calculated in previous works by different authors. In Table C-1 in Appendix C it can be seen that JMatPro prediction is in very close approximation to Smith, 1966 [159] for 0.005 wt. % Nb and 0.01 wt. % Nb, where JMatPro gives (1004.5°C and 1053.7°C) and Smith solubility product equation predicts (1009°C and 1065°C). However as the niobium content reaches 0.02 wt. % it is nearly identical to that predicted by Palmiere, et al., 1994 [160], JMatPro predicts a solubility limit temperature is 1109°C and Palmiere, et al., solubility product equation predicts 1106°C. It can be seen that regardless of which solubility product equation is used all of the equations show a trend with the increase in the niobium content there is an increase in the solubility temperature. The remaining solubility temperatures of 0.2, 0.4, 0.6, and 0.8 wt. % carbon are also given in Table C-2, Table C-3, Table C-4, and Table C-5 respectively in Appendix C and show similar trends.

Table 6-1: A section of available literature concerning different methods of obtaining a solubility product.

Authors	Product	Process	Year	Ref.
Palmiere, et al.,	Log[C][Nb] = 2.06 - 6700/T	Atom Probe	1994	[68]
Nordberg, et al.,	$Log[C][Nb]^{0.87}$ = 3.4 - 7200/T	Thermodynamic Calc	1968	[107]
Meyer, et al.,	Log[C][Nb]= 3.04 - 7290/T	Chemical Separation	1967	[161]
Smith ,	Log[C][Nb]= 3.7 - 9100/T	Equilibrating	1966	[159]
DeKazinsky, et al.,	Log[C][Nb]= 2.9 - 7500/T	Hardness Testing	1963	[162]
Nordberg, et al.,	$Log[C][Nb]^{0.87}$ = 3.11 - 7520/T	Statistical	1968	[107]

6.3 0.08 wt. % Carbon

The microstructure in all the figures from Figure C-1 to Figure C-2 for this carbon composition are shown in Appendix C, were obtained after reheating to the respective reheat temperature for 1 hour (60 minutes) in an argon atmosphere and immediately quenching in ice water. On quenching the initial microstructure for all the specimens was fully martensitic as shown in the light optical micrograph in Figure 6-1.

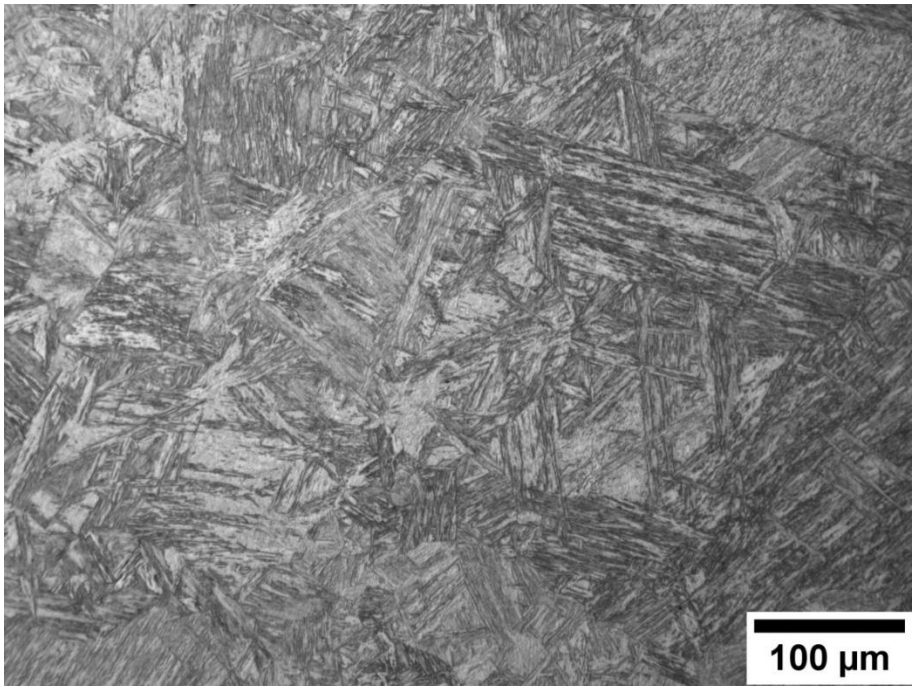

Figure 6-1: The initial structure after quenching in ice water after a holding at 1250°C for 1 hour. 20 x magnification (2% Nital).

6.3.1. Grain Growth during Reheating

The light optical micrographs showing the prior austenite grain boundaries can be seen for the ranging from Plain C-Mn steel and 0.02 wt. % Nb compositions, in Figure C-1 (Plain C-Mn), and Figure C-2 (0.02 wt. % Nb) for the reheating temperatures from 950°C to 1250°C in 50°C increments. A trend present in the steels is that the prior austenite grain size increases with increasing temperature.

However the plain C-Mn steel experiences a continuous growth from 950°C to 1250°C, which produces a gradual growth and relatively uniform prior austenite structure with equiaxed grains. On the other hand grain growth in the microalloyed steel is discontinuous; this abnormal grain growth is suppressed at certain lower temperatures presumably because of the pinning effect of the second phase carbides on the grain boundaries. Depending on the niobium concentration in the steel at certain higher temperatures when the pinning force of the second phase particles weakens, the grains begin to coarsen rapidly.

The average prior austenite grain growth as a function of the different reheating temperatures for plain C-Mn steel to 0.02 wt. % Nb is shown in below in Figure 6-2. It can be noticed that the addition of Nb decrease the prior austenite grain size. The graphical representation of the quantitative analysis (Table C-6 in Appendix C) shows the prior austenite grain size increases with increasing temperature for all of the steel compositions. At higher temperatures from 1150°C to 1200°C there is a larger increase

in the mean prior austenite grain size and after 1200°C there is an intense increase in the mean prior austenite grain size.

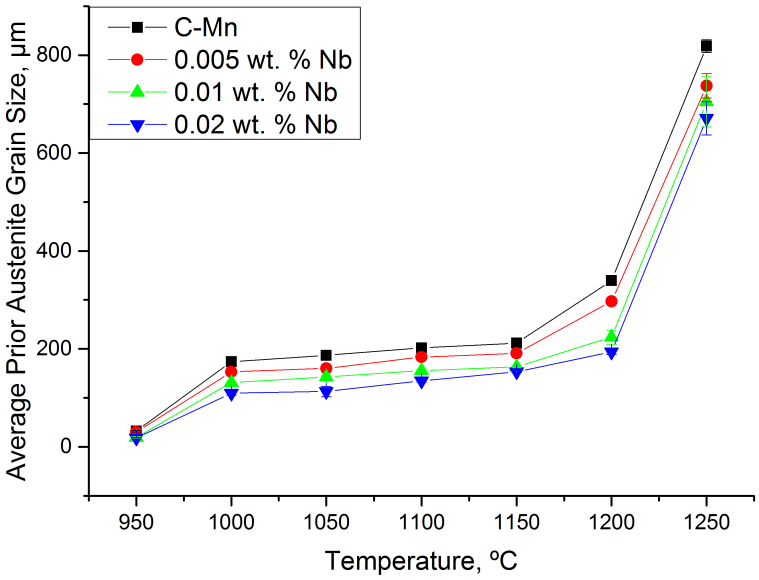

Figure 6-2: The average prior austenite grain size evolution as a function of reheating temperatures from 950°C to 1250° with a hold time of 1 hour for plain C-Mn steel and C-Mn-Nb microalloyed steels. Error bars represent ± 95% CL (Confidence limit).

6.3.2. Standard deviation of grain size (SD)

The standard deviation (SD) values are plotted against the reheat temperatures for each of the 4 steel compositions (plain C-Mn and 3 C-Mn-Nb) as shown in Figure 6-3. It can be observed that the SD values for the plain C-Mn steel keep relatively constant throughout the reheat temperatures from 1000°C to 1250°C with a slight increase from 950°C to 1000°C, which is to be expected as there are no second phase NbC particles in it.

A different trend is observed for the microalloyed steel with 0.005 wt. % Nb additions, where the SD value has a short broad peak starting from 950°C where the prior austenite grain size starts to deviate from the mean value reaching its peak at 1000°C and returning to a closer value to the mean at 1100°C and remains constant until 1150°C. After this temperature there is a sharp increase in the SD value from 9.2µm to 116µm, at 1200°C, implying abnormal grain growth is taking place.

The SD values, for 0.01 wt. % Nb steel show a similar trend to the previous steel as in there are two peaks which occur. One at 1000°C and then the other after 1250°C. The first peak at 1000°C indicates that there a large deviation in the prior austenite grain size

from the mean prior austenite grain size as compared to the previous reheat temperature of 950°C and the SD value then starts to decrease at 1050°C and remains constant until 1150°C where there is a sharp deviation increase from the mean value.

Finally for 0.02 wt. % Nb content the characteristics are similar to that of 0.01 wt. % Nb; with the increase in niobium there is an increase in the solubility temperature of the NbC precipitates. In Figure 6-3 it can be observed for 0.02 wt. % Nb that there is a transformation of normal to abnormal and back to normal growth, which starts at after 1000°C at which point the prior austenite grain size start to have a larger deviation from the mean size and there is a bimodal distribution at 1050°C as shown in the optical light micrograph in Figure 6-4(a) and by the histogram in Figure 6-4(b). The SD value then starts to return to a value which is closer to the mean grain size at 1100°C indicating a return to normal grain growth as shown in Figure C-2 in Appendix C where the transformation of normal to abnormal and back to normal can be seen visibly. However unlike the previous two microalloyed steels the (0.005 and 0.01 wt. % Nb) the second peaks do not start until 1200°C and keeps increasing to 1250°C. The standard deviation values corresponding to Figure 6-3 are given in Table C-7 in Appendix C.

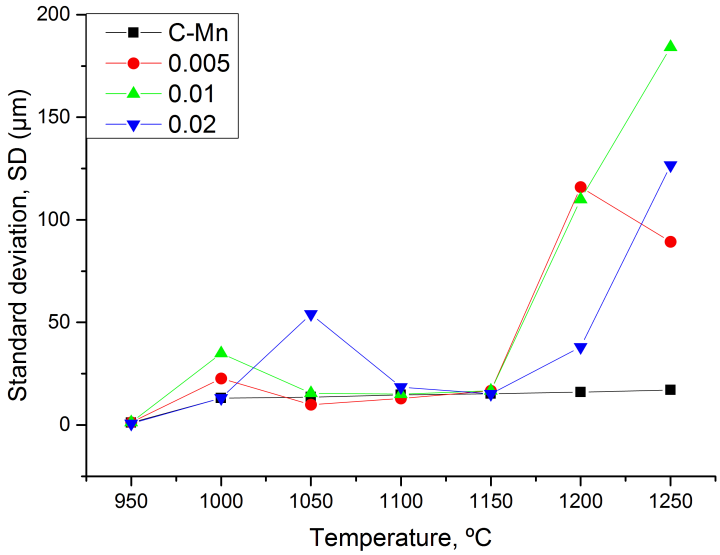

Figure 6-3: Standard deviation values at different temperatures for the 4 different steel compositions from plain carbon to 0.02 wt. % Nb addition.

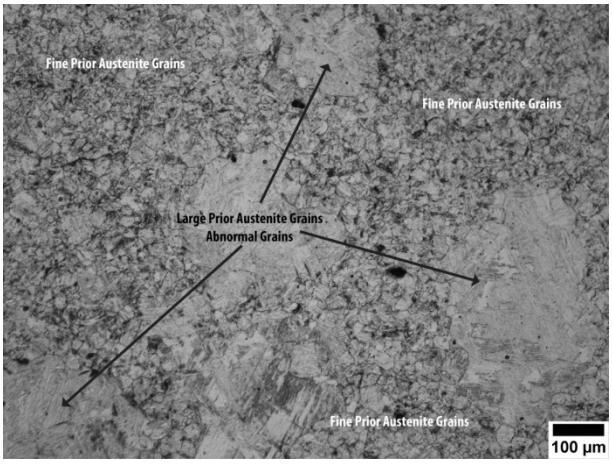

(a)

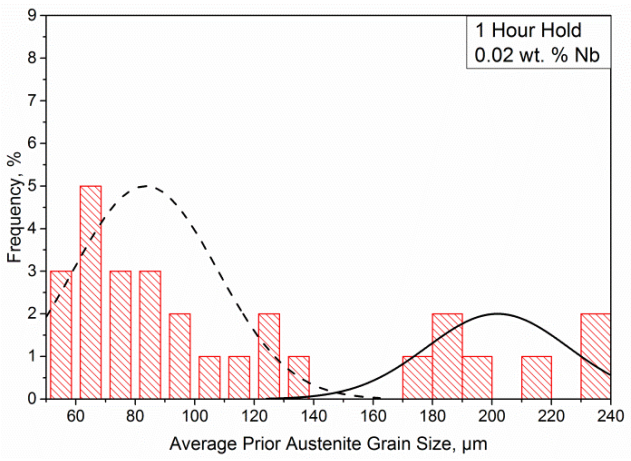

(b)

Figure 6-4: (a) Region showing abnormal grain growth giving it a duplex structure in a C-Mn-Nb (0.02 wt. % Nb) steel held at a temperature of 1050°C for 1 hour and ice water quenched, (b) grain size histograms showing two distinct size distributions.

6.4 0.2 wt. % Carbon

6.4.1. Grain Growth during Reheating

The light optical micrographs of the prior austenite grain growth for C-Mn-Nb steels as a function of different temperatures is shown in Figure C-3 (0.005 wt. % Nb) and Figure C-4 (0.01 wt. % Nb) in Appendix C. The effect of niobium on the prior austenite grain coarsening can be seen in all these figures.

The graphical representation of the grain size as a function of increasing temperature is shown in Figure 6-5. However, it can be the observed that upon reheating at lower temperatures (950°C and 1000°C) the specimens all have similar average prior austenite grain size (18.3µm to 26.4µm) for 950°C and (98.9µm to 119.8µm) for 1000°C.

However, from the 4 compositions, 3 of them have a similar growth trend apart from 0.02 wt. % which shows a gradual increase with temperature to 1200°C after which a sharp increase in prior austenite grain size is observed in this composition and the remaining 3 compositions. The quantitative analysis for the austenite grain size can be seen in Table C-8 in Appendix C.

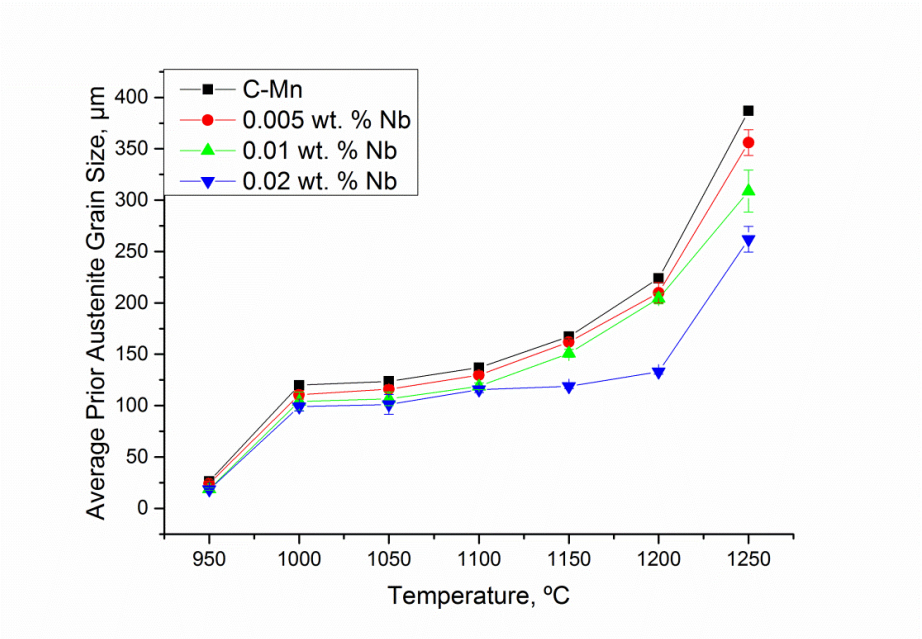

Figure 6-5: The average prior austenite grain size evolution as a function of reheating temperatures from 950°C to 1250° with a hold time of 1 hour for plain C-Mn steel and C-Mn-Nb microalloyed steels. Error bars represent ± 95% CL (Confidence limit).

6.4.2. Standard deviation of grain size (SD)

The standard deviation (SD) values for the 4 different compositions for the 0.2 wt. % Carbon steel are shown in Figure 6-6. The C-Mn steel without any niobium addition does not show much deviation from the mean prior austenite grain size from 950°C to 1250°C; which is expected as there are no second phase niobium particles. However, it can be seen that there are 3 peaks which occur in the temperature range between 1000°C to 1050°C. All of these peaks are related to the microalloyed compositions (C-Mn-Nb).

Starting with the microalloyed steel with 0.005 wt. % Nb, the results indicate that there is a small peak indicating a duplex prior austenite grain structure with a deviation of 6.3µm from the mean prior austenite grain size of 110.6 ± 4.3µm at 1000°C; furthermore the SD value remains constant from 1050°C to 1150°C indicating a return to normal growth of the prior austenite grains until after 1150°C when there is a sharp increase in the SD value.

Secondly the peak indicating the abnormal grain growth temperature for 0.01 wt. % Nb also occurs at 1000°C. However the deviation of the prior austenite grains size from the mean grain size is much higher at 23.3µm in comparison to 0.005 wt. % Nb. This higher SD value indicates that the abnormal duplex prior austenite structure is at its peak at this temperature; however this SD value decreases at 1050°C and moves closer to the mean prior austenite grains size at 1100°C, remaining relatively constant until 1200°C where after there is a sharp peak in the SD value.

Finally for the steel with 0.02 wt. % Nb addition the peak indicating the start of abnormal grain growth occurs at 1000°C where the SD value is 10.4µm, peaking at 1050°C where there is a deviation of 24.5µm from the mean value of 101.1 ± 9.6µm. At higher reheat temperatures the SD value returns closer to the mean of the overall prior austenite grain size and remains constant until 1200°C where just like the previous composition there is a sharp peak in the SD value. The standard deviation values for the austenite grain size corresponding to Figure 6-6 are given in Table C-9 in Appendix C.

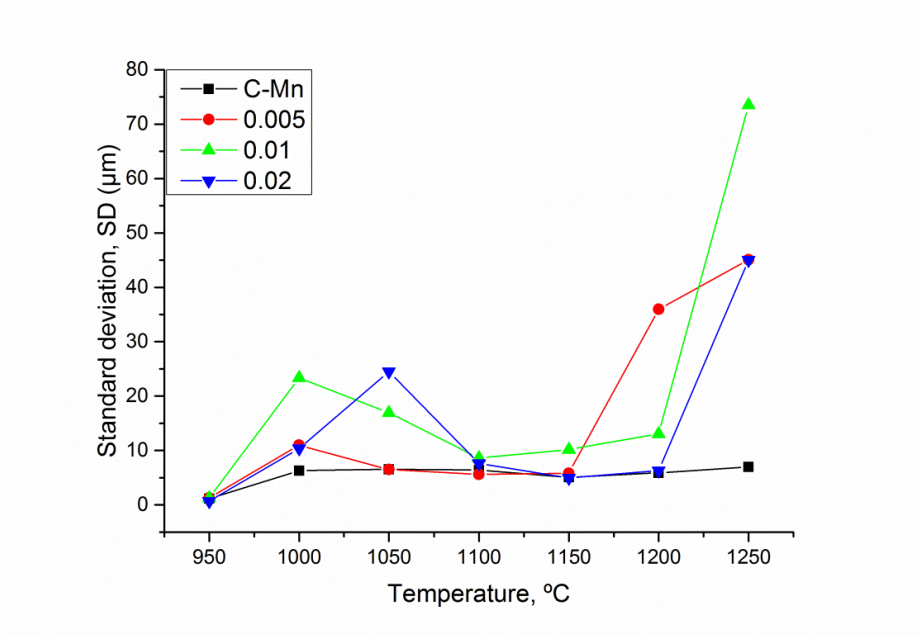

Figure 6-6: Standard deviation values at different temperatures for the 4 different steel compositions from plain carbon to 0.02 wt. % Nb addition for 0.2 wt. % Steel.

6.5 0.4 wt. % Carbon

6.5.1. Grain growth during Reheating

Figure 6-7 shows the evolution of the prior austenite grain size as a function of reheating temperature from 950°C to 1250°C for 4 different compositions of varying niobium content and an identical carbon level. As expected the prior austenite grains coarsen with increasing temperature for plain C-Mn steel and the 3 microalloyed steels. The effect of the niobium additions in the steel is clearly visible for the 3 microalloyed steels at a low temperature of 950°C when compared to the plain C-Mn steel as the austenite grain are much smaller. The grain size data is give in Table C-10 in Appendix C.

The optical light micrographs of the grain coarsening characteristics for medium 0.4 wt. % carbon steel alloyed with 0.02 wt. % Nb is shown in Figure C-6 in Appendix C. The microstructure for plain C-Mn steel consists of equiaxed and uniform prior austenite grains which coarsen with increasing temperature without any discontinuity; which is to be expected as no second phase particles are present. An interesting point to note is that in Figure C-5 (in Appendix C) at the reheat temperature of 950°C there is an intense duplex structure which occurs for 0.005 wt. % Nb alloyed steel.

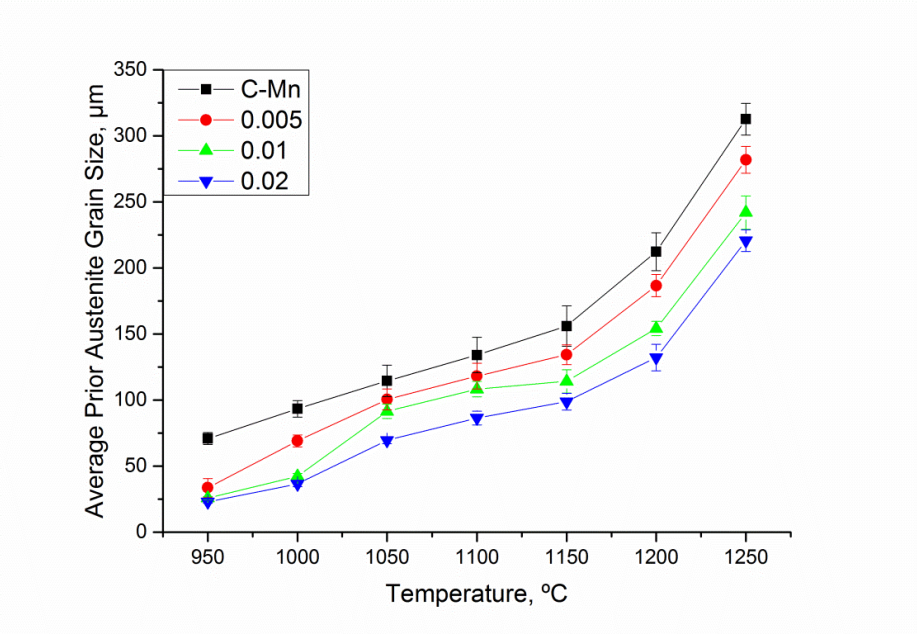

Figure 6-7: The average prior austenite grain size evolution as a function of reheating temperatures from 950°C to 1250° with a hold time of 1 hour for plain C-Mn steel and C-Mn-Nb microalloyed steels. Error bars represent ± 95% CL (Confidence limit).

6.5.2. Standard deviation of grain size (SD)

Figure 6-8 illustrates the standard deviation (SD) as a function of increasing temperature from 900°C to 1250°C, for the plain C-Mn steel and the 3 microalloyed compositions. It can be seen that the grain coarsening behaviour of plain C-Mn steel is indicative of normal grain coarsening due to the fact that the value of standard deviation remains relatively constant with increasing reheat temperature. It is to be expected that the prior austenite grains in plain C-Mn steel are relatively constant in size as there are no second phase particles which pin the grain boundaries.

However as expected, 0.005 wt. % Nb microalloyed steel shows a distinct case of abnormal grain growth as represented by the standard deviation peak at 950°C which indicated that the prior austenite grains deviate 17.8 µm from a mean of 33.6 ± 1.6µm. This duplex structure of the small and large prior austenite grains at 950°C is shown in

the light optical micrograph in Figure 6-9(a) and by the bimodal distribution histogram shown in Figure 6-9(b). As the reheat temperature increases, the standard deviation returns closer to the mean value indicating a return to a normal grain growth until after 1100°C where it once again deviates further from the mean.

Secondly, abnormal growth for 0.01 wt. % Nb occurs at 1000°C with a deviation of 15.8µm from the mean of 42.1 ± 2.3µm. The standard deviation of the prior austenite grains indicates a return back to characteristics of normal growth as the SD value comes closer to the mean value of the measured prior austenite grain size, this occurs as the reheat temperature increases. However this normal growth only occurs until 1150°C and after that there is an increase in the SD value indicating a return to abnormal growth.

Lastly at temperatures below to 1050°C, at temperature 900°C and 950°C the prior austenite grain growth is indicative of normal grain growth as is shown by the constant and low SD value. The abnormal prior austenite grain growth temperature is indicated by the standard deviation (SD) peak at 1050°C, which at the peak has a deviation value of 25.1 from the mean of 69.4 ± 2.6µm. As the reheat temperature is increased the SD value returns closer to the mean and therefore implies a return to normal grain growth until 1150°C after which it has an intense increase to 1250°C.

Table C-11 represents all the standard deviation values for the reheat temperature from 900°C to 1250°C for all the compositions.

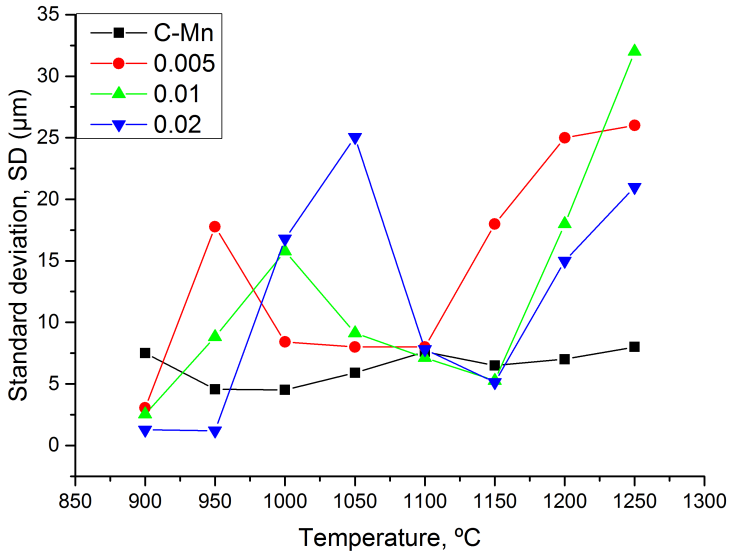

Figure 6-8: Standard deviation values at different temperatures for the 4 different steel compositions from plain carbon to 0.02 wt. % Nb addition for 0.4 wt. % Carbon Steel.

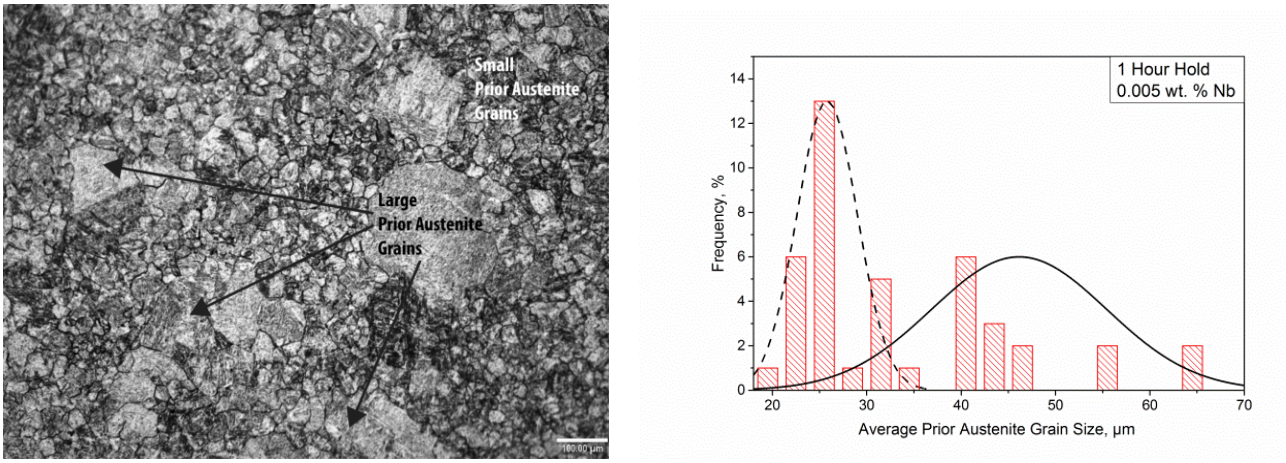

(a) (b)

Figure 6-9: (a) Region showing abnormal grain growth giving it a duplex structure in a C-Mn-Nb (0.005 wt. % Nb) steel held at a temperature of 950°C for 1 hour and ice water quenched, (b) grain size histograms showing two distinct size distributions.

6.6 0.6 wt. % Carbon

6.6.1. Grain Growth during Reheating

Figure 6-10 shows the prior austenite grain size as a function of reheat temperature from 950°C to 1250°C. The plain C-Mn steel and 0.005 wt. % Nb microalloyed steel both show gradual increase in the prior austenite grain size as a function of increasing temperature. An interesting point to note on the graphical representation is that at the temperature of 1000°C both 0.01 wt. % Nb and 0.02 wt. % Nb steels have near average prior austenite grain size of (38 ± 2.6µm and 32.8 ± 1.6µm) at a higher reheat temperature of 1050°C. The 0.01 wt. % Nb steel has much larger average prior austenite grain size increase of 79.4 ± 9.8µm in comparison to 0.02 wt. % Steel which has a small increase in the average prior austenite grain size of 40.5± 2.1µm. However this average prior austenite grain size becomes double the size at 1100°C increasing to 80.5 ± 4µm. In Appendix C, Table C-12 show the quantitative analysis of the mean prior austenite grain size for the plain C-Mn and 3 microalloyed steels.

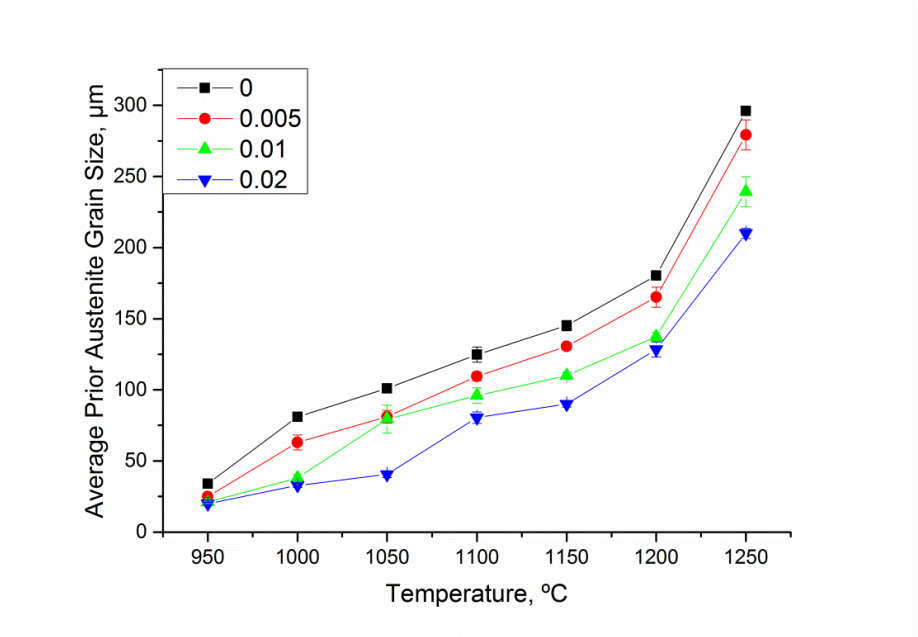

Figure 6-10: The average prior austenite grain size evolution as a function of reheating temperatures from 950°C to 1250° with a hold time of 1 hour for plain C-Mn steel and C-Mn-Nb microalloyed steels. Error bars represent ± 95% CL (Confidence limit).

6.6.2. Standard deviation of grain size (SD)

Figure 6-11 illustrates standard deviation (SD) values plotted against the reheat temperatures for the plain C-Mn steel and 3 microalloyed steels. It is to be expected that the standard deviation value for plain C-Mn steel remains constant throughout as the reheat temperature is increased.

Standard deviation (SD) trend for 0.005 wt. % Nb has a peak occurring at 1000°C. This deviation of 13.3µm from the average prior austenite grain size of 63 ± 5.2 µm suggests that abnormal grain growth is observed at this temperature when the specimen is held for a hold time of one hour. The SD value starts to return closer to the average prior austenite grain size suggesting a return to normal grain growth as the reheat temperature increases and after 1150°C an intense increase in the SD value occurs.

As the niobium content increases to 0.01 wt. Nb the SD peak moves to higher reheat temperatures. In this instance the peak is at 1050°C which has a SD value of 25µm from the average prior austenite grain size of 79.4 ± 9.8 µm at this temperature. An interesting point to note is that the start of the second peak occurs at 1200°C whereas for 0.005 wt. % it occurs at 1150°C. This second peak only occurs in the microalloyed steels and not in the plain C-Mn steel.

Finally the abnormal grain growth is indicated by the peak at 1100°C for the 0.02 wt. % Nb. It should be noted this is also the temperature where the transition from normal to abnormal and back to normal grain growth occurs. This continuous and discontinuous

grain growth trend can be seen from the SD value being constant from 950°C to 1050°C suggesting normal grain growth (continuous) until 1100°C where it goes through an abnormal grain growth (discontinuous) transition and back to normal grain growth at 1150°C. However after 1200°C the SD value starts to increase slightly and keeps increasing until 1250°C. This increase is not as intense as the one which occurs for 0.01 wt. % Nb. The standard deviation values shown in Figure 6-11 are given Table C-13 in Appendix C.

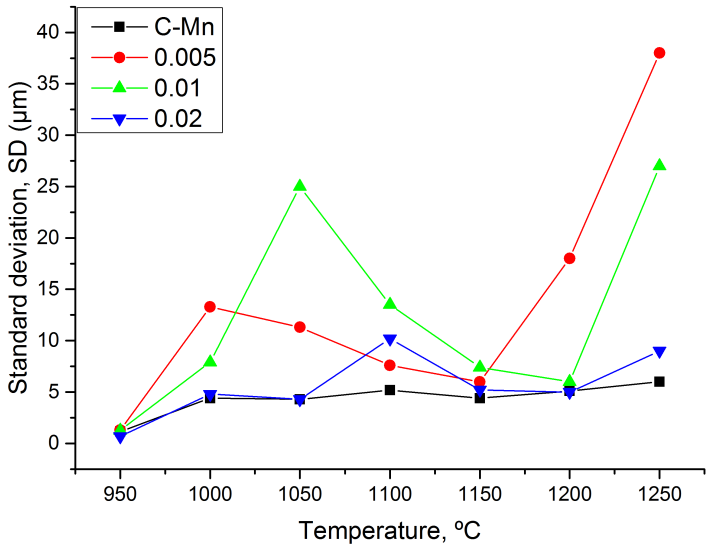

Figure 6-11: Standard deviation values at different temperatures for the 4 different steel compositions from plain carbon to 0.02 wt. % Nb addition for 0.6 wt. % Carbon Steel.

6.7 0.8 wt. % Carbon

6.7.1. Grain Growth during Reheating

Figure 6-12 illustrates the evolution of prior austenite grain size for plain C-Mn and 3 microalloyed steels against increasing reheating temperatures from 950°C to 1250°C. The quantitative analysis of the prior austenite grain size for the plain C-Mn and the 3 microalloyed steels is given in Table C-14 in Appendix C. As can be seen in Figure 6-12 the prior austenite grain size increases gradually with the increase in the reheat temperature. It also demonstrates that the addition of niobium decreases the average grain size and this trend is seen at all the different reheat temperatures.

The light optical micrographs are shown in Figure C-7 (0.005 wt. % Nb) in Appendix C, show abnormal grain growth (discontinuous) at 1000°C.

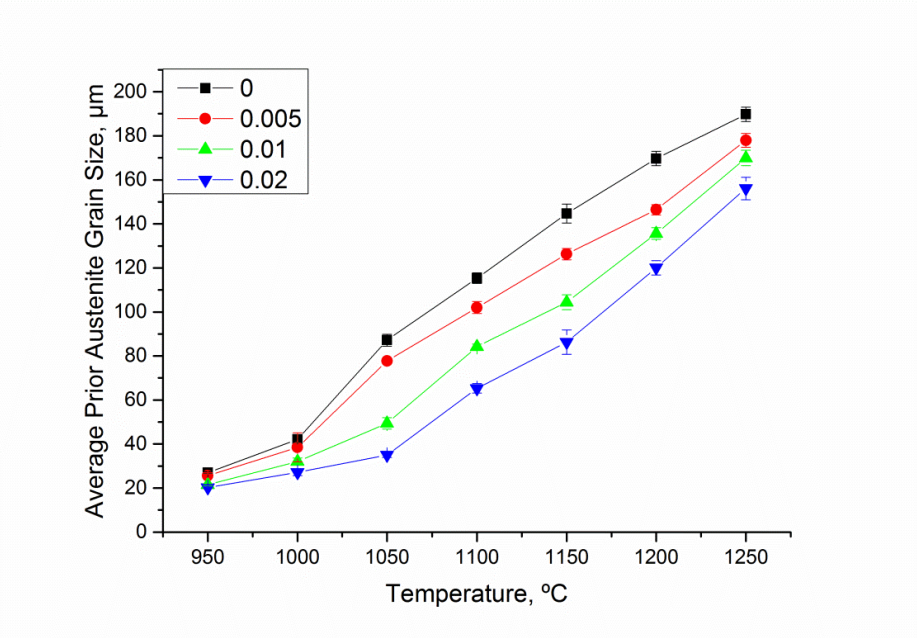

Figure 6-12: The average prior austenite grain size evolution as a function of reheating temperatures from 950°C to 1250° with a hold time of 1 hour for plain C-Mn steel and C-Mn-Nb microalloyed steels. Error bars represent ± 95% CL (Confidence limit).

6.7.2. Standard deviation of grain size (SD)

The Figure 6-13 illustrates the standard deviation (SD) as a function of increasing temperature from 950°C to 1250°C, for the plain C-Mn steel and the 3 microalloyed steel compositions. The results demonstrate that there is no abnormal grain growth (discontinuous) which occurs in the plain C-Mn steel as is indicated by the constant standard deviation value of 4.1µm to 6.2µm for 1000°C to 1250°.

The abnormal prior austenite grain growth (discontinuous) for 0.005 wt. % Nb can be seen to take place at 1000°C as is suggested by the high standard deviation value of 16.8µm from the mean prior austenite grain size of 38.5 ±5.5 µm. As shown in the earlier results of the standard deviation, as the temperature increases, the SD value comes closer to the mean prior austenite grain size until 1200°C after which there is a sharp peak to indicate abnormal grain growth once again.

Secondly, abnormal grain growth for the steel with 0.01 wt. % Nb occurs at 1050°C as suggested by the high standard deviation value of 8.3µm from the average prior austenite grain size of 49.4 ± 2.6 µm. The SD value returns closer to the mean as the reheating temperature is increased until 1250°C where it starts to deviate from the mean again to 8.6µm.

Lastly, the abnormal grain growth (discontinuous) temperature is suggested at 1150°C for 0.02 wt. % Nb. This is indicated by the high standard deviation of 13.4µm

from the average prior austenite grain size of 86.3 ± 5.5 µm. Once again as with previous trends the grain growth mechanisms return to normal growth as the reheat temperature increases, similar to the previous composition of 0.01 wt. % Nb, and the prior austenite grains start to deviate again at 1250°C. Table C-15 in Appendix C shows the standard deviations grain size values for Figure 6-13.

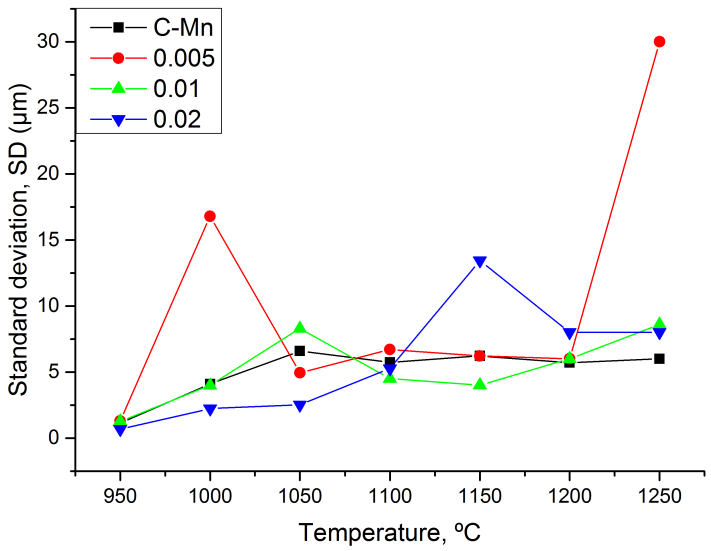

Figure 6-13: Standard deviation values at different temperatures for the 4 different steel compositions from plain carbon to 0.02 wt. % Nb addition for 0.8 wt. % Carbon Steel.

6.8 Summary

The results presented in this chapter are summarized and shown in Figure 6-14(a, b, c, and d). The illustration shows the varying carbon content with increasing reheat temperature (X axis) and the influence these two parameters have on the average prior austenite grain size (Y axis). The overall results suggest that with an increase in carbon content without any microalloyed additions for plain C-Mn steel there is a decrease in the average prior austenite grain size as illustrated in Figure 6-14(a). Similar trends can be seen in the 3 microalloyed steels shown in Figure 6-14(b, c, and d). Figure 6-15 shows the light micrograph images of the prior austenite grains comparing the different carbon content for a fixed niobium content of 0.01 wt. % at a fixed temperature of 1050°C. As it can be seen, increasing carbon decreases the prior austenite grain size.

The standard deviation results have shown that the amount of niobium addition in the steel determines at what temperature the prior austenite grain growth would transition

from normal grain growth (continuous) to abnormal (discontinuous) grain growth. It has also been shown that as the carbon content is increasing so does the temperature at which the abnormal grain growth starts to occur.

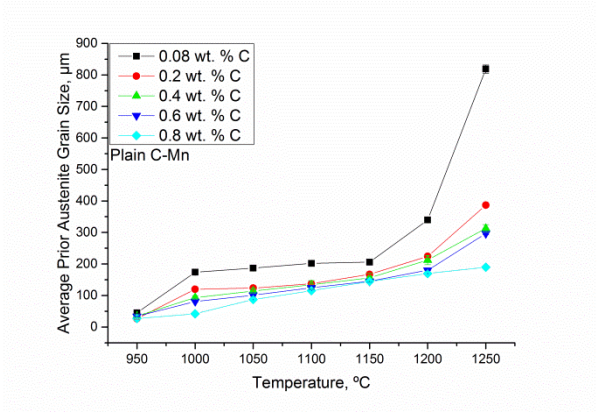

(a) Plain C-Mn Steel

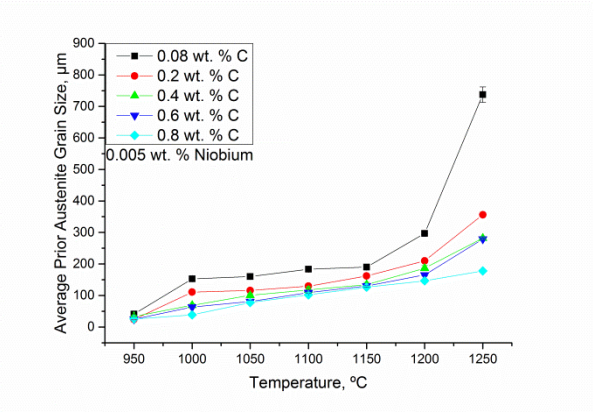

(b) 0.005 wt. % Nb

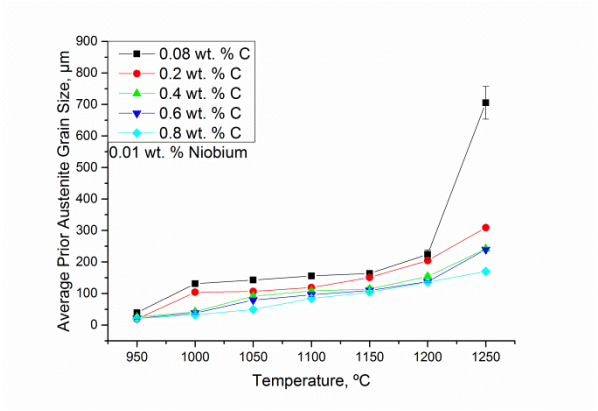

(c) 0.01 wt. % Nb

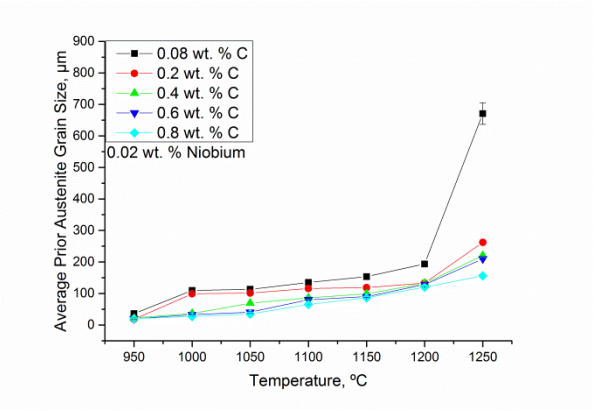

(d) 0.02 wt. % Nb

Figure 6-14: Profiles of prior austenite grain size (Y-axis) for plain C-Mn steel and 3 microalloyed steels with increasing temperature (X-axis) for the 5 different carbon contents.

0.08 wt. % Carbon

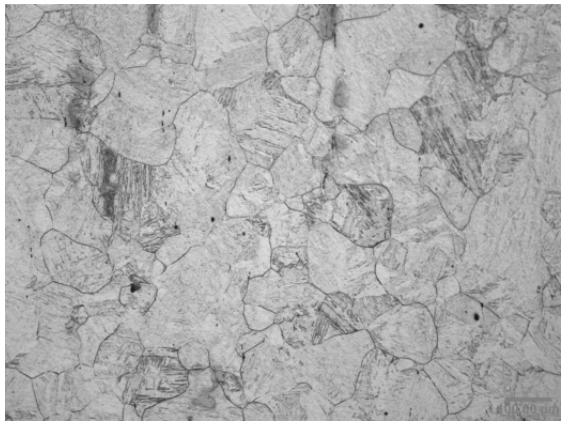

0.2 wt. % Carbon

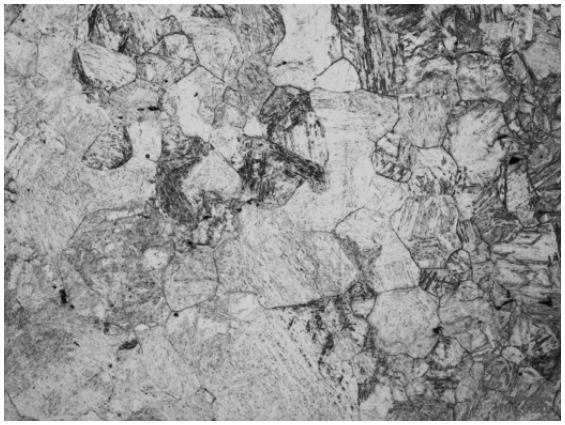

0.4 wt. % Carbon

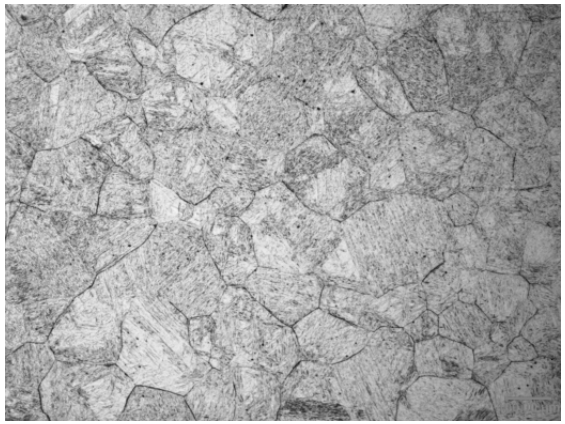

0.6 wt. % Carbon

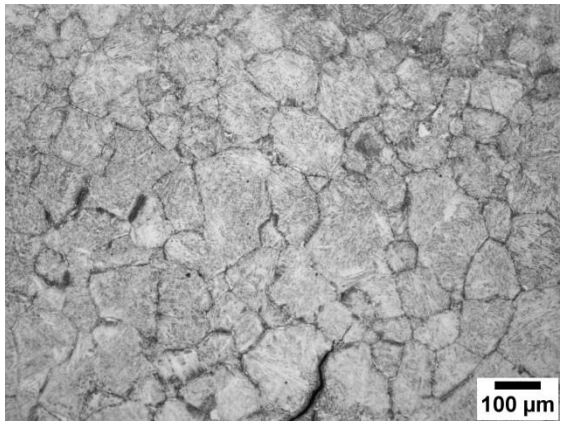

0.8 wt. % Carbon

- 0.01 wt. % Nb
- Tube Furnace
- Argon Atmosphere
- 1 Hour Hold
- Ice Water Quench

Figure 6-15: Shown above are a set of light optical micrographs of prior austenite grains for different Carbon content with a fixed allying addition of 0.01 wt. % Nb steel after isothermally reheating temp of 1050°C for 1 hour and ice water quenching. (Etched with Saturated Picric Acid)

6.9 Discussion of the Initial Austenite Grain Condition

Many factors influence the conditioning of the prior austenite grain in microalloyed steels. These factors can be traced back to the initial solidification process prior to the thermomechanical processing, where solute partitioning creates variations in composition throughout the continuously cast slab or ingot resulting in microsegregation. This does not constitute a major problem since it can be removed when the material experiences further processing such as, soaking at high temperatures. The rationale behind soaking at high temperatures is to homogenise the microstructure with a more uniform solute distribution. Soaking is often followed by high temperature deformation to produce a semi-finished slab in terms of geometrical and metallurgical significances.

6.9.1. Effect of Reheat Temperature (Microstructure of Austenite)

The first stage of any deformation process or heat treatment process is the determination of what temperature is the material going to be reheated at. There have been numerous investigations [68, 67, 5, 163, 95, 164] on the austenite grain coarsening behaviour of low, medium and high [165, 166] carbon microalloyed steel during reheating. In all the investigations the results are similar to those shown in Figure 6-2, Figure 6-5, Figure 6-7, Figure 6-10 and Figure 6-12, where the prior austenite grain size increases with increasing temperature. The characteristics of the prior austenite grains changes with increasing temperature. At temperatures below the respective grain coarsening temperature, (T_{GC}), for each carbon and niobium concentration the austenite grains have a fine uniform distribution. The presence of the second phase particles which suppress the austenite grain growth below the (T_{GC}), is the reason for the uniform grain structure. Hillert [62], Gladman [72] and Gladman, et al., [73] have shown in Equation (2-5) that the inception of abnormal prior austenite grain growth may be due to Ostwald ripening of the precipitates. Ostwald ripening is when the precipitates start coarsening at the expense of smaller ones which dissolve. As the NbC particle coarsens there is a critical particle radius r_{crit} and if the particle radius $r > r_{crit}$, the prior austenite grains will grow and consume the neighbouring grains. If the $r < r_{crit}$ the particles shrink. Furthermore, as precipitates coarsen and/or go into solution in the austenite region, the abnormal growth of the prior austenite grains start to occur as the volume fraction of the precipitates decreases.

The prior austenite grain growth characteristics for plain C-Mn steel without any alloying elements can be seen in Figure 6-16 (a) for all the five carbon concentrations. As the reheat temperature increases there is no significant change in the standard

deviation, SD value remains relatively constant, indicative of normal grain growth. In Figure 6-17(a) it can be seen that the normal grain growth is systematically increasing with increasing temperature, maintaining a constant normal distribution of the austenite grain microstructure, which is represented by the standard deviation, giving only one grain growth regime. This normal grain growth in plain carbon steel is expected as there are no second phase precipitate particles which restrict grain growth or experience an Ostwald ripening effect as the temperature increases. Similar results have been reported by Palmiere, et al., [68] for low carbon plain C-Mn steel.

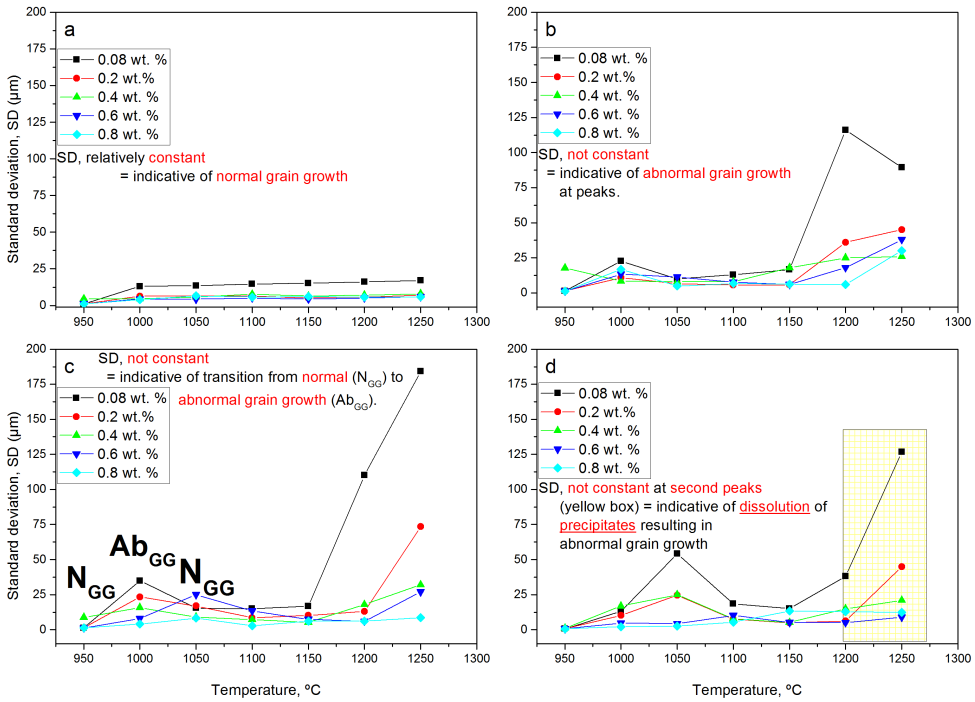

Figure 6-16: (a) Plain C-Mn. (b) 0.005 wt. % Nb, (c) 0.01 wt. % Nb and (d) 0.02 wt. % Nb Steel

Figure 6-16 (b), (c) and (d) illustrates the standard deviations for the microalloyed steel with the five different carbon concentrations, where the peaks indicate the microstructural heterogeneity of the overall prior austenite grain size, indicating regime changes. Palmieres investigation on low carbon steel alloyed with Nb reported three grain growth regimes. Coladas, et al., [165] reported two stages of grain growth for prior austenite grains in medium and high carbon steels.

All of the microalloyed steel compositions show four regime behaviours. First, a uniform distribution of prior austenite grains due to the presence of precipitates

hindering abnormal growth and causing normal grain coarsening. Secondly, inception of heterogeneity of the microstructure exhibiting retained initial small austenite grains and a small number of new abnormally coarsened grains. As explained earlier this is due to the Ostwald ripening and a decrease in volume fraction of particles. Thirdly, the austenite microstructure returns back to a uniform distribution consisting of larger prior austenite grains and finally, the last regime exhibits accelerated rapid growth of abnormal grain coarsening, resulting in larger average prior austenite grain size. This occurs when the number and size of the precipitates are no longer adequate to exert any pinning. These four regimes are shown in more detail for low carbon (0.08 wt. %) steel in Figure 6-17 (b).

Overall the number of different regimes which occur during reheating is related to the composition of the steel. For lower (0.08 wt. %, and 0.2 wt. %) and medium (0.4 wt. %, 0.6 wt. %) carbon range alloyed with (0.005 wt. % Nb, 0.01 wt. % Nb and 0.02 wt. % Nb) four grain growth regimes were observed, similar to those observed by Palmiere, et al., [68] as mentioned earlier.

The high (0.6 wt. % and 0.8 wt. %) carbon steel alloyed with 0.02 wt. % Nb, exhibited 3 regimes, the prior austenite grain characteristics remain those of normal grain coarsening, indicating the stability of the second phase particles at the high end of the temperature range.

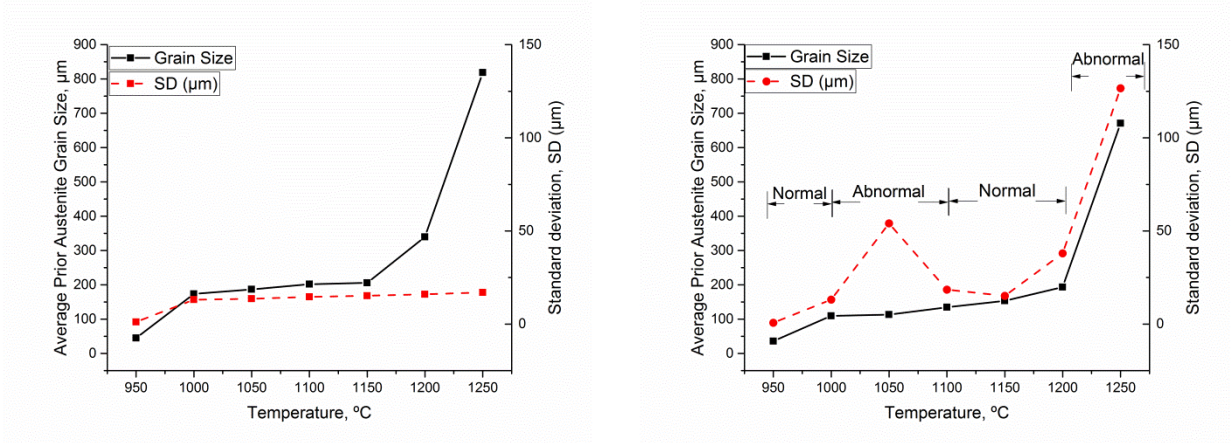

(a) (b)

Figure 6-17: Overlap of austenite grain growth and standard deviation of the overall austenite grain size, for 0.08 wt. %, plain C-Mn and microalloyed steel.

Coladas el al., [165] investigated carbon composition varying from 0.4 wt. % Carbon to 0.81 wt. % Carbon with different Nb additions. However the investigation does not indicate the degree of heterogeneity in the prior austenite grain microstructure and the effect of the different compositions on the degree of heterogeneity. In this work the effect of increasing carbon concentration is shown to have an effect on the

heterogeneity of the prior austenite grain structure in the alloyed steel containing 0.02 wt. % Nb. This is shown in Figure 6-18. The standard devation method used in this work clearly indicates the heterogenity is much lower as carbon increases from 0.08 wt. % to 0.8 wt. %. This is indicative of the NbC precipitates being more thermodynamically stable with an increase in carbon content and a higher volume fraction of precipitates avilable to restrict grain growth at higher temperatures.

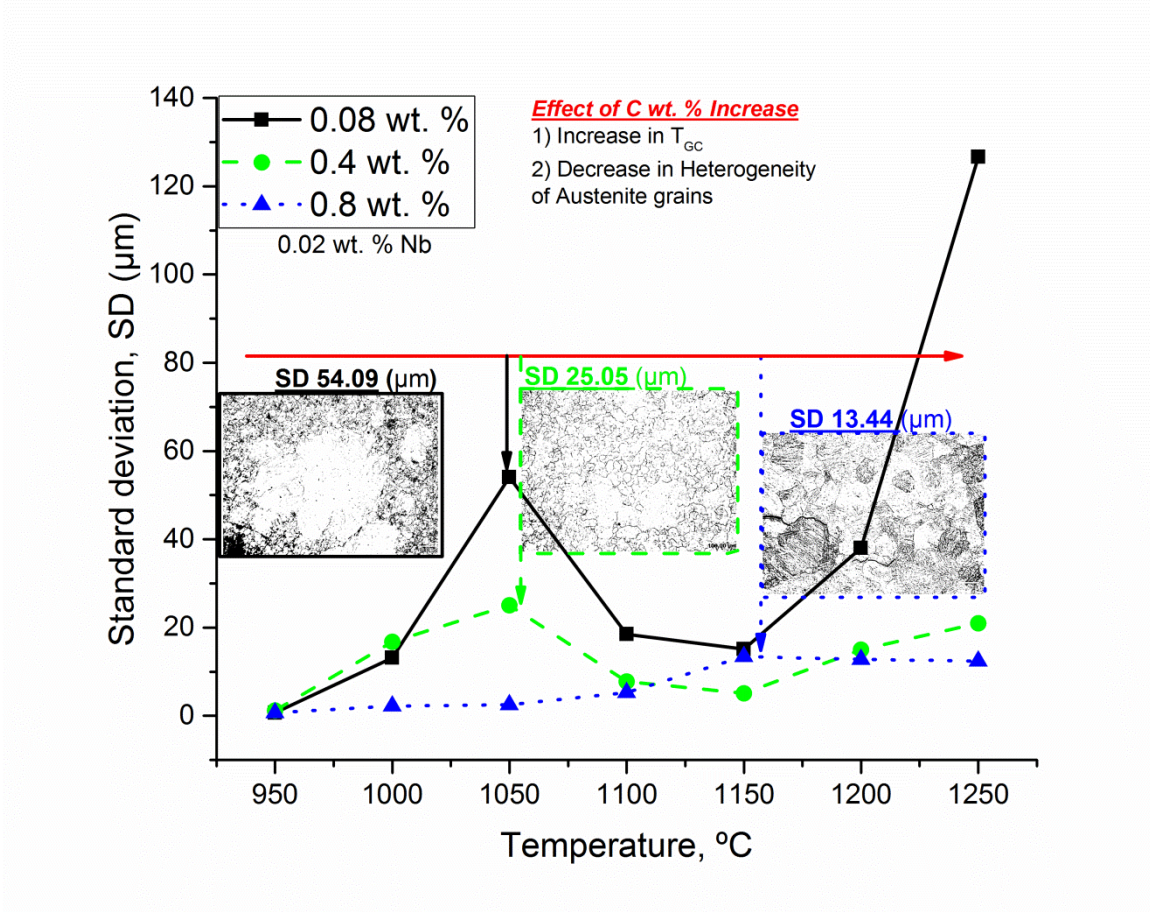

Figure 6-18: Comparison of the effect of carbon wt. % and heterogeneity of the prior austenite grain size, microalloyed with 0.02 wt. % Nb.

There is an effect of carbon content on the austenite grain size and the decreasing prior austenite grain size as can be seen in Figure 6-14 (a) for plain C-Mn steel. This can be explained by the solute drag effect on the grain boundary migration [6, 7, 8, 9]. According to the solute drag theory, the solute atoms diffuse and segregate to the grain boundaries to reduce the internal stresses, and therefore exerting drag forces on the moving grain boundaries.

The prior austenite grain size for the microalloyed steels of the different carbon compositions all show a decrease in grain size with increasing Nb concentration as shown in Figure 6-14 (b), (c) and (d), as a result of the NbC pinning the grain

boundaries. As the carbon content increases, the solubility temperature for NbC increases as shown by the various solubility equations given in Table C-1 (0.08 wt. % C), Table C-2 (0.2 wt. % C), Table C-3 (0.4 wt. % C), Table C-4 (0.6 wt. % C) and Table C-5 (0.8 wt. % C) in Appendix C.

6.9.2. Relationship between T_{DISS} and T_{GC}

The relationship between the complete precipitate dissolution temperature (T_{Diss}) and grain coarsening temperature (T_{GC}) can be useful for the approximation of the prior austenite grain structure prior to the heat treatment process, since it vastly changes the microstructure and therefore influences the mechanical properties of steels. Cuddy [5] has reported that once a heterogeneous prior austenite microstructure is formed it cannot be removed by further deformation.

The solubility products given in Table 6-1 and with the actual values given in Table C-1 in Appendix C, indicate a wide range of solubility temperatures for low (0.08 wt. %) carbon steel alloyed with different niobium content. This varying solubility trend can also be seen in the remaining solubility temperature in Table C-2 (0.2 wt. % C), Table C-3 (0.4 wt. % C), Table C-4 (0.6 wt. % C) and, Table C-5 (0.8 wt. % C). Palmiere et al., [68] investigated the dissolution of NbC by using an atom probe field ion microscope (APFIM) and found that the temperature of dissolution was 100°C - 200°C higher than those observed by other techniques [107, 161, 159, 162] used to estimate the solubility products e.g. thermodynamic, chemical separation, equilibrating a series of steels with different Nb contents, hardness and statistical techniques underestimated compete dissolution temperatures.

Cuddy et al., [67] reported that the grain coarsening temperature starts 35°C - 115°C below the complete dissolution temperature. Palmiere et al., [68] reported a higher temperature difference of 200°C below the dissolution temperature. The solubility product expression Palmiere has formulated is shown in Equation (6-1) and is the most accurate to date [22]. Therefore using this equation for the dissolution temperature and Equation (2-7) we can predict the abnormal grain coarsening temperature.

$$\log[Nb][C] = 2.06 - \frac{6700}{T} \tag{6-1}$$

Based on the value obtained by Equation (6-1) and Equation (2-7), it can in the graph give in Figure 6-19 that the approximation made by Palmiere et al., [68] as presented in Equation (2-7) is considerably different to that to that obtained in this work. In this work, the temperature at which abnormal grain growth commences is below the complete dissolution temperature and it gradually increases with higher carbon content. This difference between the values of 125°C given by Palmiere et al., [68] in Equation

(2-7) and varying temperatures in this work could be attributed to a number of factors, longer holding times, differences in carbon concentration and the fact that the specimens had been homogenised for 2 hours to dissolve all the precipitates. This discrepancy can be attributed to highly stable precipitates due to higher C concentration in this study.

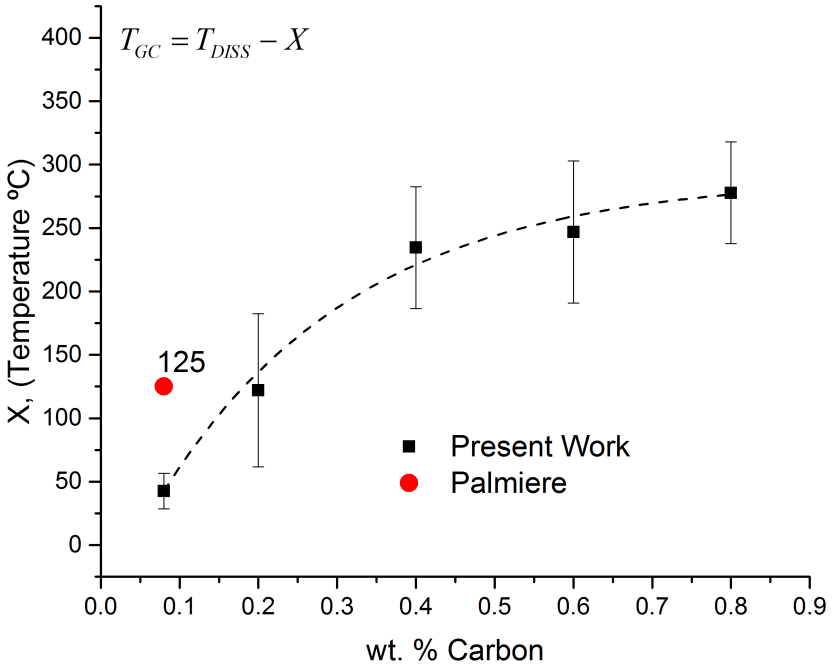

Figure 6-19: X value changing with an increase in carbon wt. %. Error bars represent ± 95% CL. Dashed line is used only as a guide for the eye. 125°C taken from Palmiere et al., [68].

The following Equations (6-2), (6-3), (6-4), (6-5) and (6-6) have been adjusted from the original Equation (2-7) to fit the grain coarsening temperatures with increasing carbon content in the present work. In Figure 6-20 (b) it can be seen that the calculated values for temperatures below T_{DISS} show a closer fit to that of the experimentally observed T_{GC}, than that of keeping a single value of 125°C as shown in Figure 6-20 (a).

$$T_{GC}{}^{0.08\ wt.\ \%\ C} = T_{DISS} - 43°C\ \pm 14 \tag{6-2}$$

$$T_{GC}{}^{0.2\ wt.\ \%\ C} = T_{DISS} - 122°C\ \pm 60.4 \tag{6-3}$$

$$T_{GC}{}^{0.4\ wt.\ \%\ C} = T_{DISS} - 235°C \pm 48.1 \tag{6-4}$$

$$T_{GC}{}^{0.6\ wt.\ \%\ C} = T_{DISS} - 247°C\ \pm 56.1 \quad (6\text{-}5)$$

$$T_{GC}{}^{0.8\ wt.\ \%\ C} = T_{DISS} - 278°C\ \pm 40.1 \quad (6\text{-}6)$$

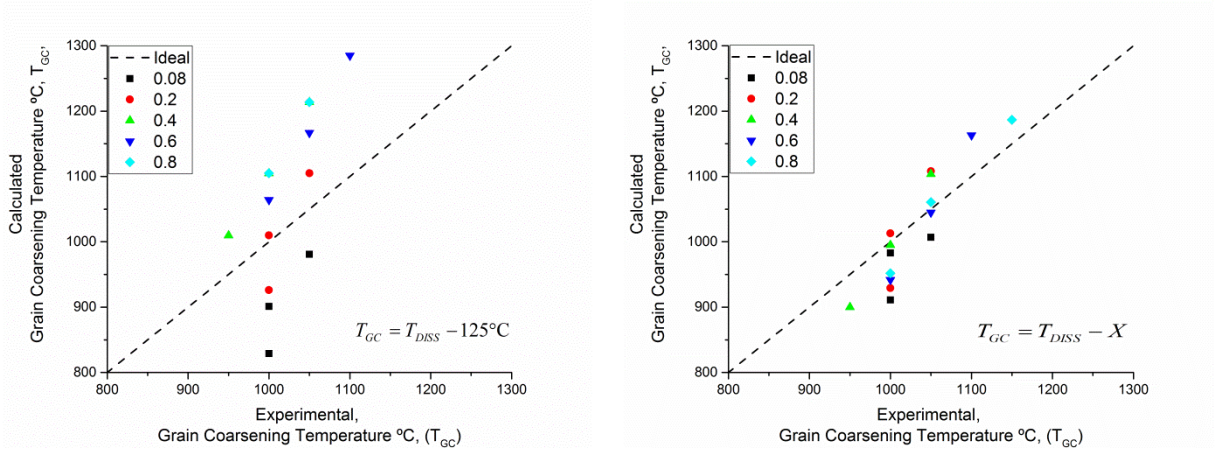

(a) (b)

Figure 6-20: Comparison between predicted grain coarsening temperature and calculated grain coarsening temperature using (a) Equation (2-7) and (b) (6-2) to (6-6).

As explained earlier the importance of getting the T_{GC} and T_{DISS} right is vital to understanding and optimising the mechanical properties of the steel, since reheating below T_{GC}, ensures the prior austenite microstructure is uniform as shown by the standard deviation values in Figure 6-17 for low carbon (0.08 wt. %) alloyed with 0.02 wt. % Nb. Having a uniform structure promotes a fine austenite structure during hot rolling [68]. On the other hand reheating above the T_{DISS} allows for maximum precipitation in austenite or ferrite later down the processing route. The trend of increasing T_{GC} with increasing Nb concentration was observed in all microalloyed steels for all the carbon concentrations. These findings are in agreement with previous investigations [74, 68]. The increase in carbon concentration when keeping the Nb content constant and resulting higher T_{GC} indicates that the NbC becomes more thermodynamically stable with higher carbon amounts.

The method of using standard deviation (SD) to analyse the heterogeneity of the austenite structure at different reheat temperatures has been shown to give quick and reliable results.

7. Hold Time at Different Isothermal Temperatures

As mentioned in the previous results Chapter 6 reheating is the initial stage of any thermo-mechanical rolling process. The amount of physical deformation needed to obtain the desired mechanical properties is influenced by the starting prior austenite microstructure; therefore it is of paramount importance that the prior austenite grain size is kept small and uniform as possible during the reheating and holding stage.

7.1 Introduction

The work presented in this chapter describes the effect of different hold times for different reheat temperatures and the effects on microstructure evolution of low, medium and high carbon microalloyed steel. This work analyses the starting prior austenite grain evolution and the presence of precipitates at different hold times for two different reheat temperatures, characterising the normal or abnormal prior austenite grain growth and precipitate distribution.

The influence of precipitates on the grain growth evolution in steel microstructures is well established. The presence of precipitates provides the pinning effect needed to inhibit the grain growth process at elevated temperatures. Therefore these second phase particles are used as a method for grain growth control in microalloyed steel during hot working. However the pinning force of the second phase particles decreases with annealing time as a result of dissolution or coarsening of the precipitates.

This work has been performed using a tube furnace for the various hold times and the experimental aspect is explained in detail in the Experimental Work Chapter 3. The light optical micrograph images of the specimens have been etched with saturated picric acid with a wetting agent to reveal the prior austenite grain boundaries. The full details can be found in the Chapter 4. The austenite grain size was measured using the intercept method ASTM standard E 112.

7.2 Hold at 1050°C (0.08 wt. % Carbon)

7.2.1. Light Optical Microscope (Prior Austenite Grain Analysis)

The prior austenite grain growth evolution is shown in Figure 7-2 for all four compositions ranging from Plain C-Mn steel to 0.02 wt. % Nb. The microstructure shows the evolution of prior austenite grains as a function of hold time of 1 (3600), 3

(10800) and 6 (21600) Hours (Seconds). The corresponding graphical representation of the prior austenite grain size evolution as a function of different hold times is shown in Figure 7-1 with the quantitative analysis is given in Table D-1 in Appendix D.

A linear growth trend is observed for plain C-Mn steel as the time is increased from 1 to 6 hours. However for the 3 niobium alloyed steel a logarithmic growth trend occurs having a steady rapid growth initially until the 3 hour mark followed by slower growth. There is no substantial overlapping of the error bars which are representative of the 95% confident intervals, therefore indicating that there is a real difference in the prior austenite grain size for the low carbon (0.08 wt. C) steel during different holding times. The effect of niobium additions can be seen as the niobium additions are increased the size of the prior austenite grain size decreases as expected due to the formation of the second phase particles which inhibit the growth of the prior austenite grains.

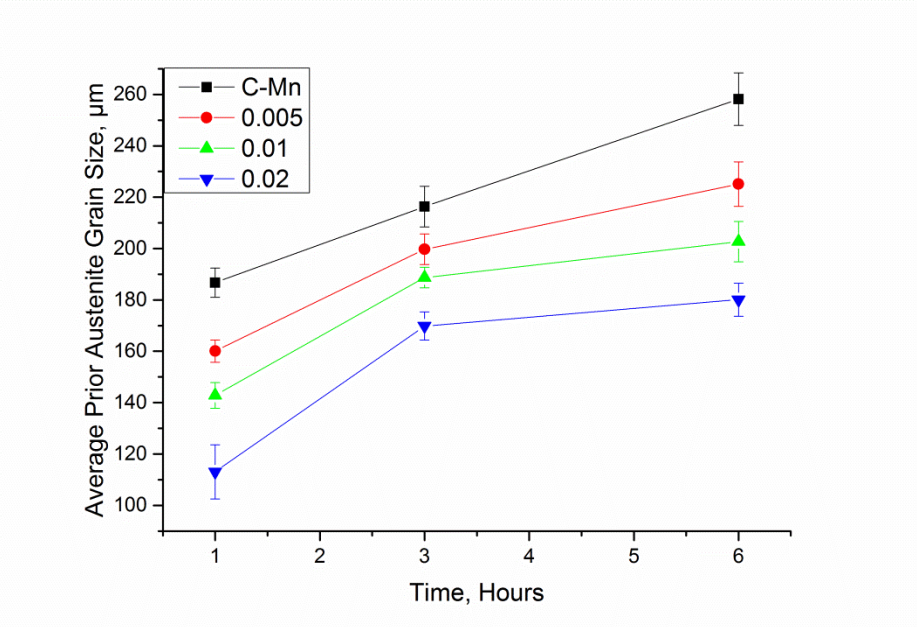

Figure 7-1: Prior Austenite grain size evolution during different hold times at an isothermal temperature of 1050°C. Error bars represent ± 95% CL (0.08 wt. % Carbon)

It is visible that Plain C-Mn steel shown in Figure 7-2 (a, b, and c) does not show any abnormal grain growth increasing hold times at 1050°C. Nonetheless, this is not the case with the niobium bearing steel. There is a decrease in the grain growth rate with steels microalloyed with niobium. This trend is represented in all three steels micro-alloyed with 0.005 wt. % Nb represented in Figure 7-2 (d, e, and f), 0.01 wt. % Nb represented in Figure 7-2 (g, h, and i) and 0.02 wt. % Nb illustrated in Figure 7-2 (j, k, and l).

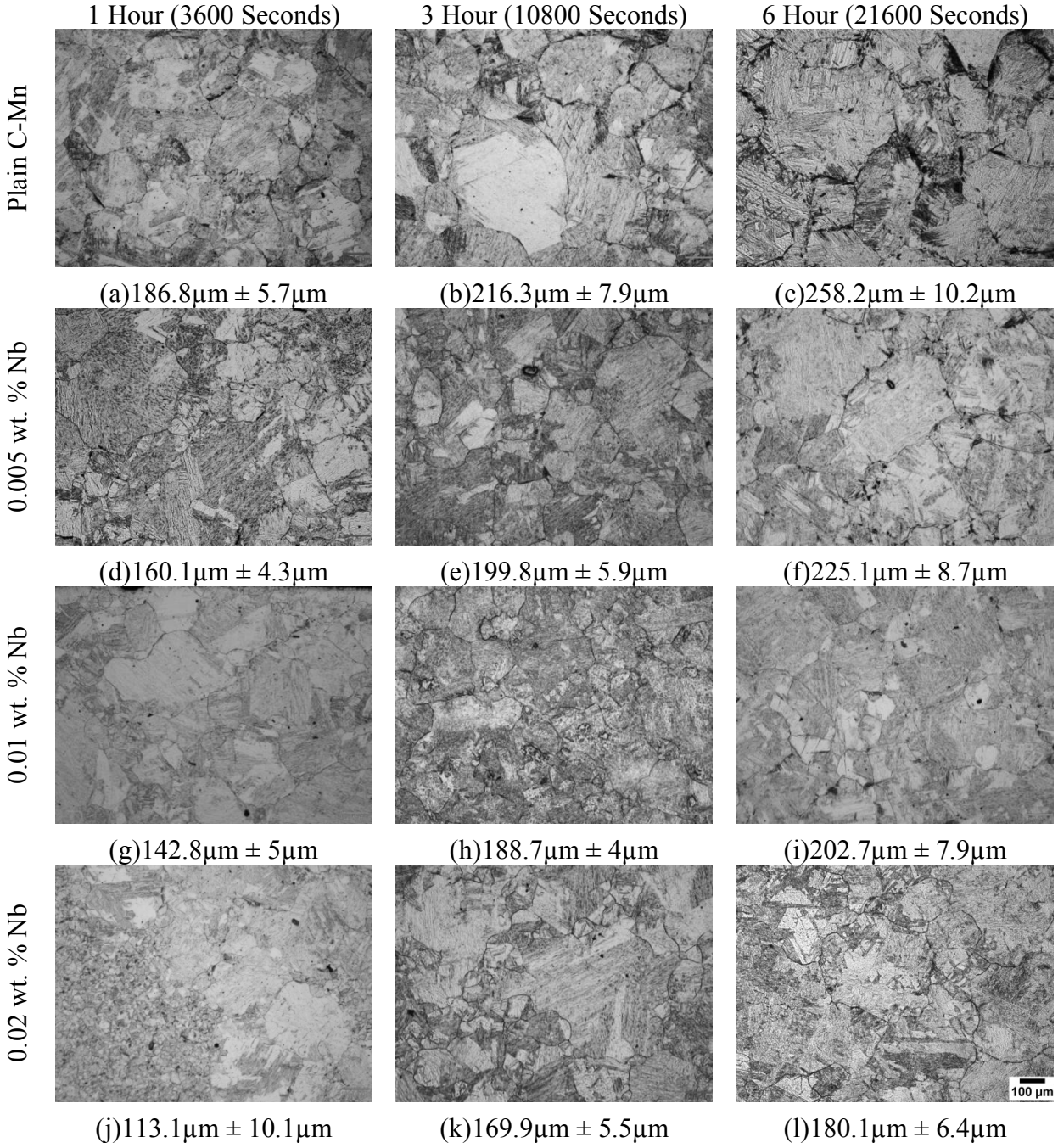

Figure 7-2: Optical micrographs of the evolution of Prior Austenite Grain Size as a fucntion of different hold times at 1050°C. Images (a), (b), and (c) are plain C-Mn Steel. Images (d), (e), and (f) are 0.005 wt. % Nb Steel. Images (g), (h), and (i) are 0.01 wt. % Nb Steel and images (j), (k), and (i) are 0.02 wt. % Nb Steel. (Etched with Picric Acid), 10x magnification and magnification bar (black) 100µm.

Figure 7-3 below shows the graphical representation of the standard deviation (SD) values for the mean size of prior austenite grain size at different holding times. The standard deviation gives an indication of the characteristics of bimodal prior austenite grain microstructure with the varying holding times. It can be seen that there is not

much difference in the standard deviation (SD) value for the C-Mn steel from 1 hour to 6 hours. The prior austenite grain size does not vary much from the mean. The standard deviation (SD) shows a larger deviation after the 3 hour mark for 0.005 wt. % Nb and 0.01 wt. % Nb steel in contrast to the C-Mn steel.

However the standard deviation (SD) value for 0.02 wt. % Nb has completely different characteristics from the other three steel compositions at this temperature. The 0.02 wt. % Nb steel deviates closer to the average prior austenite grain size at the 3 hour mark and then starts to deviate from the average at the 6 hour mark, suggesting a transition from abnormal (discontinuous) to normal (continuous) grain growth. The corresponding micrographs and histograms can be seen in Figure 7-4 for 0.02 wt. % Nb at different time intervals of 1, 3 and 6 hours.

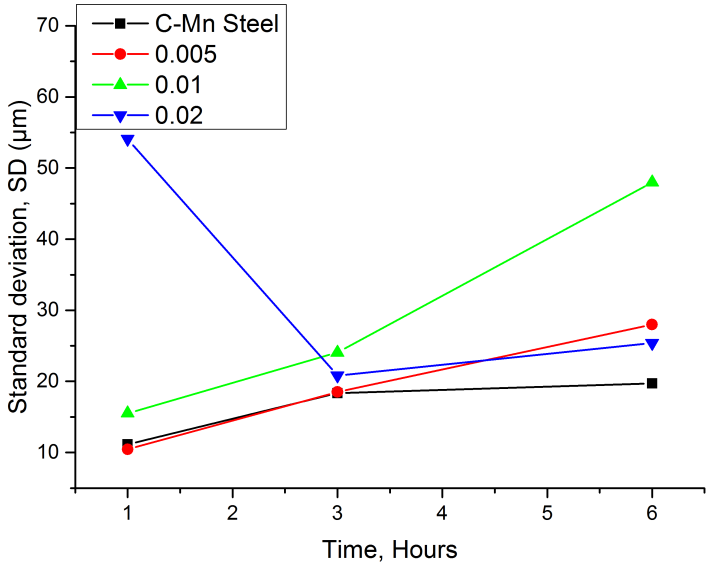

Figure 7-3: The standard deviation values for different holding times from 1 hour to 6 hours at a temperature of 1050°C.

The influence of 0.02 wt. % niobium on the prior austenite grain growth at a reheat temperature of 1050°C can be seen clearly in Figure 7-4. It represents grain evolution as a function of hold time. In Figure 7-4 (a) the bimodal distribution of fine grains and large grains can be seen visually in the optical micrograph (left) and in the corresponding histogram (right) in which two distinct distributions can be observed for a hold time of 1 hour (dotted line represents the small grains and solid line represents the larger grains) the smallest grains being in the region of 52.5µm and the largest being 231.7µm. The transition from a bimodal distribution of prior austenite grains at 1 hour to a normal distribution at 3 hours and a continuation of the normal distribution at 6 hour hold can be seen in Figure 7-4(b, c).

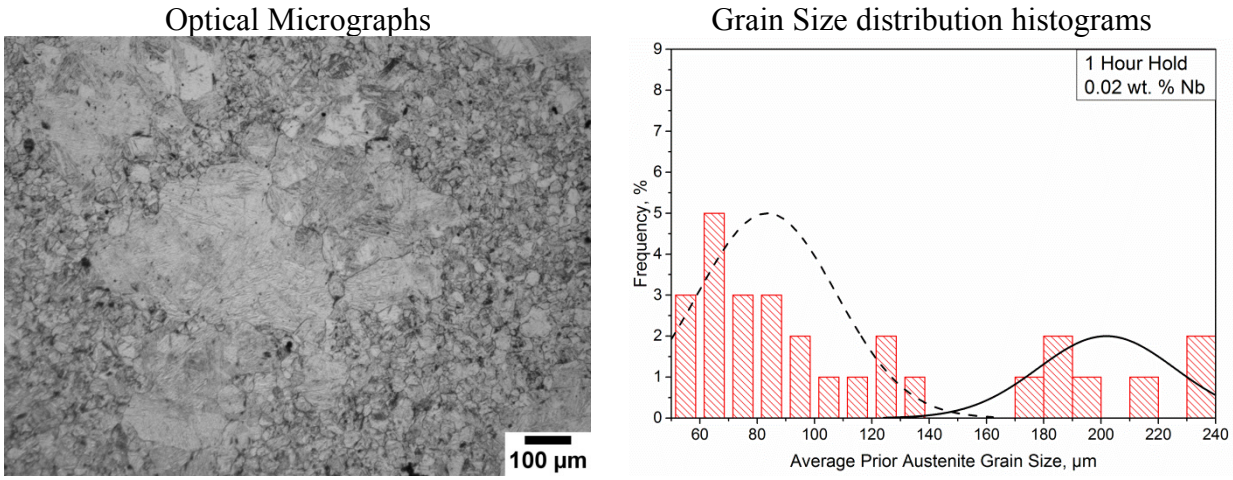

(a) 1 Hour Hold, Abnormal (bimodal distribution)

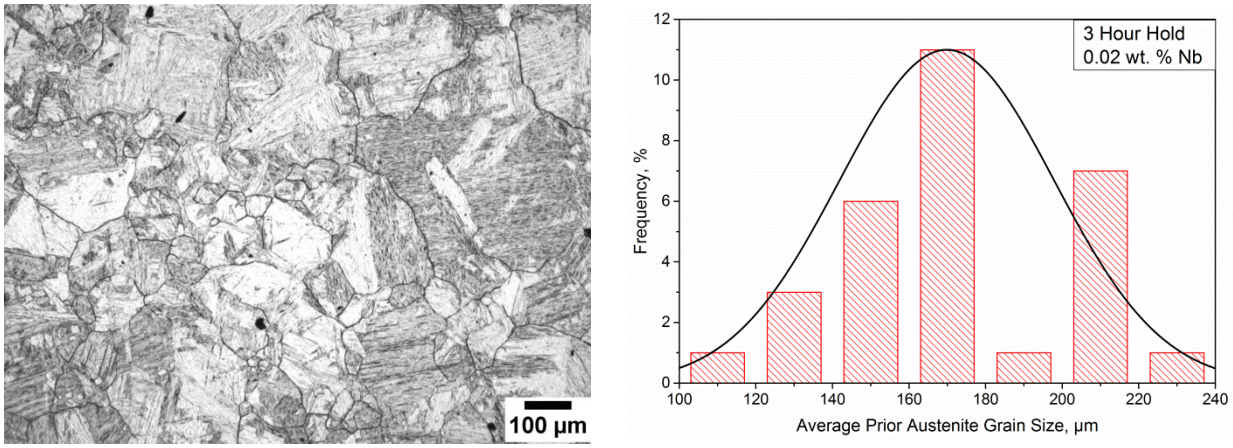

(b) 3 Hour Hold, Normal (unimodal distribution)

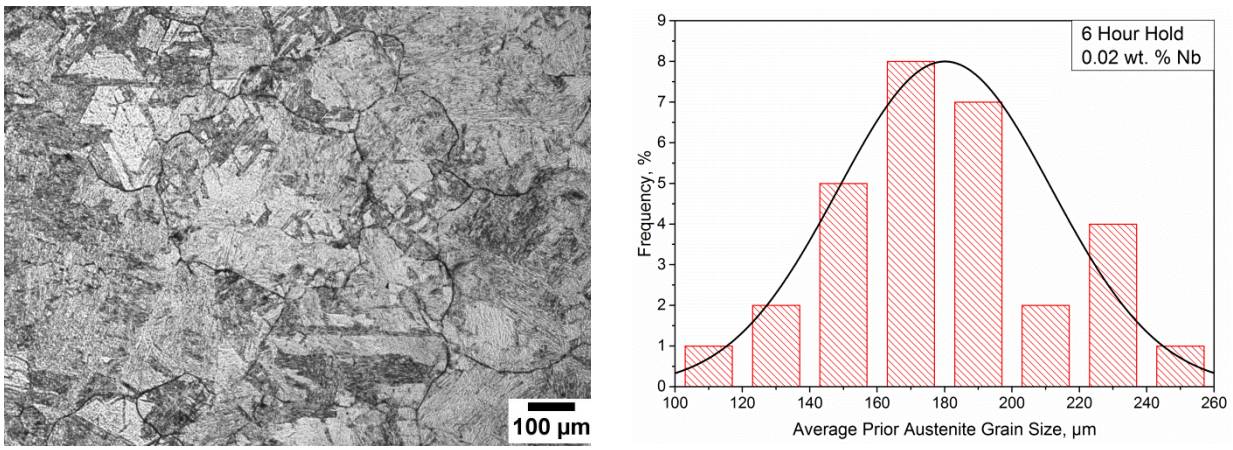

(c) 6 Hour Hold, Normal (unimodal distribution)

Figure 7-4: Optical micrographs (Left) and the corresponding grain size distribution histograms (Right) obtained for isothermal holding times of (a) 1 hour, (b) 3 hours and (c) 6 hours at a reheat temperature of 1050°C.

7.2.2. Transmission Electron Microscopy (TEM) (1050°C)

The precipitation data has been analysed using the transmission electron microscope (TEM) (Tecnai T20) for the steel composition with 0.02 wt. % Nb addition using the carbon replica extraction technique explained in chapter 3. This has been done to gain an insight into the spatial distribution and size of the precipitates. The total number of particles quantified were in the range of 265 to 271. Image J analysis software was used to count the number of precipitates. However a manual count was also carried out in such instances that the software could not distinguish between the dark contrast which was not arising from the precipitates but the carbon replica and the actual precipitates. The manual measurements were made easier because most of the precipitates were circular. The number density of NbC precipitates as a function of varying hold times is obtained by dividing the number of particles by the area of the carbon replicas analysed.

The precipitation distribution, type, and morphology are shown in Figure 7-5(b) which shows the precipitation evolution as a function of hold time of 1 hour, 3 hours and 6 hours. Both fine and large spherical precipitates and very few cuboidal precipitates can be observed at the reheat temperature of 1050°C and for the different holding times. Figure 7-5(a) shows histograms of the precipitation size distribution for the different holding times of 1 to 6 hours. The statistical size distribution analysis revealed that for the 1 hour hold at 1050°C, the mean niobium precipitate diameter size is 18.5 ± 2nm. The 3 hour hold has a mean niobium precipitate diameter size of 27 ± 1.9nm and finally for the 6 hour hold the mean diameter size is 45.5 ± 3.8nm. Figure 7-6 (a) shows a box plot with 1.5 interquartile ranges, it illustrates the distribution of the precipitates as a function of different holding times at 1050°C, and it shows the mean, median and the outliers. The outliers represent the extreme niobium carbide particles sizes which do not fall in the 1.5 interquartile ranges.

Statistical analysis was utilised to critically understand data and any possible differences. A Shapiro-Wilk's test ($p < 0.05$) [128, 129] and a visual inspection of their histograms, normal Q-Q plots and box blots showed that the precipitates were not normally distributed across the 1, 3 and 6 hour hold times, with a skewness of 2.271 (SE 0.148) and a Kurtosis of 4.601 (SE 0.295) for 1 hour hold time; a skewness of 0.611 (SE 0.150) and a Kurtosis of -0.546 (SE 0.298) for 3 hour hold time. Lastly, a skewness of 0.816 (SE 0.150) and a Kurtosis of -0.678 (SE 0.298) was observed for the 6 hour hold time [167, 168].

Further analysis was performed using the Levene test [169] to verify the equality of variances in the data (homogeneity of variance), where a significance was found; $W (2, 801) = 102.847$, $p < 0.01$. This rejected the null hypothesis as there was no equality of variance found in the data [170].

As parametric assumptions were not met, a non-parametric Kruskal-Wallis [171] analysis was carried out to analyse differences in hold times and their effect on precipitates. The analysis found precipitates were significantly affected by hold times, H (2) =166.663, $p < 0.001$.

A non-parametric Mann- Whitney test [172] was performed to look for differences between two independent samples, and a Bonferroni correction [173] (0.05/3) was applied reporting significance at 0.0167. The Bonferroni correction was applied in order to counteract the problem of multiple comparisons. In applying the correction it is considered the most conservative and simple method to help control familywise error rate (FWER). In statistical analysis the FWER is defined as the probability of making one or more false discoveries on an experimental hypothesis when carrying out multiple hypothesis analysis [173].

Data showed there was a difference in precipitates size where the 3 hour hold showed a greater significant difference compared to the 1 hour hold (U= 21665.50, Z = - 7.948, $p<0.001$. There was also a significant difference in 1 hour hold and 6 hour hold times, where the 6 hour hold time showed greater difference in the precipitate sizes (U = 14099.00, z= -12.169, $p < 0.001$. Finally, there was also a significant difference observed between the 3 and 6 hour hold times, where greater significance in precipitate size was found in the 6 hour hold time (U = 23546.50, z= -6.560, $p < 0.001$).

The precipitation number density as a function of hold time is shown in Figure 7-6 (b). It should be noted that the NbC precipitation number density has an intense decrease from 2.35 x 10^{-2} μm^2 to 0.3 x 10^{-2} μm^2 between the 1 and 3 hour hold suggesting dissolution of the precipitates and the precipitation density further decreases to 0.2 x 10^{-2} μm^2 when holding for 6 hours. It is evident that total dissolution does not occur for the NbC at the temperature of 1050°C even at a hold time of 6 hours.

Table 7-1 outlines the descriptive statistics for varying hold time at a temperature of 1050°C for low carbon steel 0.08 wt. % summarizing the mean precipitation diameter size as well as the number of precipitate counts (N).

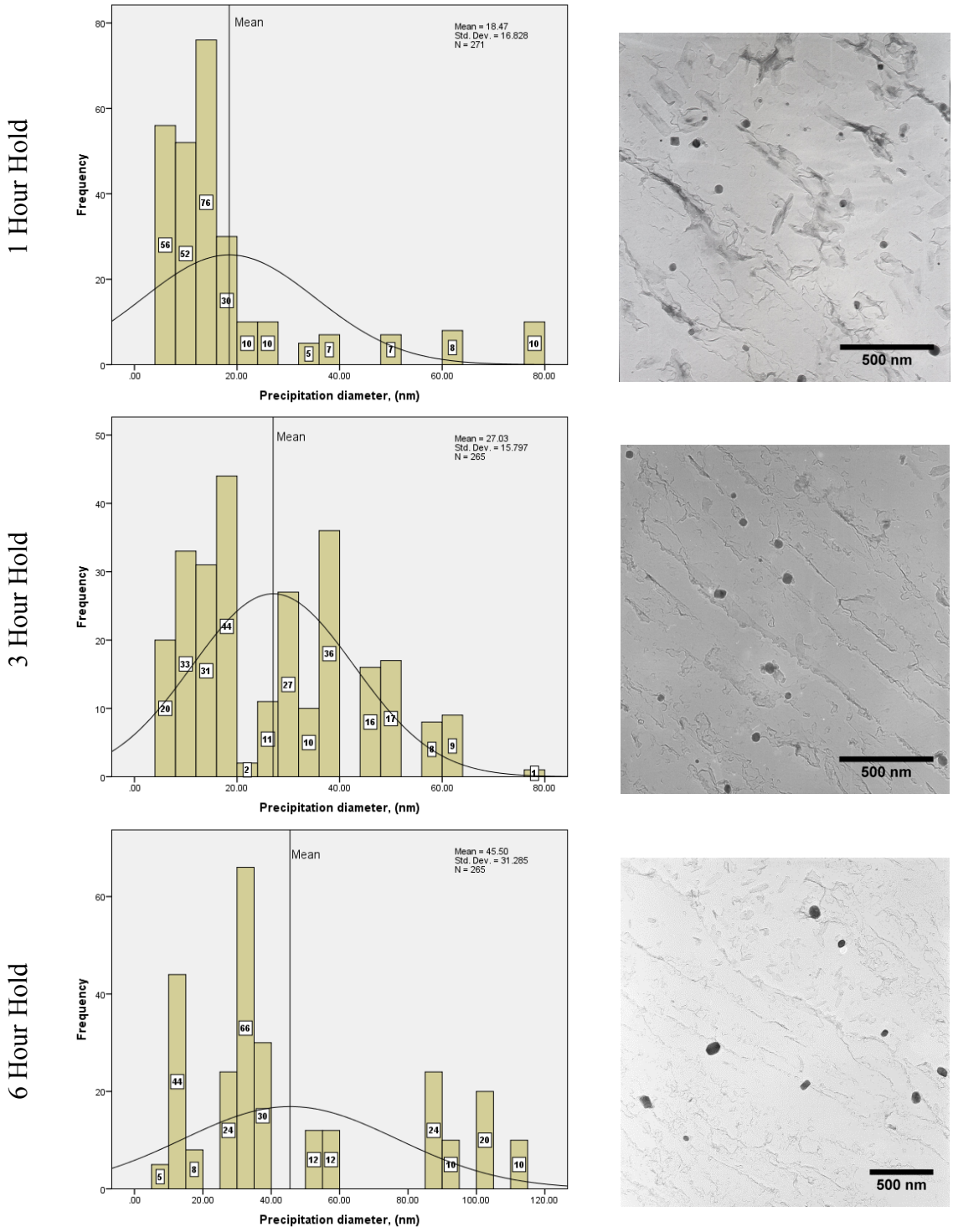

(a) (b)

Figure 7-5: (a) Histogram of the distribution of niobium carbide and (b) TEM bright field micrographs of extraction replicas showing niobium carbide precipitate evolution with respect to different holding times at 1050°C 0.08 wt. % (0.02 wt. % Nb, carbon replica, Tecnai T20).

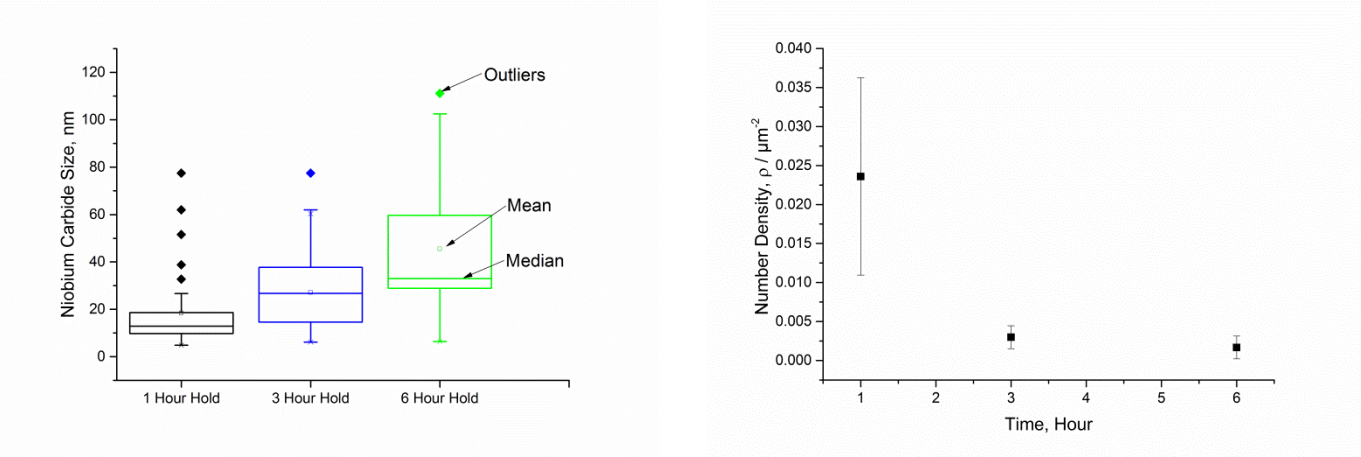

(a) (b)

Figure 7-6: Box plot representing the distribution and the growth trend of the NbC precipitate for varying hold times (b) precipitation number density versus varying hold times.

Table 7-1: Descriptive statistics for varying hold time at a temperature of 1050°C for low carbon steel 0.08 wt %.

Hold Time	Number of precipitates (N)	Minimum (nm)	Maximum (nm)	Mean (nm)	SD. Deviation (nm)
1 Hour	271	4.9	77.5	18.5	16.8
3 Hour	265	6.2	77.5	27	15.8
6 Hour	265	6.5	111.2	45.5	31.3

Figure 7-7 shows a micrograph from an extraction replica of the steel specimen with 0.02 wt. % Nb addition. It can be observed that there are spherical niobium carbide particles indicated by the black arrows, which seem to precipitate along the prior austenite grain boundary which is represented by the black line drawn on the image. The EDX analysis for the particle composition is shown in Figure 7-7 clearly indicating that the particles are niobium carbide (NbC) precipitates due to the carbon (C) and niobium (Nb) peaks. The Cu peak as indicated in the EDX spectra is due to the copper (Cu) grid used for the analysing of the carbon extraction replicas.

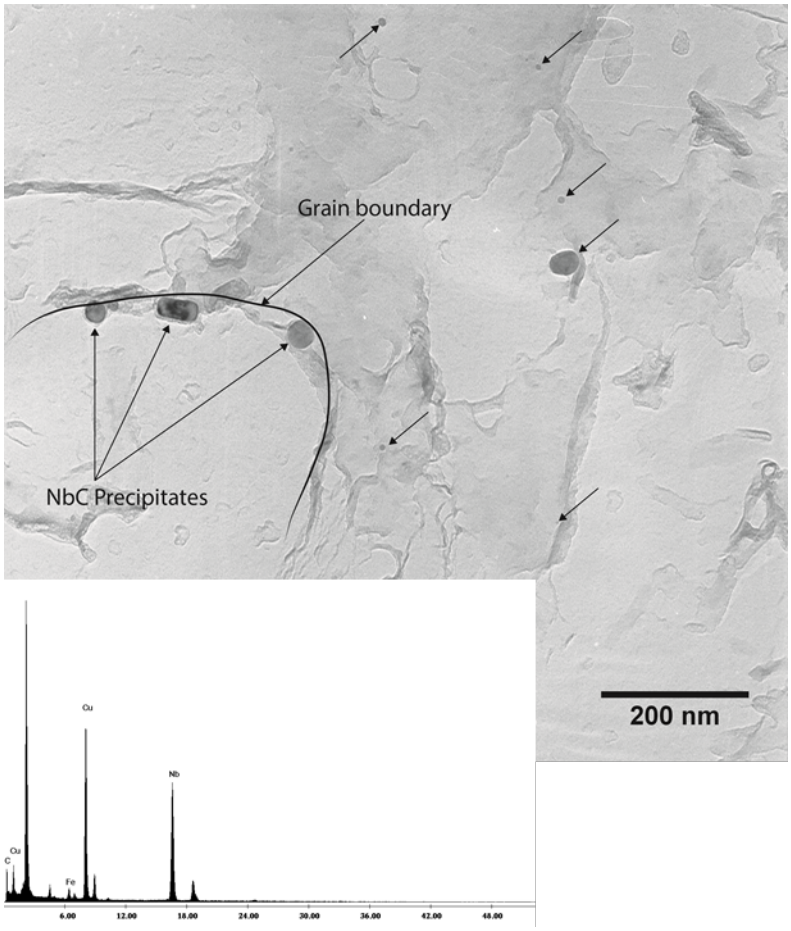

Figure 7-7: TEM image showing NbC particle precipitation along a grain boundary of the specimen held for 1 hour at 1050°C, and the EDX analysis of the NbC particles.

7.3 Hold at 1150°C (0.08 wt. % Carbon)

7.3.1. Light Optical Microscopy (Prior austenite Grain Analysis)

The graphical representation of the prior austenite grain growth against time is shown in Figure 7-8. It can be observed that both plain C-Mn (black line) and 0.005 wt. % Nb (red line) alloyed steel have a linear growth trend with increasing hold time, the linear trend is not observed for 0.005 wt. % Nb alloy at the lower temperature of 1050°C. However, a logarithmic growth trend occurs in both the 0.01 wt. % Nb (green line) and in the 0.02 wt. % Nb (blue line) steels similar to that observed in Figure 7-1 in section 7.2.1 for 1050°C. The quantitative analysis of the austenite grain size for different holding times at a fixed temperature of 1150°C is presented in Table D-2 in Appendix D.

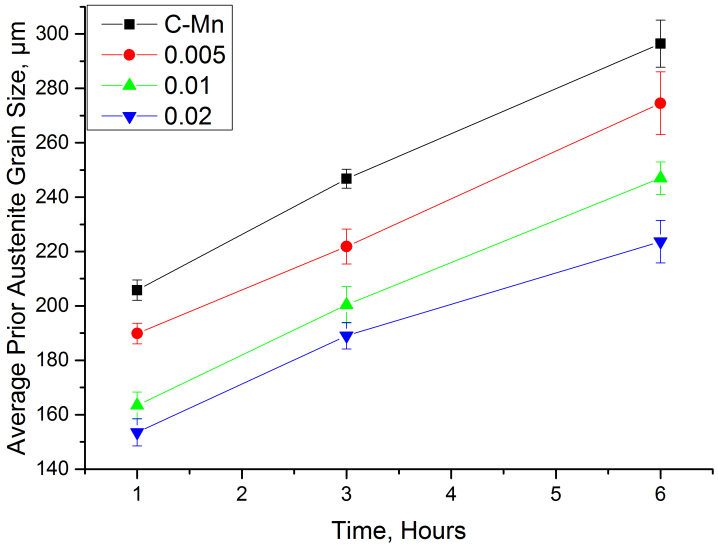

Figure 7-8: Prior Austenite grain size evolution during different hold time at an isothermal temperature of 1150°C. Error bars represent ± 95% CL

The standard deviation SD values for the isothermal hold at 1150°C are shown in the graphical plot in Figure D-1 in Appendix D. The change in SD for the plain C-Mn and 0.005 wt. % Nb bearing steel shows a distinct exponential increase trend with the increase in time from 1 hour to 6 hours. This suggests that abnormal grain growth occurs for these two steel types with increasing time. However for the two remaining steels with compositions of 0.01wt. % Nb and 0.02 wt. % Nb show a logarithmic trend as a function of time. This suggests that abnormal (discontinuous) grain growth still occurs but with a slower rate. The SD numerical values for the plain C-Mn steel and varying niobium content can be found in Table D-2 in Appendix D.

7.3.2. Transmission Electron Microscopy (TEM) (1150°C)

The results of the precipitation diameter distribution for the three different hold times can be seen in the histogram presented in Figure D-2 (a) in Appendix D. The statistical size distribution analysis revealed that for the 1 hour hold at 1150°C, the mean NbC precipitate size is 26.4 ± 2.4nm. For the 3 and 6 hour hold the mean precipitates size are 27.9 ± 2.2nm and 28 ± 6nm respectively as given in Table D-3 in Appendix D. Figure D-3 (a) in Appendix D shows a box plot with 1.5 interquartile ranges. Similar to the earlier box plot it illustrates the distributions of the precipitates as a function of hold times at a reheat temperature of 1150°C; as explained previously the outliers represent the extreme precipitate sizes.

As with the previous temperature of 1050°C, statistical analysis was applied to critically understand data and possible differences. A Shapiro-Wilk's test ($p < 0.05$)

[128, 129] and a visual inspection of their histograms, normal Q-Q plots and box blots showed that the precipitates were not normally distributed across the 1, 3 and 6 hour hold times, with a skewness of 1.333 (SE 0.234) and a Kurtosis of 2.199 (SE 0.463) for the 1 hour hold time, and a skewness of 3.365 (SE 0.190) and a Kurtosis of 18.159 (SE 0.378) for the 3 hour hold time. Lastly, a skewness of 2.119 (SE 0.347) and a Kurtosis of 4.604 (SE 0.681) was observed for the 6 hour hold time [167, 168].

Further analysis was performed using the Levene test [169] to verify the equality of variances in the data (homogeneity of variance), Where a significance was found; $W(2, 317) = 3.972$, $p < 0.05$. This rejected the null hypothesis as there was no equality of variance found in the data [170] meaning it was not a normal distribution.

As parametric assumptions were not met, a non-parametric Kruskal-Wallis [171] analysis was carried out to analyse differences in hold times and their effect on precipitates. The analysis found that precipitate size were not significantly affected by hold times, $H(2) = 2.783$, $p > 0.05$.

The decrease in the precipitation number density as a function of hold time is shown in Figure D-3 (b) in Appendix D. It should be noted that the very low number of precipitates per area μm^2 is due to the high temperatures. Figure D-2 (b) in Appendix D shows the TEM bright field micrographs of the extraction replicas. The TEM micrographs show both small and large spherical and cuboidal precipitates morphologies for the 1 and 6 hour hold. It should be noted that most of the precipitate morphologies were cuboidal. Figure 7-9 shows the morphology and the EDX analysis clearly indicates the composition of the particle being a titanium/niobium carbonitride TiNb(C,N) precipitate with a cuboid morphology. The Cu (copper) peak is that of the Cu grid being used for the analysis of the carbon replicas. It should be pointed out that titanium concentration in the steel is negligible and was not indicated in the inductively coupled plasma optical emission spectrometry (ICP-OES) test. The determination limit for the test for Ti is 0.0004 ppm (parts per million) therefore the Ti concentration in the steel is below this and should be negligible. However it was found that for the reheat temperature of 1150°C and hold times of 1 to 6 hours the majority of the precipitates showed a titanium addition in the precipitates.

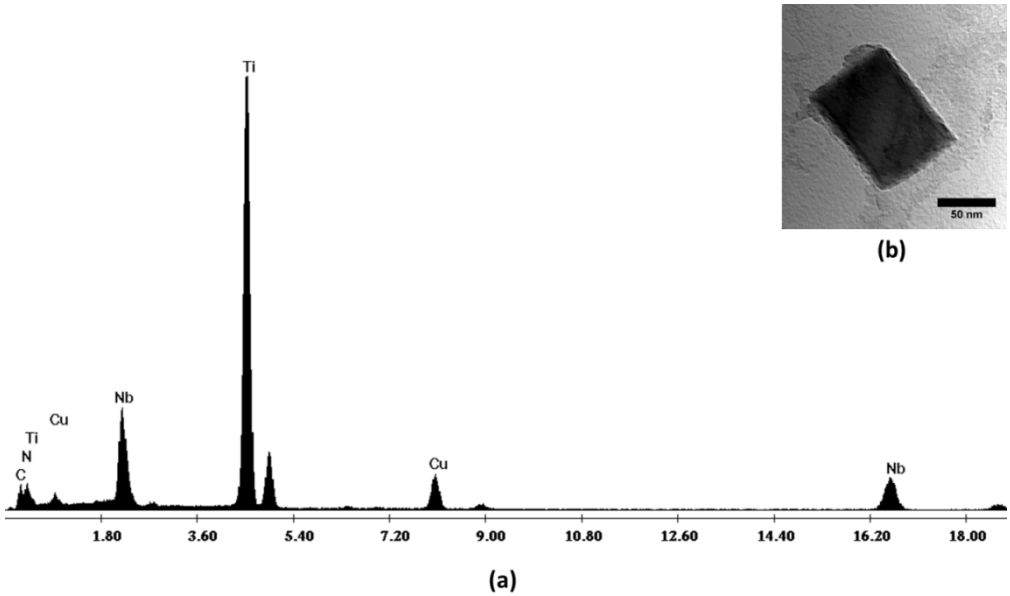

Figure 7-9: (a) EDX of a mixed (Ti,Nb)(C,N) particle, (b) TEM micrograph showing a cuboidal TiNb (C,N)precipitate at 1150°C for 3 hour hold.

7.4 Hold at 1050°C (0.4 wt. % Carbon)

7.4.1. Light Optical Microscopy (Prior Austenite Grain Analysis)

The light optical micrographs for the prior austenite grain growth evolution for medium carbon steel at a temperature of 1050°C with the hold varying from 1 hour to 6 hours is shown in Figure D-4 in Appendix D. The parameters are identical to those presented in the previous section for 0.08 wt. % Carbon steel. The corresponding graphical representation for the micrographs in Figure D-4 is given in Figure D-5 which is for the prior austenite grain growth as a function of time. It can be observed that a similar growth trend is present as for the low carbon (0.08 wt. % Carbon) steel microalloyed with niobium at a temperature of 1050°C. The measurements of the austenite grain size for the different niobium additions are given in Table D-4 in Appendix D.

As shown previously for low carbon steel, the standard deviation values have been used to analyse the abnormality in the prior austenite grain microstructure evolution as a function of time and this is shown in Figure 7-10. It can be observed that there is not much difference and that the standard deviation value remains relatively constant with times from 1 hour to 6 hours for the plain C-Mn, 0.005 wt. % Nb and 0.01 wt. % Nb steels hence implying that there is relatively continuous grain growth (normal grain growth) with increasing hold time.

However the standard deviation (SD) value for 0.02 wt. % Nb decreases with increasing hold time at 1050°C, indicating a similar trend seen previously in Figure 7-3 (0.08 wt. C alloyed with 0.02 wt. % Nb at a reheat temperature of 1050°C) in section 7.2. The standard deviation for this 0.4 wt. % C steel is 25.1µm, which is lower in comparison to 0.08 wt. % where the SD value is 54.1µm both at an initial hold of 1 hour at 1050°C. Overall the trend is indicative of the transition from a discontinuous prior austenite grain growth mechanism to a continuous mechanism.

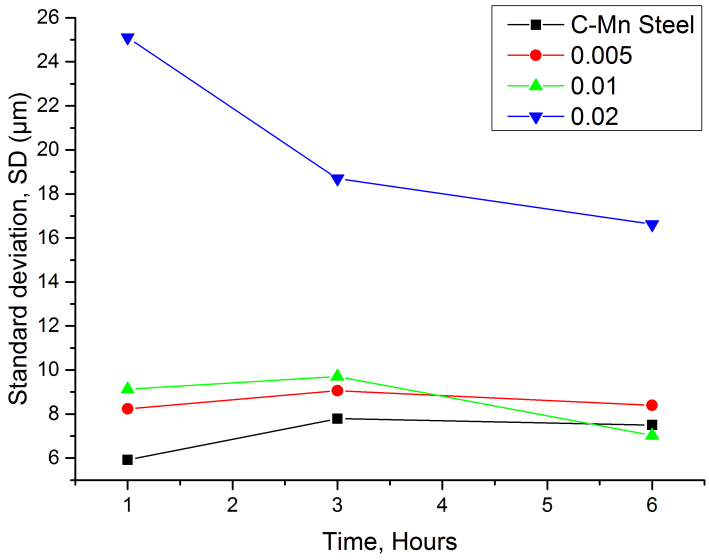

Figure 7-10: The standard deviation (SD) values as a function of different holding times for medium carbon steel (0.4 wt. % Carbon) at a temperature of 1050°C.

7.4.2. Transmission Electron Microscope (TEM) (1050°C)

Figure D-6 (a) shows a distribution histogram for the precipitation size distribution for the different holding times of 1, 3 and 6 hours. The statistical size distribution analysis revealed that for a hold time of 1 hour at a reheat temperature of 1050°C; the mean niobium precipitation diameters are given in

Table D-5 in Appendix D. The extraction replica TEM micrographs can be seen in Figure D-6 (b); both large and small precipitate particles can be observed. The morphologies of the precipitates include cuboidal, and large and small spherical.

As done previously a statistical analysis was applied to critically understand the particle size and distribution differences. A Shapiro-Wilk's test ($p < 0.05$) [128, 129] and a visual inspection of their histograms, normal Q-Q plots and box blots showed that the precipitates were not normally distributed across the 1, 3 and 6 hour hold times, with a skewness of 1.367 (SE 0.173) and a Kurtosis of 1.929 (SE 0.344) for the 1 hour hold

time; a skewness of 1.739 (SE 0.133) and a Kurtosis of 5.901 (SE 0.265) for the 3 hour hold time. Lastly, a skewness of 2.139 (SE 0.140) and a Kurtosis of 6.421 (SE 0.279) was observed for the 6 hour hold time [167, 168].

Further analysis was performed using the Levene test [169] to verify the equality of variances in the data (homogeneity of variance), Where a significance was found; $W(2,839) = 63.16$, $p < 0.01$. This rejected the null hypothesis as there was no equality of variance found in the data [170].

As parametric assumptions were not met, a non-parametric Kruskal-Wallis [171] analysis was carried out to analyse differences in hold times and their effect on precipitates. The analysis found precipitates were significantly affected by hold times, $H(2) = 248.24$, $p < 0.001$.

A non-parametric Mann- Whitney [172] test was performed to look for differences between two independent samples, and a Bonferroni correction [173] (0.05/3) was applied reporting significance at 0.0167. Data showed there was a difference in precipitates where the 3 hour hold showed a greater significant difference compared to the 1 hour hold ($U = 15651.00$, $z = -10.20$, $p < 0.001$). There was also a significant difference in the 1 hour hold and 6 hour hold times, where the 6 hour hold time showed greater difference in the precipitate size ($U = 7383.00$, $z = -14.28$, $p < 0.001$). Finally, there was also a significant difference observed between the 3 and 6 hour hold times, where greater significance in precipitates was found in the 6 hour hold time ($U = 30147.00$, $z = -8.99$, $p < 0.001$).

Figure D-7 in Appendix D illustrates a box plot with 1.5 interquartile ranges, indicating the mean, median and outliers as a function of increasing hold time at a reheat temperature of 1050°C. Figure D-7 (b) in Appendix D indicates the number density of the precipitates as a function of increasing hold time, it should be noted that the precipitation number density has a sharp decrease from 3.49 x 10^{-2} μm^2 to 0.3 x 10^{-2} μm^2 between the 1 and 3 hour hold; suggesting dissolution of the majority of the unstable precipitates. The precipitation number density remains relatively constant for a hold of 6 hours at 0.3 x 10^{-2} μm^2. It is evident that total dissolution does not occur at a reheat temperature of 1050°C even when held for a period of 6 hours.

7.5 Hold at 1150°C (0.4 wt. Carbon)

7.5.1. Light Optical Microscope (Prior Austenite Grain Analysis)

The light optical micrographs of the prior austenite grain growth for plain C-Mn steel and the 3 niobium microalloyed steels at a reheat temperature of 1150°C and hold times of 1, 3 and 6 hours are illustrated in Figure D-8. It can be observed that at a reheat temperature of 1150°C a linear trend is seen with increasing hold time from 1 to 6 hours

hold for the plain C-Mn (black line), 0.005 wt. % Nb (red line) and 0.01 wt. % Nb (green line). However for the 0.02 wt. % Nb (blue line) a logarithmic growth trend with increasing hold time is observed. The quantitative analysis of the austenite grain size for the different holding times at a fixed reheat temperature of 1150°C is shown in Table D-6 in Appendix D.

As shown previously for low carbon steel the standard deviation (SD) values have been used to analyse the abnormality in the prior austenite grain evolution as a function of time. Figure D-9 represents the standard deviation (SD) values measured for all the four different compositions and plotted against a varying hold time of 1 to 6 hours. Firstly the standard deviation (SD) value for plain C-Mn steel indicates that as the hold time increases from 1 to 6 hours at a reheat temperature of 1150°C so does the degree of abnormality present in the overall microstructure of the prior austenite grains. Secondly for the 0.005 wt. % Nb microalloyed steel the standard deviation (SD) indicates that abnormality in the prior austenite grain microstructure also increases with holding time, however the increase in abnormality with time is not as intense as indicated in the plain C-Mn steel. Thirdly a similar trend of abnormality in the prior austenite grains microstructure observed for the 0.01 wt. % Nb steel as was indicated for the 0.005 wt. % Nb steel. Finally the standard deviation (SD) for 0.02 wt. % Nb, indicates normal growth until the 3 hour mark as shown by the constant SD values from 1 to 3 hour hold; however the SD values increase more at the 6 hour mark.

Table D-6 in Appendix D shows the quantitative analysis of PAGS for different holding times at a fixed temperature of 1150°C for medium carbon steel.

7.5.2. Transmission Electron Microscope (TEM) (1150°C)

The statistical analysis for the mean particle size for reheat temperature of 1150°C for hold times of 1 to 6 hours is shown in Table 7-2. Figure D-10(a) illustrates a box plot with 1.5 interquartile ranges, indicating the mean, median and outliers as a function of increasing hold time at a reheat temperature of 1150°C.

As done previously a statistical analysis was applied to critically understand the particle size and distribution differences. A Shapiro-Wilk's test ($p < 0.05$) [128, 129] and a visual inspection of their histograms, normal Q-Q plots and box plots showed that the precipitates were not normally distributed across the 1, 3 and 6 hour hold times, with a skewness of 0.953 (SE 0.160) and a Kurtosis of 1.106 (SE 0.319) for the 1 hour hold time; a skewness of 1.814 (SE 0.222) and a Kurtosis of 4.645 (SE 0.440) for 3 the hour hold time. Lastly, a skewness of 0.61 (SE 0.337) and a Kurtosis of -0.771 (SE 0.662) was observed for the 6 hour hold time [167, 168].

Further analysis was performed using the Levene test [169] to verify the equality of variances in the data (homogeneity of variance), Where a significance was found; W (2, 400) = 18.638, $p < 0.01$. This rejected the null hypothesis as there was no equality of variance found in the data [170].

As parametric assumptions were not met, a non-parametric Kruskal-Wallis [171] analysis was carried out to analyse differences in hold times and their effect on precipitates. The analysis found precipitates were significantly affected by hold times, H (2) =91.061, $p < 0.001$.

A non-parametric Mann- Whitney [172] test was performed to look for differences between two independent samples, and a Bonferroni correction [173] (0.05/3) was applied reporting significance at 0.0167. Data showed there wasn't a significant difference in precipitates between 1 hour and 3 hour hold times (U= 12075.00, Z = -1.862, $p>0.0167$. There was a significant difference in the 1 hour hold and 6 hour hold times, where the 6 hour hold time showed greater precipitate (U = 868.00, z= -9.419, $p < 0.001$. Finally, there was also a significant difference observed between the 3 and 6 hour hold times, where greater significance in precipitate size was found in the 6 hour hold time (U = 716.00, z= -7.781, $p < 0.001$).

Figure D-10 (b) indicates the number density of the precipitates as a function of increasing hold time, it should be noted that the precipitation number density gradually decreases from 1.6 x 10^{-3} μm^2 to 1.5 x 10^{-3} μm^2 between the 1 and 3 hour hold; suggesting dissolution of the majority of the unstable precipitates has already taken place and the remaining precipitates which are stable take longer to dissolve. The precipitation number density remains relatively constant for a hold of 6 hours at 8.5 x 10^{-4} μm^2.

Figure D-11 (a) and (b) in Appendix D represent the chemical composition using EDX analysis and the TEM micrograph of the particle morphology. The EDX peaks indicate that the particle has strong Nb peaks and a weak Ti peak similar to previous EDX measurements, therefore indicating that it is a NbTiC (niobium titanium carbide) particle where the Cu (Copper) peaks occur due to the Cu grid which the extraction replica is placed on.

Table 7-2: Descriptive statistics for varying hold time at a temperature of 1150°C for low carbon steel 0.4 wt %.

Hold Time	Number of precipitates (N)	Minimum (nm)	Maximum (nm)	Mean (nm)	SD. Deviation (nm)
1 Hour	231	6.8	126.5	44.8	21.9
3 Hour	119	15.3	192.59	52.6	31.1
6 Hour	50	23	185.5	111.4	41.3

7.6 Hold at 1050°C (0.8 wt. % Carbon)

7.6.1. Light Optical Microscope (Prior Austenite Grain Analysis)

The micrographs for high carbon steel as a function of 3 different hold times are shown in Figure 7-11. The micrographs can be seen for all the 4 steel compositions from the plain C-Mn steel (without any additions of Nb) to the remaining 3 with niobium additions. It can be seen that for plain C-Mn steel images (a), (b) and (c) the prior austenite grains follow a continuous grain growth mechanism (normal grain growth) as a function of increasing time, which is to be expected as there are no second phase particles exhibiting pinning on grain boundaries. A transition from continuous (normal grain growth) to a discontinuous (abnormal grain growth) can be seen with increasing time in images (d), (e) which show normal grain growth and (f) which shows severe abnormal grain growth at the 6 hour hold mark. Figure D-12 in Appendix D illustrates the isothermal grain growth of the prior austenite grains as a function of hold time from 1 to 6 hours at a reheat temperature of 1050°C.

Figure 7-12 shows the standard deviation (SD) which gives an indication of the bimodality characteristics of the prior austenite grain size in the microstructure by calculating the spread of the prior austenite grain sizes with the varying holding times.

Firstly the standard deviation (SD) for plain C-Mn steel from 1 to 6 hour hold at 1050°C stays relatively constant, implying that the spread of the average prior austenite grain size with increasing hold time remains relatively constant. The corresponding optical micrograph images for plain C-Mn steel are shown in Figure 7-11 (a), (b) and (c).

Secondly, the SD value for the 0.005 wt. % Nb steel illustrates a sharp increase in the bimodality after the 3 hour mark, suggesting that the spread of prior austenite grains from the mean prior austenite grain size becomes severe at the 6 hour mark which can be seen in Figure 7-11 (f).

Thirdly, the bimodality in the prior austenite grains in the 0.01 wt. % microalloyed steel suggests that there is a linear increase in the abnormal grain growth with time; this can also be seen visually in Figure 7-11 (g), (h) and (i).

Finally, the SD for the 0.02 wt. % Nb steel indicates that the transition from continuous (normal grain growth) to discontinuous (abnormal grain growth) occurs after the 3 hour mark and this trend can be seen in Figure 7-11 (j), (k) and (l).

The quantitative analysis of the average prior austenite grain size with the 95% confident limits and their standard deviation values are given in Table D-7 in Appendix D.

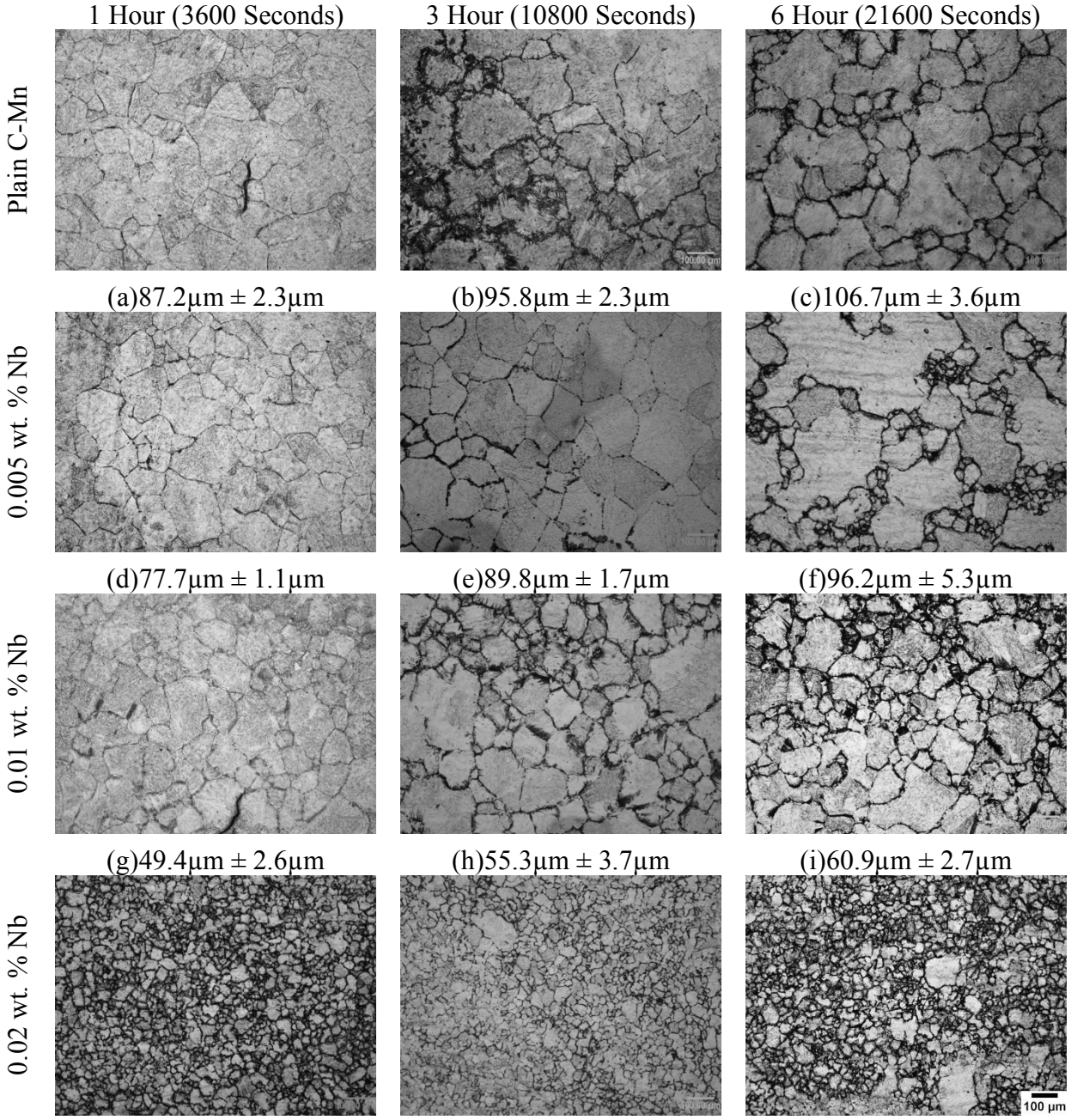

Figure 7-11: Optical micrographs of the evolution of Prior Austenite Grain Size for high carbon steel (0.8 wt. % C) as a function of different hold times at 1050°C. (Etched with Saturated Picric Acid), 10x magnification and magnification bar (white) 100µm.

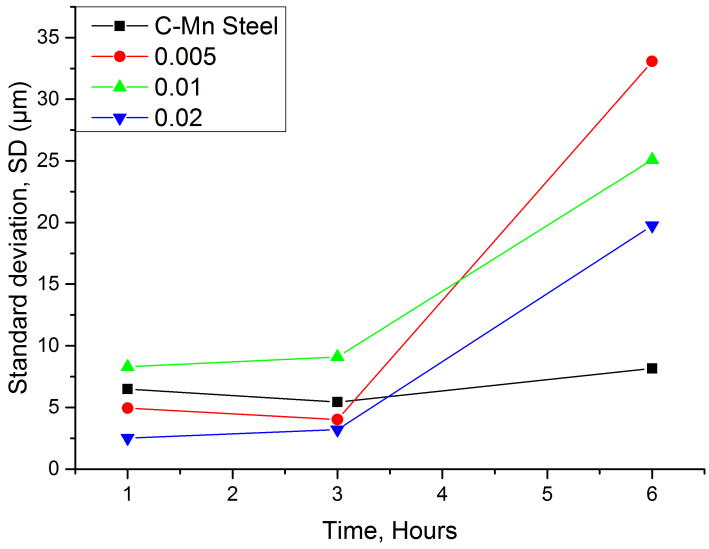

Figure 7-12: The standard deviation (SD) values as a function of different holding times for high carbon steel (0.8 wt. % Carbon).

7.6.2. Transmission Electron Microscope (TEM) (1050°C)

The histogram shown in left hand side of Figure D-13 (a) represents the size distribution of the precipitate particles from a 1 hour hold to a 6 hour hold and the corresponding bright field TEM micrographs are shown on the right hand side of Figure D-13 (b). The statistical distribution analysis of the average particle size indicates an increase in size with increasing holding time. At a hold of 1 hour the average particle size is 55.4 nm, for the 3 hour hold it is 60.2 nm and for a hold of 6 hours it is 71.1 nm. The increasing trend in the mean particle size can also be seen in the box plot shown in Figure D-14 (a).

As with the previous temperatures of 1050°C statistical analysis was applied to critically understand the data and possible differences. A Shapiro-Wilk's test ($p < 0.05$) [128, 129] and a visual inspection of their histograms, normal Q-Q plots and box blots showed that the precipitates were not normally distributed across the 1, 3 and 6 hour hold times, with a skewness of 0.995 (SE 0.122) and a Kurtosis of 1.052 (SE 0.243) for the 1 hour hold time; a skewness of 2.609 (SE 0.165) and a Kurtosis of 8.337 (SE 0.328) for the 3 hour hold time. Lastly, a skewness of 1.906 (SE 0.110) and a Kurtosis of 3.681 (SE 0.220) was observed for the 6 hour hold time [167, 168].

Further analysis was performed using the Levene test [169] to verify the equality of variances in the data (homogeneity of variance), Where a significance was found; W (2,

1109) = 44.058, $p < 0.01$. This rejected the null hypothesis as there was no equality of variance found in the data [170].

As parametric assumptions were not met, a non-parametric Kruskal-Wallis [171] analysis was carried out to analyse differences in hold times and their effect on precipitates. The analysis found precipitates were not significantly affected by hold times, H (2) =4.559, $p > 0.05$.

Figure D-14 (b) illustrates the precipitation number density as a function of increasing hold time from 1 hour to 6 hours at a temperature of 1050°C. As with previous results reported the precipitation number density decreases dramatically after 1 hour when the number density is 9.2 x 10^{-2} μm^2 to 3.7 x 10^{-3} μm^2 for a 3 hour hold, and remains relatively constant for a 6 hour hold at 3.3 x 10^{-3} μm^2. The suggesting dissolution of the majority of the unstable precipitates has already taken place between hold times of 1 to 3 hours and the remaining precipitates which are stable take longer to dissolve in between 3 and 6 hours. Table D-8 shows the descriptive statistics for the precipitate sizes presented above.

7.7 Hold at 1150°C (0.8 wt. % Carbon)

7.7.1. Light Optical Microscope (Prior Austenite Grain Analysis)

The effect of holding at temperature of 1150°C for high carbon steel alloyed with different niobium concentrations is shown in Figure 7-13. As reported with previous for 0.4 wt. % C composition at a reheat temperature of 1150°C plain C-Mn (black line) and 0.005 wt. % Nb (red line) show a linear growth trend with increasing time. However both 0.01 wt. % Nb (green line) steel 0.02 wt. % Nb steel (blue line) show a logarithmic growth. The quantitative analysis of the measurements of the prior austenite grain size for the different holding times for the reheat temperature of 1150°C is shown in Figure 7-13. Table D-9 in Appendix D show the quantitative analysis for the austenite grain size.

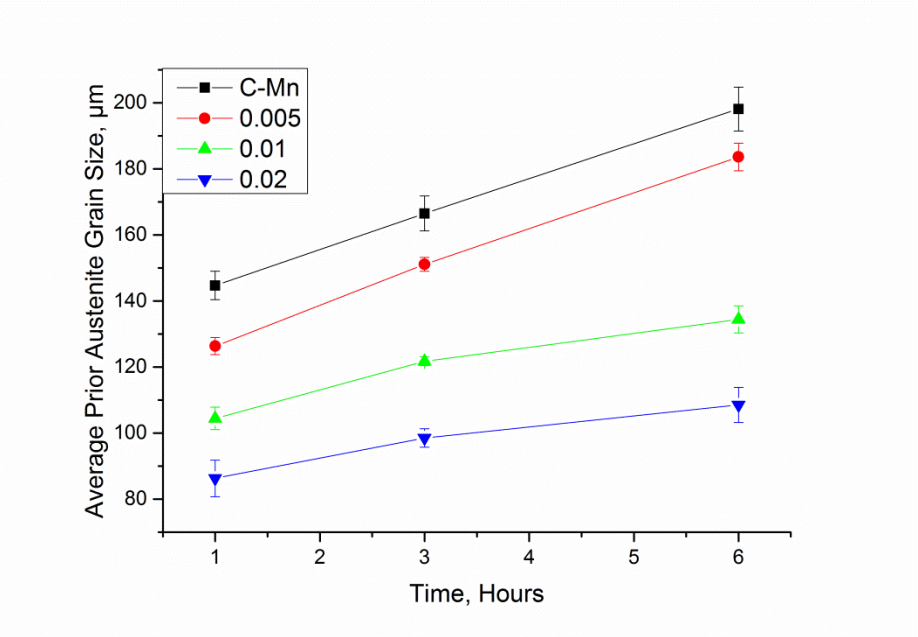

Figure 7-13: Prior austenite grain growth as a function of hold time for 1, 3 and 6 hours at 1150°C.

The standard deviation (SD) values have been used to analyse the abnormality in the prior austenite grain evolution as a function of time at the reheat temperature of 1150°C and are shown in Figure D-15. An interesting point to note is that for plain C-Mn the SD value increases after a hold of 1 hour; therefore suggesting that the degree of abnormality increases even for plain C-Mn steel without any niobium alloying elements.

Secondly, the 0.005 wt. % microalloyed steel has a relatively constant SD value with increasing time, and so this suggests that as the time increases from 1 to 6 hours the prior austenite grains grow in a continuous manner (normal grain growth).

Thirdly, the SD value for 0.01 wt. % Nb steel indicates that abnormality occurs with increasing hold times.

Finally, the 0.02 wt. % Nb steel indicates a different trend as it shows a transition from a high SD value of 13.4µm which is indicative of discontinuous growth (abnormal grain growth) to a continuous growth (normal grain growth) mechanism with increasing time.

7.7.2. Transmission Electron Microscope (TEM) (1150°C)

As previously the statistical analysis show an increase in the average particle size with time is shown in Table D-10 in Appendix D. Figure D-16 shows a box plot representing the median, mean and the outliers as a function of time.

The statistical analysis was performed as with all the previous results to understand if there is any significant difference other than the average particle size. A Shapiro-Wilk's test ($p < 0.05$) [128, 129] and a visual inspection of their histograms, normal Q-Q plots and box plots showed that the precipitates were not normally distributed across the 1, 3 and 6 hour hold times, with a skewness of 2.171 (SE 0.155) and a Kurtosis of 5.311 (SE 0.309) for 1 hour hold time; a skewness of 4.939 (SE 0.219) and a Kurtosis of 30.140 (SE 0.435) for the 3 hour hold time. Lastly, a skewness of 1.907 (SE 0.247) and a Kurtosis of 4.489 (SE 0.490) was observed for the 6 hour hold time [167, 168].

Further analysis was performed using the Levene test [169] to verify the equality of variances in the data (homogeneity of variance), Where a significance was found; $W (2, 460) = 17.285$, $p < 0.01$. This rejected the null hypothesis as there was no equality of variance found in the data [170].

As parametric assumptions were not met, a non-parametric Kruskal-Wallis [171] analysis was carried out to analyse differences in hold times and their effect on precipitates. The analysis found precipitates were significantly affected by hold times, $H (2) =123.179$, $p < 0.001$.

A non-parametric Mann- Whitney [172] test was performed to look for differences between two independent samples, and a Bonferroni correction [173] (0.05/3) was applied reporting significance at 0.0167. Data showed there was a difference in precipitates where a 3 hour hold showed a greater significant difference compared to a 1 hour hold ($U= 7666.00$, $Z = - 7.641$, $p<0.001$. There was also a significant difference in 1 hour hold and 6 hour hold times, where 6 hour hold time showed greater difference in precipitate size (being larger) ($U = 3839.000$, $z= -9.614$, $p < 0.001$. Finally, there was also a significant difference observed between 3 and 6 hour hold times, where a greater significance in precipitates size (being larger) was found in the 6 hour hold time ($U = 3683.500$, $z= -4.602$, $p < 0.001$).

The decrease in the precipitation number density as a function of hold time is shown in Figure D-16 (b). It can be noted that the precipitate number density decreases with time, however an interesting point is that even at this high temperature all the precipitates do not dissolve in solution at 6 hours.

7.8 Summary

The results presented in this chapter with regards to the effect of the alloying addition with increasing hold time and for different carbon contents at a reheat temperature of 1050°C and 1150°C are summarized. As expected for plain C-Mn steel without any niobium additions, the growth of the prior austenite grains are linear as a function of increasing time. When niobium additions are present in the specimen

at1050°C the growth trend is logarithmic. It has also been demonstrated that increasing the carbon content alone decreases the austenite grain size during holding for different times. The effect of niobium on the grain size becomes more pronounced as the carbon content increases; this has also been shown to change the abnormal grain growth behaviour of the austenite grains.

On the other hand, when the reheat temperature is raised to 1150°C the growth trend for plain C-Mn and 0.005 wt. % Nb steel are linear with increasing time. As for 0.01 wt. % Nb and 0.02 wt. % Nb steels, both experience a logarithmic growth trend.

The standard deviation (SD) was used to measure the bimodality of the prior austenite grains and has shown that other than hold time, reheat temperature also plays a major part in normal/abnormal grain structure together with the wt. % of Nb that the majority of the precipitates are of niobium carbides (NbC)

7.9 Discussion on Effect of Hold Time

It was shown earlier that abnormal grain growth occurs for certain compositions at specific reheat temperatures due to the Ostwald ripening and once a heterogeneous initial austenite structure is formed it is difficult to remove [5], as well as being detrimental to the mechanical properties. The effect of Zener pinning and solute drag factors are important considerations when deciding on the reheat and hold time.

Figure 7-1, Figure D-5 and Figure D-12 show grain coarsening with increasing hold time at 1050°C and Figure 7-8, Figure D-8 and Figure 7-13 show grain coarsening with increasing hold time at 1150°C for plain C-Mn and C-Mn-Nb steels. Moreover, the grain growth rate during reheating depends on the composition, heating temperature and hold time. The prior austenite grain size was much bigger in plain C-Mn steel and becomes smaller as the Nb concentration increased due to the pinning of the grain boundaries by the NbC particles.

In Figure 7-1 the plain C-Mn steel prior austenite grain size shows a linear increase as the hold time increases. This is to be expected as there are no second phase NbC particles restricting grain growth, this trend is not seen in the microalloyed steels.

Low (0.08 wt. %) carbon steel alloyed with 0.005 wt. % Nb indicates normal grain growth for a hold time of 1 hour with a standard deviation of 10.46μm but with a gradual increase to 18.5μm and 28μm for 3 and 6 hours respectively. The equilibrium dissolution temperature for this composition is calculated using Equation (6-1) which indicates that all the NbC particles should be in solution at 954°C. Taking the solubility temperature into account it would be reasonable to assume that a slight increase in the heterogeneity of the prior austenite grain distribution can be a result of the solute drag theory [9, 6, 7]. Because Nb atoms segregate to the grain boundaries exhibiting a strong solute dragging effect, the magnitude of the retarding on grain growth is governed by the concentration of the solute element [43]. The solute drag theory according to Cahn [6] is that the drag effect exerted by the Nb solutes reduce the grain interface mobility in a non-linear fashion depending on the velocity. This can be seen in Figure 7-1 where plain C-Mn steel shows a linear increase and 0.005 wt. % Nb shows a non-linear increase with time. The influence of solute drag on grain growth decreasing with increasing temperature can been observed in Figure 7-8 for 1150°C, where the specimen alloyed with 0.005 wt. % Nb shows an linear increase with time similar to that of plain C-Mn steel. This implies that the drag effect exerted by Nb solute atoms has a larger effect on retarding austenite grain growth at lower temperatures of 1050°C than at higher temperatures of 1150°C.

When microalloyed with 0.01 wt. % Nb, prior austenite grain characteristics at the lower temperature range of 1050°C also show a non-linear grain growth and indicate a standard deviation of 15.52μm which is indicative of normal grain growth. However a gradual increase up to 24.06μm at the 3 hour mark after which a sharp increase in heterogeneity of the prior austenite grains occurs to 48μm at the 6 hour mark when the reheat temperature is 1050°C. Once again taking into account the solubility temperature and the reheat temperature for this composition which is 1026°C and 1050°C, it can be assumed that both NbC precipitates and Nb solute atoms play a part in retarding of the austenite grain growth giving it non-linear grain growth characteristics. The observed heterogeneity in the austenite grains during holding to such a close range of the dissolution temperature is attributed to progressive particle dissolution and coarsening. At a higher temperature of 1150°C the austenite grain growth becomes linear, similar to that of plain C-Mn steel. This is expected as all of the NbC precipitates should be in solution and that any hindrances to grain growth occurs due to solute Nb atoms which at higher temperatures (1150°C) do not exert significant drag at the grain boundaries, hence the heterogeneity of the austenite grains in the microstructure is lower (this can be seen in Table D-2 in Appendix D) than that observed at the lower temperature of 1050°C.

The solute drag effect on the austenite grain boundary motion is primarily dependent on the diffusion of the solute atoms in the solvent Fe (iron) matrix and the short range self-diffusion of Fe atoms to the growing austenite grains. During the reheating process, the solute Nb atoms have a strong tendency to spontaneously segregate to the grain boundaries in order to reduce the overall energy of the matrix. The segregation occurs because the Nb atoms are not the same size as the Fe atoms and do not fit perfectly in to the vacant Fe lattice sites. The atomic radius of Nb is about 15% larger than that of Fe [174] therefore the Nb atoms introduce a local energy increase by pushing the neighbouring Fe atoms. The highest amount of disorder is at the grain boundaries which provide a large driving force for the solute atoms to segregate at the grain boundaries reducing the overall energy. The Nb atoms have different diffusion speeds in different temperature regions. At the lower temperature range the diffusion of Nb solute atoms is slow and the grain boundary mobility is also low in velocity. As the grain boundary mobility is low at the lower temperature it cannot break away from the solute Nb atoms at the grain boundary interface and therefore as the grain growth takes place the segregated Nb atoms at the grain boundary exert a solute drag effect, inhibiting the grain growth process. This process of inhibiting grain growth by solute drag is similar to that of Cottrell atmospheres[11] [175] inhibiting the movement of dislocations. In this case

[11] Condition for Cottrell atmospheres formation is that the temperature has to be sufficiently high for defect migration to take place, but not high enough for the entropy contribution to the free energy to result in evaporation of the atmosphere into the solvent.

it is the solute Nb atoms that have the dominating effect of inhibiting austenite grain growth lower temperatures. At higher temperatures, the grain boundary mobility velocity increases and the atmosphere of segregated Nb solute atoms at the grain boundaries starts to decrease. As the temperature reaches a critical value, the grain boundary eventually breaks away from the Nb solute atmosphere. At this critical point the grain boundary undergoes a transition from dragged grain boundary migration to free migration. As a consequence of the diffusion rate of Nb above this critical point of 1150°C, Nb atoms cannot keep up with the grain boundary velocity, hence the Nb solute drag is no longer obvious above the critical temperature [9, 6].

Implying that as diffusion of Nb atoms to the grain boundary increases with time, the solute Nb atoms would further reduce the mobility of the austenite grain boundaries with increase in hold time at either of the two temperatures of 1050°C and 1150°C.

Initially, abnormal grain growth is observed at a reheat temperature of 1050°C for low (0.08 wt. %) carbon steel alloyed with 0.02 wt. % Nb for a hold time of 1 hour. There is a transition from abnormal to normal grain growth for holding at an extended period of 3 and 6 hours. The initial abnormal grain growth is a result of the reheat temperature being very close to the complete dissolution temperature of 1106°C, hence the less stable NbC precipitates start to dissolve or will begin to coarsen due to coalescence. This leads to abnormal grain growth at the depleted zones where the pinning force is no longer enough to restrict growth of the austenite grains. The heterogeneous grain structure can be seen in the optical micrographs in Figure 7-4 with the corresponding austenite grain distributions. Two distinct peaks can be seen, showing small grains and large grains. As the hold time increases from 3 to 6 hours further dissolution/coarsening and a decrease in number density of NbC precipitates occurs reducing the effect on grain boundary retarding during grain growth.

When holding this composition (0.08 wt. % C, 0.02 wt. % Nb) at 1150°C (which is 44°C above the dissolution temperature) the majority of the NbC precipitates would be in solution and grain growth would be retarded by a mixture of the remaining NbC precipitates and solute Nb atoms. A more detailed analysis regarding the NbC precipitates will be discussed later.

Figure 7-14 indicates the percentile change in the grain growth with time intervals of 1 to 3 hours and 3 to 6 hours. An interesting point to note is that for plain C-Mn steel the rate of grain growth increases at both temperatures. However the rate of growth is higher at higher temperatures. On the other hand, the microalloyed steel indicated an increase in grain size change during the 1 to 3 hour hold with increasing Nb content, and during the second half of the hold time from 3 to 6 hour holds the rate of change in the grain size decreases once again with increasing Nb content. As explained earlier this is due to the dissolution/coarsening of NbC precipitates. As for the percentile change at

higher temperature (1150°C), the change does not slow down for 0.005 wt. % Nb, due to the ineffective retarding of the austenite grain boundaries by Nb solute atoms. However because of the higher concentration of the remaining two Nb content alloyed steels which both show a decrease in the change during the 1 to 6 hour hold, this is explained by solute theory.

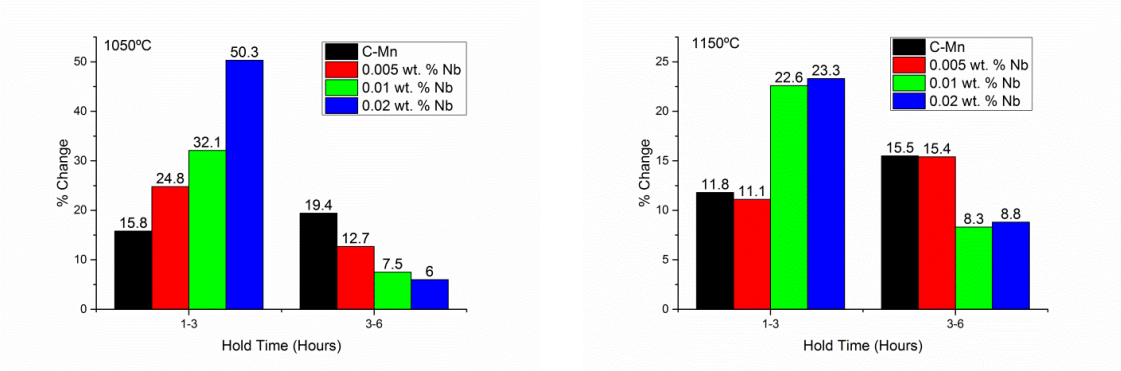

(a) (b)

Figure 7-14: The percentile change in grain growth at two different temperatures for hold times of 1 to 3 hours and 3 to 6 hours for low carbon (0.08 wt. %) steel.

Further detailed analysis on grain growth for both the holding temperatures (1050°C and 1150°C) can be made using TEM to observe the characteristics of NbC precipitate diameter (nm) using from carbon extraction replicas[12]. The mean NbC precipitate diameter increase in size as the hold time changes is shown in Figure 7-5. Fine and large spherical precipitates and very few cuboidal precipitates can be observed at the reheat temperature of 1050°C and for the different holding times, with the EDX analysis indicating the particles are NbC (shown in Figure 7-7). At a hold time of 1 hour the average particle diameter was 18.5nm with the smallest particle size at 4.9nm and the largest being at 77.5nm. As explained earlier, fine dispersions of precipitates ≤ 20nm (diameter) are the most effective forms of precipitates [176, 177]. This increase in the NbC precipitate size (diameter) can explain why abnormal grain growth occurs at 1050°C at a hold time of 1 hour. Gladman, et al., [73] have shown in Equation (2-5) that the inception of abnormal prior austenite grain growth may be due to Ostwald ripening of the precipitates. As holding time increases the NbC particle coarsens above a critical particle radius $r > r_{crit}$, reducing the pinning force required for pinning the prior austenite grains which in turn will grow and consume the neighbouring grains. The less thermodynamically stable NbC precipitates will shrink if the $r < r_{crit}$ and dissolve into solution, this would also result in a decrease of the number density of the precipitates

[12] The TEM analyses have only been done for the highest niobium content (0.02 wt. % Nb) steel specimens.

from 2.35 x 10^{-2} μm^2 to 0.3 x 10^{-2} μm^2 between 1 to 3 hours and further decreases to 0.2 x 10^{-2} μm^2 when holding for 6 hours with increasing hold time at 1050°C. Therefore the transition back to normal grain coarsening occurs because the Zener pinning is ineffective on the austenite grain boundaries due to the increase in the NbC precipitate size and the decrease in the number density of the precipitates.

At the higher temperature of 1150°C, a low number of NbC precipitates where observed in total. 1 hour (107), 3 hour (165) and 6 hour (47) compared to 1 hour (271), 3 hour (265) and 6 hour (265) at 1050°C. The mean NbC precipitate size and the decrease of the number density of the precipitates are shown in Table D-3 in Appendix D. The solubility temperature calculated by Palmiere et al., [68] suggests a complete dissolution temperature for NbC to be at1106°C. The coarse precipitates at this temperature all had elemental traces of Ti with cuboid and irregular spherical morphology. This suggests that the presence of even a small amount of Ti significantly retards the dissolution kinetics of Nb and therefore increases the thermodynamic stability of the complex TiNb(CN), even for hold times of up to 3 hours at 1150°C which was not adequate to dissolve precipitates. Qin et al., [178] investigated the effect of trace amounts of Ti on Nb precipitates during reheating of steel and also indicated that the TiNb(CN) precipitate morphology is cuboid and irregular spherical, Ti has also been shown to increase the thermodynamic stability of the complex TiNb(CN) precipitate compared to NbC, therefore increasing the complete dissolution temperature. These findings are consistent with this work.

An interesting point to note is that the number of precipitates observed at the 6 hour mark had decreased dramatically. This could suggest that all the NbC precipitates have dissolved, and that the larger TiNb(CN) precipitates have little or no effect on restricting austenite grain growth [176, 177].

As explained earlier, particle coarsening is observed by the Ostwald ripening mechanism which is described by Lifshitz, Slyozov and Wagner in Equation (7-1). The growth rate of the second phase particles increases with increasing temperature and time [1]. The particle coarsening depends on the diffusivity coefficient and the diffusion flux. The diffusion flux effected by an increase in the diffusion rate and the effect of temperature on the solubility of the elements in the matrix.

$$r^3 - {r_0}^3 = \frac{8DC_e\sigma V_m^2}{9RT}t = Kt \tag{7-1}$$

Where D is the diffusivity coefficient, C_e the equilibrium solute concentration, σ is the interfacial energy, V_m^2 is the molar volume, R is the gas constant, T is the temperature, and K is the coarsening rate in $m^{-3}s^{-1}$ with time, t.

During reheating at 1050°C the stable carbide precipitates have a tendency to coarsen due to the dissolution of less thermodynamically stable carbides, which is indicated by the decrease in number density.

Similar results have been shown for microalloyed [1, 165, 179, 180, 181] steels in that the higher the temperature before the precipitates completely dissolve, the coarser the Nb(C) particles become and the number density (volume fraction) of the precipitates present in the matrix decreases.

7.9.1. Effect of Different Carbon and Niobium Content

The Discussed earlier was the effect of grain growth and carbide precipitate characteristics of 0.02 wt. % Nb in low (0.08 wt. %) carbon steel. Now the effect of varying carbon content will be discussed. First of all it is known that the increasing the carbon content reduces the solubility of Nb in austenite phase during reheating, which is a contributing factor to the re-precipitation of NbC during rolling later down the processing route. Although, much attention has been given to the effect of carbon concentration with respect to hot deformation and on unreformed austenite grain growth particularly in regards to plain C-Mn steel [182, 87, 183, 184], little research has been done on microalloyed steels with increasing carbon content especially with Nb alloying additions. Speer & Hansen, [180] investigated a series of steels containing a constant level of 0.05 wt. % Nb, with carbon levels varying from 0.008 to 0.25 wt. %. They showed that the carbon content has a substantial effect on the recrystallization behaviour, indicating that solute drag had a relatively small effect compared to carbonitride precipitation. Coladas el al., [165] investigated Nb content of (0.03 wt. % to 0.10 wt. %) with carbon content of (0.4 wt. % to 0.8 wt. %) and its effect on austenite grain growth. The findings were unable to conclude a concrete correlation to the effect of increasing carbon on the prior austenite grain size, as the compositions were not kept constant as they have been in this work. In Figure 7-15, the effect of different carbon content on the austenite grain size during holding at 1050°C can be seen for plain C-Mn and microalloyed steels.

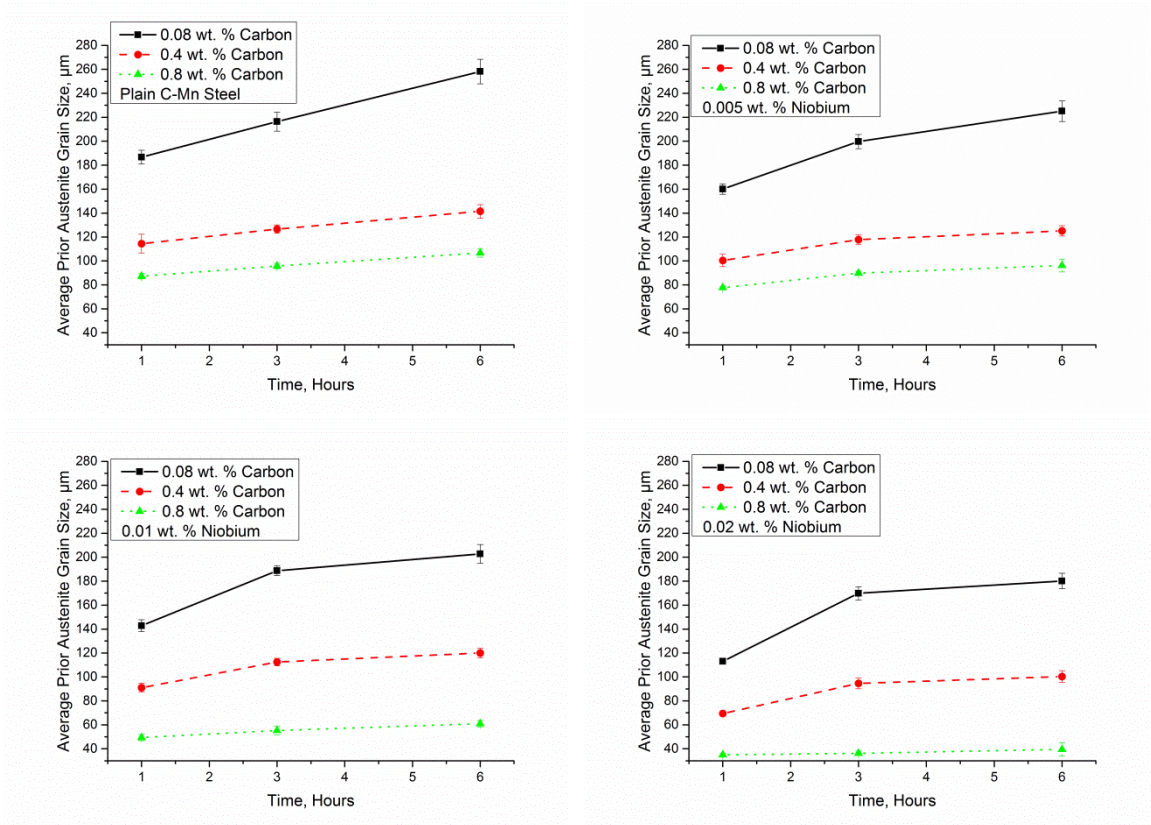

Figure 7-15: The effect of carbon and niobium on the average austenite grain size at low temperature 1050°C.

The characteristics for prior austenite grain growth regarding low (0.08 wt. %) steel have already been discussed. However, increasing the carbon content from 0.08 w. % C to 0.4 wt. % and 0.8 wt. % in plain C-Mn steel compositions, without any alloying elements, gives the same linear austenite grain growth trend irrespective of the carbon content. This linear growth rate is because no second phase particles are present to pin the grain boundaries and is indicative of normal grain coarsening behaviour as shown by the standard deviation values in Figure 7-10 for 0.4 wt. %C and Figure 7-12 for 0.8 wt. %C. The standard deviation values remained relatively constant at 5.9µm to 7.8µm for medium (0.4 wt. %) carbon and 6.5µm to 8.2µm for high (0.8 wt. %) carbon steel. For the initial 1 hour hold there is a 38.7% decrease in austenite grain size when increasing the carbon content to 0.4 wt. % C from 0.08 wt. % C. This decrease in the austenite grain size is further observed when further increasing the carbon content from 0.4 wt. % C to 0.8 wt. % C with a 23.8 % decrease in the austenite grain size. As there are no carbide forming elements in the plain C-Mn steels, responsible for grain growth suppression, solute drag is expected to be the primary reason for the decrease in the austenite grain size. This indicates that the higher the carbon solute content in steel the more pronounced the solute drag effect becomes. These findings are consistent with other investigations on plain C-Mn steels with different carbon content [87, 183].

All microalloyed steels experience a non-linear growth. Starting with 0.005 wt. % Nb, a non-linear trend is seen. The explanation of this for low (0.08 wt. %) carbon steel is given earlier and is attributed to the solute drag effect. The non-linear trend is observed in medium (0.4 wt. %) and higher (0.8 wt. %) carbon steels. It is important to consider the complete dissolution temperature for this composition which is 1134.9°C (0.4 wt. % C) and 1229.9°C (0.8 wt. % C).

However for the medium (0.4 wt. %) carbon steel it has been shown by Equation (6-4) that the T_{GC} is 899.9°C and the heterogeneous austenite microstructure is experimentally observed at 950°C as shown in Figure 6-9(a). Therefore it would be acceptable to assume that the non-linear trend of austenite grain growth is a combination of solute drag by the dissolved Nb atoms and NbC precipitate pinning grain boundaries. However the constant standard deviation values with increasing holding time indicate a homogenous austenite microstructure (normal grain coarsening), therefore it could be concluded that no dissolution/coarsening occurs during this temperature (1050°C) and all the precipitates are relatively thermodynamically stable. Further, when returning to the earlier discussion regarding different reheating temperatures it can be seen from Figure 6-8 that the austenite grain structure remains homogenous between 1000°C - °1100°C, indicating that normal grain coarsening is occurring with the remaining stable precipitates until above 1100°C where there is a transition to abnormal grain coarsening (heterogeneous austenite structure) as the temperature gets closer to the complete dissolution temperature.

When analysing the high (0.8 wt. %) carbon steel it can be seen in Figure 7-12 that a heterogeneous austenite grain structure forms after the 3 hour mark which is clearly visible in Figure 7-11 (f) at 1050°C. The start of dissolution/coarsening of NbC precipitates for this composition are first seen at 1000°C (Figure C-7 in Appendix C), which indicates that prior to holding at 1050°C, dissolution/coarsening had already started to commence. However total dissolution does not occur till 1229.9°C. Therefore, thermodynamically stable fine NbC precipitates are still present, restricting abnormal grain growth from occurring at this temperature (1050°C). Nonetheless, isothermal holding at elevated temperatures close to that of the complete dissolution temperature results in an Ostwald ripening effect of the precipitates. Since the pinning force on the grain boundaries is a function of NbC precipitate size and volume fraction [74], and that the volume fraction of particles pinning the grain boundaries decreases with longer holding times, they are no longer able to exert the pinning force needed for restricting grain growth. Hence, it can be seen in Figure 7-11 (f) that the larger grains grow at the expense of smaller ones, reducing the overall energy of the structure.

Furthermore, for 0.01 wt. % Nb content in medium (0.4 wt. %) carbon steel the austenite grain growth evolution with holding time is similar to that of lower Nb (0.005

wt. %) content, giving homogenous grain structure indicative of normal grain coarsening growth with increasing hold time as shown by Figure 7-10, for similar reasons to those given earlier for 0.005 wt. % Nb steel. An interesting point to note is that increasing the carbon content to 0.8 wt. % carbon whilst keeping the Nb wt. % constant (0.01 wt. %), the initial starting microstructure at 1050°C is heterogeneous containing abnormal grains as shown by the standard deviation peak (8.3μm) in Figure 6-13. The heterogeneity in the structure does not decrease or return to homogenous state with increasing hold time but the heterogeneity in the structure further increases. This is opposite to the effect observed for low (0.08 wt. %) carbon steel alloyed with 0.02 wt. % Nb, where the initial state is also of a highly heterogeneous structure, however the heterogeneity decreases with increasing holding time as shown by Figure 7-3 and Figure 7-4. As explained earlier this is because the precipitates are unstable and coarsen at a high rate (shown in Figure 7-19, having the highest precipitate growth exponent) or dissolve rapidly (shown by the decrease in number density in Figure 7-18 (c)). The effect of different carbon content on the precipitation kinetics will be discussed later on. This suggests that increasing the carbon content results in a slower decrease in the pinning force, therefore occurrence of precipitate coarsening or dissolution is also slower due to the stability of the NbC precipitates, which increases the susceptibility of obtaining an overall abnormal grain growth structure with longer hold times.

Finally, the highest Nb content of 0.02 wt. % in medium (0.4 wt. %) carbon steel, has a similar starting heterogeneous austenite grain structure as described above for low (0.08 wt. %) carbon alloyed with 0.02 wt. % Nb and high (0.8 wt. % C) alloyed with 0.01 wt. % Nb. However, the austenite grain characteristics have more similarities to that of low (0.08 wt. %) carbon, as the heterogeneity in the overall austenite structure decreases with increasing holding time. Nonetheless the degree of abnormality in the structure does not return to that of normal grain coarsening even for a hold of 6 hours this is evident by the standard deviation value of 16.6μm in comparison to other compositions with SD values ranging from 5.9μm to 9.1μm. This once again points to the coarsening/dissolution kinetics of NbC precipitates which are affected by the carbon content and the total dissolution temperature of the specific composition as shown in Figure 7-19. This prevents a return to normal grain coarsening so that a homogenous austenite structure is achieved, therefore maybe longer hold times maybe required for a return to a homogenous austenite grain structure. Further analysis of the precipitates for this composition (0.4 wt. % C with 0.02 wt. % Nb) shows (Figure D-6 in Appendix D) that there are still a large number of precipitates which are within the range of ≤ 20nm (diameter) [176, 177] for restricting austenite grain growth, even when the average precipitate diameter increases from 21nm (1 hour), 35.7nm (3 hour) to 59nm (6 hour). However with the increase in diameter there is a decrease in the number density of the

precipitates as shown in Figure 7-18 (a) mean diameter, nm and (b) number density. These findings are consistent with previous work done on the abnormal grain coarsening in the presence of second phase particles [185, 186, 187, 188].

Increasing the holding temperature to 1150°C as would be expected varies the austenite grain growth characteristic and also the carbide precipitation kinetics. There is no change in the linear growth rate of the plain C-Mn steel due to reasons stated earlier. However compared to the earlier austenite grain structure which was homogeneous at holding temperatures of 1050°C, the austenite grain structure obtained for extended periods of holding at 1150°C, shows an apparent difference in the normal grain coarsening and the structure becomes heterogeneous, which is observed in all the three carbon concentrations (0.08 wt. %, 0.4 wt. % and 0.8 wt. %) as shown in Figure 7-16. This suggests that the increase in the standard deviation is a result of the slight differences in the normally coarsened austenite grains with time and the rate at which the grains grow. As there are no second phase precipitate carbides to cause a pinning or solute effect to restrict grain growth, it can be related to the pre strain present in the initial specimen caused by slight deformation (rough rolling at 1100°C) prior to the isothermal heat treatment as explained in Chapter 3. The prior deformation present in the specimens leads to an increase in dislocation density, this corresponds to stored strain energy in the grain structure which when annealed at elevated temperatures, leads to recovery and recrystallization in which the dislocations undergo enhanced motion, reducing the dislocation density by dislocation annihilation. This in turn forms low energy configurations and therefore reduces the internal strain energy [189, 190]. Conrad et al., [191], Narutani & Takamur [192] and Jiang et al., [193] have shown that the dislocation density is proportional to the reciprocal of the grain size, therefore smaller grains would have a higher dislocation density and larger grains would have a smaller dislocation density. The dislocations are immobilized by a strong pinning force exerted on them by interstitial carbon atoms which diffuse and segregate at the dislocations, giving the Cottrel effect in reducing the mobility of dislocations [175] and therefore also the mobility of the primary grain boundaries. Therefore certain grains which are larger in size with lower dislocation density would fit the requirement for further growth at the expense of smaller grains which would remain relatively stationary due to the Cottrel effect still in place. However as a result of thermal activation at high temperature, dislocations can escape from the carbon atmosphere and grain boundary migration occurs at different rates. Computer simulation to explain the initial nucleation stage for the abnormal grain growth process has been done by Novikov [66]. In his work he concludes that large grains with high mobility boundaries are small in number and they are surrounded by stagnated low mobility smaller grains, therefore allowing

the larger grains to keep growing, resulting in the high standard deviation values for plain C-Mn steel.

Many previous studies have shown the influence of deformation on the kinetics of abnormal grain growth in pure materials [194, 195, 196]. Observations made by Antonione et al., [195] on high purity iron investigating the behaviour of normal grain growth with different strains indicate that for low deformations (~2%), abnormal grain growth does not occur. However, as the strain rate increases, the microstructure starts to show trends of abnormal grain growth. Conclusions from the investigation show similar results found in this work.

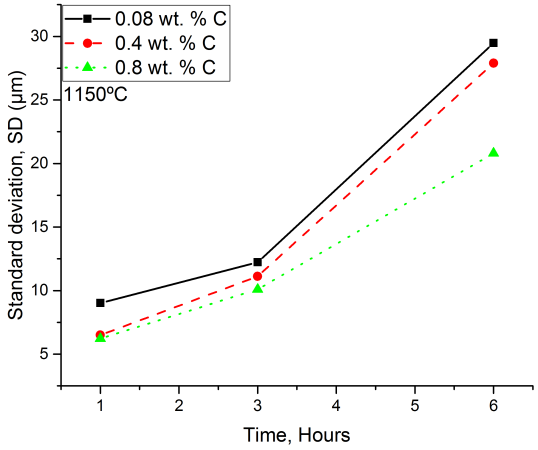

Figure 7-16: The standard deviation for plain C-Mn steel at an isothermal temperature of 1150°C for a hold time of 1 to 6 hours.

For the microalloyed compositions as stated earlier, depending on the solubility temperature, the NbC would act to either pin or exert an drag effect on the grain boundaries. As shown previously the predicted (using Equation (6-1)) dissolution temperature for 0.005 wt. % Nb in low (0.08 wt. %) carbon steel is $T_{DISS}^{0.08\,wt.\ \%} = 954°C$, for medium (0.4 wt. %) and for high (0.8 wt.%) carbon steel is $T_{DISS}^{0.4\,wt.\ \%} = 1134.9°C$ and $T_{DISS}^{0.8\,wt.\ \%} = 1229.9°C$. The austenite grain size indicates a linear increase with time for 0.005 wt. % Nb as can be seen in Figure 7-17 (b). However the austenite grain structure is not a homogenous one but heterogeneous or consists of highly abnormal grains. As indicated in Figure 6-16 the secondary peaks can be associated with further dissolution of the second phase precipitates leading to another regime of abnormal grain growth during the reheating temperature stage which is shown in Chapter 6 and discussed in Section 6.9.1. The high standard deviation value of 18µm is indicative of abnormal grain growth due to further dissolution which is understandable as it is above the T_{DISS} for the composition. It can therefore be assumed

that hindrance to grain coarsening is controlled primarily by solute drag by the solute Nb atoms at the grain boundaries. As explained previously the solute drag effect on grain boundary mobility is a function of impurity concentration and temperature. As the composition is constant in regards to medium carbon steel alloyed with 0.005 wt. % Nb, the effect of temperature is taken into account (1050°C and 1150°C). At higher temperature there is an increase in the activation energy for Nb and Fe atoms, so the atmosphere of the segregated Nb solute atoms at the grain boundaries disappear and there is no tension stress exerted on the grain boundaries, and the velocity of the grain boundary motion is much faster. This is called a "breakaway" phenomenon and is due to the increased diffusion rate of Nb atoms at the higher temperature as they keep up with the austenite grain boundary mobility. Hence the larger grains grow at the expense of smaller ones. This can explain the difference why the standard deviation is constant, and indicative of normal grain coarsening at the lower temperature of 1050°C as compared to the increasing values at 1150°C for the 3 different hold times of 1 hour (18μm) 3 hour (18.3μm) and 6 hours (25.3) which is indicative of abnormal grain coarsening with increasing time. Keeping Nb concentration at 0.005 wt. % and increasing the carbon content to 0.8 wt. %, austenite grain growth is still linear with time but the austenite grain characteristic are homogenous with holding time as seen in Figure D-15 in Appendix D as opposed to those seen at 1050°C in Figure 7-12, where the formation of the duplex heterogeneous austenite grain structure has been attributed to the Ostwald ripening effect which can be seen in Figure 7-11 (f) at the six hour mark. However, with increasing the isothermal temperature to 1150°C and holding from 1 to 6 hours, it can be assumed that the remaining NbC precipitates are highly thermodynamically stable; this is also shown by the fact that the secondary peak shown in Figure 6-16 (b) starts to occur after 1200°C, for further dissolution of the NbC precipitates, which is close to the T_{DISS}.

Thirdly, for medium (0.4 wt. %) and high (0.8 wt. %) carbon steel alloyed with 0.01 wt. % Nb there is a linear and slightly non-linear austenite grain growth trend indicating that the grain growth starts to slow with time for the higher carbon steel. In terms of the overall austenite microstructure, both compositions experience an increase in the heterogeneity of the overall austenite microstructure with increasing hold time as shown in Table D-6 (0.4 wt. % C) and Table D-9 (0.8 wt. %C) in Appendix D. Nonetheless, the heterogeneity in the austenite grain structure is higher in medium (0.4 wt. %) carbon steel compared to that in high (0.8 wt. %) carbon steel. This is attributed to the increase in the stability of the carbides with increasing carbon content as shown by $T_{DISS}^{0.4\,wt.\%} = 1229.9°C$ and $T_{DISS}^{0.8\,wt.\%} = 1338.8°C$. The T_{GC} for medium (0.4 wt. %) carbon alloyed with 0.01 wt. % Nb has been observed at 1000°C, indicating that dissolution of less stable precipitates has already occurred and that at 1150°C further

coarsening/dissolution (Ostwald ripening) starts to occur at extended hold times. This results in certain grain boundaries becoming unpinned and others remaining pinned due to the coarsening/dissolution of the precipitates and overall the number density of the precipitates decreases dramatically as can be seen for 0.02 wt. % Nb in Figure 7-18(d). Therefore it would be accurate to assume that the number density decrease would be much lower for 0.01 wt. % Nb, thereby resulting in the increase in heterogeneity of the austenite grains. Increasing the carbon to 0.8 wt. % also increase the stability of the carbide precipitates as shown by the solubility temperatures, resulting in a much more homogenous austenite structure than that of medium carbon (0.4 wt. %).

Finally, when the alloying element is increased to 0.02 wt. % Nb, the dissolution temperature also increases for both of the steels for medium (0.4 wt. %) and for high (0.8 wt. %) carbon steel, where $T_{DISS}^{0.4\,wt.\ \%} = 1338.8°C$ and $T_{DISS}^{0.8\,wt.\ \%} = 1464.6°C$. Other than a non-linear austenite grain growth trend which is seen for all three carbon contents shown in Figure 7-17 (d), an interesting observation is that relatively normal grain coarsening takes place for medium (0.4 wt. %) carbon steel and a transition from abnormal to normal austenite grain coarsening in high (0.8 wt. %) carbon steel. In regards to the relatively normal grain coarsening observed in medium (0.4 wt. %) steel this can be explained by Figure D-10 (a) showing the average precipitate size and (b) showing the decrease in number density of the precipitates. The number density of the precipitates decreases from 1.6 x 10^{-3} μm^2 to 1.5 x 10^{-3} μm^2 between a 1 and 3 hour hold, suggesting dissolution of the majority of the unstable precipitates has already taken place and the remaining precipitates are larger and are unable to exert a reasonable pinning force to restrict grain growth. The precipitation number density further decreases to 8.5 x 10^{-4} μm^2 at a hold of six hours. This indicates that at higher temperatures and longer holding times, the majority of the NbC precipitates are unable to sufficiently restrict austenite grain growth, which in turn facilitates normal grain coarsening and due to the high temperature Nb solute drag does not seem to have a high effect. A similar reason can be given to the high (0.8 wt. %) steel for the transition from abnormal to normal grain coarsening characteristics.

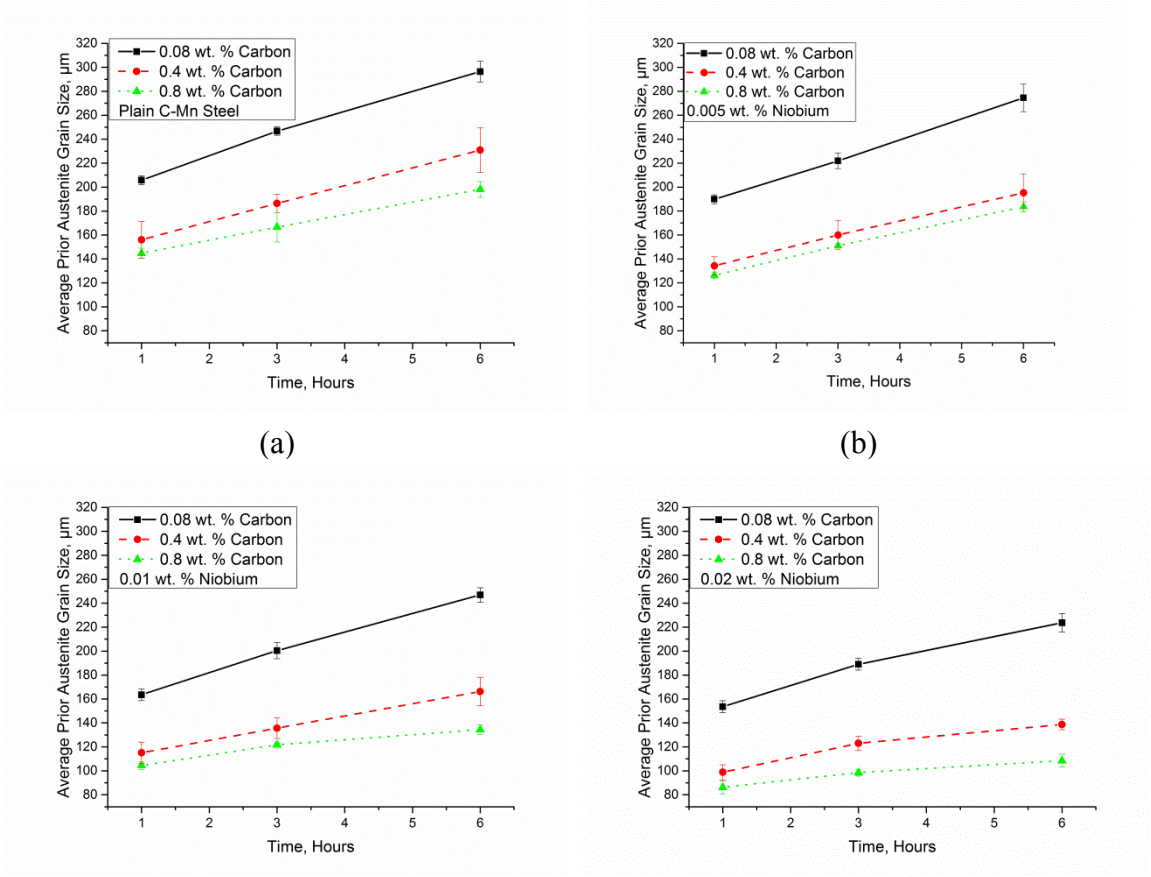

Figure 7-17: The effect of carbon at a reheat temperature of 1150°C.

In summary, abnormal grain growth is observed in plain C-Mn steel at the higher temperature of 1150°C after periods of longer than 1 hour hold and not at the lower temperature of 1050°C. This has been attributed to the strain present in the specimen prior to the heat treatment.

7.9.2. Precipitation Characteristics

Second phase carbide particle have been extensively used to control the characteristics of austenite grain growth and so improving the strength of steels. As discussed above, the characterization of the kinetics of NbC precipitates during different holding times at different reheating temperatures is important as it controls the austenite grain coarsening characteristics, resulting in normal or abnormal growth. Figure 7-7 (a) and (b) show the morphology and the EDX analysis of the Nb carbide precipitate in low (0.08 wt. %) carbon steel.

7.9.2.1. Isothermal Hold at 1050°C

Figure 7-18 indicates the growth and dissolution kinetics of the NbC precipitates with different durations of times (1, 3 and 6 hours) at 2 different temperatures (a) 1050°C and (b) 1150°C.

7.9.2.2. Isothermal Hold at 1150°C

At the higher temperature of 1150°C a complex TiNb (C, N) precipitate was observed in low (0.08 wt. %) carbon steel having a large cuboidal shape as shown in Figure 7-9(b), as well as in medium (0.4 wt. %) and high (0.8 wt. %) steels as shown in Figure D-11 and Figure D-17 in Appendix D. The solubility temperature calculated by Equation (6-1) suggests that complete dissolution of NbC should be at 1106°C in low (0.08 wt. %) carbon steel, all the coarse precipitates show traces of Ti with cuboid and irregular spherical morphology, however point out earlier Ti acts to stabilise NbC precipitates. In Figure D-17 in Appendix D the morphologies of the precipitates are compared with the EDX analyses and indicate that the amount of Titanium alters the shape of the carbide precipitate. This suggests that the presence of even a small amount of Ti significantly retards the dissolution kinetics of NbC and therefore increases the thermodynamic stability of the complex TiNb(CN), even for hold times of up to 6 hours at 1150°C which was not adequate to dissolve precipitates. Qin, at el., [178] reported similar results in which Ti additions have been shown to increase the thermodynamic stability of the complex TiNb(CN) precipitates as compared to NbC, therefore increasing the complete dissolution temperature. According to Chen et al., [197] TiN particles will form during solidification of the steel and is a preferred site for nucleation of NbC to occur, therefore it is reasonable to believe that these TiN particles in the steel samples would have come as impurities from a previous melt.

The NbC precipitate diameter size (nm) increases with increasing hold time for both the medium (0.4 wt. %) and high (0.8 wt. %) carbon steel as the number density of the precipitate decreases. Similar coarsening behaviour has been reported previously by Hansen et al., [198] in niobium microalloyed steels. However the coarsening effect for low (0.08 wt. %) carbon steel is interesting. This is because the precipitate size increases extremely slowly as seen in Figure 7-18(b) with increasing hold time. This is related to the high isothermal temperature, as it is 44°C above the complete $T_{DISS} = 1106°C$ and the majority of the precipitates have gone into solution or are dissolving as shown by the precipitate number density decrease in Figure 7-18(d). The number density is extremely low compared to 1050°C which is shown in Figure 7-18(c), but the mean precipitate diameter size is smaller at the lower temperature too.

The effect of carbon on the stability of NbC precipitates can be seen in Figure 7-18, where number density is the highest for high carbon and the lowest for low carbon irrespective of either of the two hold temperatures. This increase in stability could be the reason for the increased tendency of precipitate coarsening for the higher carbon content. However another parameter that needs to be considered is the isothermal temperature at which extended holding occurred which will be discussed later on. One conclusion is that increasing the carbon content affects the NbC coarsening/dissolution kinetics.

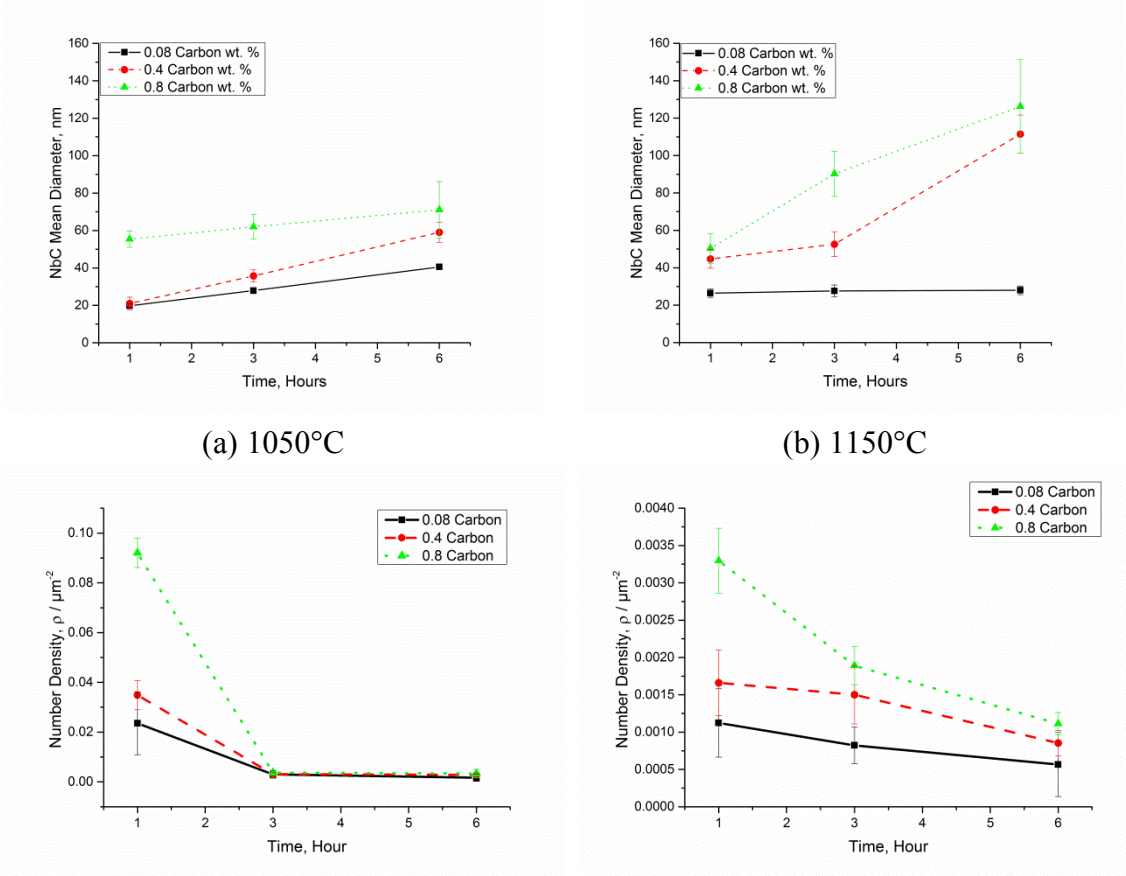

(a) 1050°C (b) 1150°C

(c) 1050°C (d) 1150°C

Figure 7-18: The effect of carbon content alloyed with 0.02 wt. % Nb on the characteristics of NbC precipitates.

7.9.2.3. Precipitate Coarsening Rate

The precipitation coarsening rates predicted by Equation (7-1) define the average slope as R^3 vs t data, the R^3 implying that the coarsening mechanism is by bulk diffusion. However, different rate controlling mechanisms result in different coarsening rates. Equation (7-2) can be rearranged to obtain the exponent "*n*" *for* the rate controlling mechanism and these are given in Table 7-3. The change in the rate

controlling exponent can be seen in Figure 7-19, it reveals that the coarsening mechanism exponent "n" is dependent on the temperature and the carbon content. The coarsening mechanism which dictates the rate of growth for carbide precipitates decreases with increasing temperature for low (0.08 wt. %) carbon steel, as can be seen when increasing from 1050°C to 1150°C. This can be explained by taking the $T_{DISS} = 1106°C$ in to account. At the lower temperature of 1050°C the *"n"* value is 0.39 ± 0.06 which indicates that the controlling mechanism for coarsening is diffusion along dislocations [199] and for the higher temperature 1150°C the *"n"* value is 0.03 ± 0.0057 which is very low and the coarsening mechanism could be associated with surface interface kinetic reactions which gives a value of *"n"* = 1 [199]. This is expected as the isothermal hold temperature and time is above the T_{DISS}, therefore the carbide precipitates are further going through dissolution. As shown in Figure 7-18(d) the precipitate number density for low (0.08 wt. %) carbon steel is extremely low which also reconfirms the low "*n"* value. This is because the driving force for precipitation coarsening is very low. The less thermodynamically stable precipitates will shrink if the radius is below the critical r ($r < r_{crit}$) and dissolve into solution and this would further reduce the coarsening exponent.

Increasing the carbon content to 0.4 wt. %, indicates a change in the rate controlling mechanism for precipitation coarsening to be faster at 1050°C compared to low (0.08 wt. %) carbon steel, which is also indicative of diffusion along dislocations. This effect of increasing carbon on the precipitation coarsening rate, can be attributed to the $T_{DISS} = 1338.8$ for the carbide precipitates which indicates that the isothermal reheat temperature of 1050°C is significantly below the temperature for total dissolution for the carbide precipitates. Therefore a higher number density of precipitates shown for the 1 hour hold in the histogram in Figure D-6 (a) and Figure D-7 (b) would result in a higher total interfacial energy providing the driving force for carbide coarsening to occur. The decrease in the smaller particles can be seen in the remaining 3 and 6 hour histograms. The higher carbon content increases the stability of the carbides, therefore smaller carbide particles with a radius smaller than a critical radius will dissolve into the matrix and the solute is diffused to the larger carbide particles. At the higher isothermal temperature (1150°C) the coarsening exponent *"n"* is lower than that observed at the lower temperature with the coarsening mechanism still indicating diffusion along dislocations. The lower coarsening rate should not be expected, as at the higher temperature of 1150°C, the majority of the precipitates should still be relatively stable due to the high total dissolution temperature. Coarsening rate should increase with temperature as smaller particles are dissolved and diffuse to larger particles, unless the isothermal temperature at which the hold occurs is above the total dissolution temperature as seen for low (0.08 wt. %) carbon steel at 1150°C. The effect of increased

stability of the carbide precipitates in high (0.8 wt. %) carbon steel is shown in Figure 7-19 where the *"n"* value is very low (0.14 ± 0.03) indicative of interface reaction as a coarsening mechanism for growth [199]. Figure 7-18(c) shows that the number density of the precipitates for the isothermal temperature of 1050°C is the highest in high (0.8 wt. %) carbon steel compared to medium (0.4 wt. %) and low (0.08 wt. %) carbon steels. The initial higher number density at 1 hour can be explained by the total dissolution temperature $T_{DISS} = 1464.6°C$ being much higher compared to the other carbon compositions. The high T_{DISS} contributes to the stability of the carbide particles, and this is also translated in the precipitate diameter size increase in the box plot shown in Figure D-14 (a). Increasing the isothermal hold temperature to 1150°C indicates a clear change in the coarsening mechanism from interface reaction at 1050°C to a dislocation diffusion mechanism at the higher temperature. This can be attributed to the dissolution of smaller less thermodynamically stable particles which then diffuses though dislocations to larger particles.

$$r^n = Kt \tag{7-2}$$

Table 7-3: The Rate Controlling mechanism exponent for different carbon contents.

	Rate Controlling Mechanisms (n)	
Carbon wt. %	1050°C	1150°C
0.08	0.39 ± 0.06	0.03 ± 0.01
0.4	0.57 ± 0.07	0.48 ± 0.254
0.8	0.14 ± 0.03	0.51 ± 0.012

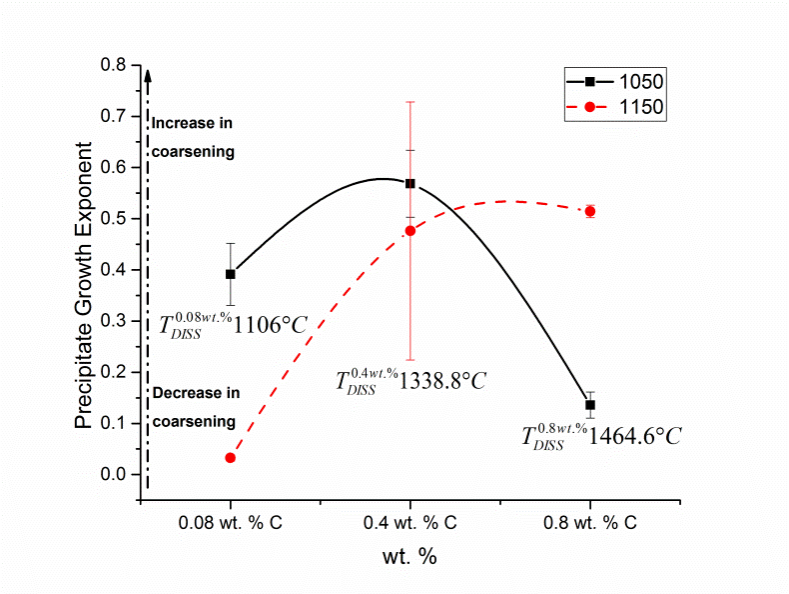

Figure 7-19: The coarsening rate of precipitate particles for different carbon concentrations at two different temperatures. Error bars represent ± 95% CL. Dashed line is used only as a guide for the eye.

In summary, as the duration of the hold increases, the carbide precipitates become larger with the total number density decreasing which is very well described by the Ostwald ripening theory. The controlling coarsening mechanism for carbide precipitate growth varies with temperature and carbon content, and can be related to the total dissolution temperature for NbC precipitates. The rate of coarsening has been shown to have low values for two cases. The first being if the isothermal hold is above the total dissolution temperature and the second, when there is high stability of the carbide precipitates as in the case of high (0.8 wt. %) carbon. Apart from the low coarsening rate exceptions mentioned, the main coarsening mechanism was diffusion through dislocations.

8. Grain Growth Activation Energy

The previous two results chapters (Reheat Temperature) and (Hold Time) show the austenite grain growth behaviour of plain C-Mn and Nb microalloyed steels from low carbon content to high carbon content. It is indicated in those two chapters that the prior austenite grains grow with increasing reheat temperature and holding times. The results from these two chapters have been combined to calculate the time exponent n, material constant A_1, A_2 and the activation energy for grain growth, the results of which are presented in this chapter.

8.1 Introduction

The work presented in this chapter evaluates the activation energy[13] at two different temperatures of 1050°C and 1150°C for the 3 different carbon contents mentioned in the results section (reheat temperature) and (Hold Time). The activation energy is needed for grain growth to occur and also to obtain a mathematical equation for modelling grain growth. The initial empirical equation for normal grain growth kinetics for isothermal temperatures was first proposed by Beck, [75] and is expressed in Equation (2-8).

$$D = A_1 \cdot t^n \tag{2-8}$$

Austenite grain growth kinetics have been modelled using the classic isothermal grain growth relationship given by Anelli, [82] which is shown in Equation (2-14).

$$D - D_0 = A_3 \cdot \exp \cdot \left(\frac{-Q}{RT}\right) \cdot t^n \tag{2-14}$$

Where D_0 and D are the initial and final grain size (μm) respectively, n is the time exponent, A_3 is a material constant, R is the universal gas constant (8.31 J mol^{-1}K^{-1}), t is the time at the austenitisation temperature T in Kelvin (K) and Q is the activation energy for boundary motion (grain growth).

The initial grain size D_0 is experimentally difficult to determine as grain growth might have started before the specimen reaches the isothermal hold temperatures of 1050°C and 1150°C.

[13] Activation energy: the additional energy necessary to initiate a thermally activated chemical or physical process (Grain Growth in this work).

8.2 Time Exponent (n) and Material Constant A_1

Taking the natural logarithm of Equation (2-8) gives Equation (2-12)

$$\ln D = n \ln t + \ln A_1 \tag{2-12}$$

The time exponent n and material constant A_1 can be obtained by a plot of $[\ln D]$ versus $[\ln t]$ and yields a straight line with n as the gradient and A_1as the y-intercept. Figure E-1 in Appendix E shows all the $[\ln D]$ versus $[\ln t]$ plots for low, medium and high carbon steels. In doing so a value of n = 0.17651 and A_1= 3.77128 were determined for low carbon 0.08 wt. % steel at a reheat temperature of 1050°C. The remaining calculated values for the time exponent n and material constant A_1 are shown in Table E 1 in Appendix E along with the coefficient of determination (R-Squared).

These R-Squared factor values represent an important aspect of information, which is to indicate if the grain growth follows a similar trend throughout the entire data range. It should be pointed out that the R-Squared values below a value of 0.9 do not follow a one stage trend and could imply a two stage grain growth trend. For example where grain growth experiences a stage of fast growth and later slower growth or the opposite.

The compositions which have an R-Squared value less than (0.9) are the 0.02 wt. % Nb steel with different Carbon wt. % of 0.08 wt. % and 0.4 wt. % and both at the reheat temperature of 1050°C. These two compositions at this reheat temperature have been shown to have abnormal grain growth occurrence in the both results Chapter 6 and 7.

Figure 8-1 (a, b, c and d) show the time exponent (n) varying with Nb (niobium) wt. % and C (Carbon) wt. %. The shaded area represents the error margin of 95% confidence limit. In (a) it can be seen that as the Nb wt. % increases for 0.08 wt. % C the time exponent n increases to 0.2701. A similar trend is observed for 0.4 wt. % C where there is also an increase to 0.2514. An interesting point to note is in regards to 0.8 wt. % C where with the increase in Nb wt. % the time exponent decreases to 0.0384.

However in (b) the n values are presented for a temperature of 1150°C and it can be seen that the time exponent n value stays around 0.2 (the exact values can be seen in Table 8-1) for both 0.08 wt. % C and 0.4 wt. % C. The point of interest is once again for 0.8 wt. % C with a Nb content of 0.1 wt. % and above where the n value are 0.1407 and 0.1274 respectively.

On the other hand (c) and (d) represent the similar values presented in (a) and (b) but the n values have been presented as a function of varying Carbon content. The main difference in presenting the variation of the data is that the effect of Carbon wt. % can be understood. It can be seen in (c) that plain C-Mn steel, 0.005 wt. % Nb and 0.01 wt. % Nb steels have a gradual decrease in n value from a range of 0.2008 – 0.1765 as the carbon content increases (for the temperature of 1050°C). The effect of carbon content

alone has been shown to decrease the growth of the prior austenite grains at the lower temperature of 1050°C. A point to be noted is that the 0.02 wt. % Nb (blue line) steel has a sharp decrease in the n value between 0.4 wt. % C to 0.8 wt. % C which is indicative of very slow grain growth kinetics, which is exhibited by the time exponent n = 0.0384.

On the other hand at a higher temperature of 1150°C the time exponent n values are higher than those calculated at 1050°C which can be seen in Figure 8-1 (d). It can be seen that for plain C-Mn steel and 0.005 wt. % Nb steel the n value remains constant at around 0.2 regardless of the increasing Carbon wt. %. The only significant decrease in the n value occurs for 0.01 wt. % Nb and 0.02 wt. % Nb steels as the Carbon wt. % reaches to 0.8. But still the value is higher than that calculated for 1050°C. Table 8-1 presents the exact time exponent n values for all the 12 compositions at both 1050°C and 1150°C.

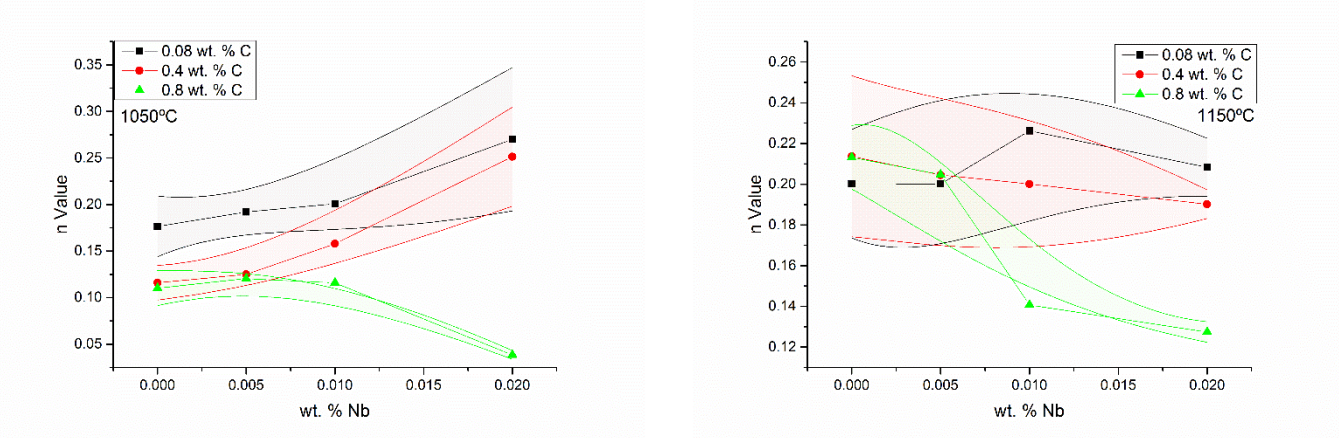

(a) n as a function of varying Nb wt. % at 1050°C (b) n as a function of varying Nb wt. % at 1150°C

(c) n as a function of varying C wt. % at 1050°C (d) n as a function of varying C wt. % at 1150°C

Figure 8-1: Relationship between the plain C-Mn steel, Nb microalloyed steel and the time exponent, n for 3 different carbon steels (low, medium and high).

Table 8-1: Values of the n at different temperatures for 12 different compositions.

		Time Exponent (n), (1050°C)		
Carbon wt. %	Plain C-Mn	0.005 wt. % Nb	0.01 wt. % Nb	0.02. wt. % Nb
0.08	0.1765	0.1921	0.2008	0.2701
0.4	0.116	0.1249	0.1578	0.2514
0.8	0.1102	0.1204	0.1159	0.0384
		Time Exponent (n), (1150°C)		
0.08	0.2002	0.2001	0.2262	0.2083
0.4	0.2137	0.2045	0.2001	0.1902
0.8	0.2132	0.2047	0.1407	0.1274

8.3 Growth Model of Austenite Grains (Hold Time)

The isothermal grain growth models for low medium and high carbon steels for hold times of 1 to 6 hours and at different temperature of 1050°C and 1150°C, demonstrates that the calculated average austenite grain size using the kinetic equations (solid circles) compared with the experimental measurements of the actual austenite grain size (solid square). The results show a good agreement for the different holding times at both of the temperature of 1050°C and 1150°C, this holds true for all the compositions the results can be seen in Appendix E starting from page 247 to 252.

8.4 Activation Energy ($\boldsymbol{Q}$)

The activation energy can be can be obtained by a plot of $[\ln\left(\frac{D}{t^n}\right)]$ versus $[\frac{1}{T}]$ (temperature in Kelvin) and therefore yields a straight line with $\left(\frac{-Q}{RT}\right)$ as the gradient. The value of n has been changed in accordance to those calculated from Figure E-1 and the values are given in Table E 1 in Appendix E for each composition with respect to the two different temperatures e.g. 1050°C and 1150°C. The coefficient of determination, R-Squared (R^2) values for the goodness of fit are low (~0.7 – 0.8) for low carbon steel (0.08 wt. % C) which is not a very good fit. The R-Squared (R^2), for medium carbon steel (0.4 wt. % C) had a better value in the range of (~0.8 – 0.95) and for the high carbon steel (0.8 wt. % C) the R-Squared (R^2) value is (~0.9 – 0.95). The importance of the R-Squared (R^2) value will be illustrated later on.

The calculated activation energies are shown in Figure 8-2. It is indicative from the results that as the Nb wt. % increase the activation energy for grain growth increases too. The Nb content can also be seen to have an effect on the activation energy. At the

lower concentrations of Nb wt. % the activation energy remains relatively constant for 0.08, 0.4 and 0.8 carbon steels until 0.005 wt. % Nb; after which it increases for both 0.4 and 0.8 carbon steels. The exact activation energies and calculated material constant A_3 values for each composition are shown in Table E-2 in Appendix E.

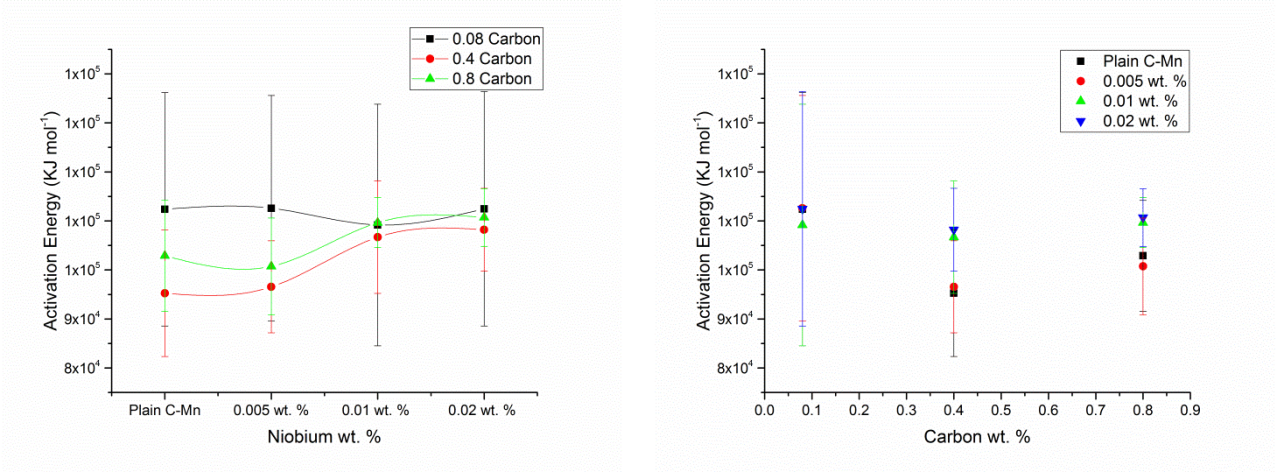

(a) (b)

Figure 8-2: The activation energy for the different carbon and niobium concentrations.

8.4.1. Low Carbon Steel

The Arrhenius plots values for the calculation of activation energy Figure E-8 in Appendix E are based on the assumption that there is only one growth regime taking place. This is not however the case as the coefficient of determination (R-Squared (R^2)) values for the goodness of fit are low (~0.7). When multiple growth regimes are taken into consideration a better coefficient of determination is achieved (~0.9 to 1). This is illustrated in Figure 8-3 where the 3 different grain growth regimes can be seen for plain C-Mn steel. The regression analysis shows that the Q_G (activation energy for grain growth) for the temperature range of 950°C – 1000°C (regime 1) is 349.88 kJmol^{-1}, for 1000°C – 1150°C (regime 2), a lower activation energy of grain growth is predicted being 17.73 kJmol^{-1}, and finally at a higher temperature of 1150°C – 1250°C (regime 3) an activation energy of 248 kJmol^{-1} is predicted.

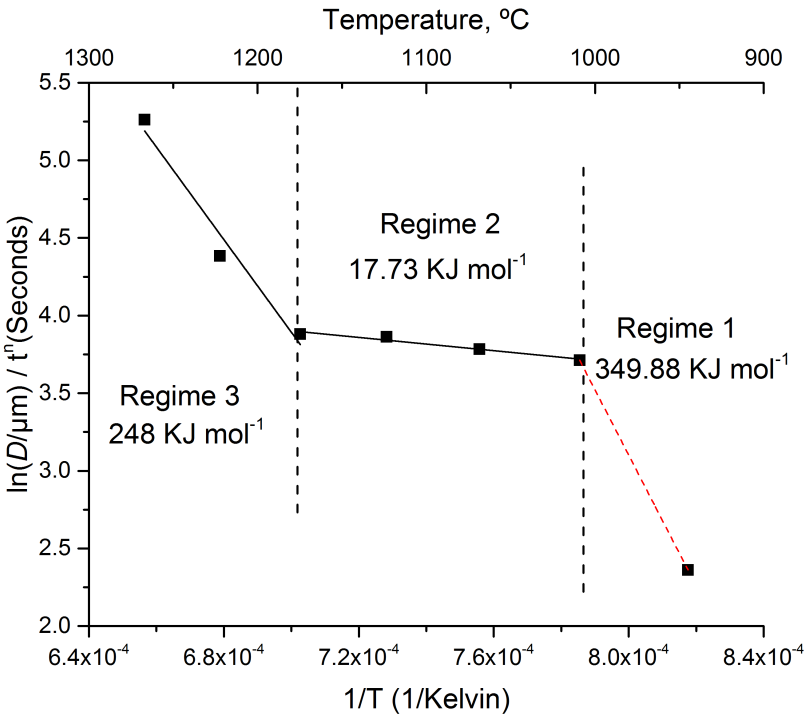

Figure 8-3: Arrhenius plot showing the 3 different regimes of activation energy for grain growth in low 0.08 wt. % plain C-Mn steel.

The different growth regimes observed for plain C-Mn steel in Figure 8-3, are also observed for microalloyed steels as shown in Figure 8-4, where the 3 different grain growth regimes can be seen for plain C-Mn steel and the 3 microalloyed steels. The regression analysis shows the Q_G (activation energy for grain growth) for the temperature range of 950°C – 1000°C (regime 1), for 1000°C – 1150°C (regime 2) and for 1150°C – 1250°C (regime 3). It can be noted there is a transition in the behaviour at each regime; the activation energies are given for each regime in Table 8-2. It can be seen from the activation energy for grain growth, with increasing niobium concentrations the activation energy for regime 1 decreases. For regime 2 and 3 the opposite is observed in which the activation energy for grain growth increases with increasing niobium content.

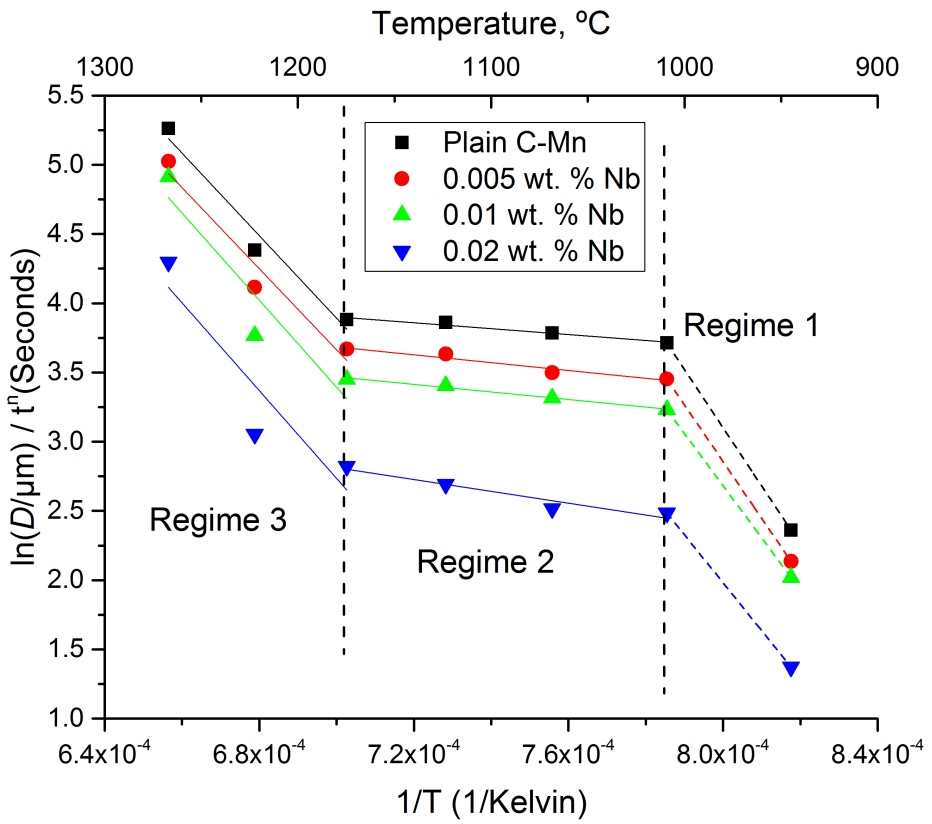

Figure 8-4: Arrhenius plot showing 3 different regimes of activation energy for grain growth in Plain C-Mn and Microalloyed steels in low carbon steel.

Table 8-2: Activation Energies for plain C-Mn and Nb microalloyed steels at different grain growth regimes in low carbon steel.

Composition	Activation Energy ($kJmol^{-1}$) Regimes		
	1 (950°C – 1000°C)	2 (1000°C – 1150°C)	3 (1150°C – 1250°C)
Plain C-Mn	349.88 ± (N/A)[14]	17.73 ± 2.5	248 ± 44.12
0.005 wt. % Nb	341 ± (N/A)	23.55 ± 4.06	243.53 ± 52.91
0.01 wt. % Nb	313.88 ± (N/A)	22.67 ± 1.55	261.62 ± 91.83
0.02 wt. % Nb	288.21 ± (N/A)	35.51 ± 6.88	263.67 ± 110.31

[14] Due to only being 2 (950°C – 1000°C) points, an error value could not be calculated.

8.4.2. Medium Carbon Steel

As shown previously for the low carbon steel, there are also different grain growth regimes observed for medium carbon steel, this is shown in Figure E-9 in Appendix E. It can be noted that there is an transition behaviour at each regime which is shown by the activation energy in Table 8-3.

Table 8-3: Activation Energies for plain C-Mn and Nb microalloyed steels at different grain growth regimes in medium carbon steel.

Composition	Activation Energy ($kJmol^{-1}$) Regimes		
	1 (Dashed line)	2	3
Plain C-Mn	253.94 ± (N/A)	51.27 ± 1.52	125.08 ± 10.64
0.005 wt. % Nb	148.02 ± 23.52	45.55 ± 1.97	133.42 ± 11.27
0.01 wt. % Nb	170.25 ± 25.8	34.86 ± 9.72	135.13 ± 18.12
0.02 wt. % Nb	148.97 ± 16.98	55.37 ± 6.37	144.41 ± 25.91

8.4.3. High Carbon Steel

The Arrhenius plot for high carbon steel showing the grain growth regimes in seen in Figure E-10 in Appendix E. Compared to the earlier Arrhenius plots where 3 regimes are observed, in the high carbon only 2 regimes are observed; indicative of 2 grain growth mechanisms instead of 3 this can be seen in Table 8-4.

Table 8-4: Activation Energies for plain C-Mn and Nb microalloyed steels at different grain growth regimes in high carbon steel.

Composition	Activation Energy ($kJmol^{-1}$) Regimes	
	1 (950°C – 1050°C)	2 (1050°C – 1250°C)
Plain C-Mn	157.08 ± 213.4	65.47 ± 41.98
0.005 wt. % Nb	148.66 ± 26.26	67.86 ± 2.94
0.01 wt. % Nb	111.79 ± 5.36	99.4 ± 9.35
0.02 wt. % Nb	73.43 ± 1.4	121.44 ± 10.37

8.5 Growth Model of Austenite Grains (Reheat Temperature)

The grain growth model presented in this section is based on Equation (2-14), which as shown previously has an Arrhenius component from which the activation energy can be taken into account.

8.5.1. Low Carbon Steel

The Figure 8-5 shows a comparison between the calculated and experimental measurements of the austenite grain size for low carbon steel for different heating temperatures.

In (a) the calculated (C-Mn, K – 1) sizes are calculated with the activation energy (Q), material constant (A_3) and time exponent calculated at a temperature of 1050°C. For (C-Mn, K – 2) the values used have been calculated at a temperature of 1150°C. The difference in using the different material constant (A_3) values obtained from either of the two temperatures is not noticeable. In fact they overlap in all the calculations (b), (c) and (d).

The mathematical model shows the prediction from the calculated austenite grain size and experimental measurements are in reasonable agreement with each other. The points where it does not fit with the experimental measurements are at the low and high end of the temperatures from 1000°C and to above 1150°C. It should be taken into consideration that this mathematical model is based on regression from Figure E-8 (a), where the coefficient of determination, R-Squared (R^2) values for the goodness of fit are low (~0.7 – 0.8).

However, when the 3 different regimes are taken into consideration (shown in Figure 8-4), where the coefficient of determination, R-Squared (R^2) values for the goodness of fit are high (~0.9 – 0.99) a much more accurate prediction of the prior austenite grain growth is observed for all the compositions (indicated by the niobium composition, regimes).

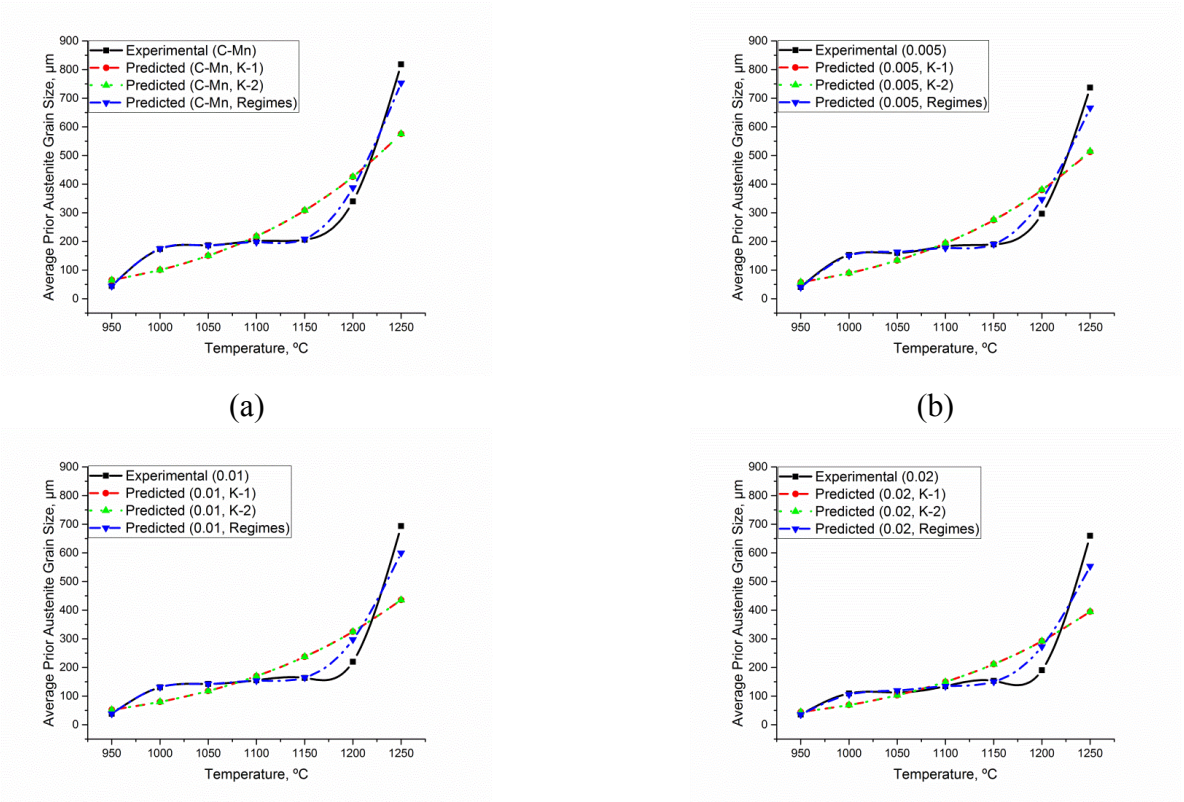

Figure 8-5: Comparison of the Calculated and the experimental austenite grain size for low carbon steels.

Figure 8-6 illustrates the comparison between the predicted and experimental measurements of the austenite grain size using the Arrhenius type predictive equation for low carbon steel held at different holding times (1, 3 and 6 hours). In (a) it can be seen that the predicted values are underestimated or overestimated. In the case of (b); these predictions of the grain sizes were made from obtaining values without consideration of different regimes.

Furthermore, in Figure 8-6 (c) and (d) it can be seen that there is a good agreement between the predicted and experimental values throughout the different hold times regardless of the 4 different compositions or the 2 different temperatures when accounting for the different regimes which occur.

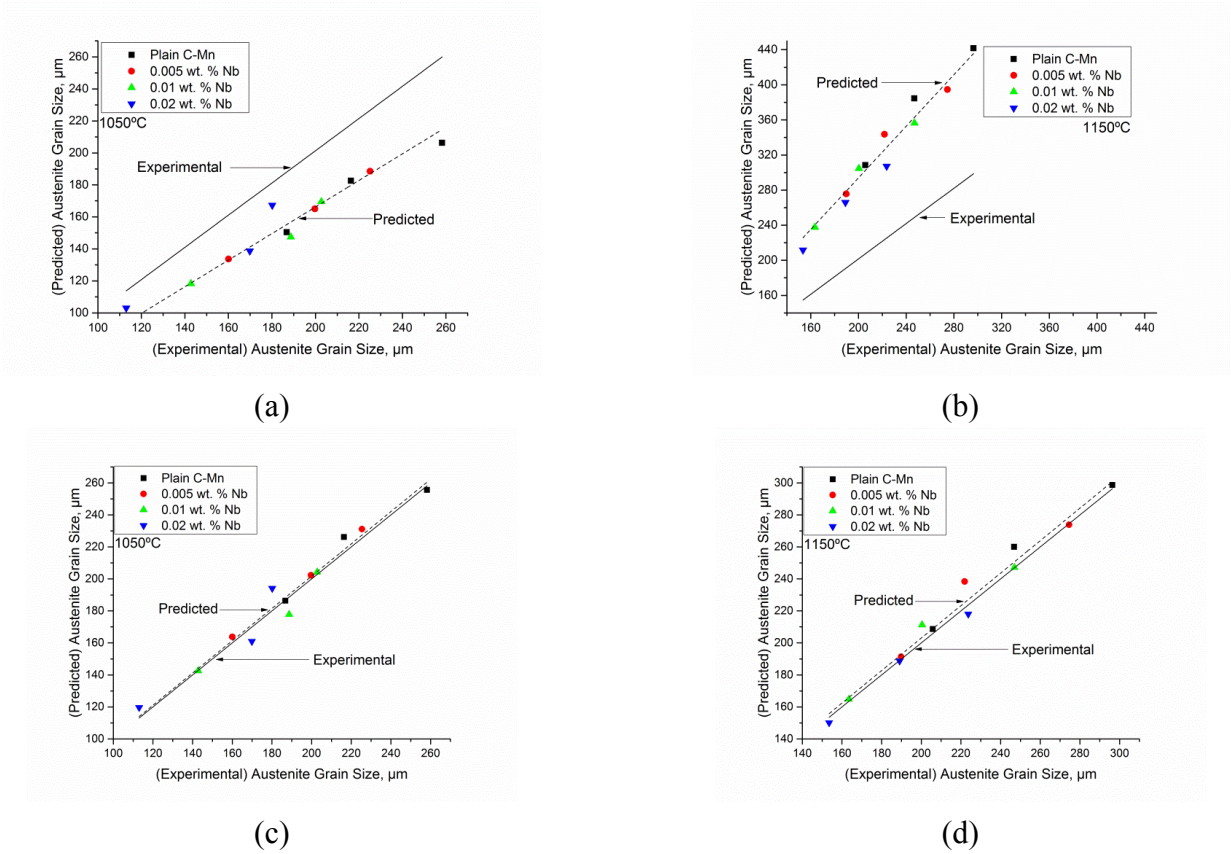

Figure 8-6: Comparison of the predicted with the experimental austenite grain size in low carbon steel for different holding times from 1 to 6 hours, at two different reheat temperatures of 1050°C and 1150°C (a) and (b) without regime considerations, (c) and (d) with regimes taken in to account.

8.5.2. Medium Carbon Steel

The Figure E-11 in Appendix E shows the accuracy of the mathematical model, for the predicted austenite grain size and experimental measurements during different heating temperatures for a hold of 1 hour.

As shown previously two different values were used to calculate the austenite grain size, in (a) the calculated (C-Mn, K[15] – 1) austenite grain sizes are calculated with the activation energy (Q), material constant (A_3) and time exponent calculated at a temperature of 1050°C; for (C-Mn, K – 2) the values used have been calculated at the temperature of 1150°C. As seen previously the material constant (A_3) values calculated are once again overlapping. The predicted grain growth trend is similar to that of the predicted trend when taking the different regimes into account (shown in Figure E-9). Both predict an increase in the grain size with increasing temperature and both are in good agreement with the experimental calculations. Nonetheless the predicted (regimes)

[15] Is the material constant (A_3) value on the graph.

grain size are much more accurate as calculations without considering regimes underestimate or overestimate the grain size at certain temperatures.

Figure 8-7 (a), (b), (c) and (d) illustrates the comparison between the calculated and experimental measurements of the austenite grain size for medium carbon steel held for different holding times (1, 3 and 6 hours). Figure 8-7 (a) and (b) in which the grain growth regimes have not been taken into consideration, have predicted values that are underestimated and overestimated at temperatures of 1050°C and 1150°C. An interesting point to note is that at these 2 temperatures a similar underestimate and overestimation occurs in Figure E-11, for grain growth predictions taking into account the different regimes.

In Figure 8-7 (c) and (d), when considering the values obtained at different grain growth regimes it can be seen that there is a good agreement without any under or overestimations for the different temperatures of 1050°C and 1150°C.

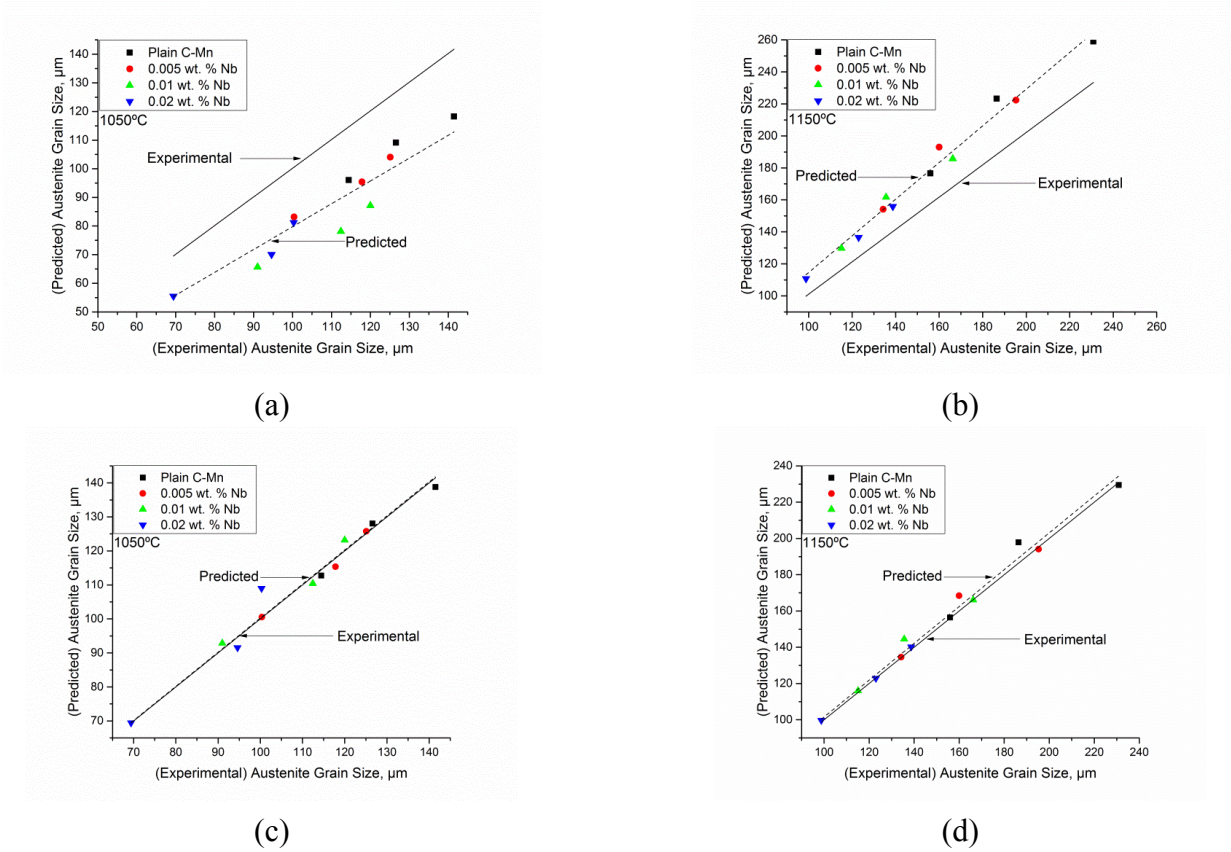

Figure 8-7: Comparison of the calculated with the experimental austenite grain size in medium carbon steel for different holding times from 1 to 6 hours, at two different reheat temperatures of 1050°C and 1150°C (a) and (b) without regime considerations, (c) and (d) with regimes taken in to account.

8.5.3. High Carbon Steel

Figure E-12 in Appendix E shows the austenite grain size calculated from the Arrhenius based equation which incorporates the activation energy. As previously (a), (b), (c) and (d) show the accuracy of the mathematical model, for the predicted austenite grain size and experimental measurements during different heating temperatures for a hold of 1 hour.

As previously two different values were used to calculate the austenite grain size, (K – 1) uses values of the activation energy (Q), material constant (A_3) and time exponent calculated at a temperature of 1050°C. For (K – 2) the values used have been calculated at a temperature of 1150°C. The material constant (A_3) values once again overlap.

The predicted values of the prior austenite grain size show similar trends in which the grain size increases with increasing temperature and are reasonably close to the calculated experimental values. Taking the two different regimes (shown in Figure E-10) into consideration make the predicted values more accurate in (a) and (b) over the ones where a single regime is assumed, where an underestimation occurs near the temperature range of 1050°C to 1150°C and an overestimation at 1200°C to 1250°C. At higher Nb concentrations (c) and (d) it is suggested that the predicted values of grain size is in good agreement with the measured experimental values for both cases with and without taking into consideration the 2 regime steps. It can be seen that the consideration of the 2 regimes, plays an important role in the prediction of the austenite grain size at different times for specific temperatures.

Figure 8-8 illustrates the comparison between the calculated and experimental measurements of the austenite grain size for high carbon steel held at different holding times, (a) shows the predicted values are close to the experimental for 0.01 wt. % Nb and 0.02 wt. % Nb. However for the lower Nb content the predicted values are smaller than the experimental calculated grain sizes; (b) indicates that for a reheat temperature of 1150°C the predicted values are closer to experimental measurements values but still underestimated.

It can be seen that there is a good agreement throughout the different hold times regardless of the different compositions or the different temperatures, when the 2 stage growth regime is taken into account.

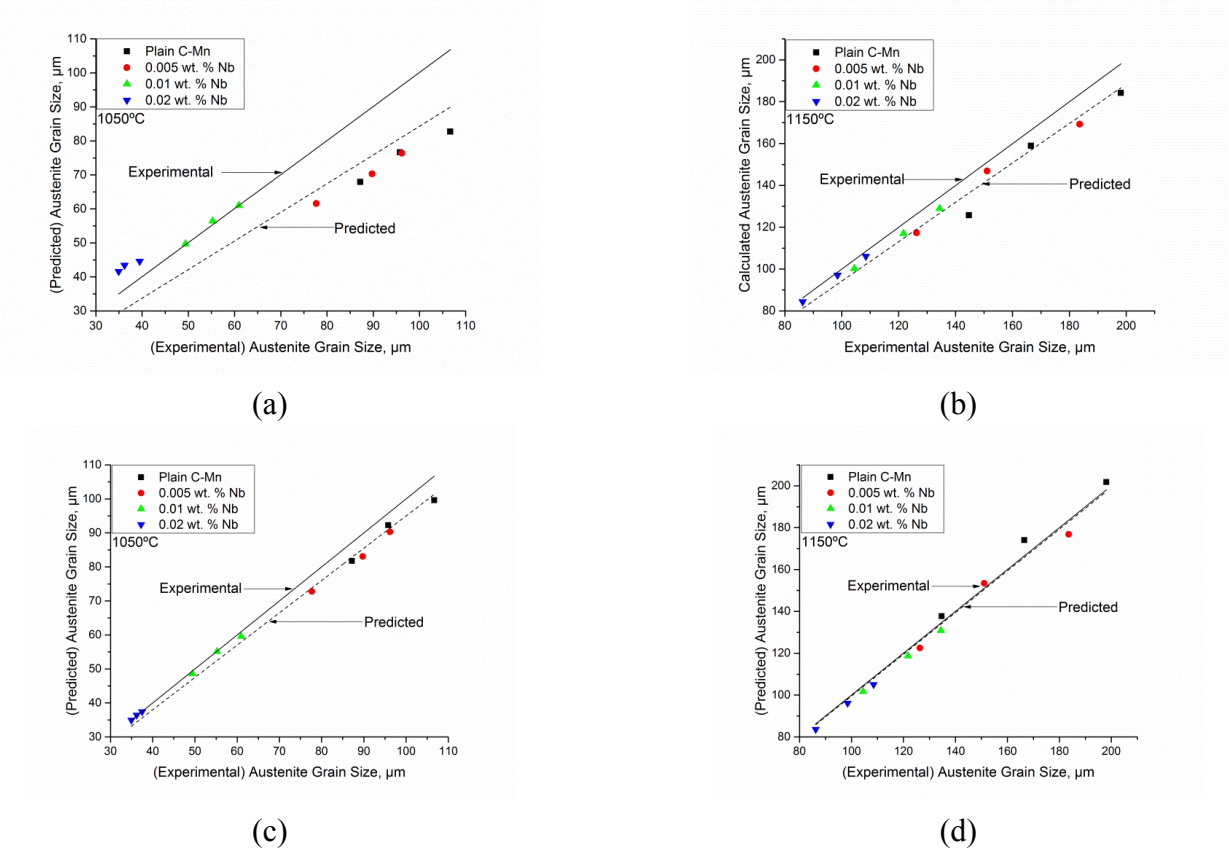

Figure 8-8: Comparison of the calculated with the experimental austenite grain size in high carbon steel for different holding times from 1 to 6 hours at two different reheat temperatures of 1050°C and 1150°C, (a) and (b) without regime considerations, (c) and (d) with regimes taken in to account.

8.6 Summary

The aim of this chapter was to form a mathematical model to describe the growth behaviour of the austenite grains under different reheating temperatures and holding times. This has been done for low, medium and high carbon steels; the exact compositions of which can be seen in the experimental procedure chapter. Two types of mathematical models have been used to predict austenite grain growth behaviour Equation (2-8) and Equation (2-14).

It was found that the time exponent *n* values are higher for 1150°C and lower for 1050°C. An interesting point to note was that the *n* value increased dramatically for both 0.08 wt. % and 0.4 wt. % carbon steels when microalloyed with 0.02 wt. % Nb at 1050°C. On the other hand the *n* value decreases dramatically for 0.8 carbon steel for the same niobium content. At the higher temperature of 1150°C the *n* value remains relatively constant for all the carbon contents; however for the 0.8 wt. % carbon steel there is, a decrease in the *n* value for the 0.01 and 0.02 wt. % Nb microalloyed steels.

The calculated austenite grain growth size according to Equation (2-8) were in good agreement to the experimental measurements of the austenite grains at the two different reheat temperatures and the different holding times.

The calculated grain growth model for different reheat temperatures based on Equation (2-14) did not have a good agreement with 0.08 wt. % carbon steel, regardless of the composition. Similar predictions given for 0.4 wt. % and 0.8 wt. % carbon steel, however when taking into account the different regimes that take place during grain growth the model gives excellent results matching the experimental date for austenite grain growth.

However, when using the same mathematical model for the evolution of the austenite grain size during different holding times at the two different reheat temperatures, the calculated predictions were in extremely good agreement with all the compositions.

8.7 Discussion of Grain Growth

8.7.1. Time Exponent (*n*)

The time exponent (n) values are obtained by taking the logs of Equation (2-8) to give Equation (2-12) and are shown in a graphical form in Figure 8-1 and the corresponding values are given in Table 8-1. The time exponent value usually approaches a value of 0.5 in high purity materials nearing its melting point as shown by Beck, et al. [75] for high purity aluminium. The n values which are obtained in this work deviate significantly from the theoretical value of 0.5. To further understand why these n values deviate from 0.5 in this study there are two parameters that would be needed to be investigated; first the composition and second the reheat temperature [200]. Previous investigations [77, 200] have been carried out to explain this deviation from the theoretical value of 0.5. In these investigations the lower n value has been attributed to numerous factors; pinning, the force exerted on the grain boundaries from second phase particles, solute drag effect, and specimen thickness effect and so on. When analysing the plain C-Mn steel compositions it can be seen from the n values given in Table 8-1 that austenite grain growth becomes slower with increasing carbon wt. %. This has been explained previously and is due to the solute drag effect [6, 9] as there are no carbide forming elements. At the higher isothermal temperature of 1150°C, the n values are higher with little variation with the increasing carbon content. These higher n values at the higher temperature are in good agreement to previous investigations on plain C-Mn steels [87] in which the chemical composition also indicated little effect at a similar temperature range. This small difference of the n values at the higher temperature is due to "breakaways" which occur when the grain boundary velocity is faster, therefore the atmosphere of carbon atoms do not exert any significant force on the grain boundaries [9]. Therefore at a lower temperature of 1050°C the grain boundary velocity is not as fast and hence the carbon solute atoms exert much more of a pulling force. Hence at lower temperature, increasing the carbon concentration has much more of a pronounced solute drag effect on the grain boundaries as compared to higher temperature. This finding is in good agreement with a previous investigation on hypoeutectoid and hypereutectoid plain C-Mn steels [183].

The time exponent n value for low (0.08 wt. %) and medium (0.4 wt. %) carbon microalloyed specimens at the lower temperature of 1050°C indicates relatively constant n values for 0.005 wt. % Nb (0.192 ± 0.01) and 0.01 wt. % Nb (0.201 ± 0.04) compositions as shown in Figure 8-1 (a). However an interesting point to note is that for 0.02 wt. % Nb composition, the time exponent value *n* increases in both the carbon contents, when the opposite should occur because of the high alloying element, as

higher Nb elements should exert more of a pinning or solute drag. In order to understand this behaviour it is important to understand what grain growth behaviour occurs at this temperature (1050°C) for this specific composition. It has been shown previously by the standard deviation values that abnormal grain growth occurs for both of these compositions at 1050°C in Figure 6-18. Therefore the much higher time exponent values could be related to the abnormal grain growth which is occurring at the beginning of the duration of the hold. In previous studies regarding grain growth, high time exponent values have been reported when abnormal grain growth occurs [194, 196, 81, 80]. When analysing the time exponent without initial abnormal grain growth for a 1 hour hold as shown in Figure 8-9 (with the values given in Table 8-5), more acceptable results are produced, indicating the effect of alloying elements on the kinetics of austenite grain growth, where the plain C-Mn steel experiences the fastest growth compared to when it is alloyed with Nb. This indicates that the initial abnormal grain structure which is produced for low (0.08 wt. %) and medium (0.4 wt. %) carbon steels is indeed the reason for the higher time exponent n value. These findings are consistent with previous research for low carbon steels [80, 81]. However, abnormal grains leading to a higher time exponent n value is not the case for high (0.8 wt. %) carbons steel as will be discussed next.

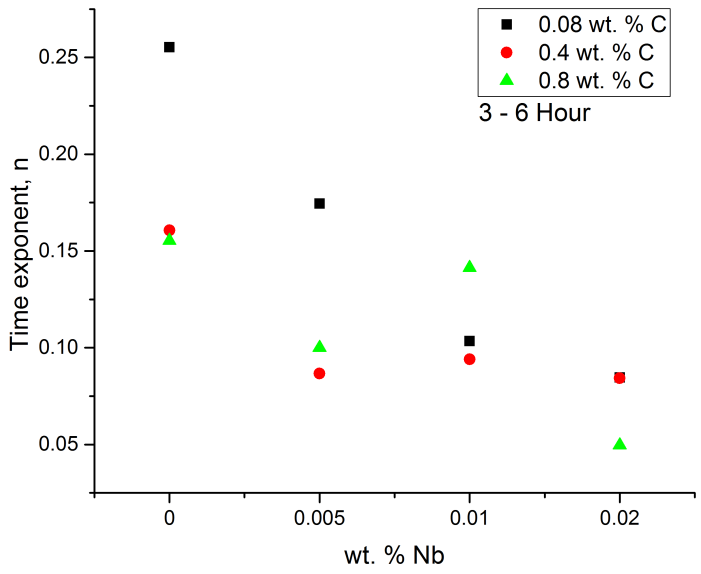

Figure 8-9: The relationship of plain C-Mn and microalloyed steels with the time exponent n for a 3 to 6 hour hold.

Table 8-5: Time exponent values for 3 – 6 hour hold at 1050°C.

	Time Exponent (n), (1050°C)			
Carbon wt. %	Plain C-Mn	0.005 wt. % Nb	0.01 wt. % Nb	0.02. wt. % Nb
0.08	0.2553	0.1745	0.1035	0.0846
0.4	0.1607	0.0866	0.094	0.0843
0.8	0.1554	0.1	0.1414	0.0497

The microalloying effect on the time exponent *n* is much more pronounced in high (0.8 wt. %) carbon steel as indicated in Figure 8-1 (a) at the lower temperature of 1050°C. This is due to the solute drag from the Nb solute atoms for the lower end of the Nb content (0.005 wt. %), a solute and pinning effect for the (0.01 wt. %) and a pinning effect exerted on the grain boundaries for the higher end (0.02 wt. %), as shown by the TEM analysis in Figure D-13 in Appendix E. A high time exponent *n* value is not observed for the 0.01 wt. % Nb even though it has been shown to have an initial abnormal structure (standard deviation peak at 1050°C in Figure 6-13) as seen previously for low (0.08 wt. %) and medium (0.4 wt. %) carbon steel alloyed with 0.02 wt. % Nb. This could be because of the lower amount of heterogeneity which was observed in the structure because of increased carbon content as indicated in Figure 6-18.

At the high temperature (1150°C), all but two of the microalloyed compositions have a mean time exponent *n* value ~ 0.21. This indicates that at higher temperature the alloying elements do not affect the time exponent *n*. Moon et al., [201] indicated a time exponent *n* value of 2.432 and Yao et al., showed similar results for microalloyed steel where the time exponent *n* value was 2.8 ± 0.02, and which remained relatively constant at higher temperatures of 1000°C and 1150°C. The two composition variants in high (0.8 wt. %) which do not have a time exponent n value of 0.21 are 0.01 and 0.02 wt. % Nb. These both still show lower *n* values of 0.1407 ± 0.001 and 0.1274 ± 0.005. As TEM analysis was not performed on 0.01 wt. % Nb steel compositions, it could be assumed that the low time exponent value could be a result of Nb solute atoms and NbC pinning on grain boundaries. Nonetheless TEM analysis for 0.02 wt. % Nb indicates that there are significant NbC precipitates available to slow austenite grain growth.

In summary, the time exponent *n* value is influenced by both the composition and temperature. In general the time exponent increases towards higher temperatures, the time exponent reaches a constant value for the majority of the compositions giving an *n* = 0.21 which is consistent with previous work [78, 87, 201]. Abnormal grain growth only increases the time exponent for low (0.08 wt. %) and medium (0.4 wt. %) carbon steels which is also in agreement with other investigations [80, 81] and not for high (0.8

wt. %) carbon steel. The increase in carbon content also decreases the time exponent at lower temperatures.

8.7.2. Isothermal Hold Grain Growth Model

The grain size can be expressed using an empirical Equation (2-8) given by Beck el al., [75] to analyse isothermal kinetics of austenite grain growth. The expressions for isothermal grain growth are given in Section 8.3 in Chapter 8. They demonstrate a good agreement to the experimental calculations for isothermal austenite grain growth at both the lower and higher temperatures as shown in Appendix E.

8.7.3. Activation Energy

In theory, the activation energy for the transfer of atoms across the grain boundary should be half of that for self-diffusion[16] [52, 202]. A large amount of information is reported in numerous studies regarding the values for activation energies, as listed in Table 2-6.

The activation energy can be can be obtained by a plot of $[\ln\left(\frac{D}{t^n}\right)]$ versus $[\frac{1}{T}]$ (temperature in Kelvin), which therefore yields a straight line with $\left(\frac{-Q}{RT}\right)$ as the gradient. In Figure E-8, a singular fit to the entire data set was made, with the values for the activation energy and rate constant calculated for each composition at both temperatures listed in Table E-2. The activation energies in this work have been calculated for plain C-Mn and microalloyed steel for all three carbon contents, low (0.08 wt. %), medium (0.4 wt. %) and high (0.8 wt. %) carbon steels. The activation energy for plain C-Mn steels is 112.4 ± 23.8 kJ mol^{-1} for low carbon, 95.3 ± 12.9 kJ mol^{-1} for medium carbon and 102.9 ± 11.3 kJ mol^{-1} for high carbon steel, as shown in Figure 8-2 where a trend of activation energy decreasing with carbon content can be seen visually. However, the activation energies indicate a different trend for Nb microalloyed steel compositions, the activation energy remains relatively constant for low carbon steel 112.4 ± 23 kJ mol^{-1} for 0.005 wt. % Nb, 109.2 kJ ± 25 kJ mol^{-1} for 0.01 wt. % Nb and 112.5 ± 24 kJ mol^{-1} for 0.02 wt. % Nb. The effect of Nb on the increase in activation energy is much more pronounced in medium and high carbon steels as can be seen in Table E-2, where the addition of Nb increases the activation energy. Figure 8-10 shows the values of activation energy for plain C-Mn steel with varying carbon content obtained by previous investigations [203, 204, 205, 206, 207] and that obtained in this work. Gruzin et al., [203], Sakai and Ohashi [204], Medina and Hernandez [205], Kong et al., [206] and Serajzadeh and Taheri [207] reported a decrease in activation energy with increasing carbon content. Moreover, the tendency of activation energy reduction

[16] Self-diffusion means the diffusion of atoms of the metal, and not of the impurities.

with increasing carbon was studied by Mead and Birchenall [208]. The study demonstrated the importance of the interactions between carbon atoms and the vacancies through electrostatic effects and strains. The vacancies are formed by thermal energy, by deformation, or heating at high temperatures, and once formed can move to a neighbouring lattice by overcoming an activation barrier [209]. However, these vacancies represent insufficiency of electrons and due to electrostatic forces become a centre of compression. The interaction with the carbon atoms which have four electrons in the second outer shell and could contribute to the expansion of lattice matrix in the bulk material and subsequently result in becoming a centre of expansion. These repulsive forces generated by the moving interstitial carbon atoms create a displacement of the lattice matrix atoms in their vicinity, which would be larger than present in the bulk of the material structure and therefore Fe vacancy diffusion might occur preferentially under these conditions. This would explain the reason for the decrease in the activation energy with increasing carbon content shown in this work which is in good agreement to previous research [203, 204, 205, 206, 207, 208] as shown in Figure 8-10.

On the other hand, making a singular fit for data given in Figure E-8 for microalloyed steels gives an activation energy which is relatively constant for low (0.08 wt. %) carbon steel but increases slightly for medium (0.4 wt. %) and high (0.8 wt. %) carbon steels with increasing Nb content.

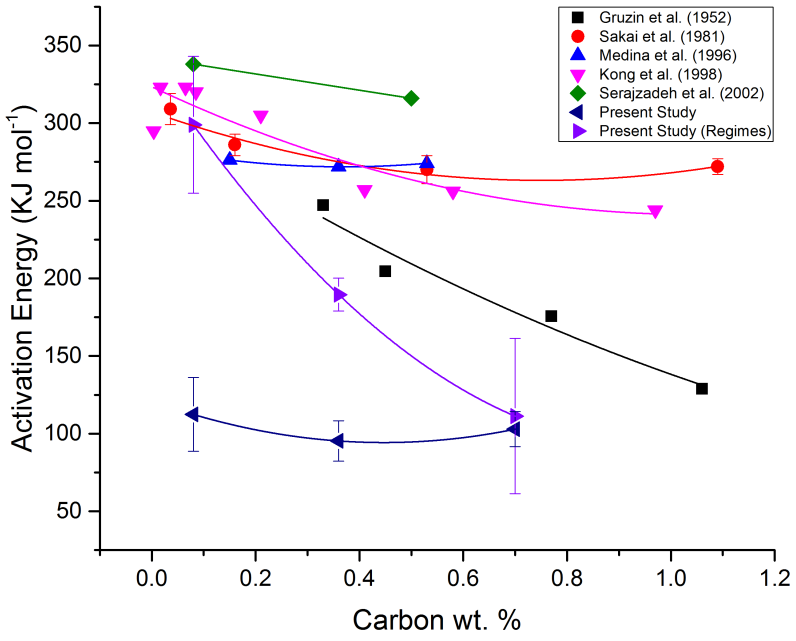

Figure 8-10: The effect of carbon content for plain C-Mn on the activation energy for iron self-diffusion and deformation.

On further analysis of Figure E-8, rather than making a singular fit to the entire data set, separate fits have been made for low (0.08 wt. %) carbon steel. Three separate fits can be seen, one for each of the three regimes as indicated for plain C-Mn steel in Figure 8-2 and for the microalloyed Nb steels in Figure 8-4. There are also three separate regimes observed in medium (0.4 wt. %) carbon steel and two separate regimes in high (0.8 wt. %) carbon steel as shown in Figure E-9 and Figure E-10 in Appendix E.

8.7.3.1. Low Carbon Steel

In Figure 8-4 (0.08 wt. %), the three regimes indicate a difference in diffusion mechanisms for grain growth e.g. volume and grain boundary diffusion. The rate at which the austenite grain growth occurred was highest between 950°C to 1000°C (regime 1) for plain C-Mn steel followed by microalloyed steels with increasing Nb content. The activation energy of Fe (iron) volume diffusion in austenite at the lower temperature range of 950°C - 1200°C is 253 – 311 $kJmol^{-1}$ and at the higher temperature range of 1170°C to 1361°C is 284 $kJmol^{-1}$ and grain boundary diffusion is in the range of 949°C - 1159°C is 38 $kJmol^{-1}$ [210]. The activation energies found for regime 1 are the following, 349.9 $kJmol^{-1}$ for plain C-Mn, 341 $kJmol^{-1}$ (0.005 wt. % Nb), 313.9 $kJmol^{-1}$ (0.01 wt. % Nb) and 288.2 $kJmol^{-1}$ (0.02 wt. % Nb). As it can be noticed, the activation energy decreases with Nb in the lower temperature region. In the temperature range of 1000°C to 1150°C (regime 2) the activation energy is lower by a factor of 13 on average, with the activation energy for plain C-Mn steel being 17.73 ± 2.5 $kJmol^{-1}$, and for the microalloyed steel being 23.55 ± 4.1 $kJmol^{-1}$, 22.7 ± 1.6 and 35.5 ± 6.9 $kJmol^{-1}$ in order of increasing niobium content. Finally, at the higher temperature range of 1150°C - 1250°C (regime 3) the activation energy increases once again but this time it increases with Nb content as it did in regime 2. This implies that the governing mechanism for grain growth changes from volume (regime 1) to grain boundary (regime 2) and back to volume diffusion (regime 3) for low (0.08 wt. %) carbon steel.

The decrease in the activation energy with increasing Nb content at the lower temperature (regime 1) range could be attributed to the dislocation density inherent in the initial structure prior to annealing. It is known that atomic migration in solids is more rapid close to or along dislocations which enhance the diffusivity, and that the dislocation density would be higher at lower temperatures than at higher temperature. With the increase in Nb concentration, the grain size become smaller and the dislocation density increase compared to coarser grains [191]. The activation energy values that are obtained at the low temperature range are in good agreement with activation energy for Fe volume diffusion in austenite, 253 – 311 $kJmol^{-1}$ [210]. The controlling mechanism for the intermediate temperature range (regime 2) is by grain boundary diffusion as the

activation energies are too low to be those for volume diffusion (Table 8-2). The activation energy values obtained for plain C-Mn steel at the high temperature range (regime 3) are in excellent agreement with those found for volume diffusion of Fe in austenite, giving a value of 249 $kJmol^{-1}$ [211] and 284 $kJmol^{-1}$ [210]. One of the reasons for the systematic increase in the activation energy with increasing Nb content in regime 3 could be the influence of Nb solute atoms exerting a dragging force. According to the solute drag theory by Cahn [6], the activation energy for volume diffusion of the solute atom in the matrix, will be found as the apparent activation energy in grain growth, if the grain growth is solute dependent. As grain growth in Nb microalloyed steels is solute dependent it would be reasonable to assume that the increase in activation energy can be related to the Nb concentration. Taking this into account, the activation energy for 0.01 wt. % and 0.02 wt. % Nb are 261.6 $kJmol^{-1}$ and 263.7 $kJmol^{-1}$, both which are in good agreement with work by Kurokawa et al., [212] for Nb diffusion in austenite in which the activation energy is 264 $kJmol^{-1}$. Cahns [6] theory also predicts that the impurities which have greater diffusivity will have a greater drag effect and it is known that Nb is one of the fastest diffusing metallic elements in Fe alloys, with a diffusivity of $7.50\ x\ 10^{-5} m^2 s^{-1}$ at higher temperatures [212].

8.7.3.2. Medium Carbon Steel

Increasing carbon content has been shown to decrease the activation energy earlier. In the case of medium (0.4 wt. %) carbon steel which also has 3 austenite grain growth regimes. A similar trend is seen in regime 1 which is shown in Table 8-3, to what was observed in low (0.08 wt. %) carbon steel, in which the activation energy decreases with increasing Nb content apart from the 0.01 wt. % Nb composition discrepancies which could be due to experimental errors or the fitting of the line. However it is still within the 95% CL error. The decrease in activation energy in regime 1 is due to the creation of high diffusivity paths created by dislocations from prior dislocations in the material or due to the smaller grain size which have a higher dislocations density due dislocation pile ups at the grain boundaries. As mentioned for plain C-Mn steel in the low carbon concentration the activation energy of Fe (iron) volume diffusion in austenite at the lower temperature range of 950°C - 1200°C is 253 – 311 $kJmol^{-1}$ therefore for the plain C-Mn composition without any Nb elements, this is excellent agreement with the activation energy of 253.9 $kJmol^{-1}$ obtained. This is still lower than that observed in low carbon steel and is a result of the increased carbon content. The governing mechanism for grain growth changes from volume diffusion to grain boundary diffusion with the addition of the Nb element, as the activation energies shown in Table 8-3 (regime 1) are close that of half of volume diffusion for Fe in austenite and are in good

agreement to the value of 167.20 $kJmol^{-1}$ [213]. As the annealing temperature increases to the intermediate range (regime 2) the grain growth mechanism is still controlled by grain boundary diffusion as the activation energy is too low for the mechanism to be of volume diffusion. The activation energies in this intermediate temperature range are similar to those given in Smithells [210] of 38 $kJmol^{-1}$ for grain boundary self-diffusion of Fe in austenite at a temperature range of 949°C – 1159°C. The Nb additions do not seem to have much of an effect on activation energies in this temperature range as it does in regime 2 for the lower carbon composition. In the higher temperature range (regime 3) the mechanism for grain boundary motion is once again diffusion of Fe by grain boundary diffusion as shown by the activation energy values given in Table 8-3. The consistent increase in the activation energy in regime 3 with Nb concentration is due to the solute drag effect exerted by the Nb solute atoms at high temperature because of their high diffusivity [212]. This is evident in Figure 6-7 for medium carbon grain growth at different reheating temperatures, where the grain size is the largest in plain C-Mn steel and gets smaller with the addition of Nb irrespective of reheat temperature.

8.7.3.3. High Carbon Steel

In high (0.8 wt. %) carbon steel there are only 2 regimes observed instead of the 3 regimes which are observed for medium (0.4 wt. %) and low (0.08 wt. %) carbon steels. In the high carbon steel grain, growth is likely governed by grain boundary diffusion in both the lower temperature range (regime 1) and higher temperature range (regime 2). It is known that diffusion is much more rapid along grain boundaries then volume diffusion of the material, therefore the diffusion coefficient is higher in polycrystalline materials. Due to the much smaller grain size in high carbon steel with increasing Nb content as shown in Figure 6-12, the diffusivity increases, which results in a decrease in activation energy as given in Table 8-4. However, at the higher temperature (regime 2) the mechanism of grain growth is still by grain boundary diffusion as the activation energies are too low to be for volume diffusion and are closer to those given in Smithells [210] for Fe grain boundary diffusion (38 $kJmol^{-1}$), for plain C-Mn steel composition without any Nb alloying element. The decrease in activation energy can be explained by the increase in diffusivity at the higher temperature. The gradual increase in the activation energy at the higher temperature is due to the solute drag effect by the Nb atoms on the migrating grain boundary, as explained by the solute drag theory [6].

In summary, the activation energies obtained for the low and high temperature ranges when not taking a singular fit are in good agreement to those found by previous authors for volume diffusion [81] and grain boundary diffusion of Fe in austenite [212,

202, 213]. Sinha, et al., for low carbon steel found that the grain growth was controlled by self-diffusion of Fe in austenite by obtaining a activation energy of 262.1 $kJmol^{-1}$ and 252.1 $kJmol^{-1}$ which is very close to the values obtained in this work for low carbon steels at the two extremes. Anelli [82] provided more similar results for activation energy of 69 $kJmol^{-1}$ and 141 $kJmol^{-1}$, for high carbon (0.71 wt. % and 0.85 wt. %) steels. However, many earlier investigations to determine the activation energy of grain growth are much larger than that of Fe self-diffusion in austenite which can be between 253 – 311 $kJmol^{-1}$. There is a lack of explanation for this, but one possibility given by Uhm, et al., [87] is that there is a non-linear relationship between the driving force boundary velocity, as the activation energy found in the investigation was also much higher than that of self-diffusion of Fe in austenite and was given to be 409±21 $kJmol^{-1}$.

8.7.4. Reheat Temperature Model

Figure 8-5, Figure E-11and Figure E-12 are comparisons of the experimental reheat grain size data obtained in Reheat Temperature Chapter 6, for low (0.08 wt. %), medium (0.4 wt. %) and high (0.8 wt. %) carbon steels. It was found that the time exponent value n changed the material constant (A_3) and not the activation energy value. Thus, inserting the time exponent value and the corresponding material constant value and keeping the activation energy constant for each composition gave near identical grain size results in all of the three models for low, medium and high carbon steels as can be seen by the Predicted (C-Mn, K – 1) and Predicted (C-Mn, K – 2) grain sizes which overlap each other. This is expected as the activation energy is not dependent on time but on the grain size. On other hand the material constant is time and temperature dependent.

In low carbon steel, the predicted grain size for plain C-Mn steel can be thought to be accurate if the experimental work of the actual grain measurements had not been made showing different grain growth mechanism. As the predicted values show an gradual exponential increase in grain size with temperature, also indicative of normal grain growth in plain C-Mn without any second phase particles. However, the trend of gradual increase in grain size is also seen for the microalloyed steel where second phase particles would restrict grain growth at particular temperature. Therefore the model does not give an accurate description of the grain growth characteristics. This trend is seen in the remaining medium and high carbon steels, hence fitting a singular line through the data points to obtain an activation energy and material constants does not take into account what is happening in regards to precipitates and abnormal grain coarsening which may occur as a result. Similar exponential grain growth from models has been

shown before [163, 87, 76], however they do not take into account the grain growth characteristics such as normal and abnormal grain growth.

In all the predicted models it can be seen that when not taking the regimes (which have just been discussed previously) into account the grain growth model does not give an accurate evolution of grain size with temperature. However, taking the regimes into consideration and not taking a linear regression gives a more accurate prediction of the grain size and the growth characteristic profile, as shown by the predicted ((composition), Regimes) Figure 8-5, Figure E-11and Figure E-12. This accuracy is due to that fact that neither the material constant nor the activation energy remains constant with increasing temperature, as shown for activation energy in Results Section 8.4.

Isothermal hold at 1050°C and 1150°C of low carbon, plain and microalloyed steel grain size is shown in Figure 8-6 (a) and (b). It is shown that taking a constant activation energy and material constant value either underestimates the grain size with holding time or over estimates it. But taking into account the activation energy for the specific regime, a more accurate fit can be achieved for the austenite grain size with increasing holding time at either of the two temperatures, as shown in Figure 8-6 (c) and (d). This holds true for the remaining medium and high carbon steels shown in Figure 8-7 and Figure 8-8.

9. Reheat Rate

Previously, results on the prior austenite grain sizes have been shown for isothermal parameters, such as in Chapter 6 (Reheat Temperature) and chapter 7 (Hold Time). In these Chapters the effect of Reheat temperature, holding time (two different temperatures 1050°C and 1150°C) on different compositions has been shown.

However in a practical sense thermo-mechanical rolling or any heat treatment processes do not occur under isothermal conditions. Hence different reheating rates of 2.5°C s^{-1}, 5°C s^{-1} and 15°C s^{-1} to the austenitization temperatures of 1000°C and 1100°C have been undertaken to understand the effect of reheating rate on the parent austenite microstructure. This is essential to understand, as control of heating rate during reheating may offer an additional process parameter to improve the properties of the steel.

9.1 Introduction

The results described in this chapter focus on austenite grain growth during continuous heating at different rates to two different temperatures for low carbon 0.08 wt. % steel microalloyed with niobium.

Previously, studies on heating rate have been shown to either have no effect on the prior austenite grain size [99], or either increase the prior austenite grain size [100] or decrease the austenite grains size. Grossmann, [99] has shown that the heating rate of 0.1°C s^{-1} (slow heating), 2°C s^{-1} (moderate rate of heating) and 3.1°C s^{-1} have no effect on the austenite grain growth when heating to a temperature of 925°C. Rosenberg & Digges, [100] presented results indicating that austenite grain size tended to increase with an increase in heating rate. The highest heating rates were 750 Fahrenheit min^{-1} (6.65°C s^{-1}) and 940 Fahrenheit min^{-1} (8.41°C s^{-1}) and the lowest was 9 Fahrenheit min^{-1} (0.2°C s^{-1}). A more recent study by Danon et al., [101] indicated that above a certain temperature there is a greater decrease in the austenite grain size with reheating rate.

The initial microstructure was martensitic obtained by heating the material to 1250°C and holding for an hour and quenching in ice water. This was done to dissolve all the precipitates which were present in the as-received material.

The light optical micrograph images of the specimens have been etched with saturated picric acid with a wetting agent to reveal the prior austenite grain boundaries similar to previous results chapters a detailed description is given in Chapter 4. The austenite grain size was measured using the intercept method ASTM standard E 112.

Precipitation characteristics were analysed at two selected conditions (2.5°C s^{-1} and 15°C s^{-1} to the temperature of 1100°C), including precipitation distribution size, average precipitation size, number density and morphology. These were examined using the carbon extraction replicas technique, using a transmission electron microscope (TEM) operating at an accelerating voltage of 200 kV. The characterisation of the distribution size was achieved by measuring at least 300 precipitates. The precipitation number densities were calculated by counting the particles for a total area; results are presented as number of particles per square micron.

9.2 Heating Rate to 1000°C

Figure 9-1 shows the light optical micrographs that illustrate the effect of heating rates of (2.5°C s^{-1}, 5°C s^{-1} and 15°C s^{-1}) and the niobium addition on the prior austenite grain microstructure for samples austenitized at 1000°C and directly water quenched. The prior austenite grain structure development is fine and uniform and indicative of normal grain growth. This is observed in all the samples regardless of the reheating rate or the niobium content. There is no evidence of any abnormal grain growth at this temperature as the samples were quenched without annealing (i.e. a zero hold time).

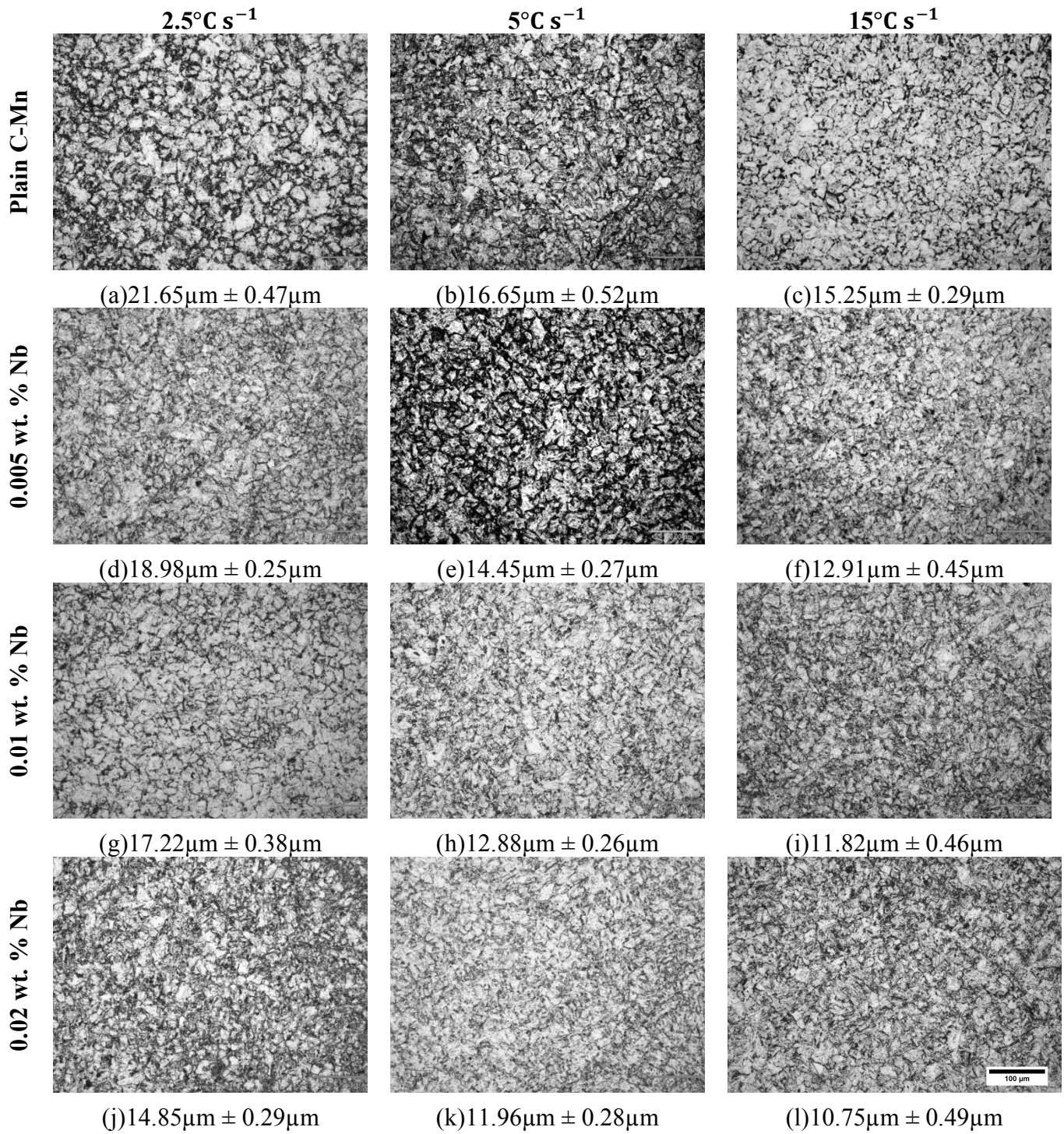

(a)21.65µm ± 0.47µm (b)16.65µm ± 0.52µm (c)15.25µm ± 0.29µm

(d)18.98µm ± 0.25µm (e)14.45µm ± 0.27µm (f)12.91µm ± 0.45µm

(g)17.22µm ± 0.38µm (h)12.88µm ± 0.26µm (i)11.82µm ± 0.46µm

(j)14.85µm ± 0.29µm (k)11.96µm ± 0.28µm (l)10.75µm ± 0.49µm

Figure 9-1: Light optical micrographs showing Austenite Grain Size at 1000°C after different heating rates. (Etched with Saturated Picric Acid), 20x magnification and magnification bar (black) 100µm.

Figure 9-2 summaries the quantitative average grain size measurements of the prior austenite grains as a function of reheating rate and for all the different niobium additions. As expected the plain C-Mn steel has the biggest prior austenite grain size but this decrease with increasing reheating rate. In plain C-Mn steel the decrease in austenite grain size is 26.1% when increasing the reheating rate from 2.5°C s^{-1} to

5°C s^{-1} and 8.8 % when increasing from 5°C s^{-1} to 15°C s^{-1}. Table 9-1 shows the percentage change in the decrease of the prior austenite grain size (PAGS) as the heating rate increases. It can be seen that the change in the prior austenite grain size become less between the reheating rates of 5°C s^{-1} to 15°C s^{-1} in comparison to 2.5°C s^{-1} to 5°C s^{-1}.

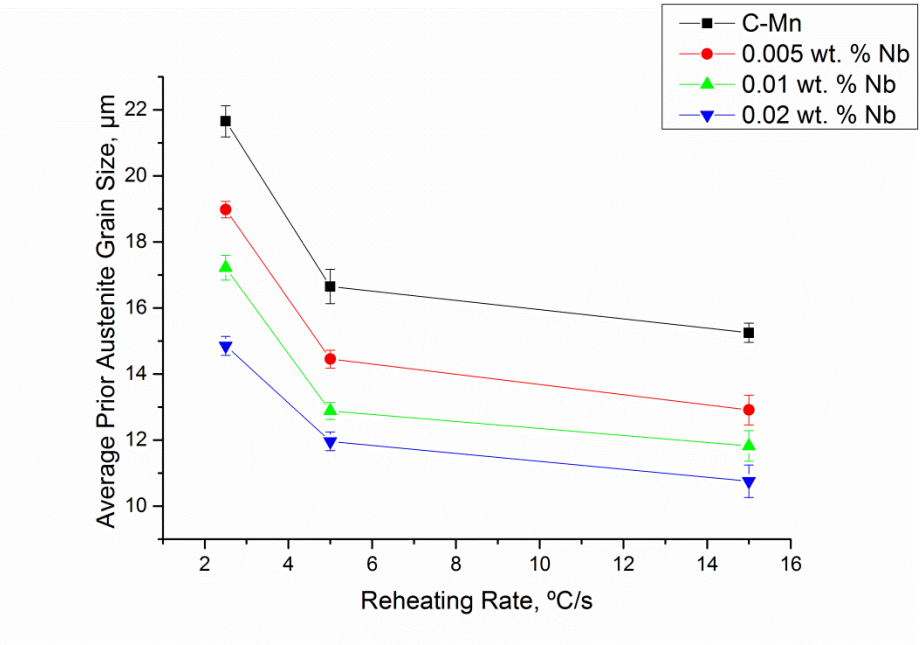

Figure 9-2: The effect of niobium content and heating rate on the average prior austenite grain size (diameter) at 1000°C.

Table 9-1: The percentage change in the decrease of the prior austenite grain size (PAGS) as the heating rate increases.

Specimen	Heating Rate (°C s^{-1})	Decrease in PAGS (%)	Heating Rate (°C s^{-1})	Decrease in PAGS (%)
Plain C-Mn	2.5 - 5	26.1	5 - 15	8.8
0.005 wt. % Nb	2.5 - 5	27.1	5 - 15	11.3
0.01 wt. % Nb	2.5 - 5	28.8	5 - 15	8.6
0.02 wt. % Nb	2.5 - 5	21.6	5 - 15	10.7

Figure 9-3 shows the light optical micrographs that illustrate the effect of heating rates of (2.5°C s^{-1}, 5°C s^{-1} and 15°C s^{-1}) and niobium addition on the prior austenite grain microstructure for samples austenitized at 1000°C with a 5 minute hold and directly water quenched. The prior austenite grain development for plain C-Mn steel shown in Figure 9-3 (a, b and c) illustrates fine/uniform austenite grains which is indicative of normal grain growth. The remaining microalloyed specimens are all

indicative of normal grain growth as shown in the micrographs, regardless of the heating rate or composition.

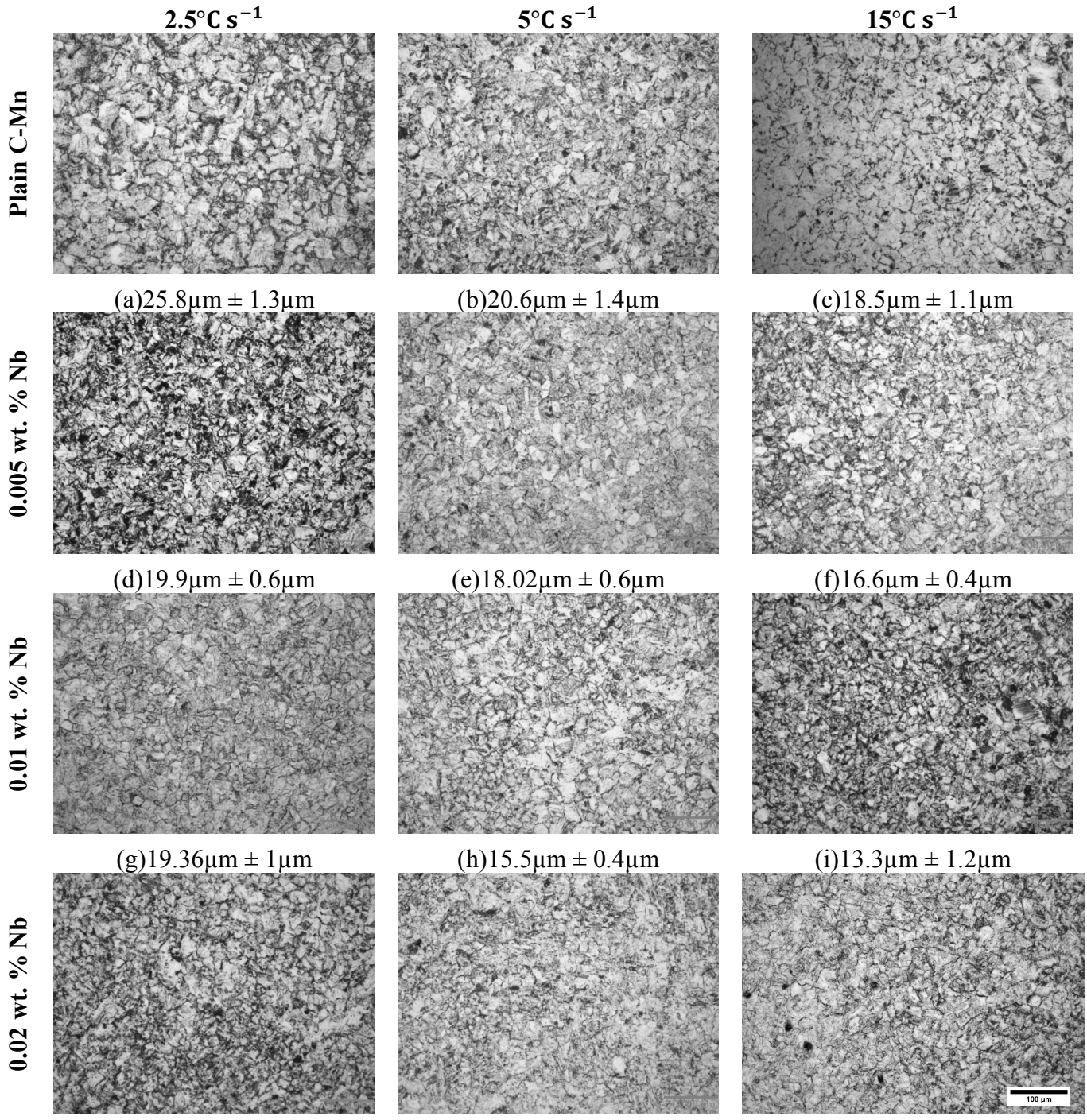

Figure 9-3: Light optical micrographs showing Austenite Grain Size at 1000°C with a 5 minute hold after different heating rates. (Etched with Saturated Picric Acid), 20x magnification and magnification bar (black) 100µm.

Figure 9-4 summaries the quantitative average grain size measurements of the prior austenite grains as a function of reheating rate and for all the different niobium addition specimens austenitized at 1000°C and held for 5 minutes. The grain size trends remain similar to those shown in Figure 9-2 with plain C-Mn steel having the biggest austenite grain size which decreases with increasing heating rate and niobium content.

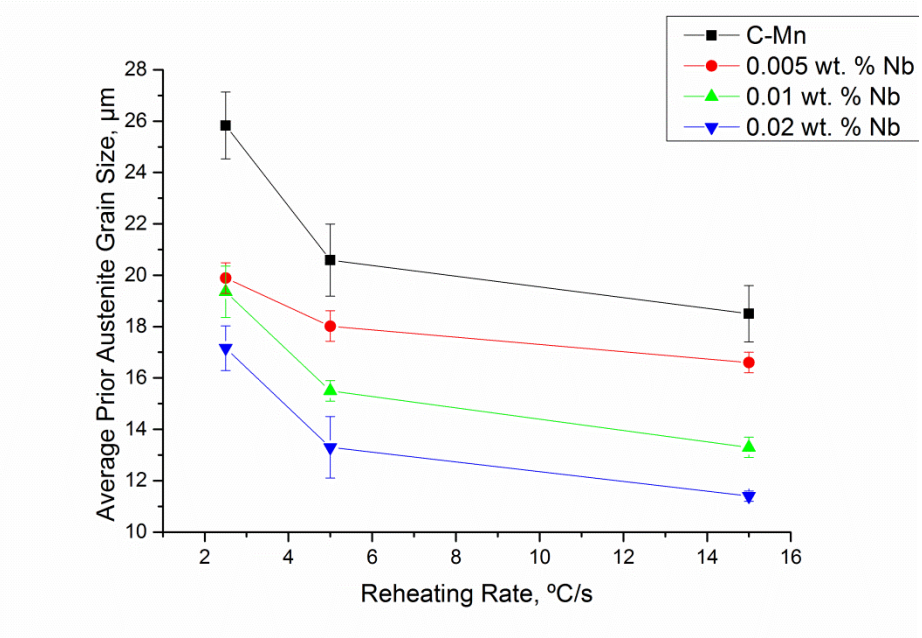

Figure 9-4: The effect of niobium content and heating rate on the average prior austenite grain size (diameter) at 1000°C with a 5 minute hold.

9.3 Heating Rate to 1100°C

Figure 9-5 shows the light optical micrographs that illustrate the effect of heating rates of (2.5°C s^{-1}, 5°C s^{-1} and 15°C s^{-1}) and niobium addition on the prior austenite grain microstructure for samples austenitized at 1100°C and directly water quenched. The prior austenite grain development for plain C-Mn steel Figure 9-5 (a, b and c) show fine/uniform grains. Abnormal austenite grain growth can be observed in the micrograph Figure 9-5 (d) for 0.005 wt % Nb steel at a reheating rate of 2.5°C s^{-1}. The austenite grains for the higher reheating rates of 5°C s^{-1} and 15°C s^{-1} indicate that the austenite grain distribution is fine/uniform, indicative of normal grain growth.

The remaining two microalloyed steel samples shown in Figure 9-5 (g, h, i, j, k and l) show fine/uniform austenite grains development for all three reheating rates (2.5°C s^{-1}, 5°C s^{-1} and 15°C s^{-1}).

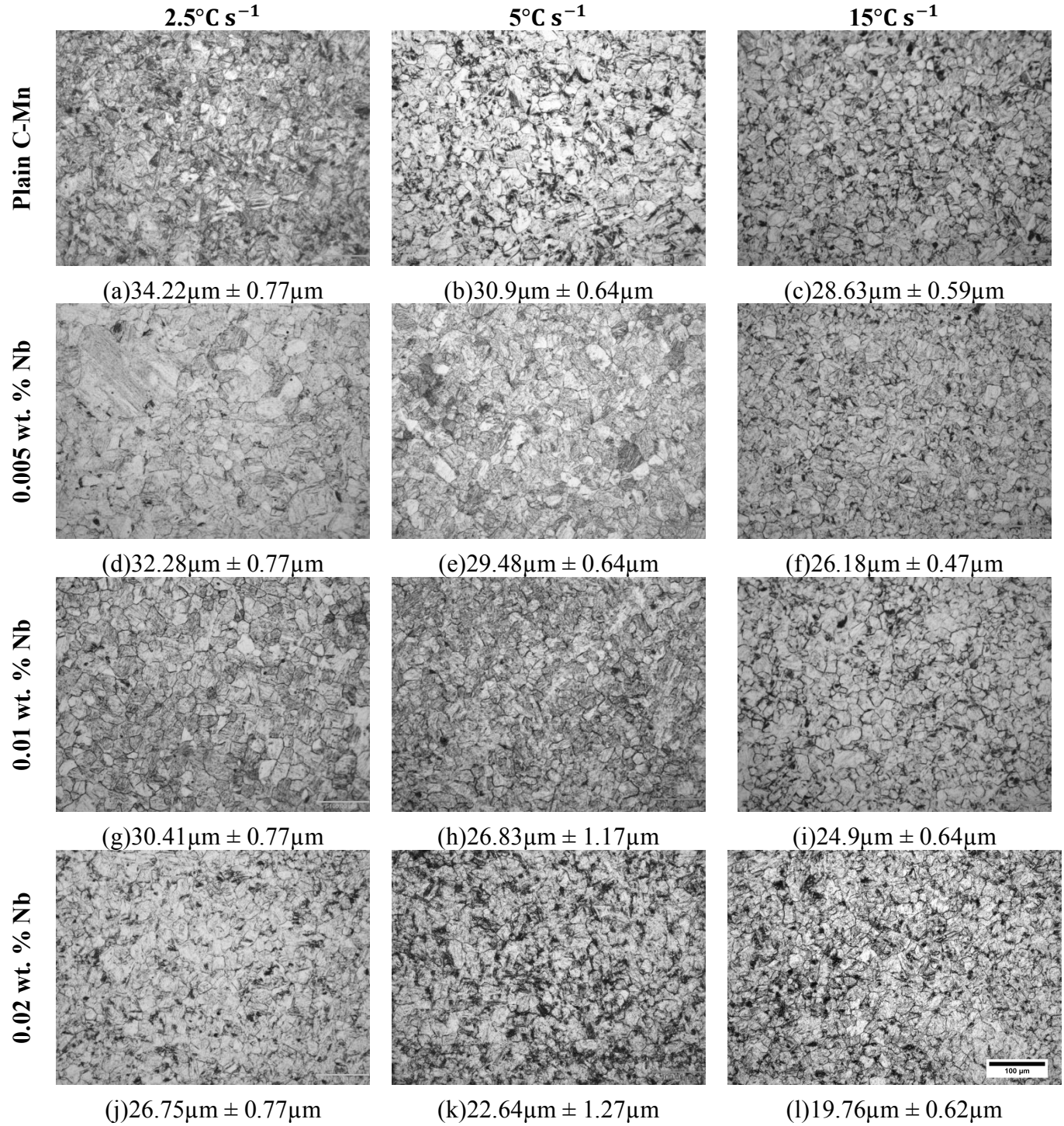

(a)34.22µm ± 0.77µm (b)30.9µm ± 0.64µm (c)28.63µm ± 0.59µm

(d)32.28µm ± 0.77µm (e)29.48µm ± 0.64µm (f)26.18µm ± 0.47µm

(g)30.41µm ± 0.77µm (h)26.83µm ± 1.17µm (i)24.9µm ± 0.64µm

(j)26.75µm ± 0.77µm (k)22.64µm ± 1.27µm (l)19.76µm ± 0.62µm

Figure 9-5: Light optical micrographs showing Austenite Grain Size at 1100°C after different heating rates. (Etched with Saturated Picric Acid), 20x magnification and magnification bar (black) 100µm.

Figure 9-6 summaries the quantitative average grain size measurements of the prior austenite grains as a function of reheating rate for all the different niobium addition specimens austenitized at 1100°C and held for 5 minutes. The percentage change in the

decrease of the prior austenite grain size (PAGS) as the heating rate increases is shown in Table 9-2. In plain C-Mn steel the decrease in austenite grain size is 10.2 % when increasing the reheating rate from 2.5°C s^{-1} to 5°C s^{-1} and 7.6 % when increasing from 5°C s^{-1} to 15°C s^{-1}. This decrease is much less then that observed for the temperature of 1000°C, indicating that the reheating rate has a much more dramatic effect on the prior austenite grains at lower temperatures. The remaining values for the decrease in the percentage of prior austenite grain are given in Table 9-2.

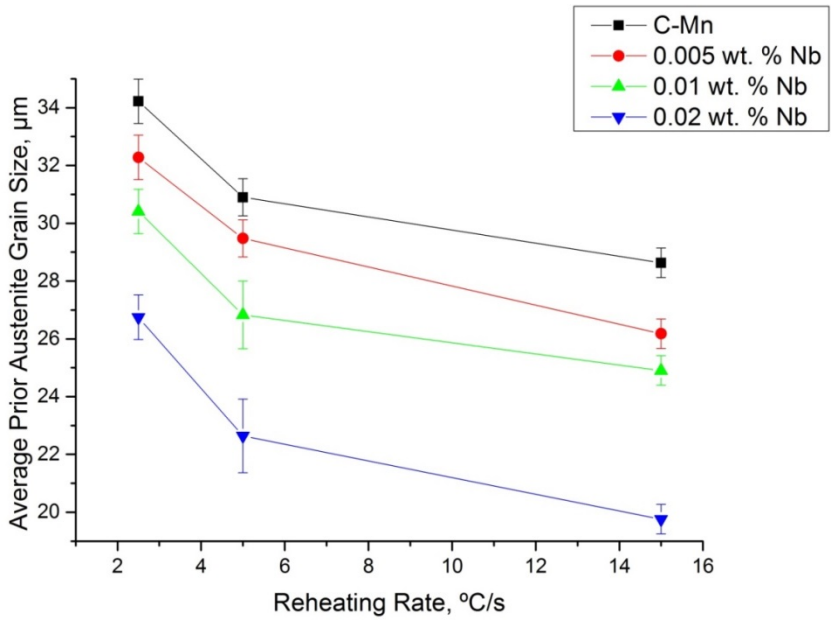

Figure 9-6: The effect of niobium content and heating rate on the average prior austenite grain size (diameter) at 1100°C.

Table 9-2: The percentage change in the decrease of the prior austenite grain size (PAGS) as the heating rate increases.

Specimen	Heating Rate (°C s^{-1})	Decrease in PAGS (%)	Heating Rate (°C s^{-1})	Decrease in PAGS (%)
Plain C-Mn	2.5 - 5	10.2	5 - 15	7.6
0.005 wt. % Nb	2.5 - 5	9.1	5 - 15	11.9
0.01 wt. % Nb	2.5 - 5	12.5	5 - 15	7.4
0.02 wt. % Nb	2.5 - 5	16.6	5 - 15	13.6

The average precipitation size (diameter), precipitation size distribution, precipitation density and morphology were quantified using the TEM micrograph images. Figure 9-7 shows the precipitation distribution histograms for 0.02 wt. % Nb alloyed steel at two reheating rates of 2.5°C s^{-1} and 15°C s^{-1}. For a martensitic structure without any

niobium carbide (NbC) precipitates present in the initial microstructure, the reheating rate does make a difference to the prior austenite grain size. Figure 9-7 (a) demonstrates that when reheating at 2.5°C s^{-1} the niobium carbide size distribution is in the range of 1.4 nm to 54.5 nm. In Figure 9-7 (b) the precipitation distribution is shown for 15°C s^{-1}; the range of the precipitates are 1.5 nm to 36 nm. Figure 9-8 shows a niobium carbide (NbC) precipitate at a very high magnification of 285000 with the EDX analysis indicating that the particle is NbC.

Table 9-3 summarises precipitation number density and average precipitation size at 1100°C for selected reheating rates obtained by the TEM carbon extraction replicas shown in Figure 9-7 (a and b). The data presented in Table 9-3 indicates that the average precipitation size and the precipitation number density decreases with increasing reheating rate. The precipitates are much finer at the higher reheating rates of 15°C s^{-1} than 2.5°C s^{-1}.

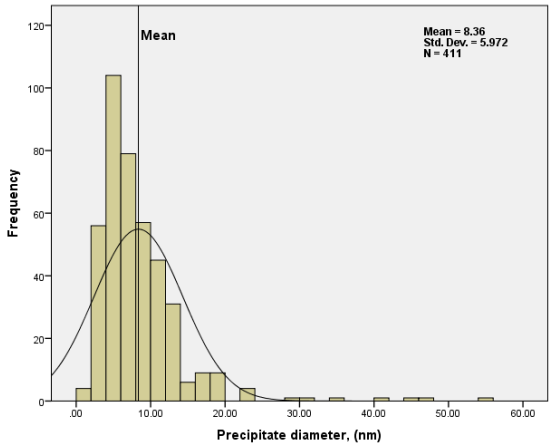

(a) 2.5°C s^{-1}

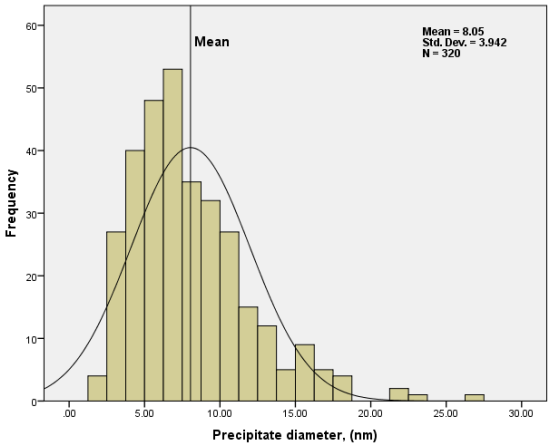

(b) 15°C s^{-1}

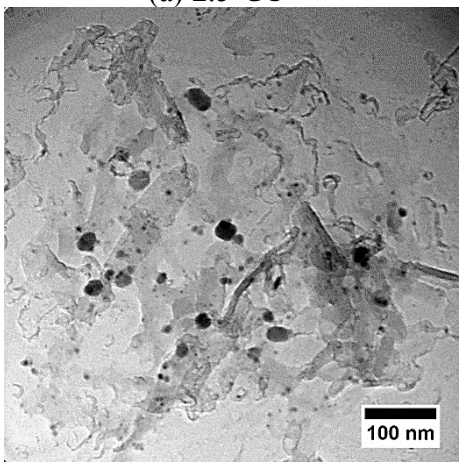

(c) 2.5°C s^{-1}

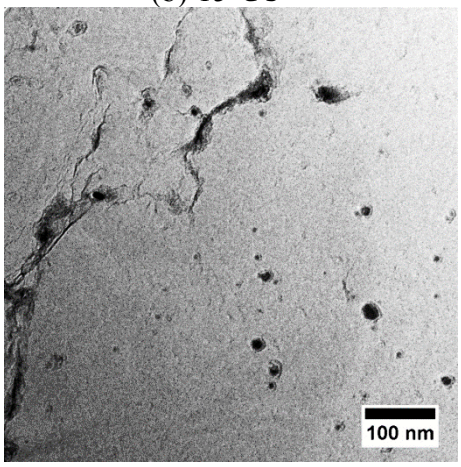

(d)15°C s^{-1}

Figure 9-7: The precipitation size distribution as a function of 2.5°$C\ s^{-1}$ and 15°$C\ s^{-1}$ with the respective TEM micrographs below them.

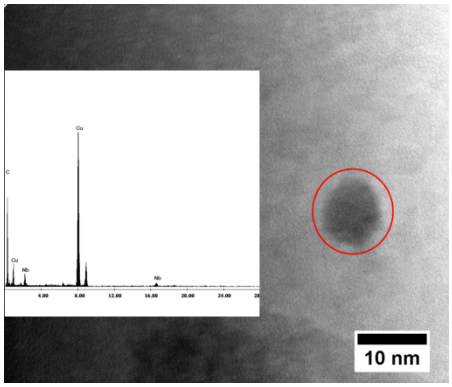

Figure 9-8: TEM bright field image micrograph showing a niobium Carbide precipitate at 285000x magnification with EDX analysis on the left.

Table 9-3: Precipitate number density and average precipitate size at 1100°C for two selected reheating rates (2.5°$C\ s^{-1}$ and 15°$C\ s^{-1}$)

Steel	Reheating Rate Condition			Precipitate number density (μm^{-2})	Average precipitate diameter size (nm)
	Temp (°C)	Time (s)	Reheating Rate (°C s^{-1})		
0.02 wt. % Nb	1100	0	2.5	0.13	8.36
			15	0.09	8.05

Figure 9-9 shows the light optical micrographs that illustrate the effect of heating rates of (2.5°C s^{-1}, 5°C s^{-1} and 15°C s^{-1}) and niobium addition on the prior austenite grain microstructure for samples austenitized at 1100°C with a 5 minute hold and directly water quenched. The prior austenite grain growth characteristics for plain C-Mn steel indicate coarse normal grains distribution which are shown in Figure 9-9 (a, b and c). Abnormal grain growth is observed in all the remaining optical light micrographs alloyed with niobium, where one large or a few large austenite grains are observed within a relatively equiaxed fine matrix of austenite grains.

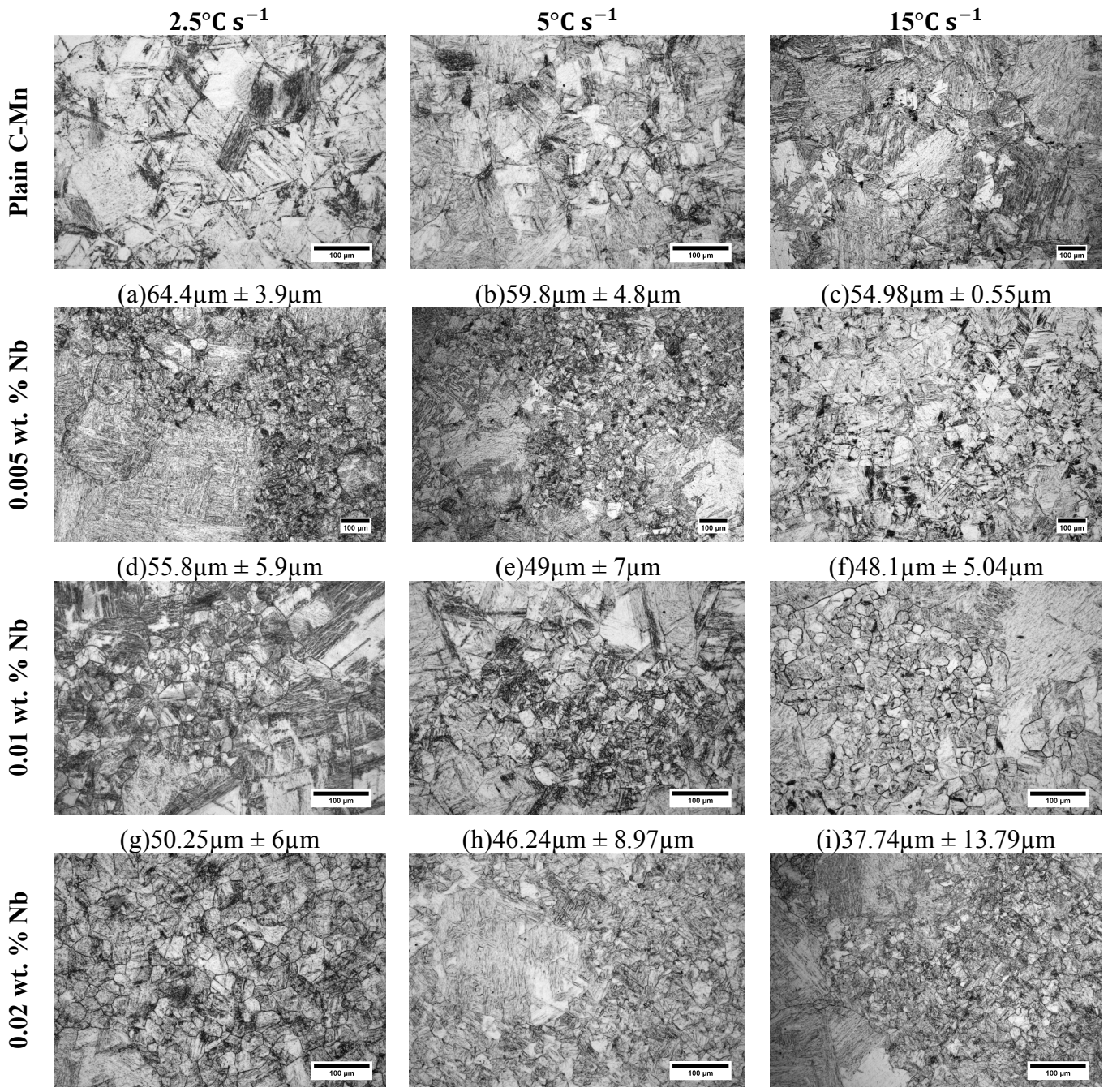

(a)64.4µm ± 3.9µm (b)59.8µm ± 4.8µm (c)54.98µm ± 0.55µm

(d)55.8µm ± 5.9µm (e)49µm ± 7µm (f)48.1µm ± 5.04µm

(g)50.25µm ± 6µm (h)46.24µm ± 8.97µm (i)37.74µm ± 13.79µm

(j)47.5µm ± 4.8µm (k)39.1µm ± 7µm (l)33.6µm ± 8.9µm

Figure 9-9: Light optical micrographs showing Austenite Grain Size at 1100°C with a 5min hold after different heating rates. (Etched with Saturated Picric Acid), 10x and 20x magnification and magnification bar (black) 100µm.

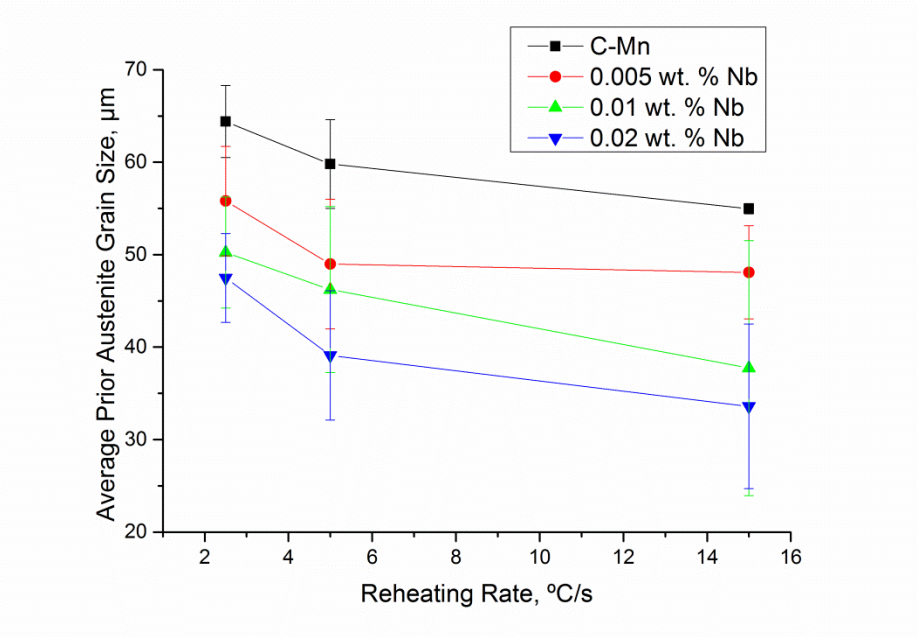

Figure 9-10: The effect of niobium content and heating rate on the average prior austenite grain size (diameter) at 1100°C with a 5 minute hold.

9.4 Summary

It has been found that increasing the reheating rate decreases the prior austenite grain size at both temperatures of 1000°C and 1100°C and when held for 5 minutes. The results did indicate that the effect of reheating rate on the decrease in the prior austenite grain size was more prominent for heating rates of 2.5°C s^{-1} and 5°C s^{-1} at lower temperatures of 1000°C. When the heating rate was 15°C s^{-1} the decrease in the prior austenite grain size was not as significant.

The two conditions used to show the effect of precipitates indicated that with increasing heating rate the precipitation number density decreases, the average precipitation size decreases and that that the precipitates are much finer at higher heating rates.

9.5 Discussion of Reheat Rate

The effect of alloying elements on low (0.08 wt. %) carbon steel at different temperatures has been shown to have an effect on decreasing the prior austenite grain size. However, the effect of reheat rate on the prior austenite grain size is not understood completely as explained in the literature review.

The austenite grain size in the plain C-Mn steel decreases with increasing reheating rate from 2.5°C s^{-1}, 5°C s^{-1} and 15°C s^{-1} up to 1000°C, exhibiting a uniform grain size as shown in light optical micrographs in Figure 9-1 (a), (b) and (c) with the grain size given below the respective micrograph. The microalloyed steels experience a further decrease in austenite grain size with increasing Nb content which is also shown in Figure 9-1. A visual representation of the reheat rate and its effect on austenite grain size is given in Figure 9-2. The percentage decrease with respect to reheating rate is shown in Table 9-1, it indicates that the highest decrease is observed between 2.5°C s^{-1} and 5°C s^{-1}, of 26.1% for plain C-Mn steel and 27.1 % for 0.005 wt. % Nb, 28.8 % for 0.01 wt. % Nb and 21.6 % for 0.02 wt. % Nb steel, and that increasing the heating rate to 15°C s^{-1} does not imply a further decrease in the austenite grain size of the same magnitude.

Figure 9-3 illustrates the effect of heating rates of (2.5°C s^{-1}, 5°C s^{-1} and 15°C s^{-1}) on prior austenite grain microstructure for samples austenitized at 1000°C with a 5 minute hold and directly water quenched. Once again a fine/uniform grain size can be observed in all micrographs, with Figure 9-4 giving the quantitative measurements of the prior austenite grains as a function of reheating. It should be noticed that at that the increase in austenite grain size for plain carbon steel when held for 5 mins at 1000°C, is also affected by the reheating rate. The principal effect of the reheating rate can be explained using the classical nucleation theory. A slow reheating rate will give fewer nuclei and will in turn lead to larger initial austenite grain size, on the other hand, a fast reheating rate will lead to more nucleii and therefore lead to a smaller initial austenite grain size.

Results of reheating to a higher temperature of 1100°C are shown in Figure 9-5 for all three reheating rates (2.5°C s^{-1}, 5°C s^{-1} and 15°C s^{-1}). What is interesting at 1100°C is that abnormal austenite grain growth can be observed in micrograph Figure 9-5 (d) for 0.005 wt % Nb steel at a reheating rate of 2.5°C s^{-1}. This could be a result of the equilibrium conditions have being attained for the precipitates due to the lower reheating rate for and therefore the rate of dissolution and coarsening increases [102], whereas the remaining microalloyed steels are still in the non-equilibrium stage which leads to a decrease in the rate of dissolution and coarsening of precipitates. It was earlier

shown in the Reheat Temperature Chapter 6 that the T_{GC} increases with Nb composition. It was shown in Figure 6-3 that the $T_{GC} = 1000°C$ for 0.005 wt. % Nb in low carbon steel for equilibrium conditions. However, reheating at 2.5°C s^{-1} increases the T_{GC} to 1100°C. This is consistent with other findings [102]. However, when being held at 1100°C for 5 minutes there is a large amount of normal grain coarsening observed in plain C-Mn steel which is expected as there are no second phase particles to pin grain boundaries [65, 67, 73, 68]. There is abnormal grain growth occurrence in the microalloyed steels as shown in Figure 9-9, where the grain size still decreases with increasing reheating rate as indicated in Figure 9-10. This indicates that for the microalloyed steels dissolution/coarsening occurs at or with a 5 minute hold. It was shown in Figure 9-5 (d) that abnormal grain coarsening starts to occur in the 0.005 wt. % Nb composition without any hold, indicating that NbC precipitates start to undergo Ostwald ripening at a reheating rate of 2.5°C s^{-1}. Now with a 5 minute hold, it is seen that at a reheating rate of 15°C s^{-1} a more homogenous austenite grain structure is obtained. As TEM analysis on the precipitate characteristics was not performed for this composition, the reason for this could not be identified.

The composition with 0.02 wt. % Nb has a uniform structure at the slower reheating rate of 2.5°C s^{-1} and this suggests that finer precipitates suppressed grain growth. Table 9-3 (for heating at 1100°C and immediately quenching) shows that a slower reheating rate produced higher precipitate number density, whilst at the same time keeping the average particle size ≤ 20nm (diameter) to restrict grain growth. However, it was found that the T_{GC} for 0.02 wt. % Nb composition is at 1050°C and that it is known that higher reheating rates increase the T_{GC}. Therefore it is reasonable to assume that coarsening/dissolution is the main reason for the abnormal grain growth occurrence explained earlier by the Ostwald ripening phenomenon. The critical particle radius increases with an increase in number density of the precipitates and as dissolution occurs, the remaining precipitates become larger and are unable to restrict grain growth. Martin, et al., [102] investigated the effect of 3 different heating rates (0.05°C s^{-1}, 0.5°C s^{-1}, and 5°C s^{-1}) at 4 different austenitization temperatures ranging from 910°C to 1250°C in ~50°C increments. This research has shown similar results to those found in this investigation in that the prior austenite grain size decreases with increasing reheating rate and is in good agreement [57, 102, 214, 104, 105].

9.5.1. Effect of Heating Rate on Precipitation

Alogab, et al., [105] has shown that varying the heating rate to the austenitization temperatures of 1050°C has a strong influence on the number density of the precipitates and the average precipitate size. As the heating rate increased from $20°C\,min^{-1}$ ($0.3°C\,s^{-1}$) to $145°C\,min^{-1}$($2.4°C\,s^{-1}$) it resulted in an increase in the average precipitate size and an decrease in the number density of the precipitates.

Figure 9-7 (a) shows a histogram of the distribution of the NbC precipitates when reheating at $2.5°C\,s^{-1}$ in the range of 1.4 nm to 54.5 nm. In Figure 9-7 (b) the precipitation distribution is shown for $15°C\,s^{-1}$; the range of the precipitates are between 1.5 nm and 36 nm. Figure 9-8 shows an EDX analysis indicating that the particle is NbC. It is shown in Table 9-3 that at slower reheating rates the number density was higher and the average precipitate size was slightly larger, than when the reheating rate was faster. These results only partially agreed with the previous findings of the author in regards to precipitate number density being higher for a slower reheating rate [105]. This may be due to the holding time differences, but it is still counterintuitive based on the conventional model for Ostwald ripening.

The results in this investigation indicate that at lower heating rates the precipitates have enough time to grow, due to the conditions being close to equilibrium conditions and more precipitates can form. At higher reheating rates due to the non-equilibrium conditions, fewer numbers of fine precipitates form.

10. A Summary of the significance of this work

The primary aim of this work was to understand the microstructural evolution of the prior austenite grains for different carbon and niobium contents at different reheating temperatures, hold times and reheating rate. The objectives which were pointed out in the beginning of this work have all been achieved.

The main novelty of this work lies primarily in the compositions investigated. Past researchers have not investigated different carbon contents whilst keeping the amounts of other elements relatively similar and microalloying elements less than 0.02 wt. %.

This research investigation has also developed an etching technique which is relatively fast and does not require much if any re-polishing of the specimens to reveal the prior austenite grains. This would aid in time saving and cost of consumables when analysing steel specimens for the prior austenite grain structure. The technique has been applied to all the compositions in this work (reheat temperature, hold time and reheat rate) and has been proven to be effective in saving time and cost. An important part of this technique is that it works with 0.8 wt. % Carbon steel compositions, as previous research have found it very difficult to chemical etch 0.8 wt. % Carbon steels, the addition of the etching technique adds the benefit of etching certain compositions previously difficult to etch.

The characterisation of bimodal austenite grain structure in this work has been calculated by using standard deviation values obtained by the ASTM E112 [126] method to describe the distribution of grain sizes. This technique was found to be simple and easy to measure the bimodal distribution of the austenite grain size. The standard test method to measure duplex grain structures is ASTM E 1181 [215]. This method works well for structures which have a distinct coarse and fine prior austenite grain distribution. However for structures where there is a small difference in austenite grain heterogeneity, as seen in the work for 0.8 wt. % Carbon, leads to problems with the usage of this method. The arbitrary division for the heterogeneity based on visual inspection to separate the austenite grain size distribution into two distinct populations could lead to inaccuracies. Therefore using the standard deviation values obtained from the ASTM E112 method which is used in this work provides a better description of the heterogeneity of the grain structure, this is provided that the field of views are kept identical in all specimens when taking the standard deviation as a measure for heterogeneity.

Clearly, the compositions of the steels used in this investigation were of simple design and were not intended to represent commercial grade steels. However, results from reheat temperature helped build on existing formulae to calculate abnormal grain

growth temperatures provided by Palmiere [68] for low carbon steel, with this work contributing 5 different carbon concentrations with 3 varying niobium contents. These formulae are useful in predicting which temperatures, with respect to the compositions, exhibit abnormal grain structure, therefore helping to avoid initial abnormal structures which are difficult to remove later down the processing route, whilst keeping the initial grain structure as small as possible.

The understanding of the abnormal grain growth behaviour of microalloyed steels is critical since it will ultimately influence the mechanical properties of the steel structure. Another significant finding from this work is the relation between temperature and hold time, principally how long it takes for the abnormality in the austenite grain structure to correct itself.

Another significant outcome of this investigation are the austenite grain growth models for low (0.08 wt. % C), medium (0.4 wt. % C) and high (0.8 wt. % C) carbon steels to estimate the austenite grain size at individual temperatures. These have the potential to be useful industrially to improve the strength of the product.

The overall combined result from this work would be an enhancement to the final product in regards to the microstructure being kept uniform throughout, therefore giving improved mechanical properties.

11. Conclusions

Investigations into the effect of low niobium concentrations of 0.005, 0.01 and 0.02 wt. % Nb for the five carbon concentrations of 0.08, 0.2, 0.4, 0.6 and 0.8 wt. % have not been investigated previously. Therefore the compositions investigated in this work are novel and the austenite grain size results for these compositions have yielded the following findings.

11.1 Delineation of Prior Austenite Grain Boundaries (PAGB)

1. This research has developed a new etching technique which is relatively fast and does not require much if any re-polishing of the specimens to reveal the prior austenite grains in high purity cast steels. An important part of this technique is that it works with 0.8 wt. % carbon steel compositions, as previous literature has reported the difficulties of chemically etching 0.8 wt. % carbon steels.
2. The wetting agent was found to have a significant influence on austenite grain boundary delineation in high purity HSLA steel. It was shown that sodium dodecyl sulfate (SDS) worked best for 0.08 wt. % to 0.6 wt. % steels and sodium dodecylbenzene sulfonate (SDBS) for 0.8 wt. % C steel and both wetting agents were shown to give significantly good results.
3. The formation of this protective etchant layer on the surface is considered to be of vital importance in the etching process as it helps stop the fresh etching solution from reacting with the specimen surface.
4. The importance of making the etching solution less acidic is important in getting the samples to etch first time around which saves time on re-polishing and re-etching.

11.2 As Received Material

1. Pearlite volume fraction increases with increasing niobium content from 0.005 to 0.02 wt. % Nb in low 0.08 wt. % and 0.4 wt. % carbon steel.
2. Micro-hardness results showed that increasing Nb in low (0.08 wt. %) carbon steel did not increase the hardness suggesting that no precipitation strengthening in ferrite or pearlite interlamellar refinement occurs.
3. A hardness increase in pearlite with increased Nb was observed and is likely to be a result of interlamellar spacing refinement due to the addition of Nb.

This was observed in both medium (0.4 wt. %) and high (0.8 wt. %) carbon steels, but not in low (0.08 wt. %) carbon steel.

11.3 Reheat Temperature

1. In plain C-Mn steels, the increasing carbon content was also found to decrease the prior austenite grain size. This was attributed to the solute drag effect of the carbon atoms.
2. Upon reheating abnormal grain growth was observed in all Nb alloyed steels. Increasing the Nb content from 0.005 to 0.02 wt. % increased the abnormal grain coarsening temperature. Increasing the carbon content from 0.08 to 0.8 wt. % was found to increase the NbC precipitate stability and was also shown to increase the abnormal grain coarsening temperature. However the extent of the heterogeneity in the austenite grain structure decreases with increasing carbon content.
3. Calculation of a relationship between the T_{GC} and the T_{DISS} can provide a useful indication in locating the start of the T_{GC}. This would further reduce steps needed to eliminate heterogeneity later down the processing route to provide a homogenous microstructure and provide an improvement in mechanical properties. These relationships are provided below- starting from low carbon to high carbon.

$$T_{GC}{}^{0.08\ wt.\ \%\ C} = T_{DISS} - 43°C\ \pm 14 \quad (11\text{-}1)$$

$$T_{GC}{}^{0.2\ wt.\ \%\ C} = T_{DISS} - 122°C\ \pm 60.4 \quad (11\text{-}2)$$

$$T_{GC}{}^{0.4\ wt.\ \%\ C} = T_{DISS} - 235°C \pm 48.1 \quad (11\text{-}3)$$

$$T_{GC}{}^{0.6\ wt.\ \%\ C} = T_{DISS} - 247°C\ \pm 56.1 \quad (11\text{-}4)$$

$$T_{GC}{}^{0.8\ wt.\ \%\ C} = T_{DISS} - 278°C\ \pm 40.1 \quad (11\text{-}5)$$

4. There are different grain growth regimes observed during the reheating stages. 3 grain growth regimes in low and medium carbon steels, and two grain growth regimes observed in high carbon steel.

11.4 Hold Time

1. Increasing the Nb content in either of the 5 carbon concentrations slowed the austenite grain growth; however the effect of Nb addition on the grain growth was shown to have a dramatic effect in 0.8 wt. % carbon steel at 1050°C.
2. It has been shown that other then hold time, reheat temperature also plays a major part in determining grain structure together with the wt. % of Nb.
3. Abnormal grain growth is observed in plain C-Mn steel for all the three carbon concentrations of 0.08, 0.4 and 0.8 wt. % at the higher temperature of 1150°C after periods of longer than 1 hour hold but not at the lower temperature of 1050°C. This has been attributed to the strain in the specimen prior to the heat treatment.
4. As the duration of the hold increases the carbide precipitates become larger with the total number density decreasing, which is very well described by the Ostwald ripening theory. The controlling coarsening mechanism for carbide precipitate growth varies with temperature and carbon content and can be related to the total dissolution temperature for the NbC precipitates. The rate of coarsening has been shown to have low values for two scenarios. Firstly if the isothermal hold is above the total dissolution temperature and secondly, when there is high stability of the carbide precipitates as in the case of high (0.8 wt. %) carbon. Apart from the low coarsening rate exceptions mentioned the main coarsening mechanism was diffusion through dislocations.
5. The time exponent n value is influenced by both the composition and temperature. In general the time exponent increases towards higher temperatures 1150°C, the time exponent reaches a constant value for the majority of the compositions giving an n = 0.21. Increasing niobium content to 0.01 and 0.02 wt. % in steel with 0.8 wt. % decreases the n value to 0.0159 and 0.0384 for the temperature of 1150°C.

11.5 Grain Growth

1. The empirical models for predicting the isothermal grain growth of austenite in C-Mn and C-Mn-Nb steels does not fit well with the experimental results when assuming that only one growth regime is taking place. However when multiple growth regimes are taken in to account the model gives an excellent fit.
2. Activation energy for grain growth is found to decrease with increasing carbon content.

11.6 Reheat Rate

1. It has been found that increasing the reheating rate decreases the prior austenite grain size at both temperatures of 1000°C and 1100°C when the samples were immediately quenched and when they were held for 5 minutes. The results did indicate that the effects of reheating rate on the decrease of the prior austenite grains were more prominent for heating rates of 2.5°C s^{-1} and 5°C s^{-1} at lower temperatures of 1000°C. When the heating rate was 15°C s^{-1} the decrease in the prior austenite grain size was not as significant.

2. The two conditions used to show the effect of precipitates indicated that with increasing heating rate the precipitation number density decreases, the average precipitation size decreases and the precipitates are much finer at higher heating rates.

12. Further Work

One of the primary aims of this work was to look at the effect of composition on microstructural development. This current investigation has focussed on steels with niobium content below 0.02 wt. %, and so there is still plenty of work to be done to investigate and understand further effects of low niobium concentrations on precipitation and mechanical properties. This chapter will discuss the possibilities for further investigation identified during this work, which are as follows

- To determine if the bimodal austenite grain structure obtained at specific temperatures can be removed during deformation.
- To investigate the mechanical properties of the specimens as a function of different reheating temperatures, taking in to consideration the evolution of the austenite grain microstructure.
- In this work precipitates were analysed at 1050°C and 1150°C, but it would be useful to analyse the precipitation evolution at different reheating temperatures. The results could be useful in formulating a solubility equation for NbC precipitates for different carbon contents.
- Formation of precipitates with rod morphology could also be investigated. Particular emphasis should be placed on the orientation relationship between the rods and the austenite matrix.
- As the experimental work looking at the effect of reheating rate was only performed on the low carbon composition, it should be expanded to the remaining carbon compositions, to investigate the effect of varying carbon content and reheating rate and to confirm if the microalloying element has an influence on the austenite grain structure.
- Further investigation can be directed towards the effect of strain and austenite grain growth characteristics during reheating temperatures and hold times, as it was found in this work that plain C-Mn steel held at 1150°C indicated abnormal grain growth characteristics when held for extended times.
- Another point of interest could be the investigation of the effect of reheating rate on the A_3 temperature with respect to the different carbon compositions.
- This work was concerned with reheating but there would be a lot of scope for investigating the transformation temperatures, microstructure formation and thermal distribution throughout the steel samples during the cooling stage.

13. Works Cited

[1] T. Gladman, The Physical Metallurgy of Microalloyed Steels, London : Maney Publishing , 2002.

[2] T. Tanaka, "Controlled rolling of steel plate and strip," *International Metals Reviews,* vol. 26, no. 1, pp. 185-212, 1981.

[3] C. M. Sellars and J. A. Whiteman, "Recrystallization and grain growth in hot rolling," *Material Science ,* vol. 13, no. March - April , pp. 187-193, 1979.

[4] A. J. DeArdo, M. J. Hua, K. G. Cho and C. I. Garcia, "On strength of microalloyed steels: an interpretive review," *Material Science and Technology,* vol. 25, no. 9, pp. 1074 - 1082, 2009.

[5] L. J. Cuddy, "Microstructure Development During Thermomechanical Treatment of HSLA Steels," *Metallurgical Transactions A,* vol. 12, pp. 1313-1320, 1981.

[6] J. W. Cahn, "The impurity-drag effect in grain boundary motion," *Acta Metallurgica,* vol. 10, pp. 789 - 798, 1962.

[7] K. Lucke and H. P. Stuwe, "On the theory of impurity controlled grain boundary motion," *Acta Metallurgica,* vol. 19, pp. 1087 - 1099, 1971.

[8] M. Hillert and B. Sundman, "A Treatment of the solute drag on moving grain boundaries and phase interfaces in binary alloys," *Acta Metallurgica,* vol. 24, pp. 731 - 743, 1975.

[9] K. Lucke and K. Detert, "A quantitative theory of grain boundary motion and recrystallization in metals in the presence of impurities," *Acta Metallurgica,* vol. 5, pp. 628 - 637, 1957.

[10] L. Sun, The Effects of Strain Path Reversal on Austenite Grain Subdivision, Recrystallisation and Phase Transformations in Microalloyed Steel, Sheffield, 2012.

[11] T. Kimura and Y. Kurebayashi, "Niobium in Microalloyed Engineering Steels, Wire Rods and Case Carburized Products," pp. 801-872, 2001.

[12] W. B. Morrison, "Overview of Microalloying in Steel," in *The Proceedings of the Vanitec Symposium*, Guilin, 2000.

[13] D. K. Matlock and J. G. Speer, "Microalloying concepts and application in long products," *Material Science and Technology,* vol. 25, pp. 1118-1125, 2009.

[14] J. Adanczyk, "Development of the microalloyed constructional steels," *Achievements in Materials and Manufacturing Engineering,* vol. 14, no. 1-2, pp. 9-20, 2006.

[15] H.-G. Hillenbrand, M. Graf and C. Kalwa, "Development and production of high strength pipeline steels," in *Europipe*, Florida, 2001.

[16] G. E. Dieter, Mechanical Metallurgy, London, UK: McGraw-Hill Book Company, 1989.

[17] Y. Weng, "Overview," in *Ultra-Fine Grained Steels*, Beijing, Springer Berlin Heidelberg, 2009, pp. 12-13.

[18] H. K. Bhadeshia and R. W. Honeycombe, Steels, Microstructure and Properties, Cambridge: Butterworth-Heinemann, 2007.

[19] K. L. Murty and I. Charit, An Introduction to Nuclear Materials: Fundamentals and Applications, Wiley VCH, 2012.

[20] C. Hatchett, "An Analysis of a Mineral Substance from North America, Containing a Metal Hitherto Unknown," *Philosophical Transactions of the Royal Society of London,* pp. 49 - 66, 1802.

[21] F. M. Becket and R. Franks, "Steel". United States of America Patent 2158651, 16 May 1939.

[22] A. J. DeArdo, "Niobium in mordern steels," *International Material Reviews,* vol. 48, pp. 371-402, 2003.

[23] British Geological Survey, "Risk list 2011," 2011.

[24] J. M. Gray and F. Sicilianco, "High Strength Microalloyed linepipe: Half a Century ofEvolution,"[Online].Available: http://www.metal.citic.com/iwcm/UserFiles/img/zlk/03_30zn/d2.pdf. [Accessed 23 May 2012].

[25] "wikipedia,"wikipedia,[Online]Available: http://en.wikipedia.org/wiki/File:World_Niobium_Production_2006.svg. [Accessed 20 1 2012].

[26] H. Stuart, Niobium: Proceedings of the International Symposium, H. Stuart, Ed., Warrendale, Pennsylvania: Tms, 1984, pp. 113-132.

[27] N. P. Lyakishev, N. A. Tulin and Y. L. Pliner, Niobium in Steels and Alloys, Araxa: Companhia Brasileira de Metaivrgia & Mineracao, 1984.

[28] Roskill, "Roskill Report on The Economics of Niobium," Roskill, London, 2012.

[29] Q. Yu, Z. Wang, X. Liu and G. Wang, "Effect of microcontent Nb in solution on the strength of low carbon steels," *Material Science and Engineering,* vol. 379, pp. 384-390, 2004.

[30] K. Hulka, "The Role of Niobium in multi-pgase steel," cbmm, Düsseldorf.

[31] H. Meuser, F. Grimpe, S. Meimeth, C. J. Heckmann and C. Trager, "Development of NbTiB micro-alloyed HSLA steels for high-strength heavy plate," in *Microalloying for New Steel Processes and Applications*, San Sebastian, Spain, 2005.

[32] B. Verlinden, J. Driver, I. Samajdar and R. D. Doherty, "Softening Mechanisms," in *Thermo-Mechanical Processing of Metallic Materials*, Oxford, Elsevier, 2007, p. 85.

[33] Z.-h. Zhang, Y.-n. Liu, X.-k. Liang and Y. She, "The effect of Nb on recrystallization behavior of a Nb micro-alloyed steel," *Material Science and Engineering,* vol. 474, pp. 254-260, 2008.

[34] T. Niu, Y.-l. Kang, H.-w. Gu, Y.-q. Yin, M.-l. Qiao and J.-x. Jiang, "Effect of Nb on the dynamic recystallization behavior of high-grade pipeline steels," *International Journal of Minerals, Metallurgy and Materials,* vol. 17, pp. 472 - 747, 2010.

[35] K. Titto, G. Fitzsimons and A. J. DeArdo, "The Effect of Dynamic Precipitation and Recrystallization on the Hot Flow Behavior of Nb V Microalloyed Steel," *Acta Metallurgica,* vol. 31, no. 8, pp. 1159 - 1168, 1983.

[36] E. I. Poliak and J. J. Jonas, "A One-parameter approach to determining the critical conditions for initiation of dynamic recrystallization," *Acta Metallurgica,* vol. 44, pp. 127 - 136, 1996.

[37] A. J. DeArdo, C. I. Garcia and E. J. Palmiere, "Thermomechanical Processing of Steel," in *Metals Handbook*, 10th ed., vol. 4, ASM International, 1991, pp. 237 - 255.

[38] C. Zener, "Relaxation phenomena in metals," *Physica,* vol. 15, no. 1 - 2, pp. 111 - 118, 1949.

[39] C. R. Hutchinson and Y. Brechet, "Solid State Transformation and Heat Treatment," in *The Coupling of Interphase Boundary Migration and Precipitation: Example of a Microalloyed Nb-Containing Steel*, A. Hazotte, Ed., Weinheim, Wiley-VCH Verlag GmbH & Co. KGaA, 2003, pp. 42 - 52.

[40] C. Zener, Transactions of the AIME, vol. 175, 1949.

[41] Y. Hui, L. Zhen-hong and Z. Zhi-liang, "Investigation on Zener-Hollomon parameter in the warm-hot deformation behavior of 20CrMnTi," *Journal od Zhejiang University Science A,* vol. 7, pp. 1453-1460, 2006.

[42] A. Le Bon, J. Rofes - Vernis and C. Rossard, "Recrystallization and precipitation during Hot Working of a Nb - Bearing HSLA Steel," *Metal Science ,* vol. 9, no. 1, pp. 36 - 40, 1975.

[43] R. E. Reed-Hill, Physical Metallurgy Principles, Boston: PSW Publishing Company, 1994.

[44] C. Jian-chun, L. Qing-you, L. Qi-long and S. Xin-jun, "Effect of Niobium on Isothermal Transformation of Austenite to Ferrite in HSLA Low-Carbon Steel," *JOURNAL OF IRON AND STEEL RESEARCH,* vol. 14, no. 3, pp. 51-55, 2007.

[45] S. M. K. Hosseini, Z. A. Hanzaki, M. J. Y. Panah and S. Yue, "ANN model for prediction of the effect of composition and process parameters on tensile strength and percent elongation of Si-Mn Trip steels," *Material Science and Engineering A,* vol. 374, pp. 122-128, 2004.

[46] S. Vercynckt, K. Verbeken, B. Lopez and J. J. Jonas, "Modern HSLA steels and role of non-recrystallisation temperature," *International Materials Reviews,* vol. 57, pp. 187-207, 2012.

[47] J. R. Davis, Metals Handbook Desk Edition, Taylor & Francis, 1998.

[48] F. B. Pickering, Physical Metallurgy and the Design of Steel, Essex UK: Applied Science , 1978.

[49] Thermo-Mechanical Processing of Metallic Materials, Amsterdam: Elserier, 2007.

[50] H. K. D. H. Bhadeshia and R. W. K. Honeycombe, Steels Microstructure and Properties, Oxford Uk: Butterworth - Heinemann, 2006.

[51] W. D. Callister , "Phase Diagrams," in *Material Science and Engineering An Introduction*, New York, John Wiley & Sons, 2007, p. 290.

[52] J. W. Christian, The Theory of Transformations in Metals and Alloys, Oxford: A Pergamon, 2002.

[53] G. R. Speich, V. A. Demarest and R. L. Miler, "Formation of Austenite During Intercritical Annealing of Dual-Phase Steels," *Metallurgical Transactions A,* vol. 12, no. 8, pp. 1419-1428, 1981.

[54] N. C. Law and D. V. Edmonds, “The formation of austenite in a low-alloy steel,” *Metallurgical and Materials Transactions A,* vol. 11, no. 1, pp. 33-46, 1980.

[55] C. I. Garcia and A. J. DeArdo, “Formation of austenite in 1.5 pct Mn steels,” *Metallurgical Transactions A,* vol. 12, no. 3, pp. 521-530, 1981.

[56] D. Z. Yang, E. L. Brown, D. K. Matlock and G. Krauss, “Ferrite Recrystallization and Austenite Formation in Cold-Rolled Intercritically Annealed Steel,” *Metallurgical Transactions A,* vol. 16, pp. 1385-1392, 1985.

[57] D. S. Martín, T. d. Cock, A. García-Junceda, F. G. Caballero, C. Capdevila and C. G. de Andrés, “Effect of heating rate on reaustenitisation of low carbon niobium microalloyed steel,” *Materials Science and Technology,* vol. 24, no. 3, pp. 266-272, 2008.

[58] C. R. Brooks, Principles of the Austenitization of Steels, Essex: Springer, 1992.

[59] J. E. Burke and D. Turnbull, “Recrystallization and Grain Growth,” *Progress in Metal Physics,* vol. 3, pp. 220-292, 1952.

[60] S. K. Kurtz and F. M. A. Carpay, “Microstructure and normal grain growth in metals and ceramics. Part I. Theory,” *Journal of Applied Physics,* vol. 51, no. 11, pp. 5725-5744, 1980.

[61] R. W. Cahn, Physical Metallurgy, vol. 3, R. W. Cahn and P. Haasen, Eds., Amsterdam: North Holland, 1996, pp. 2482-2487.

[62] M. Hillert, “On the theory of normal and abnormal grain growth,” *Acta Metallurgica ,* vol. 13, no. 3, pp. 227-238, 1965.

[63] D. J. Srolovitz, G. S. Grest and M. P. Anderson, “Computer simulation of grain growth—V. Abnormal grain growth,” *Acta Metallurgica,* vol. 33, no. 12, pp. 2233-2247, 1985.

[64] C. V. Thompson, H. J. Frost and F. Spaepen, “The relative rates of secondary and normal grain growth,” *Acta Metallurgica ,* vol. 35, no. 4, pp. 887-890, 1987.

[65] T. Gladman, “The theory and inhibition of abnormal grain growth in steels,” *The Journal of The Minerals, Metals & Materials Society ,* vol. 44, no. 9, pp. 21-24, 1992.

[66] V. Y. Novikov, “On the genesis of secondary recrystallization nuclei,” *Acta Metallurgica,* vol. 34, no. 5, pp. 685-687, 1996.

[67] L. J. Cuddy and J. C. Raley, “Austenite grain coarsening in microalloyed steels,” *Metallurgical Transactions A,* vol. 14, no. 10, pp. 1989-1995, 1983.

[68] E. J. Palmiere, C. I. Garcia and A. J. DeArdo, “Compositional and Mircostructural Changes Which Attend Reheating and Grain Coarsening in Steels Containing Niobium,” *Metallurgical and Materials Transaction A,* vol. 25, pp. 277-285, 1994.

[69] J. M. Gray and A. J. DeArdo, “Austenite conditioning alternatives for microalloyed steel products,” in *HSLA Steels Metallurgy and Applications*, Beijing, China, 1985.

[70] T. Tanaka, T. Funakoshi , M. Ueda and J. Tsuboi , “Development of High Strength Steel with Good Toughness at Arctic Temperature for Large-Diameter Line Pipe,” in *Microalloying 75*, Washington, D.C, 1975.

[71] B. K. Panigrahi, “Processing of low carbon steel plate and hot strip - an overview,” *Bulletin of Materials Science ,* vol. 24, no. 4, pp. 361-371, 2001.

[72] T. Gladman, “On the theory of the effect of precipitate particles on grain growth in

metals," *Proceedings of the Royal Society of London,* vol. 294, pp. 298-309, 1966.

[73] T. Gladman and D. Dulien, "Grain Size Control in Steels," in *Recrystallization in the Control of Microstructure*, London, 1973.

[74] P. K. Amin and F. B. Pickering, "Austenite Grain Coarsening and the effect of thermo-mechanical processing on austenite recrystallisation," in *Thermomechanical Processing of Microalloyed Austenite*, Pittsburgh, Pennsylvania, 1981.

[75] P. A. Beck, J. C. Kremer , L. J. Dener and M. L. Holzworth, "Grain Growth In High-Purity Aluminum And In An Aluminum- Magnesium Alloy - Introduction," *American Institue of Mining and Metallurgical Engineers,* vol. XIV, pp. 372-400, 1948.

[76] Y.-l. Zhao, J. Shi, W.-q. Cao, M.-q. Wang and G. Xie, "Kinetics of austenite grain growth in medium carbon niobium-bearing steel," *Zhejiang University Science A,* vol. 12, p. 171, 2011.

[77] G. T. Higgins, "Grain-Boundary Migration and Grain Growth," *Metal Science ,* vol. 8, pp. 143-150, 1974.

[78] S. Yao, L. Du, X. Liu and G. Wang, "Isothermal Growth Kinetics of Ultra-fine Austenite Grains in a Nb-V-Ti Microalloyed steel," *Material Science and Technology ,* vol. 25, no. 5, pp. 615-618, 2009.

[79] F. J. Humphreys and M. Hatherly, Recrystallization and Related Annealing Phenomena, Second ed., Oxford: Elsevier, 2004.

[80] J. Mizera, J. W. Wyrzykowski and K. J. Kurzydlowski, "Description of the Kinetics of Normal and Abnormal Grain Growth in Austenitic Stainless Steel," *Materials Science and Engineering ,* vol. A, no. 104, pp. 157-162, 1988.

[81] P. P. Sinha, K. Sreekumar, A. Natarajan and K. V. Nagarajan, "Grain growth in 18Ni 1800 Mpa maraging steel," *Material Science ,* vol. 26, pp. 4155-4159, 1991.

[82] E. Anelli, "Application of Mathermatical Modelling to Hot Rolling and Controlled Cooling of Wire Rods and Bars," *ISIJ International,* vol. 32, pp. 440-449, 1992.

[83] G. Shen, J. Rollins and D. Furrer, "Microstructure Modeling of Forged Waspaloy Discs," *Superalloys,* pp. 613-620, 1996.

[84] P. D. Hodgson and R. K. Gibbs, "A Mathematical Model to Predict the Mechanical Properties of Hot Rolled C-Mn and Microalloyed Steels," *ISIJ International,* vol. 12, pp. 1329-1338, 1992.

[85] C. Yue, L. Zhang, S. Liao and H. Gao, "Kinetic Analysis of the Austenite Grain Growth in GCr15 Steel," *Material Engineering and Performance,* vol. 19, pp. 112-115, 2010.

[86] J. Wang, J. Chen, Z. Zhao and X. Y. Ruan, "Modeling of Microstructural Evolution in Microalloyed Steel During Hot Forging Process," *Acta Metallurgica Sinica,* vol. 19, no. 4, pp. 279-286, 2006.

[87] S. Uhm, J. Moon, C. Lee, J. Yoon and B. Lee, "Prediction Model for the Austenite Grain Size in the Coarse Grained Heat Affected Zone of Fe-C-Mn Steels: Considering the Effect of Initial Grain Size on Isothermal Growth Behavior," *ISIJ International,* vol. 44, pp. 1230-1237, 2004.

[88] M. Militzer, A. Giumelli, E. B. Haqbolt and T. R. Meadowcraft, "Austenite Grain Growth Kinetics in Al-Killed Plain Carbon Steels," *Metallurgical and Material*

Transactions A, vol. 27, pp. 3399-3409, 1996.

[89] A. H. Seikh, M. S. Soliman, A. AlMajid, K. Alhajeri and W. Alshalfan, "Austenite Grain Growth Kinetics in API X65 and X70 Line-Pipe Steels during Isothermal Heating," *Advances in Material Science and Engineering ,* pp. 1-8, 2014.

[90] S.-f. Tao, F.-m. Wang, G.-l. Sun, Z.-b. Yang and C.-r. Li, "DICTRA Simulation of Holding Time Dependence of NbC Size and Experimental Study of Effect of NbC on Austenite Grain Growth," *Metallurgical and Material Transactions A,* pp. 1-9, 2015.

[91] D. Priadi, R. A. Napitupulu, E. S. Siradj and , "Austenite Grain Grpwth Calculation during Hot Rolling of 0.02% Nb Steel," *Material Science and Engineering A,* pp. 678-683, 2011.

[92] S. Nanba, M. Kitamura, M. Shimada, M. Katsumata, T. Inoue, H. Imamura, Y. Maeda and S. Hattori, "Prediction of Microstructure Distribution in the Through-thickness Direction during and after Hot Rolling in Carbon Steels," *ISIJ International ,* vol. 32, pp. 377-386, 1992.

[93] G.-w. Yang, X.-j. Sun, Q.-l. Youg, Z.-d. Li and X.-x. Li, "Austenite Grain Refinement and Isothermal Growth Behavior in a Low Carbon Vanadium Microalloyed Steel," *Iorn and Steel Research,* vol. 21, pp. 757-764, 2014.

[94] S.-J. Lee and Y.-K. Lee, "Prediction of austenite grain growth during austenitization of low alloy steels," *Material and Design,* vol. 29, pp. 1840-1844, 2008.

[95] S. S. Zhang, M. Q. Li, Y. G. Liu, J. Luo and T. Q. Liu, "The growth behavior of austenite grain in the heating process of 300M steel," *Material Science and Engineering A,* pp. 4967-4972, 2011.

[96] G. Sheard and J. Nutting, "Examination of recrystallization and grain growth of austenite with the photoemission electron microscope," *Metal Science ,* vol. 13, p. 131, 1979.

[97] K. Banerjee, M. Militzer, M. Perez and X. Wang, "Nonisothermal Austenite Grain Growth Kinetics in a Microalloyed X80 Linepipe Steel," *Metallurgical and Materials Transactions A,* vol. 41, no. 12, pp. 3161-3172, 2010.

[98] S. Jiao, J. Penning , F. Leysen, Y. Houbaert and E. Aernoudt, "The Modeling of the Grain Growth in a Continuous Reheating Process of a Low Carbon Si-Mn Bearing TRIP Steel," *ISIJ International,* vol. 40, no. 10, pp. 1035-1040, 2000.

[99] M. A. Grossmann, "Grain Size in Metals, with special reference to grain growth in austenite," in *ASM*, New York , 1934.

[100] S. J. Rosenberg and T. G. Digges, "Effect of rate of heating through the transformation range on austenite grain size," in *Trans. Am. Soc. Met*, 1940.

[101] A. Danon, C. Servant, A. Alamo and J. C. Brachet, "Heterogeneous austenite grain growth in 9Cr martensite steels: influence of the heating rate and the austenitization temperature," *Material Science and Engineering A,* pp. 122-132, 2003.

[102] D. S. Martin , F. G. Caballero, C. Capdevila and C. G. de Andres, "Austenite Grain Coarsening Under the Influence of Niobium Carbonitrides," *Materials Transactions,* vol. 45, no. 9, pp. 2797-2804, 2004.

[103] N. Z. Gutierrez, M. I. Luppo and C. A. Danon, "Heterogeneous Austenite Grain Growth in ASTM A213-T91 Steel," *ISIJ International,* vol. 47, no. 8, pp. 1178-

1187, 2007.

[104] K. A. Alogab, D. K. Matlock, G. J. Speer and H. J. Kleebe, "The Influence of Niobium Microalloying on Austenite Grain Coarsening Behavior of Ti-modified SAE 8620 Steel," *ISIJ International ,* vol. 47, no. 2, pp. 307-316, 2007.

[105] K. A. Alogab, D. K. Matlock, J. G. Speer and H. J. Kleebe, "The Effect of Heating Rate on Austenite Grain Growth in a Ti-modified SAE 8620 Steel with Controlled Niobium Additions," *ISIJ International ,* vol. 47, no. 7, pp. 1034-1041, 2007.

[106] R. C. Sharma, V. K. Lakshmanan and J. S. Kirkaldy, "Solubility of Niobium Carbide and Niobium Carbonitride in Alloyed Austenite and Ferrite," *Metallurgical Transcations A,* vol. 15 A, pp. 545 - 553, 1984.

[107] H. Nordberg and B. Aronsson, "Solubility of Niobium Carbide in Austenite," *The Iron and Steel Institute,* pp. 1263 - 1266, 1968.

[108] J. Ayache, L. Beaunier, J. Boumendil, G. Ehret and D. Laub, Sample Preparation Handbook for Transmission Electron Microscopy Techniques, New York, New York: Springer, 2010.

[109] K. Balasubramanian, A. Kroupa and J. S. Kirkaldy, "Experimental Investigation of the Thermodynamics of Fe-Nb-C Austenite and Nonstoichiometric Niobium and Titanium Carbides (T = 1273 to 1473 K)," *Metallurgical Transactions A,* vol. 23, no. 3, pp. 729 - 744, 1992.

[110] V. K. Lakshmanan and J. S. Kirkaldy, "Solubility Product for Niobium Carbide in Austenite," *Metallurgical Transactions A ,* vol. 15, pp. 541 - 544, 1984.

[111] T. M. Hoogendoorn and M. J. Spanraft, "Microalloying 75," in *Union Carbide Corporation* , New York, 1977.

[112] G. F. V. Voort, Metallography Principles and Practice, New York, USA: ASM International, 1984, p. 438.

[113] R. D. K. Misra and T. V. Balasubramanian, "Effects of microstructure on grain boundary segregation processes in low alloy steels," *Acta Metallurgica et Materialia,* vol. 38, no. 11, pp. 2357-2366, 1990.

[114] A. J. Papworth and D. B. Williams, "Segregation to prior austenite grain boundaries in low-alloy steels," *Scripta Materialia,* vol. 42, no. 11, pp. 1107-1112, 2000.

[115] S. Shenhua, Y. Zexi, S. Dongdong and W. Luqian, "Effects of phosphorus grain boundary segregation and hardness on the ductile-to-brittle transition for a 2.25Cr1Mo steel," *Journal of Wuhan University of Technology-Mater. Sci. Ed.,* vol. 22, no. 1, pp. 1-6, 2007.

[116] Z. Zhang, Q. Lin and Z. Yu, "Grain boundary segregation in ultra-low carbon steel," *Materials Science and Engineering: A,* vol. 291, pp. 22-26, 2000.

[117] D. R. Barraclough, "Etching pf Prior Austenite Grain Boundaries in Martensite," *Metallography,* vol. 6, pp. 465-472, 1973.

[118] S. W. Mahajan, G. Venkataraman and A. K. Mallik, "Grain Refinement of Steel by Cyclic Rapid Heating," *Metallography,* vol. 6, pp. 337-345, 1973.

[119] G. F. V. Voort, "Wetting Agents in Metallography," *Material Characterization ,* vol. 35, pp. 135-137, 1995.

[120] J. A. Nelson, "The Use of Wetting Agents in Metallographic Etchants," *Praktische Metallographie,* vol. 4, pp. 192-198, 1967.

[121] G. F. V. Voort, "Quantitative Microscopy," in *Metallography Principles and Practice*, New York, USA, ASM International, 1984, p. 438.

[122] C. G. d. Andres, M. J. Bartolome, C. Capdevila, D. S. Martin, F. G. Caballero and V. Lopez, "Metallographic techniques for the determination of the austenite grain size in medium-carbon microalloyed steels," *Materials Characterization,* vol. 46, pp. 389-398, 2001.

[123] C. G. d. Andres, F. G. Caballero, C. Capdevila and D. S. Martin, "Revealing austenite grain boundaries by thermal etching: advantages and disadvantages," *Material Characterization,* vol. 49, pp. 121-127, 2003.

[124] M. G. Lozinskii, "High Temperature Metallography," *Metal Science and Heat Treatment,* vol. 9, pp. 405-412, 1967.

[125] E. S. Davenport and E. C. Bain , "General Relations Between Grain-Size and Hardenability and the Normality of steels," in *ASM*, New York, 1934.

[126] "ASTM E112-13, Standard Test Methods for Determining Average Grain Size," ASTM International, West Conshohocken,, 2013.

[127] D. G. Rees, Essential Statistics, Fourth Edition ed., Chapman and Hall, 2001.

[128] S. S. Shapiro and M. B. Wilk, "An Analysis of variance test for normality (complete samples)," *Biometrika,* vol. 52, p. 591, 1965.

[129] N. M. Razail and Y. B. Wah, "Power Comparisons of Shapiro-Wilk, Kolmogorov-Smirnov, Lilliefors and Anderson-Darling Test," *Journal of Statistical Modeling and Anlytics,* vol. 2, pp. 21-33, 2011.

[130] P. Joaquim and D. S. Marques, Applied Statistics using SPSS, New York, NY: Springer, 2007.

[131] J. P. Verma, Repeated Measures Design for Empirical Researchers, New Jersey, NY: John Wiley & Sons, 2015.

[132] A. Brownrigg, P. Curcio and R. Boelen, "Etching of Prior Austenite Grain Boundaries in Martensite," *Metallography,* vol. 8, pp. 529-533, 1975.

[133] R. L. Bodnar, V. E. McGraw and A. V. Brandemarte, "Technique for Revealing Prior Austenite Grain Boundaries in CrMoV Turbine Rotor Steel," *Metallography,* vol. 17, pp. 109 - 114, 1984.

[134] L. Zhang and D. C. Guo, "A general etchant for revealing prior - austenite grain boundaries in steels," *Materials Characterization,* vol. 30, pp. 299 - 305, 1993.

[135] A. Brockmeier, F. J. S. Rodriguez, M. Harrison and U. Hilleringmann, "Surface tension and its role for vertical wet etching of silicon," *Micromechanics and Microengineering,* vol. 22, pp. 1 - 7, 2012.

[136] G. F. V. Voort, "Microstructure," in *Metallography, principles and practice*, New York, USA, ASM International, 1984, p. 196.

[137] G. Petzow, Metallographic Etching, Ohio: American Society for Metals, 1978.

[138] J. M. West, "Basic corrosion and oxidation," in *Why corrosion Happens*, New York, John Wiley & Sons, 1980, pp. 72-73.

[139] K. Trethewey and J. Chamberlain, "Differential-Aeration Corrosion," in *Corrosion for Science and Engineering*, London, Longman, 2001, p. 169.

[140] M. Hillert, "The Formation of Pearlite," in *Decomposition of austenite by diffusional*

processes, Philadelphia, Pennsylvania, 1962.

[141] C. Hui-jing, W. Fu-ming, L. Chang-rong, Z. Bo and X. Yun-jin, "Effect of Nb-V Microalloying on Microstructures and Mechanical Properties of Medium Carbon Non-Quenched and Tempered Steel," *Iron and Steel Research,* vol. 18, pp. 779 - 784, 2011.

[142] P. Zhao and J. D. Boyd, "Microstructure - property relationship in thermomechanically processed microalloyed medium carbon steels," *Material Science and Technology,* vol. 20, pp. 695 - 704, 2004.

[143] E. D. Moor and S. L. Miller , "Effects of niobium additions to a vanadium microalloyed high carbon wire steel," in *CabWire World Conference*, Milan, Italy, 2013.

[144] J. Bradford and W. S. Owen, "The Effect of Austenite Grain Size and Temperature on the Rate of the bainite transformation," *Metal Science and Heat Treatment of Metals,* vol. 4, no. 7-8, pp. 359-360, 1961.

[145] A. E. Gvozdev, A. G. Kolmakov, D. A. Provotorov, I. V. Minaev, N. N. Sergeev and I. V. Tikhonova, "Grain Size Effects of Austenite on the Kinetics of Pearlite Transformation in Low - and Medium-Carbon Low Alloy Steels," *Inorganic Materials: Applied Research,* vol. 6, no. 1, pp. 41 - 44, 2015.

[146] M. M. Aranda, B. Kim, R. Rementeria, C. Capdevila and C. C. d. Andres, "Effect of Prior Austenite Grain Size on Pearlite Transformation in a Hypoeuctectoid Fe-C-Mn Steel," *Metallurgical and Materials Transactions A,* vol. 45, no. 4, pp. 1778 - 1786, 2013.

[147] M. Fukuda, T. Hashimoto and K. Kunishige, "Effect of Controlled Rolling and Microalloying on Properties of Strips and Plates," in *Microalloying 75*, Washington D.C, 1975.

[148] A. J. DeArdo, "Metallurgical basis for thermomechaincal processing of microalloyed steels," *Ironmaking and Steelmaking,* vol. 28, pp. 138-144, 2001.

[149] J. P. Drolet and A. Galibois, "The Impurity-Drag Effect on Grain Growth," *Acta Metallurgica,* vol. 16, pp. 1387- 1399, 1968.

[150] H. J. Kestenbach, "Dispersion hardening by niobium carbonitride precipitation in ferrite," *Material Science and Technology,* vol. 13, pp. 732-739, 1997.

[151] J. M. Gray, R. B. G. Yeo, P. E. Repas and A. G. Melville, "Written Contributions," in *Strong Tough Structural Steels*, Scarborough, 1967.

[152] S. Qin, B. Liao, L. Mao and F. Xiao, "A novel method for preparing nano-NbC/Fe powder and nano-NbC particle reinforced cast low-carbon steel," *Materials Letters,* vol. 121, pp. 162-165, 2014.

[153] G. D. Hughes, S. D. Smith, C. S. Pande, H. R. Johnson and R. W. Armstrong, "Hall-Patch Strengthening for the microhardness of twelve nanometer grain diameter electrodeposited nickel," *Scripta Metallurgica,* vol. 20, pp. 93 - 97, 1986.

[154] T. Gladman, "Precipitation hardening in metals," *Material Science and Technology,* vol. 15, pp. 30 - 36, 1999.

[155] H. J. Kestenbach and J. Gallego, "On Dispersion Hardening of Microalloyed Hot Strip Steels by Carbonitride Precipitation in Austenite," *Scripta Materialia,* vol. 44, pp. 791 - 796, 2001.

[156] N. Ryum and O. Hunderi, "On the analytic description of normal grain growth," *Acta Metallurgica,* vol. 37, no. 5, pp. 1375-1379, 1989.

[157] T. O. Saetre, O. Hunderi and N. Ryum, "Modelling grain growth in two dimensions," *Acta Metallurgica,* vol. 37, no. 5, pp. 1381-1387, 1989.

[158] T. Gladman, Grain Size Control, London, UK: Maney Publishing, 2004.

[159] R. P. Smith , "The Solubility of Niobium (Columbium) Carbide in Gamma Iron," *Transactions of the Metallurgical Society of AIME,* vol. 236, pp. 220 - 221, 1966.

[160] E. J. Palmiere, C. I. Garcia and A. J. DeARDO, "Compositional and Microstructural Changes Which Attend Reheating and Grain Coarsening in Steels Containing Niobium," *Metallurgical and Materal Transactions A,* vol. 25, pp. 277 - 286, 1994.

[161] L. Meyer and Z. Metallkd, vol. 58, p. 334, 1967.

[162] F. DeKazinsky, A. Axnas and P. Pachleiter, *Jernkontoret Annaler,* vol. 147, p. 408, 1963.

[163] P. A. Manohar, D. P. Dunne, T. Chandra and C. R. Killmore, "Grain Growth Predictions in Microalloyed Steels," *ISIJ International,* vol. 36, no. 2, pp. 194-200, 1996.

[164] N. Gao and T. N. Baker, "Austenite Grain Growth Behaviour of Microalloyed Al-V-N and Al-V-Ti-N Steels," *ISIJ International,* vol. 38, no. 7, pp. 744-751, 1998.

[165] R. Coladas, J. Masounave, G. Guerin and J. P. Bailon, "Austenite grain growth in medium- and high-carbon steels microalloyed with niobium," *Metal Science,* vol. 11, no. 11, pp. 509-516, 1977.

[166] H. Ma, S.-l. Liao and S.-f. Wang, "Effects of Ti on Austenite Grain Growth Behavior in High Carbon Steels," *Iron and Steel Research,* vol. 21, no. 7, pp. 702-709, 2014.

[167] D. Cramer, Fundamental Statistics for Social Research: Step by Step Calculations and Computer Techniques Using SPSS for Windows, New York, NY: Routledge, 1998.

[168] D. P. Doane and L. E. Seward, "Measuring Skewness: A Forgotten Statistic?," *Journal of Statistics Education Volume,* vol. 19, no. 2, 2011.

[169] H. Levene, Robust testes for equality of variances., Palo Alto, CA: Stanford Univ. Press, 1960.

[170] W. E. Martin and K. D. Bridgmon, Quantitative and Statistical Research Methods: From Hypotheses to Results, San Francisco: Wiley & Sons Inc, 2012.

[171] W. H. Kruskal and A. Wallis, "Use of Ranks in One-Criterion Variance Analysis," *Journal of American Statistical Association,* vol. 47, no. 260, pp. 583-621, 1952.

[172] H. B. Mann and D. R. Whitney, "On the Test of Whether one of Two Random Variables in Stochastically Larger than the Other," *Annals of Mathematical Statistics,* vol. 18, no. 1, pp. 60-60, 1947.

[173] O. J. Dunn, "Multiple Comparisons Among Means," *Journal of the American Statistical Association,* vol. 56, no. 293, pp. 52-64, 1961.

[174] W. B. Pearson, Crystal Chemistry and Physics of Metals and Alloys, New York: John Wiley & Sons Inc, 1972, pp. 135-197.

[175] D. Hull and D. J. Bacon, "Strength of Crystalline Solids," in *Introducation to*

Dislocations, Oxford , Butterworth-Heinemann, 2001, pp. 206 - 207.

[176] W. Kesternich and D. Meertens, "Microstructural evolution of a Titanium-stabilized 15Cr-15Ni steel," *Acta Metallurgica,* vol. 34, no. 6, pp. 1071-1082, 1986.

[177] B. Dutta and C. M. Sellars , "Strengthening of austenite by niobium during hot rolling of microalloyed steel," *Material Science and Technology,* vol. 2, pp. 146 - 153, 1986.

[178] Y. L. Qin, H. W. Luo, B. Kooi and J. De Hosson, "Influence of a Trace Amount of Ti on Precipitates in Nb Microalloyed Steel during Reheating," in *Physical and Numerical Simulation of Material processing*, Shanghai, 2004.

[179] L. M. Cheng, E. B. Hawbolt and T. R. Meadowcroft, "Dissolution and Coarsening of Aluminum Nitride Precipitates in Low Carbon Steel - Distribution Size and Morphology," *Canadian Metallurgical Quarterly,* vol. 39, pp. 73-86, 2000.

[180] J. G. Speer and S. S. Hansen, "Austenite recrystallization and carbonitride precipitation in niobium microalloyed steels," *Metallurgical Transactions A,* vol. 20, pp. 25 - 38, 1989.

[181] J. G. Speer, J. R. Michael and S. S. Hansen, "Carbonitride Precipitation in Niobium/Vanadium Microalloyed Steels," *Metallurgical Transactions A,* vol. 18, pp. 211 - 222, 1987.

[182] H. Beladi, G. L. Kelly and P. D. Hodgson , "Formation of Ultrafine Grained Structure in Plain Carbon Steels Through Thermomechanical Processing," *Materials Transactions,* vol. 45, no. 7, pp. 2214 - 2218, 2004.

[183] J. Maity and D. K. Mondal, "Isothermal Grain Growth of Austenite in Hypeoutectoid and Hypereutectoid Plain Carbon Steels," *Iron and Steel Research,* vol. 17, pp. 38 - 43, 2010.

[184] A. K. Giumelli, M. Militzer and E. B. Hawbolt, "Analysis of the Austenite Grain Size Distribution in Plain Carbon Steels," *ISIJ International,* vol. 39, pp. 271-280, 1999.

[185] I. Andersen, . Ø. Grong and N. Ryum, "Analytical modelling of grain growth in metals and alloys in the presence of growing and dissolving precipitates—II. Abnormal grain growth," *Acta Metallurgica et Materialia,* vol. 43, pp. 2689 - 2700, 1995.

[186] P. R. Rios, "Abnormal growth in the presence of coarsening particles," *Acta Metallurgica et Materialia,* vol. 40, pp. 649 - 651, 1992.

[187] H. Adrian and F. B. Pickering, "Effect of titanium additions on austenite grain growth kinetics of medium carbon V–Nb steels containing 0·008–0·018%N," *Materials Science and Technology,* vol. 7, no. 2, pp. 176 - 182, 1991.

[188] B. Garbarz and F. B. Pickering, "Effect of austenite grain boundary mobility on hardenability of steels containing vanadium," *Materials Science and Technology,* vol. 4, no. 11, pp. 967 - 975 , 1988.

[189] D. Hull and J. B. D, "Dislocation Arrays and Crystal Boundaries," in *Introduction to Dislocations*, Oxford, Butterworth-Heinemann, 2001, pp. 156 -160.

[190] F. J. Humphreys and M. Hatherly, "Recovery After Deformation," in *Recrystallization and Related Annealing Phenomena*, Oxford, Elsevier, 2004, p. 169.

[191] H. Conrad, S. Feuerstein and L. Rice, "Effects of Grain Size on the Dislocation Density and Flow Stress of Niobium," *Materials Science and Engineering,* vol. 2, no. 3, pp. 157 - 168, 1967.

[192] T. Narutani and J. Takamura, "Grain-Size Strengthening in Terms of Dislocation Density Measured by Resistivity," *Acta Metallurgica et Materialia,* vol. 39, no. 8, pp. 2037 - 2049 , 1991.

[193] Z. Jiang, J. Lian and B. Baudelet, "A dislocation density approximation for the flow stress—grain size relation of polycrystals," *Acta Metallurgica et Materialia,* vol. 43, no. 9, pp. 3349 - 3360, 1995.

[194] G. Riontino, C. Antonione, L. Battezzati, F. Marino and M. C. Tabasso, "Kinetics of abnormal grain growth in pure iron," *Journal of Material Science ,* vol. 14, pp. 86 - 90 , 1979.

[195] C. Antonione, G. D. Gatta, G. Riontino and G. Venturello, "Grain growth and secondary recrystallization in iron," *Journal of Material Science ,* vol. 8, pp. 1 -10 , 1973.

[196] C. Antonione, F. Marino, G. Riontino and M. C. Tabasso, "Effect of slight deformation on grain growth in iron," *Journal of Material Science ,* vol. 12, pp. 747 -750 , 1977.

[197] Z. Chen, M. H. Loretto and R. C. Cochrane, "Nature of large precipitates in titanium-containing HSLA steels," *Materials Science and Technology,* vol. 3, no. 10, pp. 836 - 844, 1987.

[198] S. S. Hansen, J. B. V. Sande and Morris Cohen, "Niobium carbonitride precipitation and austenite recrystallization in hot-rolled microalloyed steels," *Metallurgical Transactions A,* vol. 11, pp. 387 - 402, 1980.

[199] R. D. Vengrenovitch, "On the ostwald ripening theory," *Acta Metallurgica,* vol. 30, no. 6, pp. 1079-1086, 1982.

[200] H. Hu and B. B. Rath, "On the Time Exponent in Isothermal Grain Growth," *Metallurgical Transactions,* vol. 1, pp. 3181-3184, 1970.

[201] J. Moon, J. Lee and C. Lee, "Prediction for the austenite grain size in the presence of growing particles in the weld HAZ of Ti-microalloyed steel," *Material Science and Engineering A,* vol. 459, pp. 40-46, 2007.

[202] S. Z. Bokshteyn, "Diffusion and the structure of metals," *Metal Science and Heat Treatment of Metals,* vol. 3, no. 11, pp. 473 - 480, 1961.

[203] P. L. Gruzin, Y. V. Kornev and G. V. Kurdyumov, Problems of Metallography and Metal Physics, B. Y. Lyubov, Ed., Moscow: Metallurgizdat, 1952, p. 225.

[204] T. Sakai and M. Ohashi, "The Effect of Temperature, Strain Rate, and Carbon Content on Hot Deformation of Carbon Steels," *Iron and Steel Institute of Japan,* vol. 67, no. 11, pp. 2000 - 2009 , 1981.

[205] S. F. Medina and C. A. Hernandez, "General expression of the Zener-Hollomon parameter as a function of the chemical composition of low alloy and microalloyed steels," *Acta Materialia,* vol. 44, no. 1, pp. 137-148, 1996.

[206] L. X. Kong, P. D. Hodgson and D. C. Collinson, "Modelling the Effect of Carbon Content on Hot Strength of Steels Using a Modified Artificaial Neural Network," *ISIJ International,* vol. 38, no. 10, pp. 1121-1129, 1998.

[207] S. Serajzadeh and A. K. Taheri, “An investigation on the effect of carbon and silicon on flow behavior of steel,” *Materials and Design,* vol. 23, no. 3, pp. 271-276, 2002.

[208] H. W. Mead and C. E. Birchenall, “Self-Diffusion of Iron in Austenite,” *Journal of Metals,* vol. 8, no. 10, pp. 1336-1339, 1956.

[209] C. Barrett and T. B. Massalski, “Defects in crystals,” in *Structure of Metals*, Oxford UK, Pergamon Press, 1980, p. 382.

[210] C. J. Smithells, “Diffusion in metals,” in *Smithells Metals Reference Book*, E. A. Brandes and G. B. Brook, Eds., Oxford UK, Butterworth - Heinemann, 1992, pp. 13-1 .

[211] H. Hu, “Grain growth in Zone-refined iron,” *Canadian Metallurgical Quarterly,* vol. 13, no. 1, pp. 275 - 286, 1974.

[212] S. Kurokawa, J. E. Ruzzante, A. M. Hey and F. Dyment, “Diffusion of Nb in Fe and Fe alloy,” *Metal Science,* vol. 17, pp. 433 - 438, 1983.

[213] R. V. Patil and B. D. Sharma, “Lattice and grain-boundary diffusion of 59Fe in 316 stainless steel,” *Metal Science,* vol. 16, no. 8, pp. 389-392, 1982.

[214] Y. Liu, M. Li and X. Dang, “Effect of Heating Temperature and Heating Rate on Austenite in the Heating Process of 300M Steel,” *Materials Science Forum,* vol. 749, pp. 260-267, 2013.

[215] “Standard Test Methods for Characteriziing Duplex Grain Sizes,” ASTM International, West Conshohocken,, 2008.

[216] S. J. Coakes and L. G. Steed, SPSS: Analysis without anguish: version 14.0 for Windows, Brisbane: John Wiley & Sons Australia Ltd, 2007.

[217] P. H. Westfall and K. S. Henning , Understanding Advanced Statistical Methods, Boca Raton, FL: CRC Press, 2013.

[218] J. J. Irani, D. Burton, J. D. Jones and A. B. Rothwell, “Benefical effects of controlled rolling in the processing of structural steels,” in *Strong Tough Structural Steels*, Scarborough, 1967.

[219] P. A. Manohar and T. Chandra, “Dimensions of Grain Boundary Mobility,” *ISIJ International,* vol. 37, no. 7, pp. 726-728, 1997.

Appendix A Statistics

Shapiro-Wilk test for normality:

$$W = \frac{(\sum_{i=1}^{n} a_i x_{(i)})^2}{\sum_{i=1}^{n}(x_i - \bar{x})^2} \quad (13\text{-}1)$$

Where:

- $x_{(i)}$ (with parentheses enclosing the subscripy index *i*) is the *i*th order statistic, i.e., the *i*th-smallest number in the sample;
- $\bar{x}$= (x_1+…+x_n) / n is the sample mean;
- The constant a_i are given by $(a_1, \ldots., a_n) = \frac{m^T V^{-1}}{(m^T V^{-1} V^{-1} m)^{1/2}}$ where: $m = (\, m_{1,\ldots.}\, m_n)^T$;

  $m_{1,\ldots..,}\, m_n$ = expected values of the order statistics of independent and identically distributed random variables sampled from the Standard normal distribution
  V = covariance matrix of the order statistics

Histograms were used to examine the distributions of the data, helping to provide a graphical view of how the data was skewed. Graphical data can further provide opportunity to examine data to understand whether data is parametric or nonparametric. When examining graphical data, SPSS provides Descriptive Statistics data, more specifically Skewness and Kurtosis output, which is an important component to carefully examining the distribution of the data. Skewness is a measure of the lack of symmetry, within a data set; distribution is symmetric if it looks the same on the right and left centre point. Kurtosis measures whether the data is peaked or flat relative to a normal distribution. A normal distribution has a skewness and kurtosis of 0, so if the distribution is close to those values then it is likely to be close to normally distributed, and values pertaining to be above or below 0 indicates a deviation from normal distribution.

As a general rule of thumb, when skewness is greater than or equal to +1, or less than or equal to -1, then the distribution of data is different from a normal distribution in its asymmetry. A kurtosis greater than or equal to +/-3, then the distribution of the data is not that of a normal distribution in its propensity to produce outliers (Coakes & Steed, 2007) [216] & Westfall & Henning, 2013) [217].

Another perquisite for carrying out parametric statistical analysis is the Levene test (Levene, 1960) [169] to verify the equality of variances in the data (homogeneity of variance). If the significance from the test is less than p value of 0.05, then variances are significantly different and parametric tests cannot be used, and instead non-parametric measures are to be carried out.

Levene Test for Equality of variances:

$$W = \frac{(N-k)}{(k-1)} \frac{\sum_{i=1}^{k} N_i \, (\bar{Z}_{i.} - \bar{Z}_{..})^2}{\sum_{i=1}^{k} \sum_{j=1}^{N_1} (Z_{ii} - \bar{Z}_{i.})^2} \qquad (13\text{-}2)$$

Where:

W = Levene Test Statistic

k = is the number of different groups to which the sampled cases belong

N = Is the total number of cases in all groups

N_1= is the number of cases in the $\boldsymbol{i}$th group

Y_{ij} =is the value of the measured variable for the $\boldsymbol{j}$th case from the $\boldsymbol{i}$th group

$$Z_{ij} = \begin{cases} |Y_{ij} - \bar{Y}_i|, & \bar{Y}_i \ is \ a \ mean \ of \ the \ i-th \ group \\ |Y_{ij} - \tilde{Y}_i|, & \tilde{Y}_i \ is \ a \ median \ of \ the \ i-th \ group \end{cases}$$

Within the present research study when examining Precipitate size for the different hold times, the findings concluded that parametric measures were not met when carrying out the afore mentioned pre-requisite tests of normality for statistical tests. As a result non parametric analysis was carried out using Kruskal – Wallis (1952) [171], and where appropriate Mann – Whitney (1947) [172].

Kruskal - Wallis which is a non-parametric version of One-Way Anova, and is carried out in order to compare two or more data groups, and whether or not there is a significant difference between these data groups; in the case of this present study a difference in Precipitate size between hold times and carbon content. Where the p value is found to be 0.05 or less, i.e. a significant finding; this indicates one or more of the Hold times, and or Carbon content is significantly different.

Kruskal- Wallis Test for difference in two independent groups [medians]:

Procedure:

1. Arrange the data of samples in a single series in ascending order.
2. Assign rank to them in ascending order. In the case of a repeated value, or a tie, assign to them by averaging their rank position.
3. Then sup up the different ranks for each of the different groups.

4. To calculate the value, apply the following formula:

$$H = \frac{12}{N\,(N-1)} \sum_{j=1}^{c} \frac{T_j^2}{n_j} - 3\,(N+1) \qquad (13\text{-}3)$$

Where:

H = Kruskal- Wallis Test Statistic

N = Total number of values over the combined samples

n_j= number of values in the jth sample (j = 1,2,…,c)

T^j= sum of the ranks assigned to the ***j***th sample

T_j^2= square of the sum of the ranks assigned to the ***j***th sample

c = number of groups

Whilst the Kruskal – Wallis test indicates whether a significant difference exits within the data being examined, it doesn't however indicate where the significant differences specifically lie, i.e. between which hold times. Hence, when this test is found to be significant then it can be followed by a Mann Whitney, the Mann-Whitney is the nonparametric equivalent of t-tests [172]. It compares two independent data groups, assessing whether there is a significant difference between their mean ranks.

Mann- Whitney Test for differences between two independent samples:

$$U = n_1 n_2 + \frac{N_1(N_1+1)}{2} - R_1 \qquad (13\text{-}4)$$

Where:

- U is the Mann-Whitney Statistic
- N_1 and N_2 are the number cases in samples 1 and 2
- R_1 is the sum of the ranks for the first sample

With the Mann-Whitney Test, multiple comparisons are being made simultaneously in order to establish within the data where there are significant differences, and therefore Bonferroni correction is used, in order to avoid spurious positives, the alpha value (p value) needs to be lowered to account for the number of comparisons being carried out (Dunn,1961) [173]. Therefore, p value of 0.05 is divided by the number of hypothesized comparisons [173], within this study that is comparisons of 1 hour to 3 hour hold, 3 hour to 6 hour hold, and 1 hour to 6 hour hold (3 comparisons); to give a p value of 0.0167; hence any significant differences arising in the comparisons of the data will have a p value of 0.0167 or lower.

Appendix B Etching

ScienceLab.com
Chemicals & Laboratory Equipment

Health	2
Fire	1
Reactivity	4
Personal Protection	X

Material Safety Data Sheet
Picric acid MSDS

Section 1: Chemical Product and Company Identification

Product Name: Picric acid

Catalog Codes: SLP4363, SLP1546

CAS#: 88-89-1

RTECS: TJ7875000

TSCA: TSCA 8(b) inventory: Picric acid

CI#: Not available.

Synonym: 2,4,6-trinitrophenol; 1,3,5-Trinitrophenol

Chemical Name: Picric Acid

Chemical Formula: C6H2(NO3)3OH

Contact Information:

Sciencelab.com, Inc.
14025 Smith Rd.
Houston, Texas 77396

US Sales: **1-800-901-7247**
International Sales: **1-281-441-4400**

Order Online: ScienceLab.com

CHEMTREC (24HR Emergency Telephone), call:
1-800-424-9300

International CHEMTREC, call: 1-703-527-3887

For non-emergency assistance, call: 1-281-441-4400

Section 2: Composition and Information on Ingredients

Composition:

Name	CAS #	% by Weight
Picric acid	88-89-1	100

Toxicological Data on Ingredients: Picric acid: ORAL (LD50): Acute: 200 mg/kg [Rat].

Section 3: Hazards Identification

Potential Acute Health Effects:
Very hazardous in case of skin contact (irritant), of eye contact (irritant). Hazardous in case of ingestion, of inhalation. Slightly hazardous in case of skin contact (permeator). Corrosive to eyes and skin. The amount of tissue damage depends on length of contact. Eye contact can result in corneal damage or blindness. Skin contact can produce inflammation and blistering. Inhalation of dust will produce irritation to gastro-intestinal or respiratory tract, characterized by burning, sneezing and coughing. Severe over-exposure can produce lung damage, choking, unconsciousness or death. Inflammation of the eye is characterized by redness, watering, and itching. Skin inflammation is characterized by itching, scaling, reddening, or, occasionally, blistering.

Potential Chronic Health Effects:
Slightly hazardous in case of skin contact (sensitizer). CARCINOGENIC EFFECTS: Not available. MUTAGENIC EFFECTS: Mutagenic for bacteria and/or yeast. TERATOGENIC EFFECTS: Not available. DEVELOPMENTAL TOXICITY: Not available. The substance is toxic to mucous membranes. The substance may be toxic to blood, kidneys, liver. Repeated or prolonged exposure to the substance can produce target organs damage. Repeated exposure of the eyes to a low level of dust can produce eye irritation. Repeated skin exposure can produce local skin destruction, or dermatitis. Repeated inhalation of dust

p. 1

can produce varying degree of respiratory irritation or lung damage. Repeated exposure to a highly toxic material may produce general deterioration of health by an accumulation in one or many human organs.

Section 4: First Aid Measures

Eye Contact:
Check for and remove any contact lenses. In case of contact, immediately flush eyes with plenty of water for at least 15 minutes. Cold water may be used. WARM water MUST be used. Get medical attention.

Skin Contact:
In case of contact, immediately flush skin with plenty of water for at least 15 minutes while removing contaminated clothing and shoes. Cover the irritated skin with an emollient. Wash clothing before reuse. Thoroughly clean shoes before reuse. Get medical attention immediately.

Serious Skin Contact:
Wash with a disinfectant soap and cover the contaminated skin with an anti-bacterial cream. Seek immediate medical attention.

Inhalation:
If inhaled, remove to fresh air. If not breathing, give artificial respiration. If breathing is difficult, give oxygen. Get medical attention immediately.

Serious Inhalation:
Evacuate the victim to a safe area as soon as possible. Loosen tight clothing such as a collar, tie, belt or waistband. If breathing is difficult, administer oxygen. If the victim is not breathing, perform mouth-to-mouth resuscitation. WARNING: It may be hazardous to the person providing aid to give mouth-to-mouth resuscitation when the inhaled material is toxic, infectious or corrosive. Seek immediate medical attention.

Ingestion:
If swallowed, do not induce vomiting unless directed to do so by medical personnel. Never give anything by mouth to an unconscious person. Loosen tight clothing such as a collar, tie, belt or waistband. Get medical attention immediately.

Serious Ingestion: Not available.

Section 5: Fire and Explosion Data

Flammability of the Product: Flammable.

Auto-Ignition Temperature: 300°C (572°F)

Flash Points: CLOSED CUP: 150°C (302°F).

Flammable Limits: Not available.

Products of Combustion: These products are carbon oxides (CO, CO2), nitrogen oxides (NO, NO2...).

Fire Hazards in Presence of Various Substances: Slightly flammable to flammable in presence of open flames and sparks, of heat.

Explosion Hazards in Presence of Various Substances: Explosive in presence of open flames and sparks, of shocks, of heat, of metals, of alkalis.

Fire Fighting Media and Instructions:
Explosive. Flammable solid. SMALL FIRE: Use DRY chemical powder. LARGE FIRE: Use water spray or fog. Cool containing vessels with water jet in order to prevent pressure build-up, autoignition or explosion. Do not fight fire. Evacuate surrounding areas.

Special Remarks on Fire Hazards:
Dry mixtures of picric acid and aluminum powder are inert, but addition of water causes ignition after a delay depending upon the quantity added. Flammable solid when exposed to heat or flame.

Special Remarks on Explosion Hazards:
Picric acid and bases form explosive salts. Ammonia and metals with picric acid give results similar to bases. Contact between picric acid and concrete floors leads to the formation of explosion-sensitive salts, such as calcium picrate. Mixtures with

uranium perchlorate are extremely powerful explosives. It forms unstable salts with concrete, ammonia, and bases. Many of these are heat, friction, or impact-sensitive. An explosive mixture results when the aqueous solution crystallizes. Keep Picric acid wet with water. Do not let dry picric acid (crystals) form in container or on the cap threads of container. A severe explosion hazard when shocked or exposed to heat. Dried out material may explode if exposed to heat, flame, friction or shock; treat as an explosive. Keep material wet with water or treat as an explosive. Explodes when heated to 300 C.

Section 6: Accidental Release Measures

Small Spill: Use appropriate tools to put the spilled solid in a convenient waste disposal container.

Large Spill:
Explosive. Explosive, class 1.4. Flammable solid. Corrosive solid. Poisonous solid. Stop leak if without risk. Do not touch damaged container or spilled material. Do not clean-up or dispose except under supervision of a specialist. Do not operate radio transmitters within 100 m of an electric detonator. Do not get water inside container. Do not touch spilled material. Use water spray curtain to divert vapor drift. Use water spray to reduce vapors. Prevent entry into sewers, basements or confined areas; dike if needed. Eliminate all ignition sources. Call for assistance on disposal. Be careful that the product is not present at a concentration level above TLV. Check TLV on the MSDS and with local authorities.

Section 7: Handling and Storage

Precautions:
Do not allow this material to dry out. Do not let dry picric acid (crystals) form in container or on the cap threads of container. strong incandescent light. Ground all equipment containing material. Empty containers may contain hazardous residue and pose a fire risk. Do not ingest. Do not breathe dust. Take precautionary measures against electrostatic discharges. Avoid shock and friction. In case of insufficient ventilation, wear suitable respiratory equipment. If ingested, seek medical advice immediately and show the container or the label. Avoid contact with skin and eyes. Keep away from incompatibles such as oxidizing agents, reducing agents, metals, alkalis. Keep away from heat. Keep away from sources of ignition. Keep away from direct sunlight or

Storage:
Store in a segregated, approved and labeled area away from acute fire hazards and powerful oxidizing materials. Isolate from Organic materials. Do not store in metal containers. Keep container in a cool, well-ventilated area. Do not allow this material to dry out. Keep Picric acid wetted with a minimum of 30% water. Keep container tightly closed and sealed until ready for use. Avoid all possible sources of ignition (spark or flame).

Section 8: Exposure Controls/Personal Protection

Engineering Controls:
Use explosion-proof electrical (ventilating, lighting and material handling) equipment. Use process enclosures, local exhaust ventilation, or other engineering controls to keep airborne levels below recommended exposure limits. If user operations generate dust, fume or mist, use ventilation to keep exposure to airborne contaminants below the exposure limit.

Personal Protection:
Splash goggles. Synthetic apron. Vapor and dust respirator. Be sure to use an approved/certified respirator or equivalent. Gloves. Suggested protective clothing might not be sufficient; consult a specialist BEFORE handling this product.

Personal Protection in Case of a Large Spill:
Splash goggles. Full suit. Vapor and dust respirator. Boots. Gloves. A self contained breathing apparatus should be used to avoid inhalation of the product. Suggested protective clothing might not be sufficient; consult a specialist BEFORE handling this product.

Exposure Limits:
TWA: 0.1 (mg/m3) from ACGIH (TLV) [United States] Consult local authorities for acceptable exposure limits.

Section 9: Physical and Chemical Properties

Physical state and appearance: Solid. (Crystals solid.)

Odor: Odorless.

Taste: Bitter.

Molecular Weight: 229.11 g/mole

Color: Yellow.

pH (1% soln/water): Not available.

Boiling Point: Not available.

Melting Point: 122.5°C (252.5°F)

Critical Temperature: Not available.

Specific Gravity: 1.763 (Water = 1)

Vapor Pressure: Not applicable.

Vapor Density: 7.9 (Air = 1)

Volatility: Not available.

Odor Threshold: Not available.

Water/Oil Dist. Coeff.: The product is equally soluble in oil and water; log(oil/water) = -0.02

Ionicity (in Water): Not available.

Dispersion Properties: See solubility in water, diethyl ether, acetone.

Solubility:
Easily soluble in acetone. Soluble in hot water, diethyl ether. Partially soluble in cold water. Soluble in ethanol. Solubility in ethanol: 1 g/12 ml ethanol @ 25 deg. C Solubility in water: 1.27 x 10+4 mg/l @ 25 C; 1g/78 ml water @ 25 C; 1 g/15 ml boiling water. Solubility in Benzene: 1 g/10 ml @ 25 deg. C. Solubility in Chloroform: 1 g/35 ml @ 25 deg. C. Solubility in Ether: 1 g/65 ml @ 25 deg. C

Section 10: Stability and Reactivity Data

Stability: The product is stable.

Instability Temperature: Not available.

Conditions of Instability:
High temperatures, mechanical shock, ignition sources. Keep Picric acid wet with water. Do not allow water to evaporate from product. An explosive mixture results when the aqueous solution crystallizes. Do not let dry picric acid (crystals) form in container or on the cap threads of container. Dry picric acid is explosive. It can explode on impact if water content is below 10%.

Incompatibility with various substances:
Highly reactive with metals, alkalis. Reactive with oxidizing agents, reducing agents. The product may undergo hazardous decomposition, condensation or polymerization, it may react violently with water to emit toxic gases or it may become self-reactive under conditions of shock or increase in temperature or pressure.

Corrosivity: Non-corrosive in presence of glass.

Special Remarks on Reactivity:
Incompatible with copper, lead, zinc and other metals, salts, plaster, concrete, ammonia, oxidizing materials, reducing agents, albumin, gelatin, alkaloids(bases). Can react vigorously with oxidizing materials. Dry mixtures of picric acid and aluminum powder are inert, but addition of water causes ignition after a delay depending upon the quantity added. Picric acid and bases form explosive salts. Contact between picric acid and concrete floors leads to the formation of explosion-sensitive salts, such as calcium picrate. Mixtures with uranium perchlorate are extremely powerful explosives. It forms unstable salts with concrete, ammonia, and bases. Many of these are heat, friction, or impact-sensitive.

Special Remarks on Corrosivity: Corrodes metals

Polymerization: Will not occur.

Section 11: Toxicological Information

Routes of Entry: Absorbed through skin. Inhalation. Ingestion.

Toxicity to Animals: Acute oral toxicity (LD50): 200 mg/kg [Rat].

Chronic Effects on Humans:
MUTAGENIC EFFECTS: Mutagenic for bacteria and/or yeast. Causes damage to the following organs: mucous membranes. May cause damage to the following organs: blood, kidneys, liver.

Other Toxic Effects on Humans:
Very hazardous in case of skin contact (irritant). Hazardous in case of ingestion, of inhalation. Slightly hazardous in case of skin contact (permeator).

Special Remarks on Toxicity to Animals: Not available.

Special Remarks on Chronic Effects on Humans: May affect genetic material (mutagenic)

Special Remarks on other Toxic Effects on Humans:
Acute Potential Health Effects: Skin: Causes skin irritation. It may be absorbed by the skin. If it is absorbed through the skin and it can cause symptoms similar to those of ingestion. Eyes: Causes eye irritation. May result in corneal injury. Inhalation: May cause respiratory tract irritation. May cause effects similar to those for ingestion. May affect the kidneys. Ingestion: Harmful if swallowed! May cause gastrointestinal tract irritation with abdominal pain, nausea, vomiting, diarrhea. May affect behavior/central nervous system (vertigo, headache, stupor, tremor, convulsions), cardiovascular system, metabolism, kidneys/urinary system (anuria, oliguria, renal leisons, hemorrhagic nephritis), liver (acute hepatitis, jaundice). Chronic Potential Health Effects: Skin: Prolonged or repeated skin contact may cause allergic or sensitization dermatitis. Eyes: Prolonged or repeated eye contact may cause conjunctivitis. Prolonged or repeated skin and eye contact may also cause yellow staining of skin and eyes, and "yellow vision." Ingestion: Prolonged or repeated ingestion will cause symptoms similar to that of acute ingestion.

Section 12: Ecological Information

Ecotoxicity: Not available.

BOD5 and COD: Not available.

Products of Biodegradation: Possibly hazardous short/long term degradation products are to be expected.

Toxicity of the Products of Biodegradation: The products of degradation are less toxic than the product itself.

Special Remarks on the Products of Biodegradation: Not available.

Section 13: Disposal Considerations

Waste Disposal:
Waste must be disposed of in accordance with federal, state and local environmental control regulations.

Section 14: Transport Information

DOT Classification: CLASS 4.1: Flammable solid.

Identification: : Trinitrophenol, wetted with not less than 30% water, by mass UNNA: 1344 PG: I

Special Provisions for Transport: Not available.

Section 15: Other Regulatory Information

Federal and State Regulations:
Connecticut hazardous material survey.: Picric acid Illinois toxic substances disclosure to employee act: Picric acid Rhode Island RTK hazardous substances: Picric acid Pennsylvania RTK: Picric acid Minnesota: Picric acid Massachusetts RTK: Picric acid Massachusetts spill list: Picric acid New Jersey: Picric acid New Jersey spill list: Picric acid California Director's List of Hazardous Substances: Picric acid TSCA 8(b) inventory: Picric acid SARA 313 toxic chemical notification and release reporting: Picric acid

Other Regulations:
OSHA: Hazardous by definition of Hazard Communication Standard (29 CFR 1910.1200). EINECS: This product is on the European Inventory of Existing Commercial Chemical Substances.

Other Classifications:

WHMIS (Canada):
CLASS D-1B: Material causing immediate and serious toxic effects (TOXIC). CLASS D-2B: Material causing other toxic effects (TOXIC). CLASS E: Corrosive solid. CLASS F: Dangerously reactive material.

DSCL (EEC):
R2- Risk of explosion by shock, friction, fire or other sources of ignition. R4- Forms very sensitive explosive metallic compounds. R23/24/25- Toxic by inhalation, in contact with skin and if swallowed. S28- After contact with skin, wash immediately with plenty of [***] S35- This material and its container must be disposed of in a safe way. S37- Wear suitable gloves. S45- In case of accident or if you feel unwell, seek medical advice immediately (show the label where possible).

HMIS (U.S.A.):

Health Hazard: 2

Fire Hazard: 1

Reactivity: 4

Personal Protection: x

National Fire Protection Association (U.S.A.):

Health: 3

Flammability: 4

Reactivity: 4

Specific hazard:

Protective Equipment:
Gloves. Synthetic apron. Vapor and dust respirator. Be sure to use an approved/certified respirator or equivalent. Wear appropriate respirator when ventilation is inadequate. Splash goggles.

Section 16: Other Information

References: Not available.

Other Special Considerations: Not available.

Created: 10/10/2005 11:27 AM

Last Updated: 05/21/2013 12:00 PM

The information above is believed to be accurate and represents the best information currently available to us. However, we make no warranty of merchantability or any other warranty, express or implied, with respect to such information, and we assume no liability resulting from its use. Users should make their own investigations to determine the suitability of the information for their particular purposes. In no event shall ScienceLab.com be liable for any claims, losses, or damages of any third party or for lost profits or any special, indirect, incidental, consequential or exemplary damages, howsoever arising, even if ScienceLab.com has been advised of the possibility of such damages.

Appendix C Reheat Temperature

Table C-1: Solubility limit temperature (°C) for 0.08 wt. % Carbon steel with microalloyed niobium additions.

Authors	Solubility Limit Temperature (°C)		
	0.005 wt. %	0.01 wt. %	0.02 wt. %
Palmiere, et al.,	954	1026	1106
Nordberg, et al., (T)	834.9	881	932
Smith ,	1009	1065	1127
Meyer, et al.,	859.34	914.89	976.16
DeKazinsky, et al.,	917	977	1043
Nordberg, et al., (S)	938.18	991.52	1049
JMatPro 4.0	1004.5	1053.7	1109

Table C-2: Solubility limit temperature (°C) for 0.2 wt. % Carbon steel with microalloyed niobium additions.

Authors	Solubility Limit Temperature (°C)		
	0.005 wt. %	0.01 wt. %	0.02 wt. %
Palmiere, et al.,	1051.1	1134.9	1229.9
Nordberg, et al., (T)	907.2	960.1	1018
Smith ,	1085.2	1149.1	1219.3
Meyer, et al.,	934	997.3	1067.6
DeKazinsky, et al.,	998.2	1066.5	1142.6
Nordberg, et al., (S)	1021.1	1082.2	1149.3
JMatPro 4.0	1063	1116.8	1176.7

Table C-3: Solubility limit temperature (°C) for 0.4 wt. % Carbon steel with microalloyed niobium additions.

Authors	Solubility Limit Temperature (°C)		
	0.005 wt. %	0.01 wt. %	0.02 wt. %
Palmiere, et al.,	1134.9	1229.9	1338.8
Nordberg, et al., (T)	968.4	1027.1	1091.7
Smith ,	1149.1	1219.3	1296.8
Meyer, et al.,	997.3	1067.6	1146.1
DeKazinsky, et al.,	1066.5	1142.6	1227.9
Nordberg, et al., (S)	1091.8	1159.9	1235.2
JMatPro 4.0	1104.8	1162.3	1225

Table C-4: Solubility limit temperature (°C) for 0.6 wt. % Carbon steel with microalloyed niobium additions.

Authors	Solubility Limit Temperature (°C)		
	0.005 wt. %	0.01 wt. %	0.02 wt. %
Palmiere, et al.,	1189	1291.7	1410.1
Nordberg, et al., (T)	1007.3	1069.8	1138.8
Smith ,	1189.3	1263.7	1346
Meyer, et al.,	1037.5	1112.4	1196.5
DeKazinsky, et al.,	1110	1191.3	1282.8
Nordberg, et al., (S)	1136.9	1209.7	1290.4
JMatPro 4.0	1126.9	1186.7	1251.9

Table C-5: Solubility limit temperature (°C) for 0.8 wt. % Carbon steel with micro-alloyed niobium additions.

Authors	Solubility Limit Temperature (°C)		
	0.005 wt. %	0.01 wt. %	0.02 wt. %
Palmiere, et al.,	1229.9	1338.8	1464.6
Nordberg, et al., (T)	1036.4	1101.9	1174.2
Smith ,	1219.3	1296.8	1382.8
Meyer, et al.,	1067.6	1146.1	1234.5
DeKazinsky, et al.,	1142.6	1227.9	1324.1
Nordberg, et al., (S)	1170.7	1247.1	1332.1
JMatPro 4.0	1140.4	1201.7	1268.7

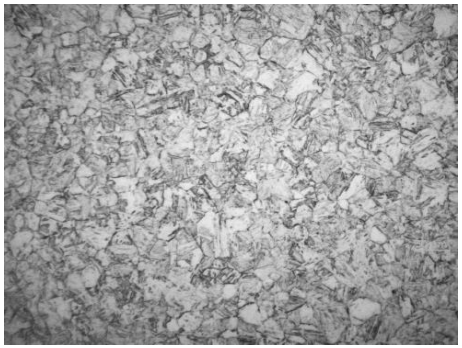

32µm ± 1.5µm
950°C

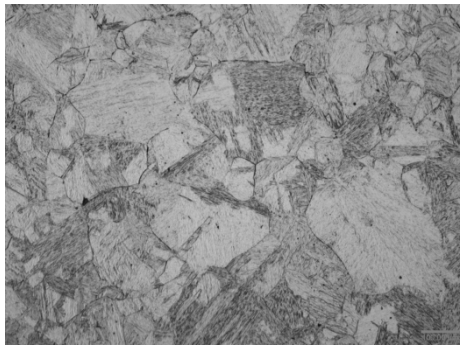

173.8µm ± 1.5µm
1000°C

186.8µm ± 5.7µm
1050°C

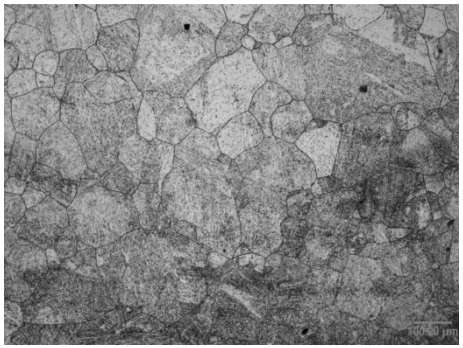

201.9µm ± 6µm
1100°C

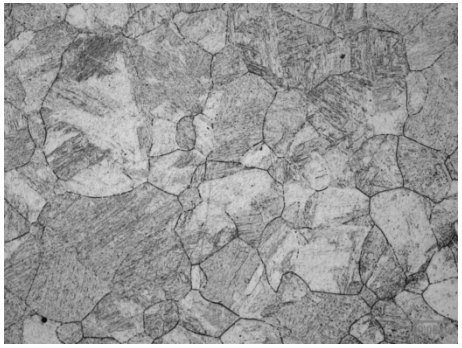

205.8µm ± 3.4µm
1150°C

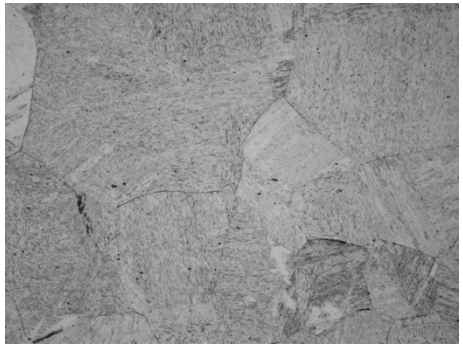

339.9µm ± 3µm
1200°C

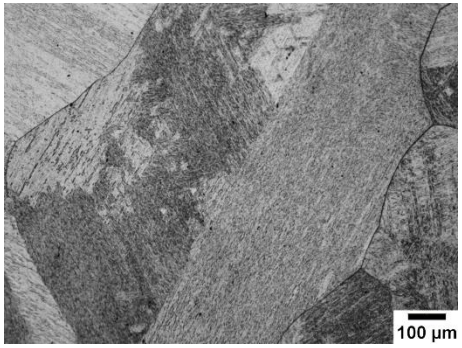

818.6µm ± 13.1µm
1250°C

- 0.08 wt. % Carbon
- Plain C-Mn (No Nb)
- 950°C - 1250°C
- Tube Furnace
- Argon Atmosphere
- 1 Hour Hold
- Ice Water Quench

Figure C-1: Shown above are a set of prior austenite grains for Plain C-Mn steel after isothermally reheating to the above temperatures (950°C - 1250°C) for 1 hour and ice water quenching. (Etched with Saturated Picric Acid) 10 x magnification.

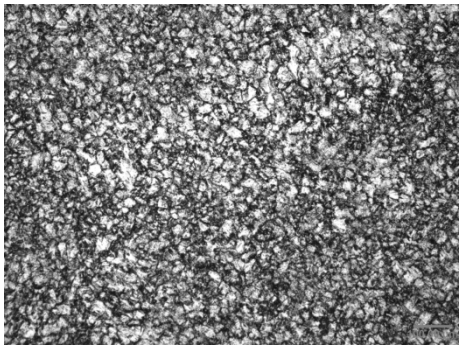

18µm ± 1.5µm
950°C

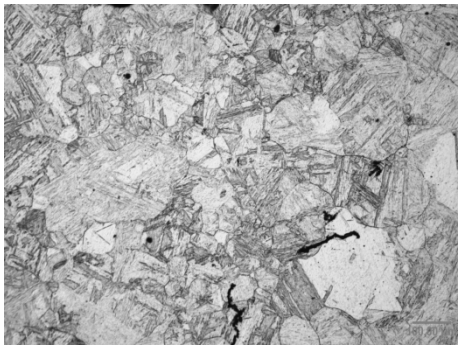

109.6µm ± 4.2µm
1000°C

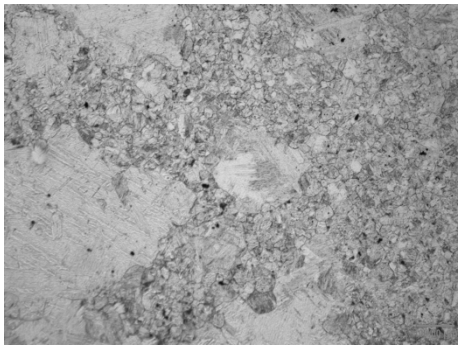

113.1µm ± 10.5µm
1050°C

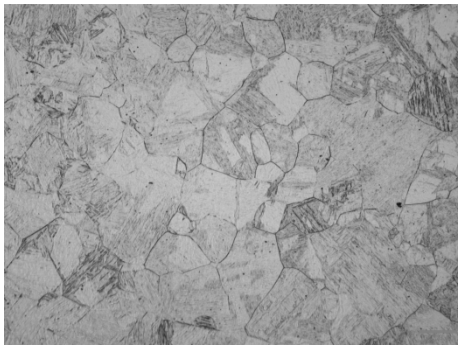

134.8µm ± 2.3µm
1100°C

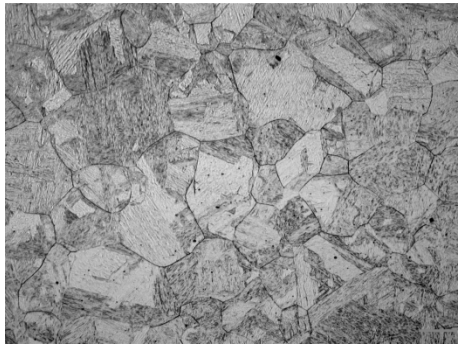

153.5µm ± 1.9µm
1150°C

193.6µm ± 5.4µm
1200°C

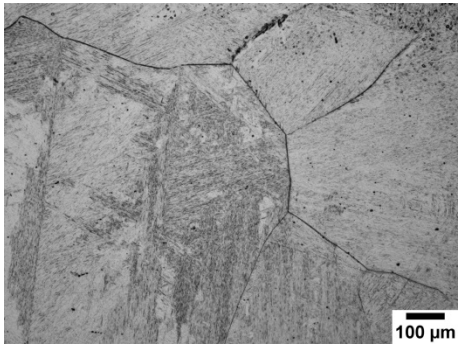

671µm ± 34µm
1250°C

- 0.08 wt. % Carbon
- 0.02 wt. % Nb
- 950°C - 1250°C
- Tube Furnace
- Argon Atmosphere
- 1 Hour Hold
- Ice Water Quench

Figure C-2: Shown above are a set of light micrographs of prior austenite grains for 0.02 wt.% Nb steel after isothermally reheating to the above temperatures (950°C - 1250°C) for 1 hour and ice water quenching. (Etched with Saturated Picric Acid) 10 x magnification.

Table C-6: Quantitative analysis of the mean PAGS (μm) for the different reheat temperatures from 950°C to 1250°C.

	Prior Austenite Grain Size, PAGS, (μm)			
Temperature (°C)	Plain C-Mn	0.005 wt. % Nb	0.01 wt. % Nb	0.02 wt. % Nb
950	32 ± 1.5	30 ± 1.5	19.2 ± 1.5	18 ± 1.5
1000	173.8 ± 1.5	153 ± 1.6	131.1 ± 2.8	109.6 ± 4.2
1050	186.8 ± 5.7	160.1 ± 4.3	142.8 ± 5	113.1 ± 10.5
1100	201.9 ± 6	183.2 ± 1.6	155.8 ± 1.7	134.8 ± 2.3
1150	205.8 ± 3.7	189.8 ± 3.8	163.5 ± 4.9	153.5 ± 5
1200	339.9 ± 3	296.9 ± 5.9	223.8 ± 14.6	193.6 ± 5.4
1250	818.6 ± 13.1	737.5 ± 24.7	705.1 ± 51.8	671 ± 34

Table C-7: The Standard deviation (SD) values for the reheat temperatures of 950°C to 1250°C.

	Standard Deviation (SD), Values (μm)			
Temperature (°C)	Plain C-Mn	0.005 wt. % Nb	0.01 wt. % Nb	0.02. wt. % Nb
950	1.2	1.3	1.3	0.7
1000	13.1	22.7	34.9	13.1
1050	13.6	9.9	15.5	54.1
1100	14.6	12.9	15	18.5
1150	15.2	16.7	13.9	15.1
1200	16	116	110	38
1250	17	89.3	184.2	126.6

Table C-8: Quantitative analysis of the mean PAGS (μm) for the different reheat temperatures from 950°C to 1250°C for 0.2wt. % carbon.

	Prior Austenite Grain Size, PAGS, (μm)			
Temperature (°C)	Plain C-Mn	0.005 wt. % Nb	0.01 wt. % Nb	0.02 wt. % Nb
950	26.4 ± 1.3	24 ± 1.2	18.6 ± 1.2	18.3 ± 1.2
1000	119.8 ± 2.5	110.6 ± 4.3	104.1 ± 9.2	98.9 ± 4.1
1050	123.6 ± 2.6	116 ± 2.7	106.6 ± 6.6	101.1 ± 9.6
1100	137 ± 2.5	129.7 ± 2.2	118.9 ± 3.4	115.6 ± 3
1150	167.2 ± 2	161.9 ± 2.3	150.8 ± 4	118.6 ± 1.9
1200	224 ± 3.1	210 ± 10	204.5 ± 5.1	133.1 ± 2.5
1250	386.9 ± 3.1	356.1 ± 12.5	308.9 ± 20.4	262 ± 12.5

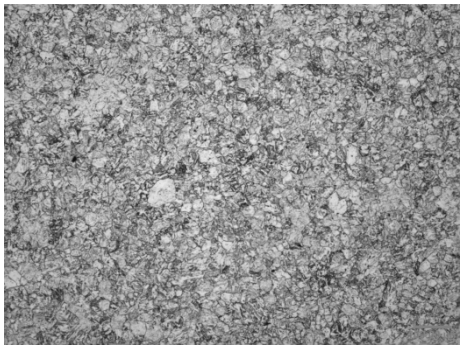

24µm ± 1.2µm
950°C

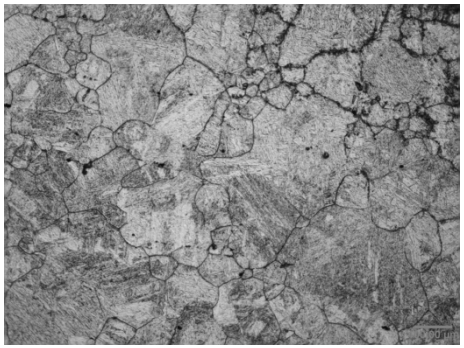

110.6µm ± 4.3µm
1000°C

116µm ± 2.7µm
1050°C

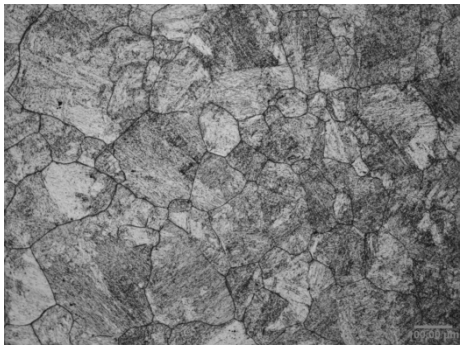

130µm ± 2.2µm
1100°C

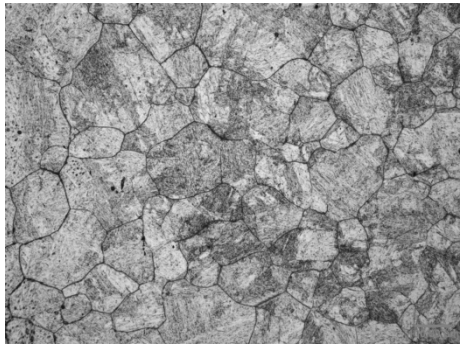

161.9µm ± 2.3µm
1150°C

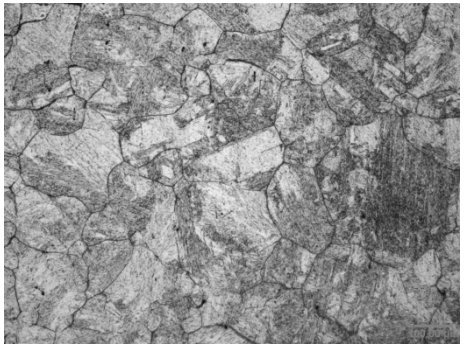

210µm ± 10µm
1200°C

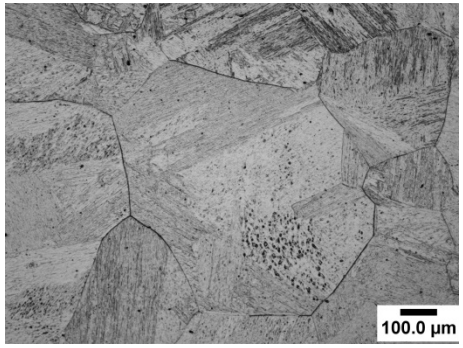

356.1µm ± 12.5µm
1250°C

- 0.2 wt. % Carbon
- 0.005 wt. % Nb
- 950°C - 1250°C
- Tube Furnace
- Argon Atmosphere
- 1 Hour Hold
- Ice Water Quench

Figure C-3: Shown above are a set of light micrographs of prior austenite grains for 0.005 wt. % Nb steel after isothermally reheating to the above temperatures (950°C - 1250°C) for 1 hour and ice water quenching. (Etched with Saturated Picric Acid) 10 x magnification.

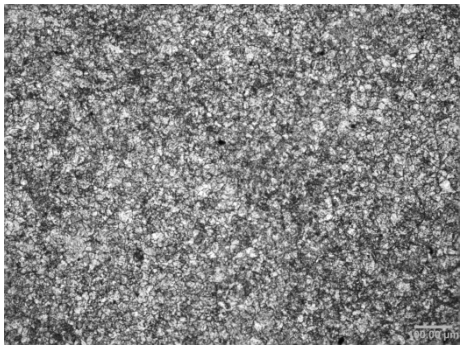

18.9µm ± 1.2µm
950°C

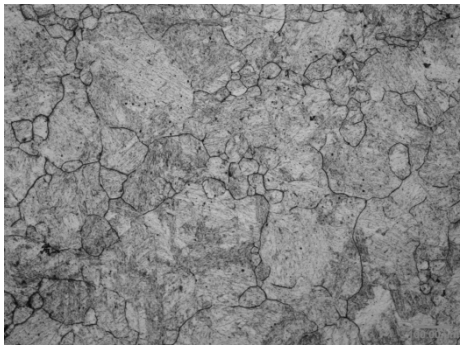

104.1µm ± 9.2µm
1000°C

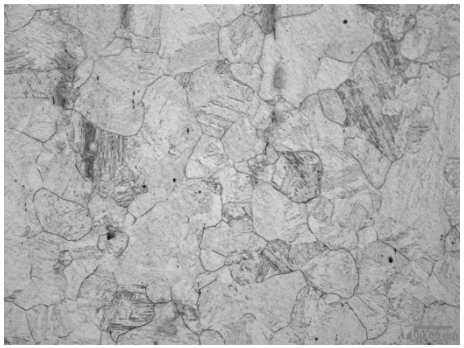

106.6µm ± 6.6µm
1050°C

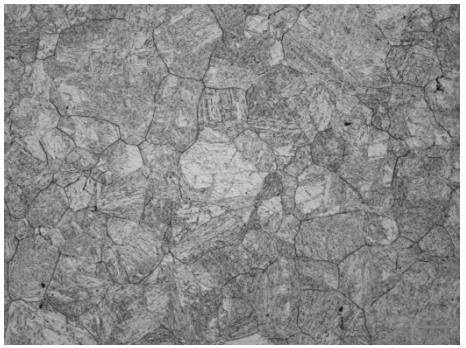

118.9µm ± 3.4µm
1100°C

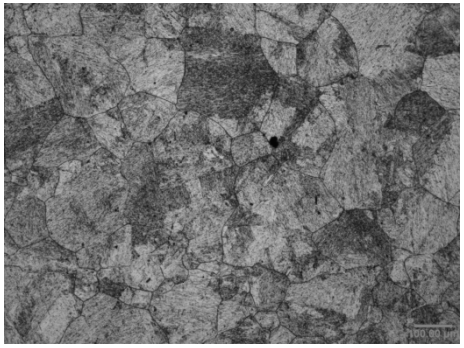

150.8µm ± 4µm
1150°C

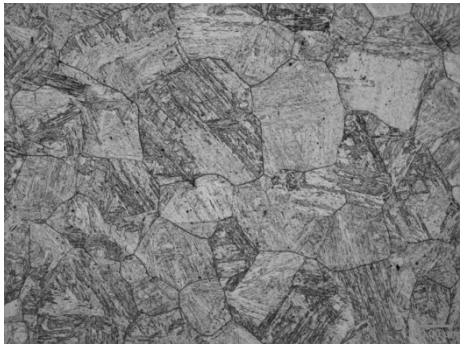

204.5µm ± 5.1µm
1200°C

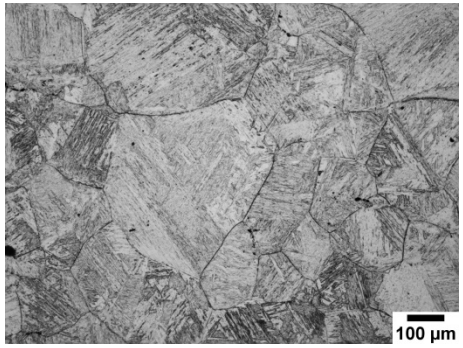

309µm ± 20.4µm
1250°C

- 0.2 wt. % Carbon
- 0.01 wt. % Nb
- 950°C - 1250°C
- Tube Furnace
- Argon Atmosphere
- 1 Hour Hold
- Ice Water Quench

Figure C-4: Shown above are a set of light micrographs of prior austenite grains for 0.01 wt. % Nb steel after isothermally reheating to the above temperatures (950°C - 1250°C) for 1 hour and ice water quenching. (Etched with Saturated Picric Acid) 10 x magnification.

Table C-9: The standard deviation (SD) of grain size values for the reheat temperature of 950°C to 1250°C for 0.2 wt. % Carbon steel.

	Standard Deviation (SD), Values (μm)			
Temperature (°C)	Plain C-Mn	0.005 wt. % Nb	0.01 wt. % Nb	0.02. wt. % Nb
950	1.2	1.3	1.3	0.7
1000	6.3	11	23.3	10.4
1050	6.5	6.5	17	24.5
1100	6.4	5.6	8.6	7.6
1150	5.1	5.8	10.2	5
1200	5.9	36	13.1	6.3
1250	7	45.1	73.5	45

Table C-10: Quantitative analysis of the mean PAGS (μm) for the different reheat temperatures from 950°C to 1250°C for 0.4wt. % carbon.

	Prior Austenite Grain Size, PAGS, (μm)			
Temperature (°C)	Plain C-Mn	0.005 wt. % Nb	0.01 wt. % Nb	0.02 wt. % Nb
950	35 ± 4.57	33.6 ± 1.6	25.7 ± 1.34	22.9 ± 1.1
1000	93.3 ± 6.23	69 ± 4.4	42.1 ± 2.3	36.5 ± 2.2
1050	114.4 ± 11.9	100.4 ± 7.9	91.4 ± 5.5	69.4 ± 2.6
1100	134 ± 13.5	118 ± 9.7	108.2 ± 5.8	86.3 ± 5.3
1150	156 ± 15.4	134.3 ± 7.5	114.1 ± 8.9	98.8 ± 6.3
1200	212.3 ± 14.4	186.6 ± 8.4	154.2 ± 5.4	132.14 ± 10
1250	312.6 ± 12	281.9 ± 3.4	241.9 ± 5.2	220.7 ± 5.2

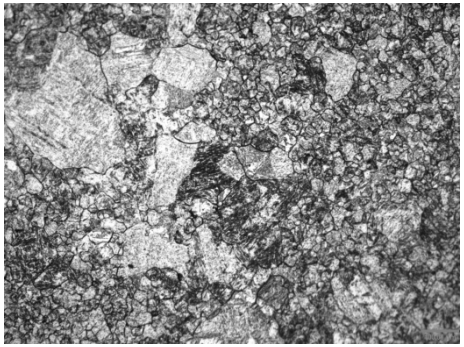

33.6µm ± 1.6µm
950°C

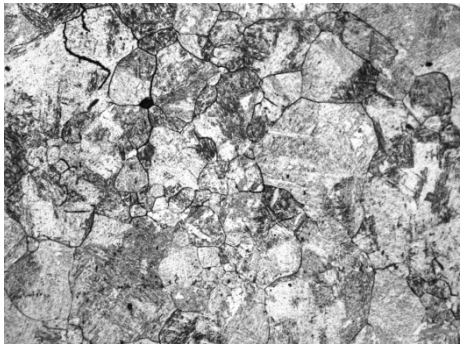

69µm ± 4.4µm
1000°C

100.4µm ± 7.9µm
1050°C

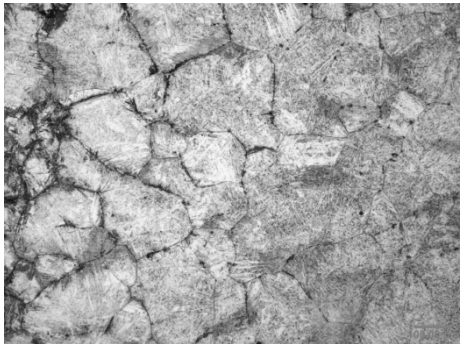

118µm ± 9.7µm
1100°C

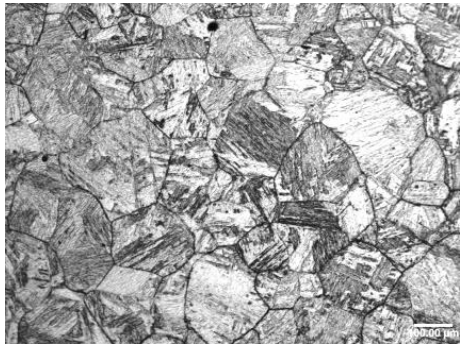

134.3µm ± 7.5µm
1150°C

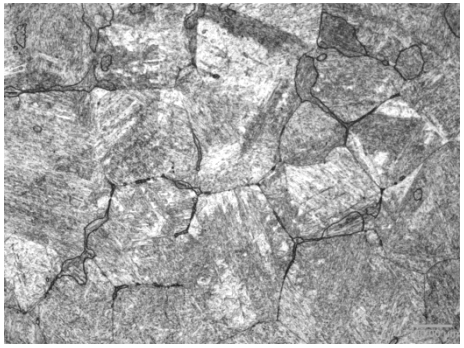

186.6µm ± 8.4µm
1200°C

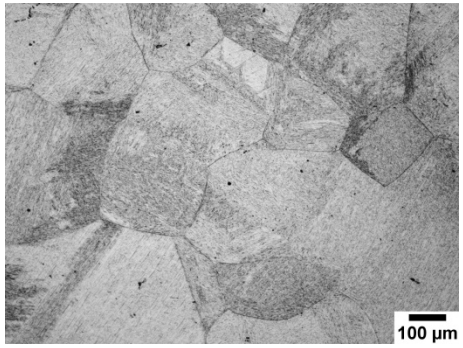

281.9µm ± 3.4µm
1250°C

- 0.4 wt. % Carbon
- 0.005 wt. % Nb
- 950°C - 1250°C
- Tube Furnace
- Argon Atmosphere
- 1 Hour Hold
- Ice Water Quench

Figure C-5: Shown above are a set of light micrographs of prior austenite grains for 0.005wt. % Nb steel after isothermally reheating to the above temperatures (950°C - 1250°C) for 1 hour and ice water quenching. (Etched with Saturated Picric Acid) 10 x magnification.

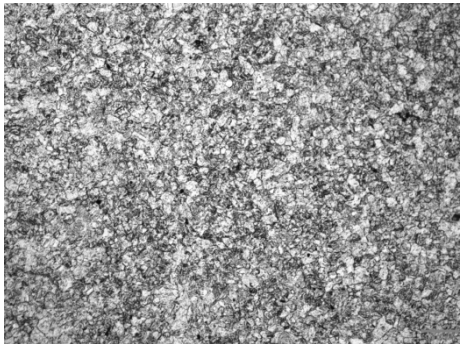

22.9µm ± 1.1µm
950°C

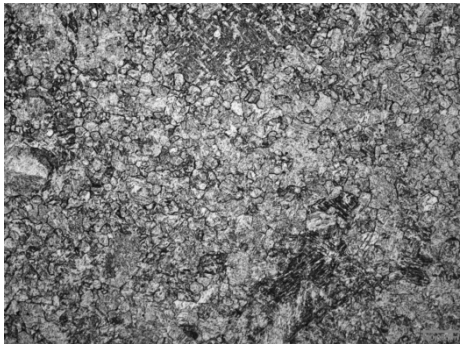

36.5µm ± 2.6µm
1000°C

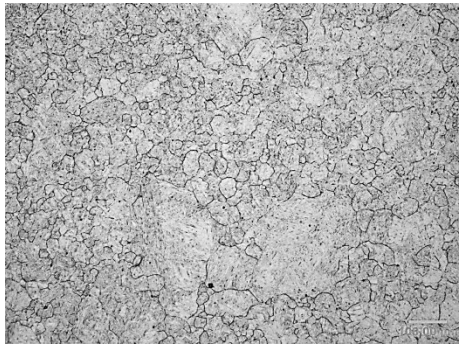

69.4µm ± 2.6µm
1050°C

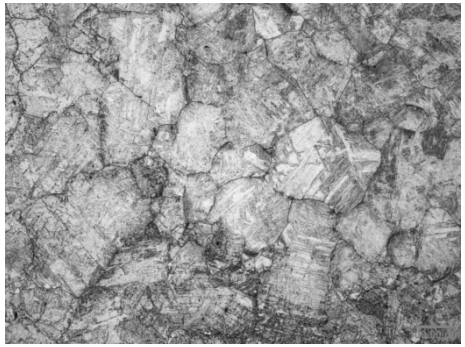

86.3µm ± 5.3µm
1100°C

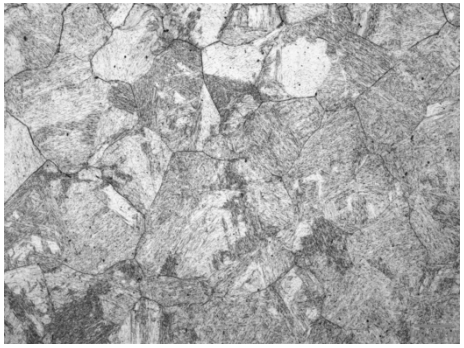

98.8µm ± 6.3µm
1150°C

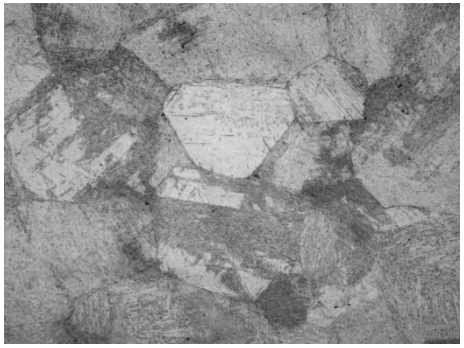

132.1µm ± 10µm
1200°C

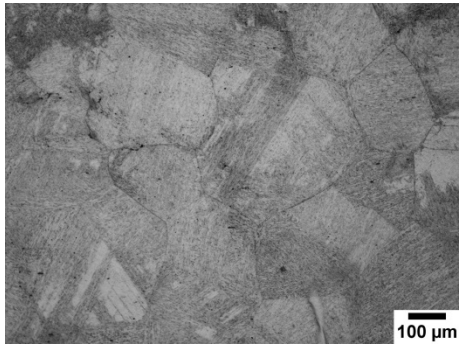

220.7µm ± 5.2µm
1250°C

- 0.4 wt. % Carbon
- 0.02 wt. % Nb
- 950°C - 1250°C
- Tube Furnace
- Argon Atmosphere
- 1 Hour Hold
- Ice Water Quench

Figure C-6: Shown above are a set of light micrographs of prior austenite grains for 0.02wt. % Nb steel after isothermally reheating to the above temperatures (950°C - 1250°C) for 1 hour and ice water quenching. (Etched with Saturated Picric Acid) 10 x magnification.

Table C-11: The Standard deviation (SD) values for the reheat temperatures of 950°C to 1250°C for 0.4 wt. % carbon steel.

	Standard Deviation (SD), Values (μm)			
Temperature (°C)	Plain C-Mn	0.005 wt. % Nb	0.01 wt. % Nb	0.02. wt. % Nb
900	7.5	3.1	2.5	1.3
950	4.6	17.8	8.8	1.2
1000	4.5	8.4	15.8	8
1050	5.9	8	9.1	25.1
1100	7.61	8	7.1	7.8
1150	6.5	18	5.3	5.1
1200	7	25	18	15
1250	8	26	32	21

Table C-12: Quantitative analysis of the mean PAGS (μm) for the different reheat temperatures from 950°C to 1250°C for 0.6wt. % Carbon.

	Prior Austenite Grain Size, PAGS, (μm)			
Temperature (°C)	Plain C-Mn	0.005 wt. % Nb	0.01 wt. % Nb	0.02 wt. % Nb
950	37 ± 1.2	25 ± 0.7	21 ± 0.8	20 ± 0.7
1000	81 ± 1.8	63 ± 5.2	38 ± 2.6	32.8 ± 1.6
1050	101 ± 3.1	81.1 ± 4.4	79.4 ± 9.8	40.5 ± 2.1
1100	124.7 ± 5.3	109.4 ± 3.2	96 ± 5.3	80.5 ± 4
1150	145.2 ± 3.7	130.5 ± 2.5	110 ± 2.3	90 ± 2.2
1200	180.3 ± 2.1	165.2 ± 7.1	137.3 ± 3.2	128.3 ± 5.3
1250	296 ± 3.1	279.2 ± 10.5	239.3 ± 10.6	210 ± 3.5

Table C-13: The Standard deviation (SD) values for the reheat temperatures of 950°C to 1250°C for 0.6 wt. % Carbon steel

	Standard Deviation (SD), Values (μm)			
Temperature (°C)	Plain C-Mn	0.005 wt. % Nb	0.01 wt. % Nb	0.02. wt. % Nb
950	1.15	1.3	1.3	0.7
1000	4.4	13.3	7.9	4.8
1050	4.3	11.3	25	4.3
1100	5.2	7.6	13.5	10.2
1150	4.4	6	7.4	5.2
1200	5.1	18	6	5
1250	6	38	27	9

Table C-14: Quantitative analysis of the mean PAGS (μm) for the different reheat temperatures from 950°C to 1250°C for 0.8wt. % carbon.

	Prior Austenite Grain Size, PAGS, (μm)			
Temperature (°C)	Plain C-Mn	0.005 wt. % Nb	0.01 wt. % Nb	0.02 wt. % Nb
950	27 ± 0.3	25.6 ± 0.8	21.5 ± 0.5	20.3 ± 0.3
1000	42.1 ± 1.3	38.5 ± 5.5	32 ± 1.6	27.1 ± 1.5
1050	87.2 ± 2.7	77.7 ± 1.1	49.4 ± 2.6	34.9 ± 1
1100	115.4 ± 2.4	102 ± 2.7	84.2 ± 1.2	65.3 ± 2.2
1150	144.7 ± 4.3	126.3 ± 2.6	104.4 ± 3.4	86.3 ± 5.5
1200	169.7 ± 3.3	146.4 ± 2.3	135.7 ± 2.6	120.1 ± 3.2
1250	189.8 ± 3.3	177.9 ± 3.2	169.9 ± 3.5	156.1 ± 5.1

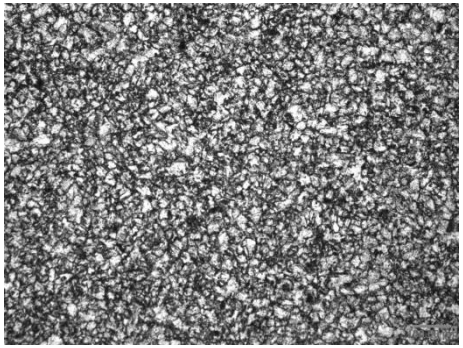

25.6µm ± 0.8µm
950°C

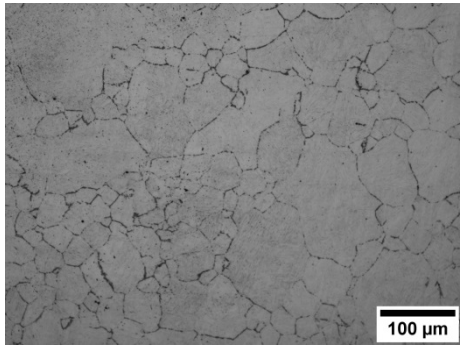

38.5µm ± 6.6µm (20x mag)
1000°C

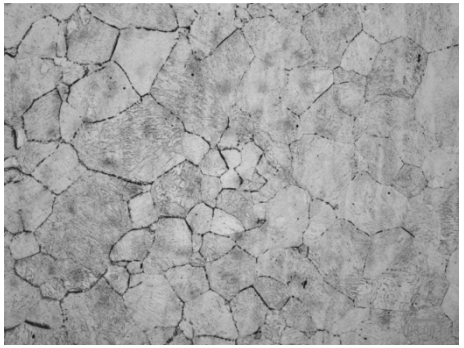

77.7µm ± 1.1µm
1050°C

102µm ± 2.7µm
1100°C

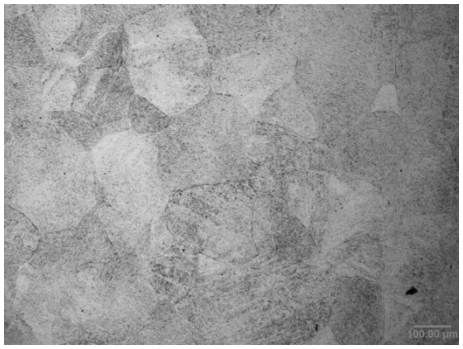

126.3µm ± 2.6µm
1150°C

146.4µm ± 2.3µm
1200°C

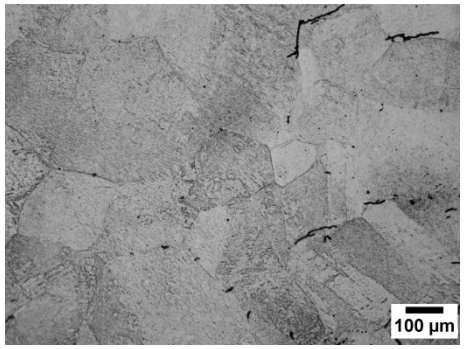

177.9µm ± 3.2µm
1250°C

- 0.8 wt. % Carbon
- 0.005 wt. % Nb
- 950°C - 1250°C
- Tube Furnace
- Argon Atmosphere
- 1 Hour Hold
- Ice Water Quench

Figure C-7: Shown above are a set of light micrographs of prior austenite grains for 0.005 wt. % Nb steel after isothermally reheating to the above temperatures (950°C - 1250°C) for 1 hour and ice water quenching. (Etched with Saturated Picric Acid) 10 x and 20 x magnification.

Table C-15: The Standard deviation (SD) values for the reheat temperatures of 950°C to 1250°C for 0.8 wt. % carbon steel.

	Standard Deviation (SD), Values (μm)			
Temperature (°C)	Plain C-Mn	0.005 wt. % Nb	0.01 wt. % Nb	0.02. wt. % Nb
950	1.2	1.3	1.3	0.7
1000	4.1	16.8	4	2.2
1050	6.6	5	8.3	2.5
1100	5.7	6.7	4.5	5.3
1150	6.2	6.2	4	13.4
1200	5.7	6	6	8
1250	6	30	8.6	8

Appendix D Hold Time

Table D-1: Quantitative analysis of PAGS for different holding times at a fixed temperature of 1050°C. (0.08 wt. % carbon)

Composition	Hold Time (Hours)	Mean PAGS (μm)	Confidence limit (μm)	SD (μm)
C-Mn	1	186.8	5.7	11.1
	3	216.3	7.9	18.3
	6	258.2	10.2	19.7
0.005 wt. % Nb	1	160.1	4.3	10.5
	3	199.8	5.9	18.5
	6	225.1	8.7	28
0.01 wt. % Nb	1	142.8	5	15.5
	3	188.7	4	24.1
	6	202.7	7.9	48
0.02 wt. % Nb	1	113.1	10.5	54.1
	3	169.9	5.5	20.8
	6	180.1	6.4	25.4

Table D-2: Quantitative analysis of PAGS for different holding times at a fixed temperature of 1150°C. (0.08 wt. % carbon)

Composition	Hold Time (Hours)	Mean PAGS (µm)	Confidence limit (µm)	SD (µm)
C-Mn	1	205.8	3.4	9.0
	3	246.8	3.5	12.2
	6	296.4	8.7	29.5
0.005 wt. % Nb	1	189.8	3.8	9.2
	3	221.9	6.4	17.7
	6	274.6	11.5	33.9
0.01 wt. % Nb	1	163.5	4.9	11.8
	3	200.4	6.7	26
	6	247	6.0	33.9
0.02 wt. % Nb	1	153.5	5	12.1
	3	189.1	4.9	18.9
	6	223.7	7.8	24.5

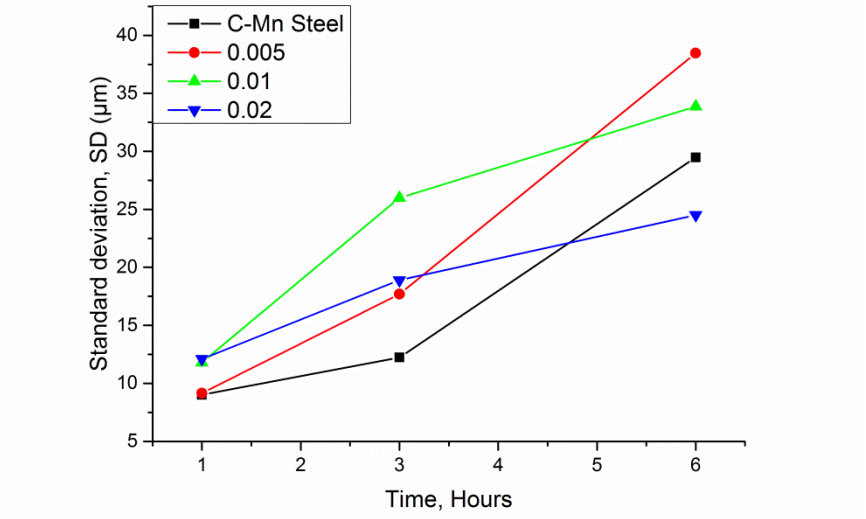

Figure D-1: The standard deviation (SD) values for different holding times from 1 hour to 6 hours at a temperature of 1150°C. (0.08 wt. % carbon)

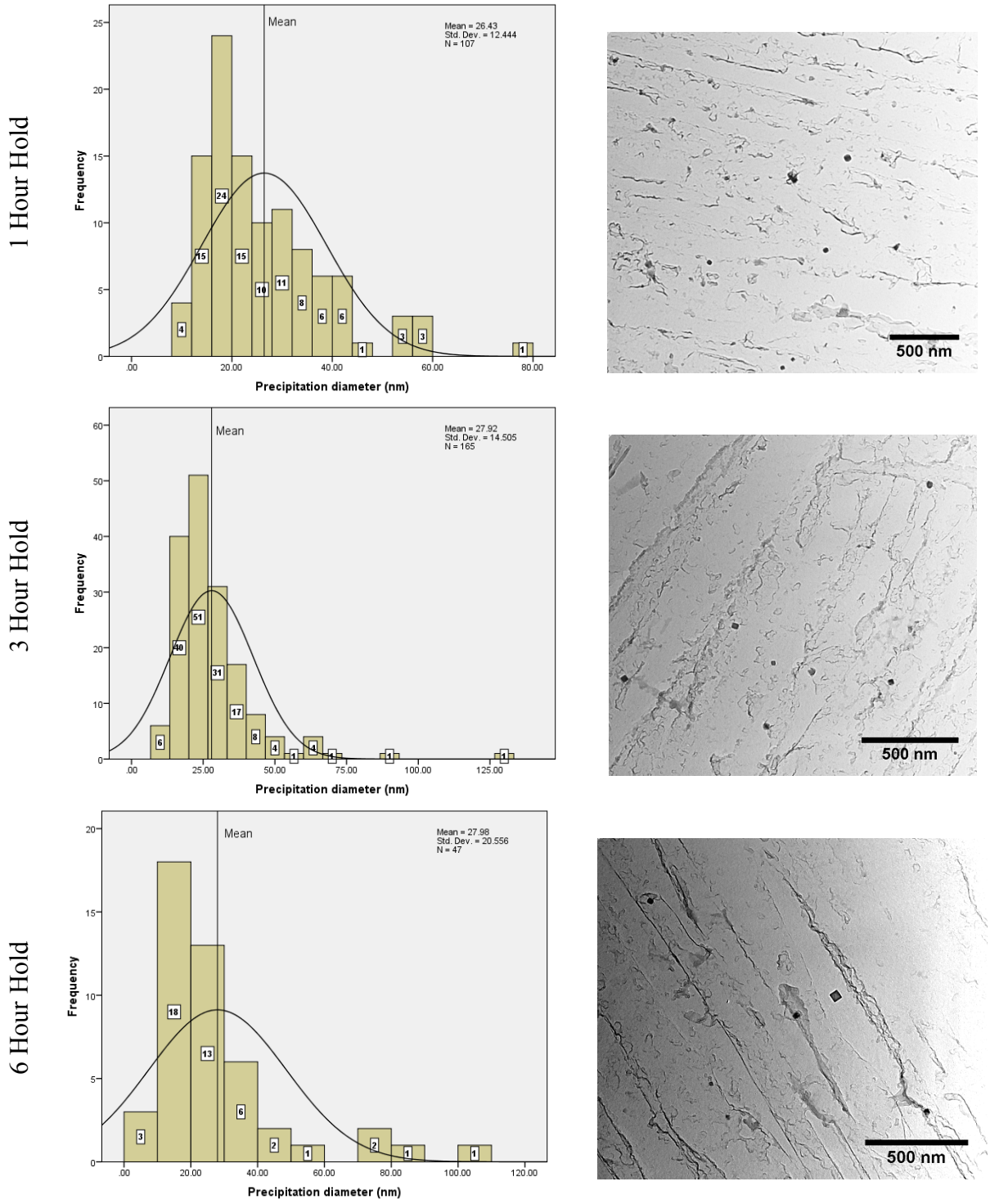

(a) (b)

Figure D-2: (a) Histogram of the distribution of niobium carbide and (b) TEM bright field micrographs of extraction replicas showing niobium carbide precipitate evolution with respect to different holding times at 1150°C 0.08 wt. % C (0.02 wt. % Nb, carbon replica, Tecnai T20).

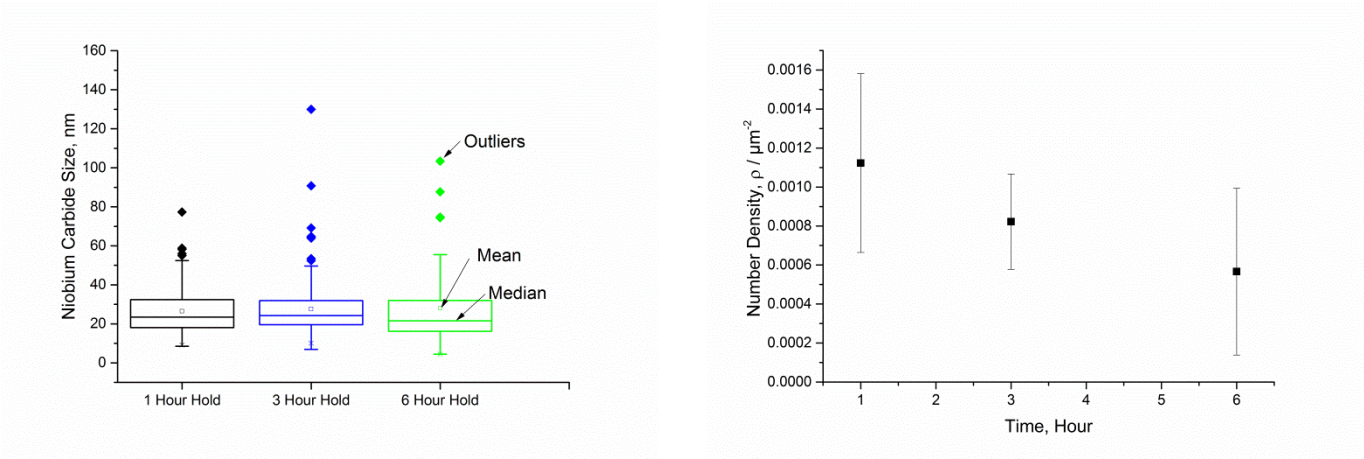

(a) (b)

Figure D-3: (a) Box plot representing the distribution and the growth trend of the NbC precipitates for varying hold times and (b) precipitation number density versus hold time.

Table D-3: Descriptive statistics for varying hold time at a temperature of 1150°C for low carbon steel 0.08 wt %.

Hold Time	Number of precipitates (N)	Minimum (nm)	Maximum (nm)	Mean (nm)	SD. Deviation (nm)
1 Hour	107	8.5	77.3	26.4	12.4
3 Hour	165	6.9	129.7	27.9	14.5
6 Hour	47	4.5	103.4	28	20.6

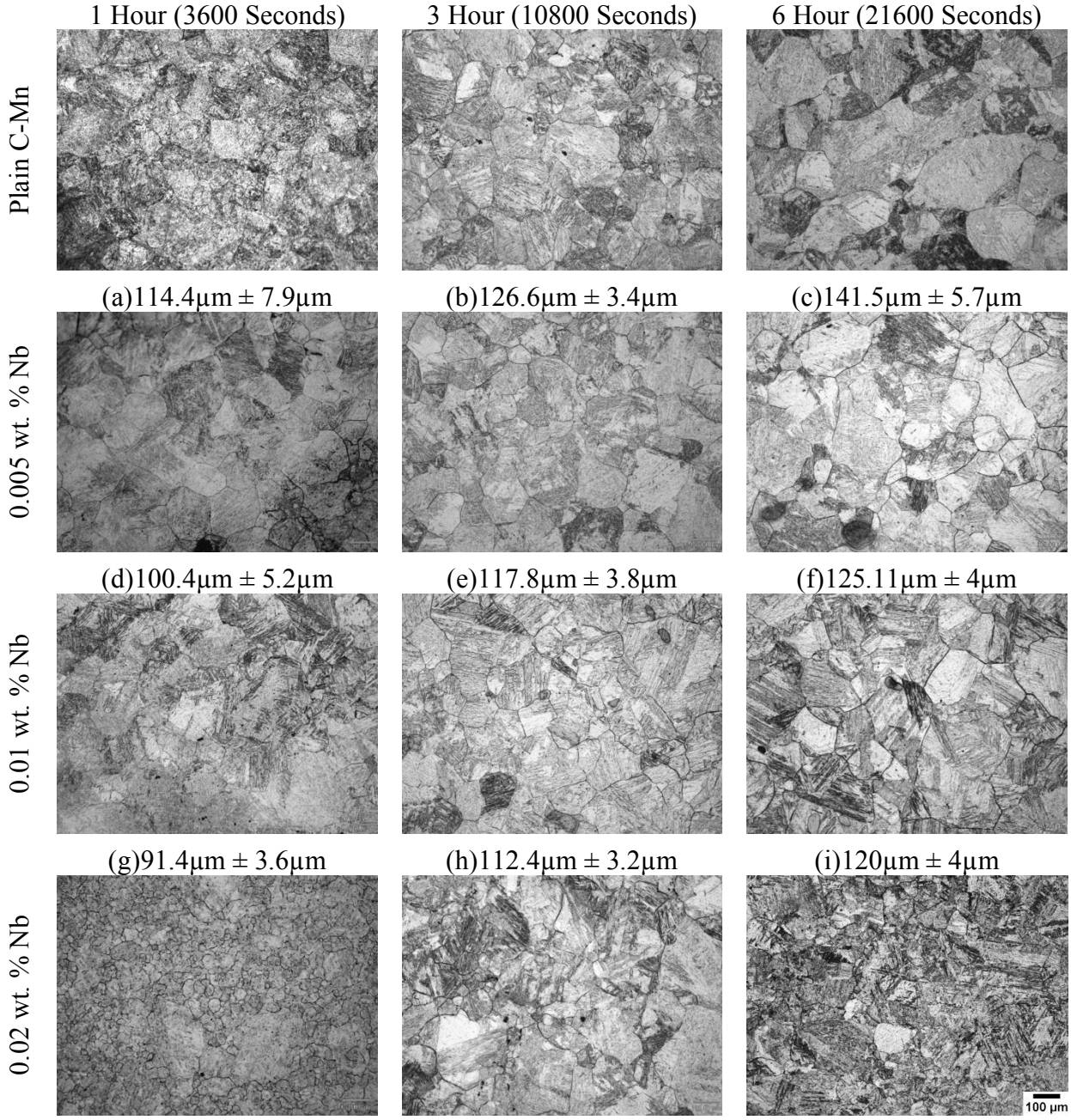

Figure D-4: Optical micrographs of the evolution of Prior Austenite Grain Size for medium carbon steel (0.4 wt. % C) as a function of different hold times at 1050°C Images (a), (b), and (c) are plain C-Mn Steel. Images (d), (e), and (f) are 0.005 wt. % Nb Steel. Images (g), (h), and (i) are 0.01 wt. % Nb Steel and images (j), (k), and (i) are 0.02 wt. % Nb Steel. (Etched with Picric Acid), 10x magnification and magnification bar (black) 100µm.

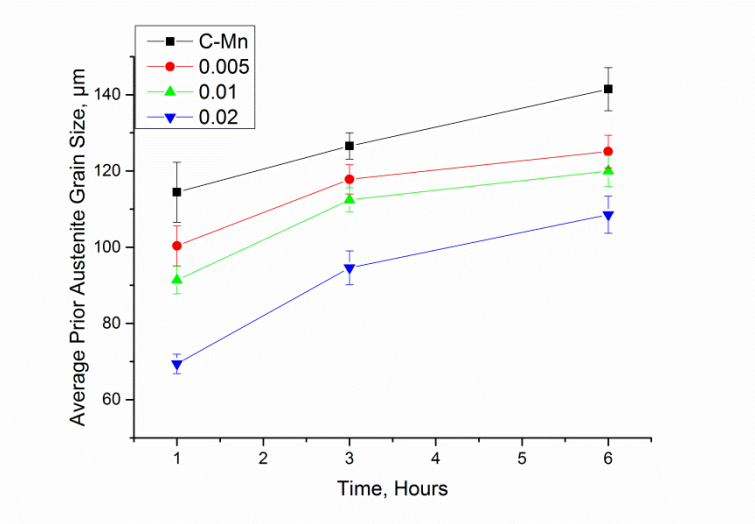

Figure D-5: Prior austenite grain growth as a function of time at an isothermal temperature of 1050°C. Error bars represent ± 95% CL. (0.4 wt. % Carbon)

Table D-4: Quantitative analysis of PAGS for different holding times at a fixed temperature of 1050°C for medium carbon steel.

Composition	Hold Time (Hours)	Mean PAGS (µm)	Confidence limit (µm)	SD (µm)
C-Mn	1	114.4	7.9	5.9
	3	126.6	3.4	7.8
	6	141.5	5.7	7.5
0.005 wt. % Nb	1	100.4	5.2	8.2
	3	117.8	3.8	9.1
	6	125.1	4.3	8.4
0.01 wt. % Nb	1	91.4	3.6	9.1
	3	112.4	3.2	9.7
	6	120	4	7
0.02 wt. % Nb	1	69.4	2.6	25.1
	3	94.6	4.5	18.7
	6	108.5	4.9	16.6

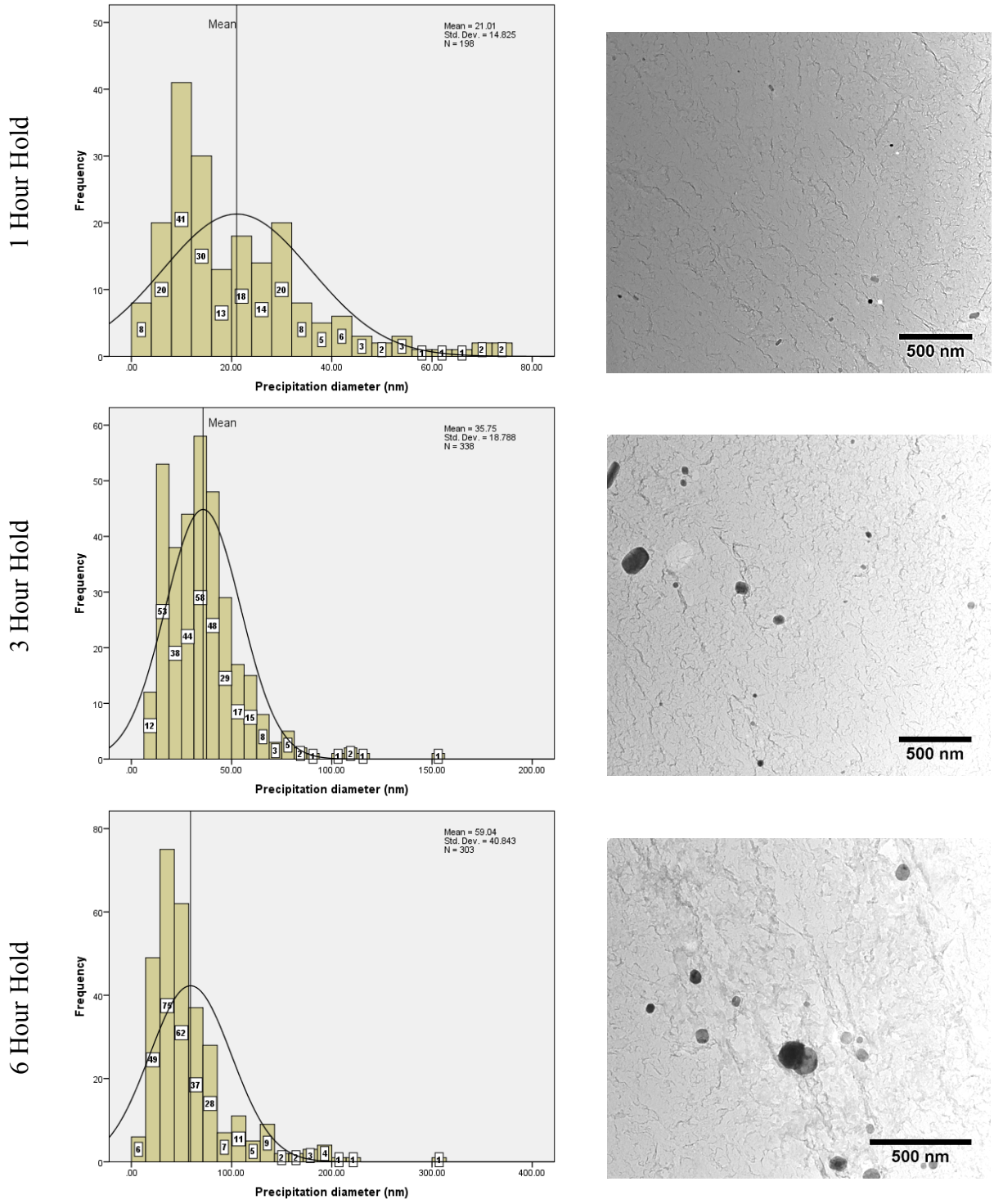

Figure D-6: (a) Histogram of the distribution of niobium carbide and (b) TEM bright field micrographs of extraction replicas showing NbC precipitation evolution with respect to different holding times at 1050°C for 0.4wt. % C (0.02 wt. % Nb, carbon replica, Tecnai T20).

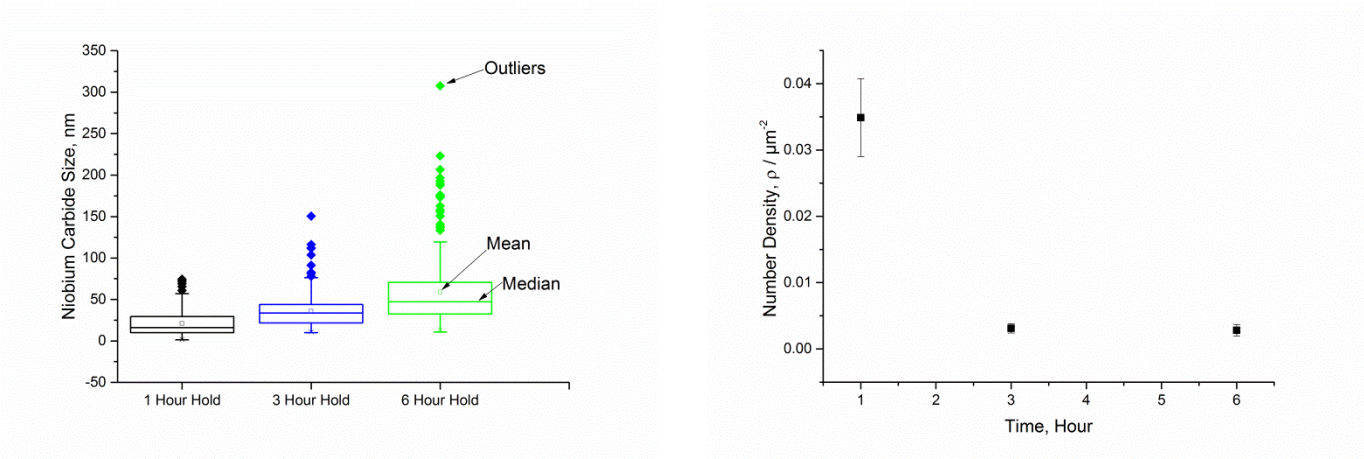

(a) (b)

Figure D-7: (a) Box plot representing the distribution and the growth trend of the NbC precipitate for varying hold times and (b) precipitation number density versus hold time. (0.4 wt. carbon, 1050°C)

Table D-5: Descriptive statistics for varying hold time at a temperature of 1050°C for low carbon steel 0.4 wt %.

Hold Time	Number of precipitates (N)	Minimum (nm)	Maximum (nm)	Mean (nm)	SD. Deviation (nm)
1 Hour	198	1.4	74.4	21	14.8
3 Hour	338	9.9	150.5	35.7	18.9
6 Hour	303	10.6	307.6	59	40.8

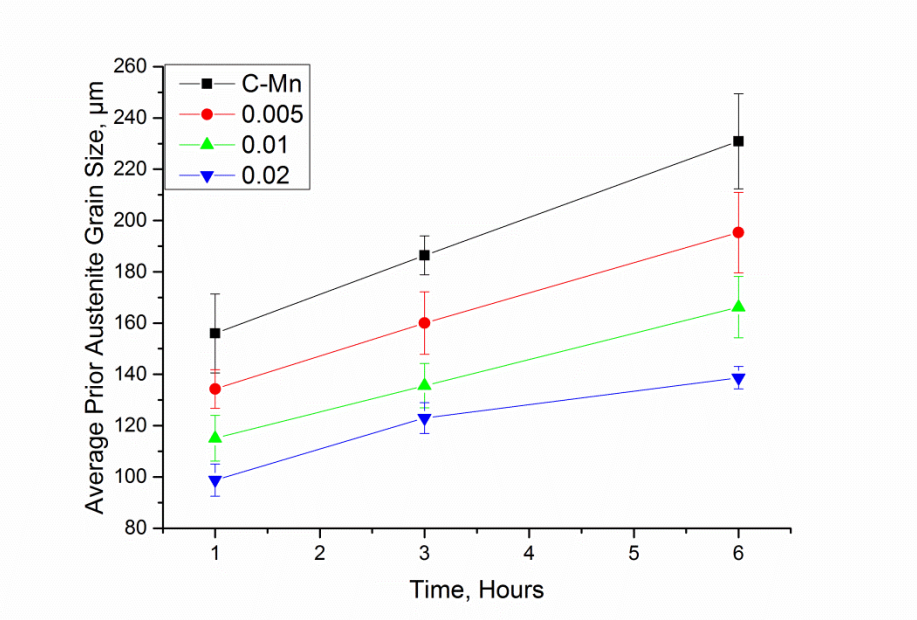

Figure D-8: Prior austenite grain growth as a function of time at an isothermal temperature of 1150°C. Error bars represent ± 95% CL. (0.4 wt. % Carbon)

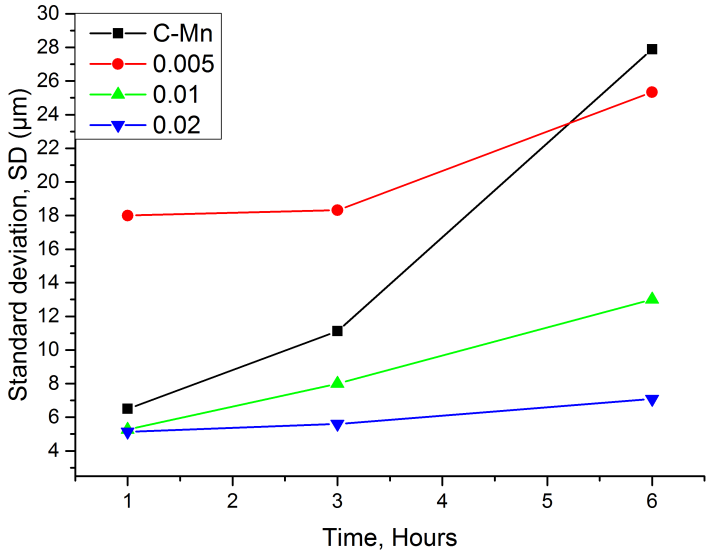

Figure D-9: The standard deviation (SD) values as a function of different holding times for medium carbon steel (0.4 wt. % Carbon) at a temperature of 1150°C.

Table D-6: Quantitative analysis of PAGS for different holding times at a fixed temperature of 1150°C for medium carbon steel.

Composition	Hold Time (Hours)	Mean PAGS (µm)	Confidence limit (µm)	SD (µm)
C-Mn	1	156	15.4	6.5
	3	186.4	7.6	11.1
	6	230.9	18.6	27.9
0.005 wt. % Nb	1	134.3	7.5	18
	3	160	12.2	18.3
	6	195.3	15.7	25.3
0.01 wt. % Nb	1	115.1	8.9	5.3
	3	135.6	8.6	8
	6	166.2	12	13
0.02 wt. % Nb	1	98.8	6.3	5.1
	3	123	4.4	5.6
	6	138.7	4.4	7.1

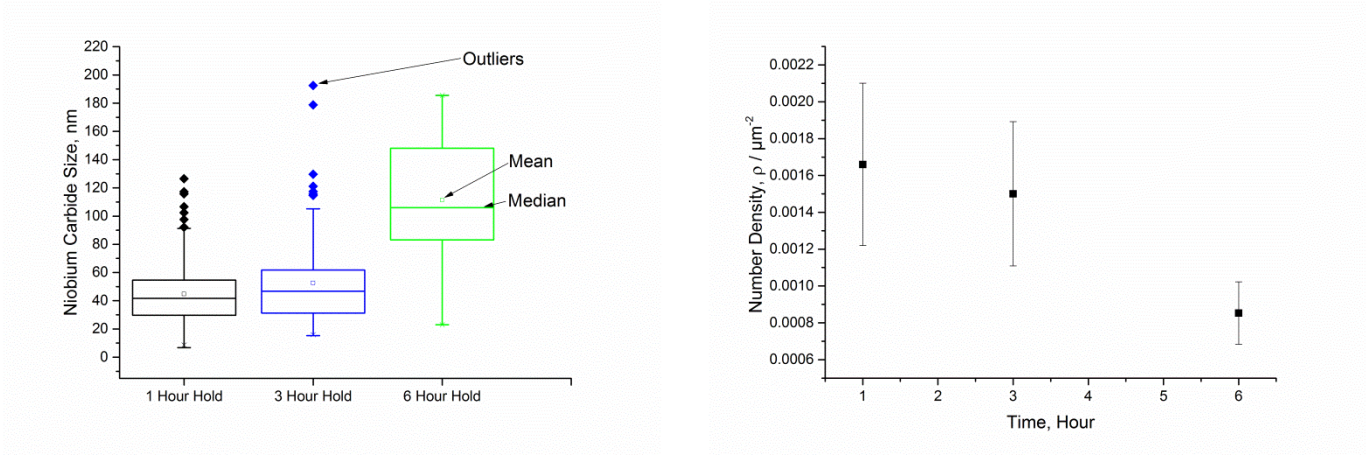

(a) (b)

Figure D-10: (a) Box plot representing the distribution and the growth trend of the NbC precipitate for varying hold times (b) precipitation number density versus hold time.

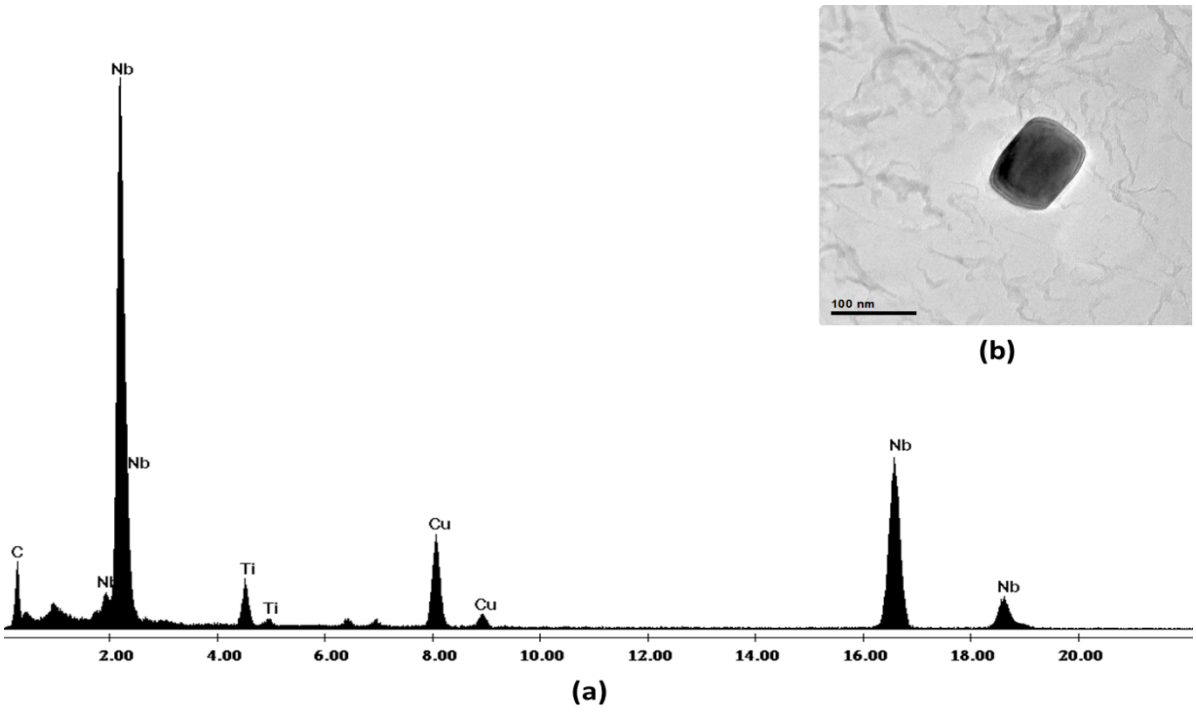

Figure D-11: (a) EDX of a mixed Ti,Nb(C) particle, (b) TEM micrograph showing a cube shape TiNbC particle at 1150°C for 1 hour hold (0.4 wt. % C).

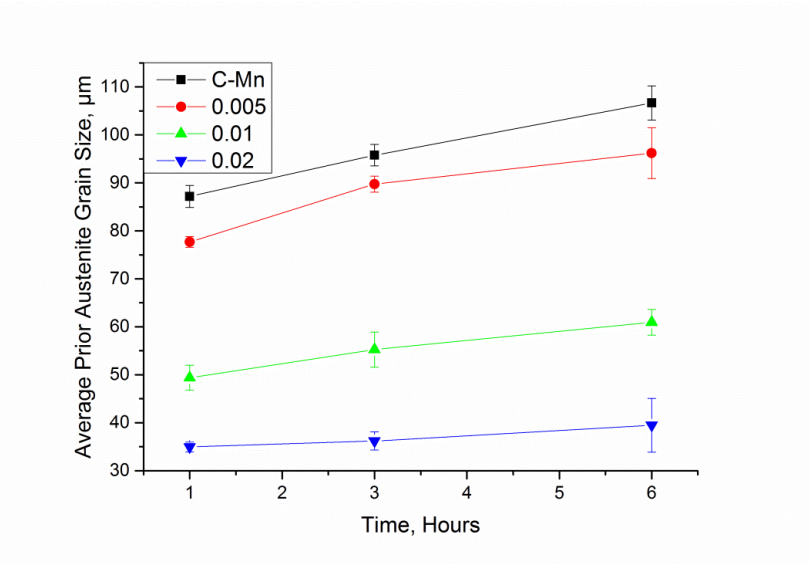

Figure D-12: Prior austenite grain growth as a function of hold time for 1, 3 and 6 hours at 1050°C. (0.8 wt. % Carbon)

Table D-7: Quantitative analysis of PAGS for different holding times at a fixed temperature of 1050°C for high carbon steel.

Composition	Hold Time (Hours)	Mean PAGS (µm)	Confidence limit (µm)	SD (µm)
C-Mn	1	87.2	2.3	6.5
	3	95.8	2.3	5.4
	6	106.7	3.6	8.2
0.005 wt. % Nb	1	77.7	1.1	5
	3	89.8	1.7	4
	6	96.2	5.3	33.1
0.01 wt. % Nb	1	49.4	2.6	8.3
	3	55.3	3.7	9.1
	6	60.9	2.7	25.1
0.02 wt. % Nb	1	34.9	1	2.5
	3	36.2	1.9	3.2
	6	39.5	5.6	19.8

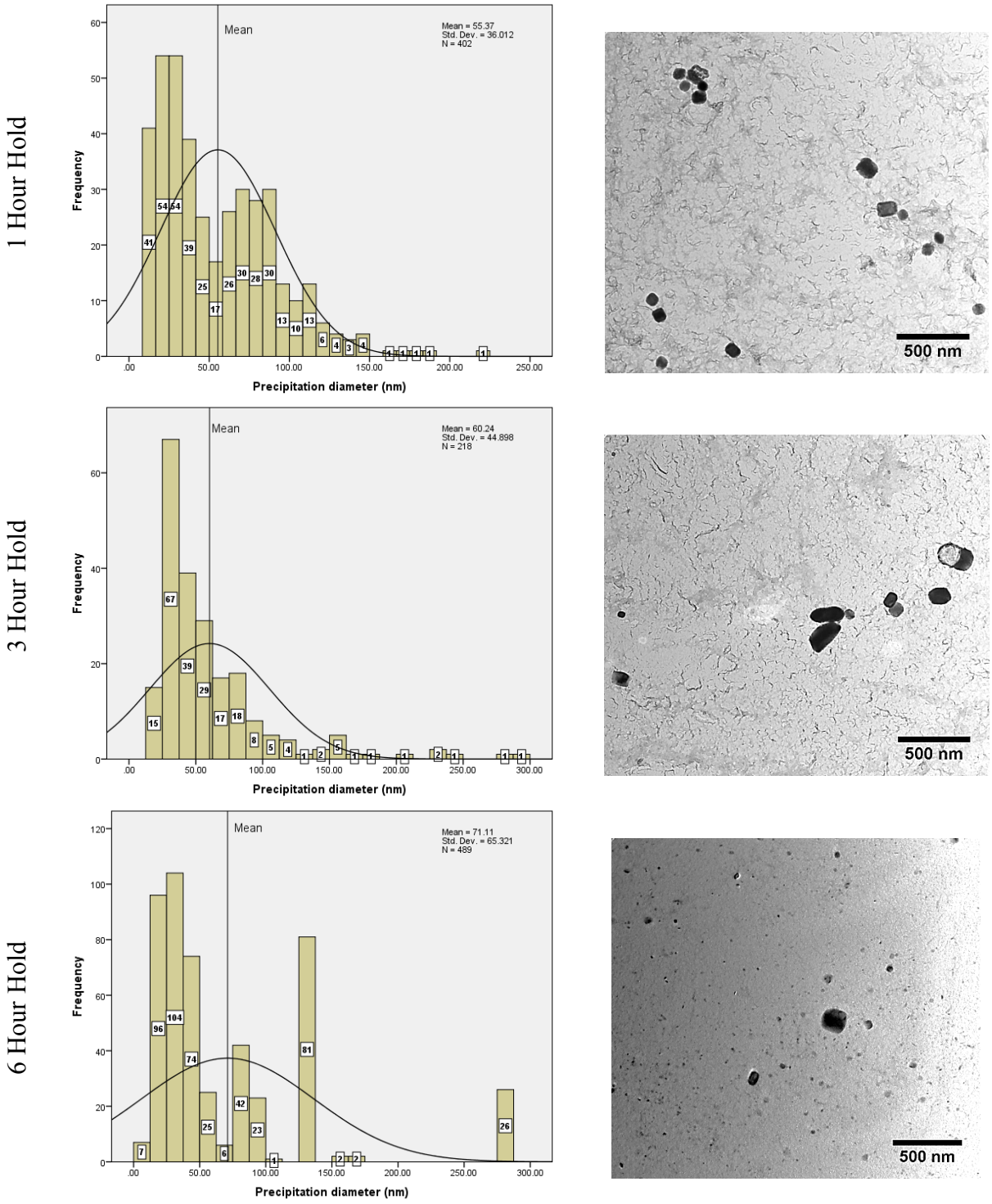

(a) (b)

Figure D-13: (a) Histogram of the distribution of niobium carbide and (b) TEM bright field micrographs of extraction replicas showing NbC precipitate evolution with respect to different holding times at 1050°C for 0.8wt. % C (0.02 wt. % Nb, carbon replica, Tecnai T20).

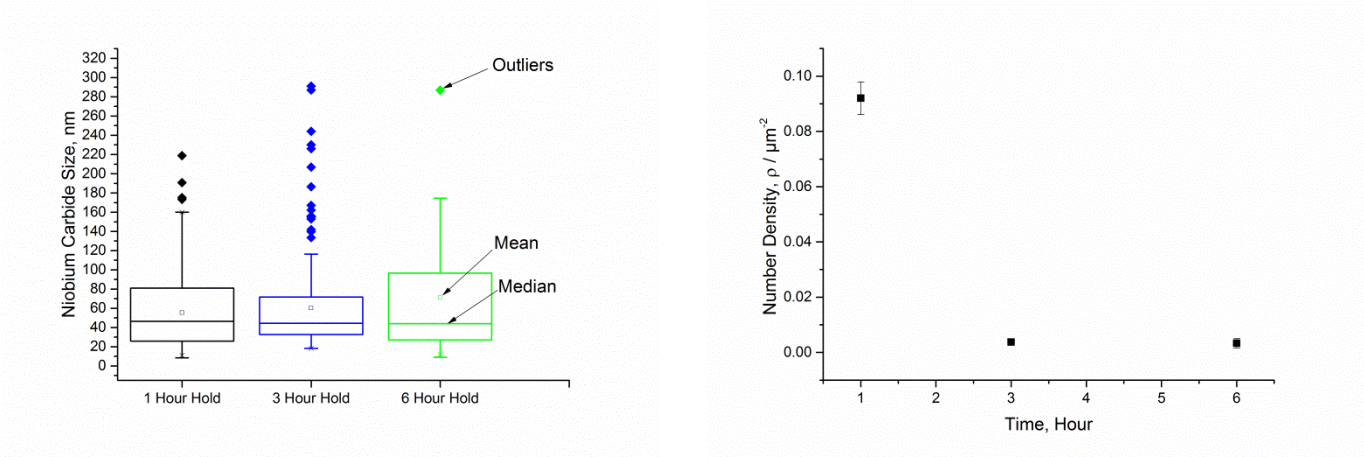

(a) (b)

Figure D-14: (a) Box plot representing the distribution and the growth trend of the NbC precipitate for varying hold times (b) precipitation number density versus hold time.

Table D-8: Descriptive statistics for varying hold time at a temperature of 1050°C for low carbon steel 0.8 wt %.

Hold Time	Number of precipitates (N)	Minimum (nm)	Maximum (nm)	Mean (nm)	SD. Deviation (nm)
1 Hour	402	8.4	218.7	55.4	36
3 Hour	218	18.3	291.1	60.2	44.9
6 Hour	489	9	286.8	71.1	65.3

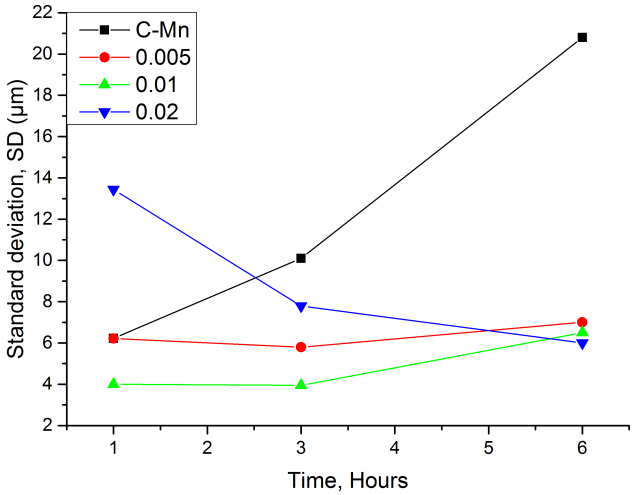

Figure D-15: The standard deviation (SD) values as a function of different holding times for high carbon steel (0.8 wt. % Carbon) at a reheat temperature of 1150°C.

Table D-9: Quantitative analysis of PAGS for different holding times at a fixed temperature of 1150°C for high carbon steel.

Composition	Hold Time (Hours)	Mean PAGS (µm)	Confidence limit (µm)	SD (µm)
C-Mn	1	144.7	4.3	6.2
	3	166.5	5.3	10.2
	6	198.1	6.6	20.8
0.005 wt. % Nb	1	126.3	2.6	6.2
	3	151.1	2.1	5.8
	6	183.6	4.2	7
0.01 wt. % Nb	1	104.4	3.4	4
	3	121.7	1.34	3.95
	6	134.4	4.1	6.5
0.02 wt. % Nb	1	86.3	5.5	13.4
	3	98.5	2.8	7.8
	6	108.5	5.3	6

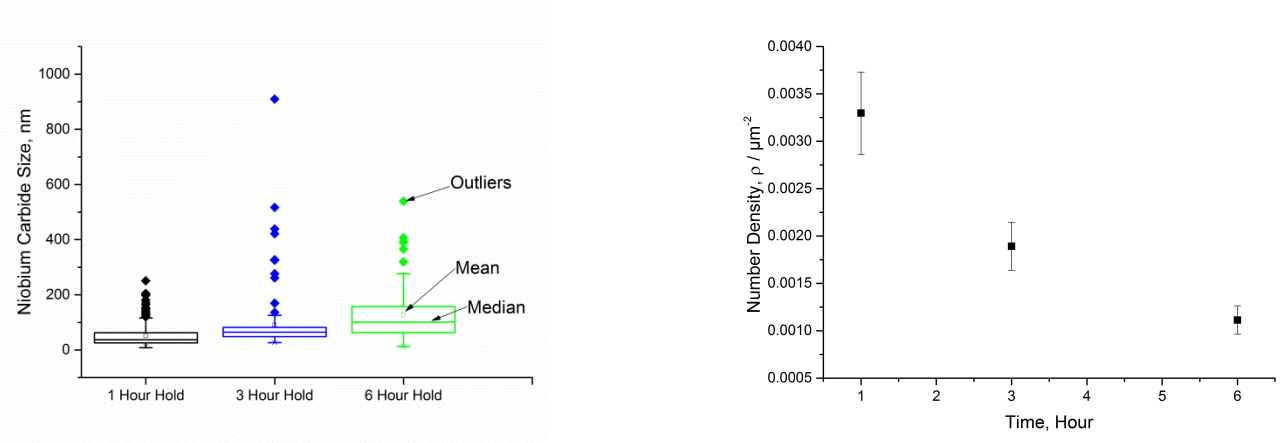

(a) (b)

Figure D-16: (a) Box plot representing the distribution and the growth trend of the NbC precipitates for varying hold times (b) precipitation number density versus hold time, 1150°C.

Table D-10: Descriptive statistics for varying hold time at a temperature of 1150°C for low carbon steel 0.8 wt %.

Hold Time	Number of precipitates (N)	Minimum (nm)	Maximum (nm)	Mean (nm)	SD. Deviation (nm)
1 Hour	246	8	251	50.4	39.7
3 Hour	122	26.4	909.9	90.2	108
6 Hour	95	12.3	539.5	126.3	94.2

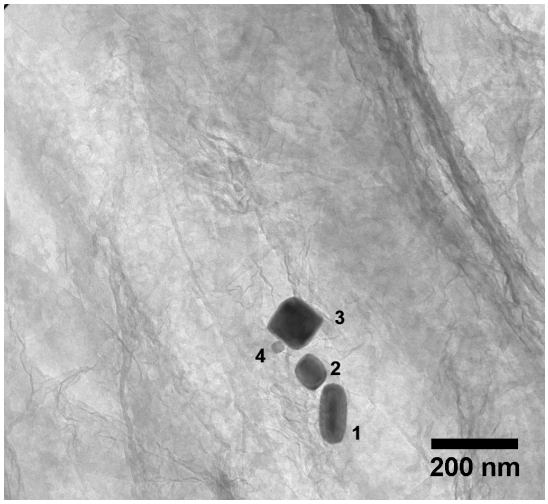

(a) TEM micrograph

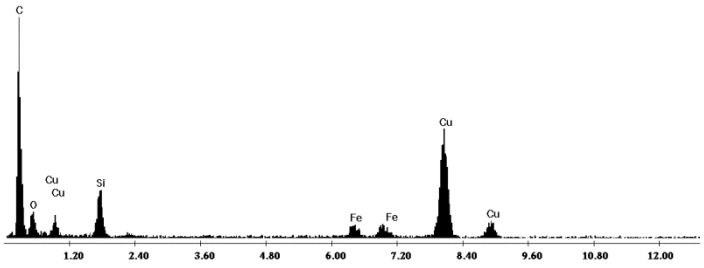

(b) EDX of the carbon coating (background)

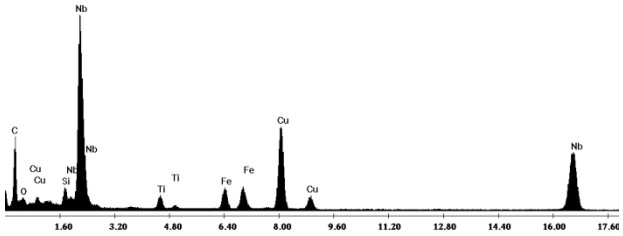

(c) EDX of Particle 1

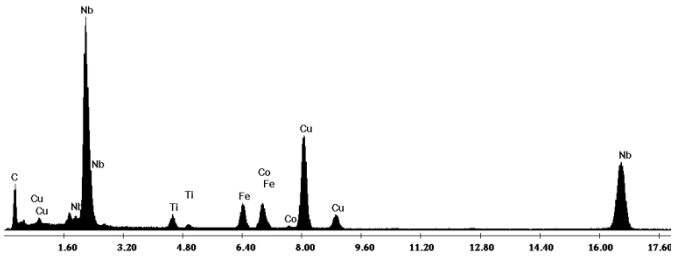

(d) EDX of Particle 2

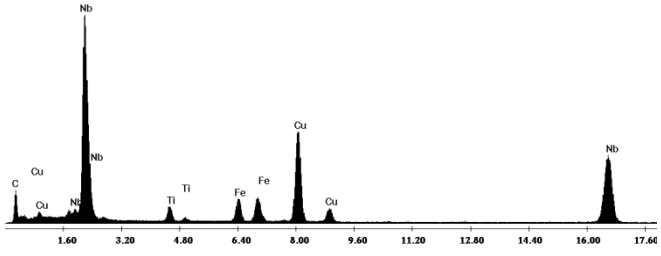

(e) EDX of Particle 3

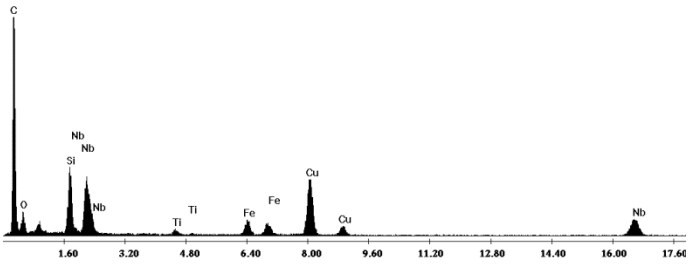

(f) EDX of Particle 4

Figure D-17: Presented above in (a) are 4 different morphologies of precipitates and their respective EDX analyses at 1150°C for a 6 hour hold.

Appendix E Grain Growth Activation Energy

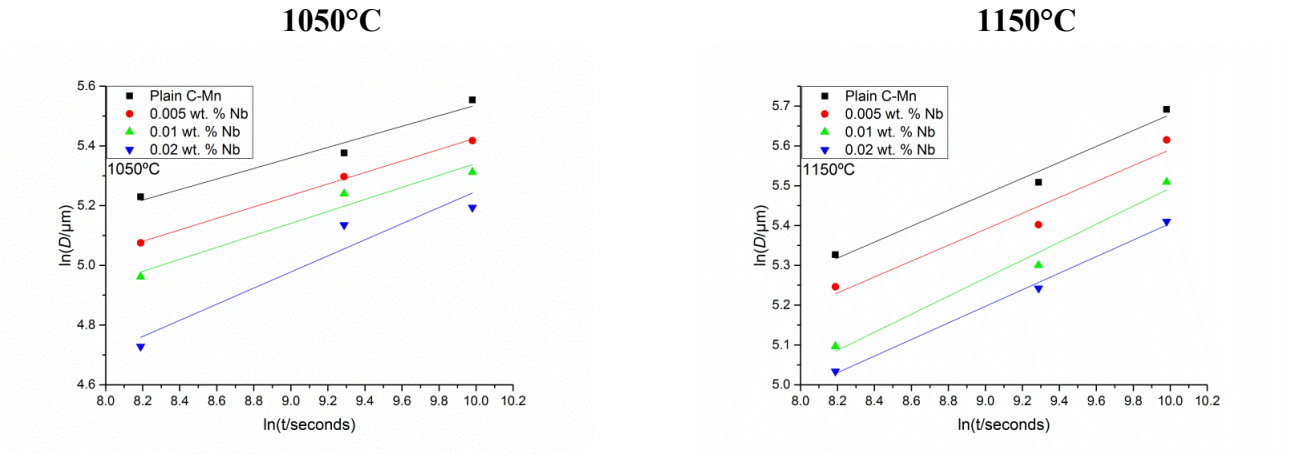

(a) 0.08 Carbon wt. %

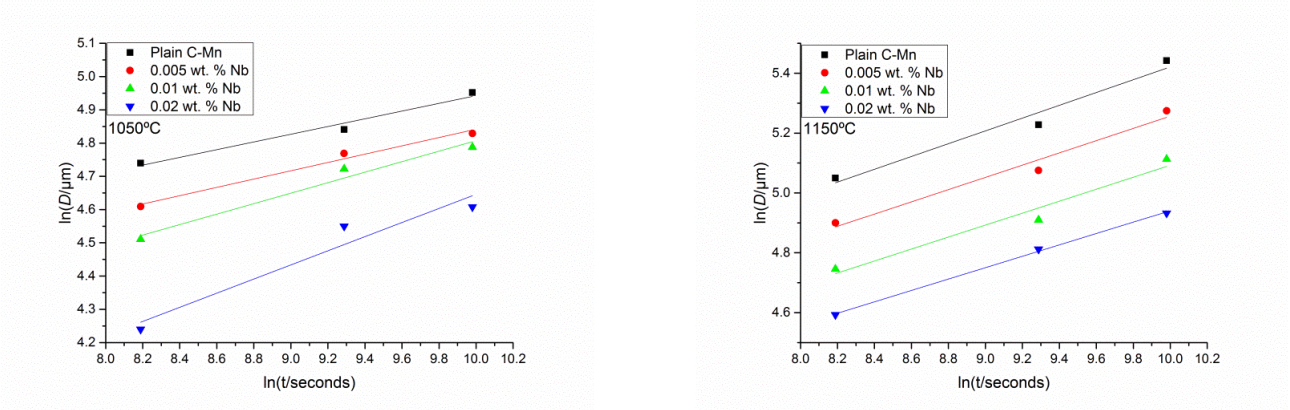

(b) 0.4 Carbon wt. %

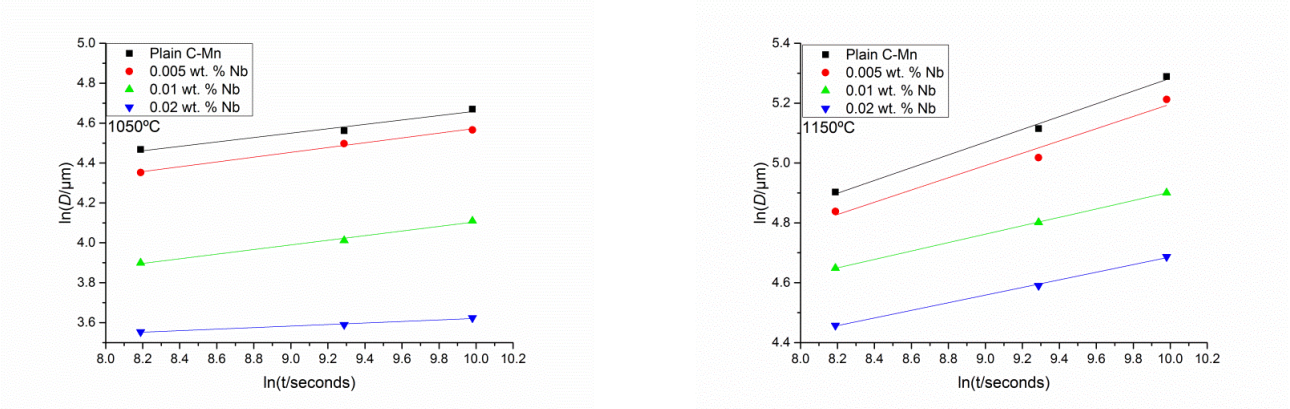

(c) 0.8 Carbon wt. %

Figure E-1: Presented above are the plots of $[ln\, D]$ versus $[ln\, t]$ of austenite grain growth for the data range of 1 to 6 hour hold for both 1050°C and 1150°C.

Table E-1: A summary of the Gradient $[n]$ and the Intercept $[A_1]$ for the three different base carbons and the microalloyed steels at 1050°C and 1150°C.

		Gradient $[n]$		Intercept $[A_1]$		Statistics
		Value	Standard Error	Value	Standard Error	Adj. R-Square
0.08 wt. % C						
1050°C	Plain C-Mn	0.17651	0.03271	3.77128	0.30035	0.93359
	0.005 wt. % Nb	0.19212	0.00733	3.50518	0.06727	0.9971
	0.01 wt. % Nb	0.20085	0.04042	3.33301	0.37113	0.92215
	0.02 wt. % Nb	0.27006	0.07703	2.54723	0.70728	0.84952
1150°C	Plain C-Mn	0.20018	0.02666	3.67695	0.24475	0.96516
	0.005 wt. % Nb	0.2001	0.04452	3.58982	0.40881	0.90565
	0.01 wt. % Nb	0.22625	0.03125	3.23151	0.28694	0.96256
	0.02 wt. % Nb	0.2083	0.01424	3.32228	0.13073	0.9907
0.4wt. % C						
1050°C	Plain C-Mn	0.116	0.01855	3.78261	0.17032	0.95014
	0.005 wt. % Nb	0.12488	0.01589	3.59293	0.14594	0.96812
	0.01 wt. % Nb	0.15781	0.0265	3.22923	0.24329	0.94516
	0.02 wt. % Nb	0.21244	0.05324	2.52158	0.48884	0.88181
1150°C	Plain C-Mn	0.21369	0.03953	3.28423	0.363	0.93381
	0.005 wt. % Nb	0.20448	0.03453	3.21184	0.31709	0.94453
	0.01 wt. % Nb	0.20009	0.03897	3.09175	0.35783	0.9269
	0.02 wt. % Nb	0.19024	0.00703	3.03811	0.06456	0.99727
0.8 wt. % C						
1050°C	Plain C-Mn	0.11015	0.01878	3.55844	0.1724	0.94353
	0.005 wt. % Nb	0.12039	0.00848	3.37014	0.07787	0.99013
	0.01 wt. % Nb	0.1159	0.0106	2.94646	0.09732	0.98341
	0.02 wt. % Nb	0.0384	0.00471	3.23729	0.04327	0.97033
1150°C	Plain C-Mn	0.21324	0.01556	3.15065	0.14288	0.98941
	0.005 wt. % Nb	0.20469	0.03172	3.14976	0.29128	0.95309
	0.01 wt. % Nb	0.14068	0.00105	3.49614	0.00964	0.99989
	0.02 wt. % Nb	0.12736	0.00504	3.41241	0.04629	0.99687

Low Carbon, (0.08 wt. % C)

$$D_{Plain\ C-Mn,1050°C} = 43.44 \cdot t^{0.1765} \quad \text{(E-1)}$$

$$D_{0.005\ wt.\%\ Nb,1050°C} = 33.29 \cdot t^{0.19212} \quad \text{(E-2)}$$

$$D_{0.01\ wt.\%\ Nb,1050°C} = 28.02 \cdot t^{0.20085} \quad \text{(E-3)}$$

$$D_{0.02\ wt.\%\ Nb,1050°C} = 12.77 \cdot t^{0.27006} \quad \text{(E-4)}$$

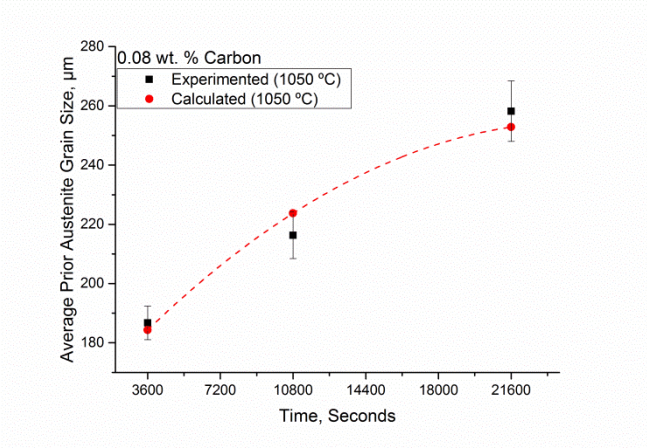

(a) Equation (E-1)

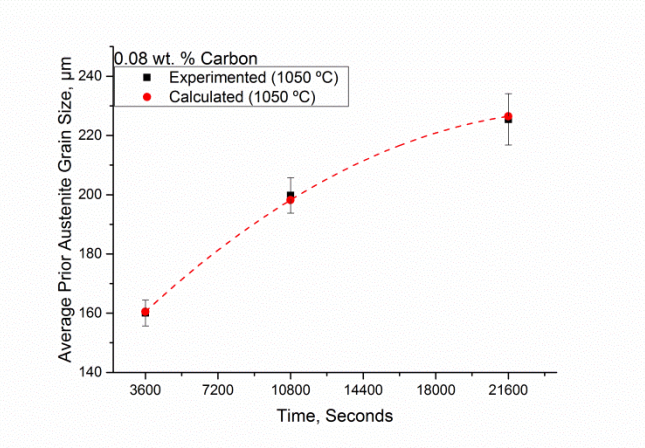

(b) Equation (E-2)

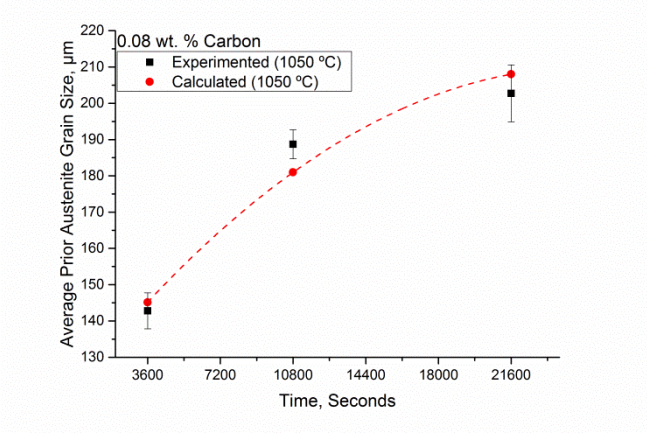

(c) Equation (E-3)

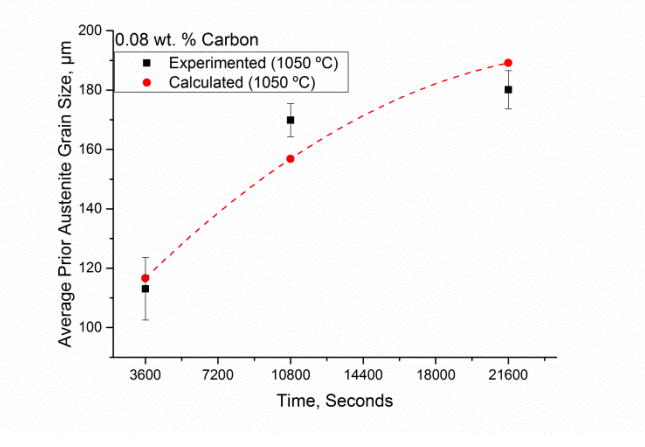

(d) Equation (E-4)

Figure E-2: Comparison of calculated austenite average grain size and the experimental measurements of the austenite grain size at a temperature of 1050°C. (0.08 wt. % Carbon)

$$D_{Plain\ C-Mn,1150°C} = 39.53 \cdot t^{0.20018} \quad \text{(E-5)}$$

$$D_{0.005\ wt.\%\ Nb,1150°C} = 36.23 \cdot t^{0.2001} \quad \text{(E-6)}$$

$$D_{0.01\ wt.\%\ Nb,1150°C} = 25.32 \cdot t^{0.22625} \quad \text{(E-7)}$$

$$D_{0.02\ wt.\%\ Nb,1150°C} = 27.72 \cdot t^{0.2083} \quad \text{(E-8)}$$

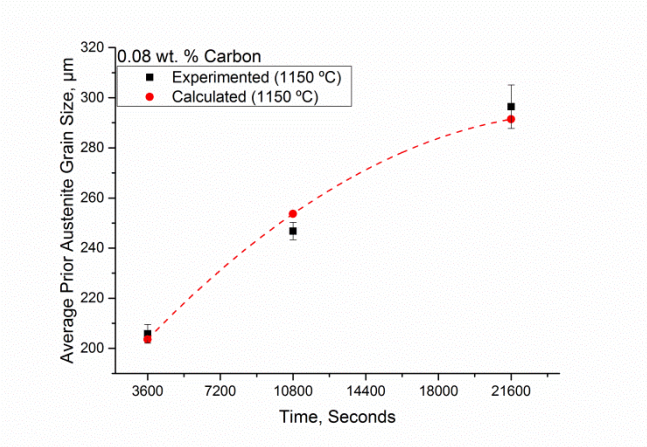

(a) Equation (E-5)

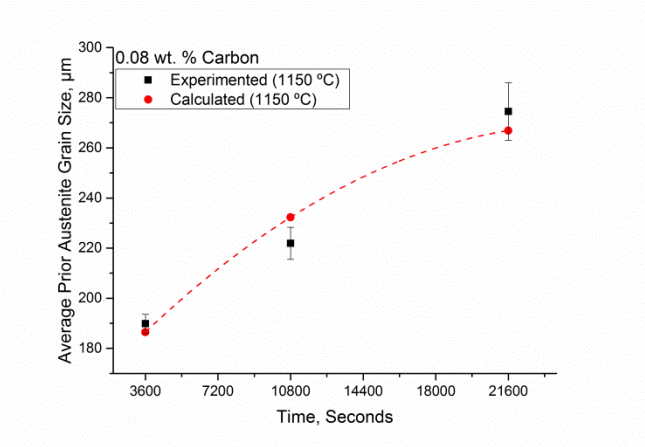

(b) Equation (E-6)

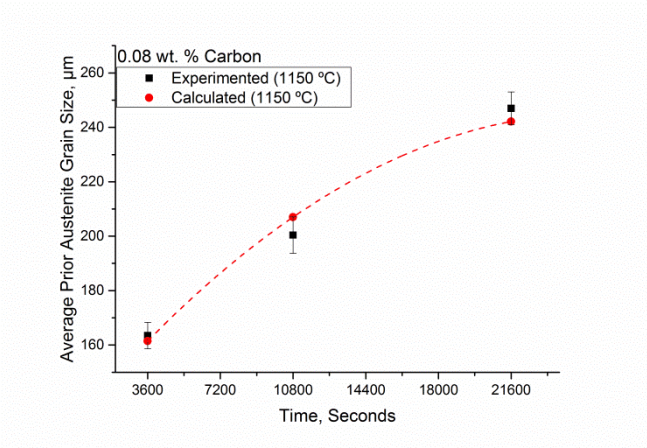

(c) Equation (E-7)

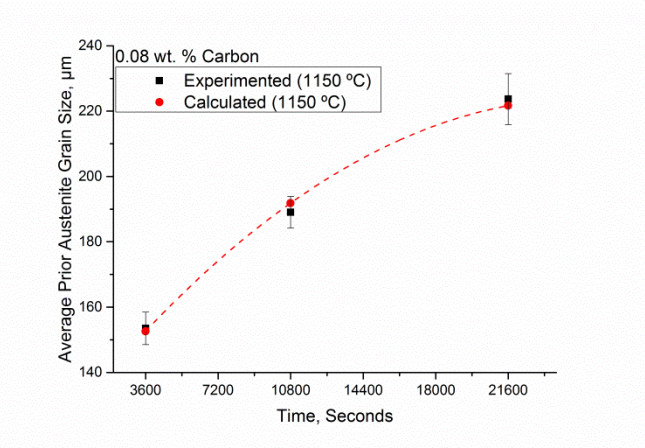

(d) Equation (E-8)

Figure E-3: Comparison of calculated austenite average grain size and the experimental measurements of the austenite grain size at a temperature of 1150°C. (0.08 wt. % Carbon)

Medium carbon, (0.4 wt. % C)

$$D_{Plain\ C-Mn,1050°C} = 43.93 \cdot t^{0.116} \quad \text{(E-9)}$$

$$D_{0.005\ wt.\%\ Nb,1050°C} = 36.34 \cdot t^{0.12488} \quad \text{(E-10)}$$

$$D_{0.01\ wt.\%\ Nb,1050°C} = 25.26 \cdot t^{0.15781} \quad \text{(E-11)}$$

$$D_{0.02\ wt.\%\ Nb,1050°C} = 12.45 \cdot t^{0.21244} \quad \text{(E-12)}$$

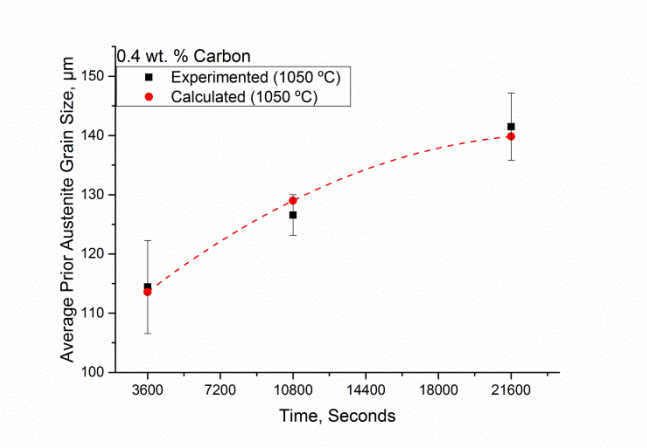

(a) Equation (E-9)

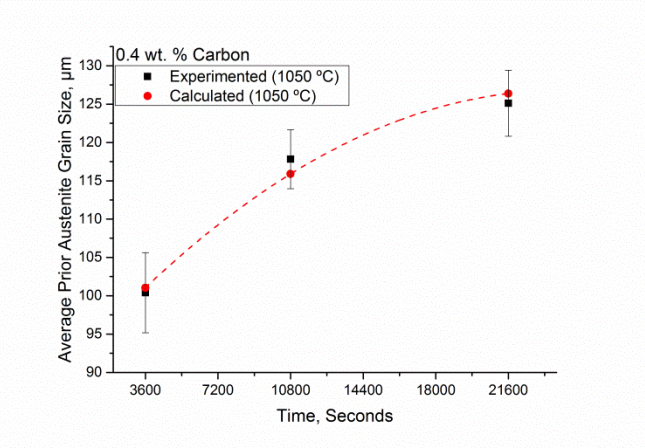

(b) Equation (E-10)

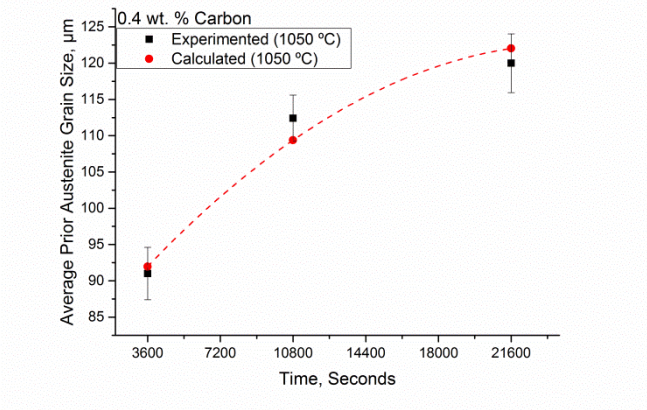

(c) Equation (E-11)

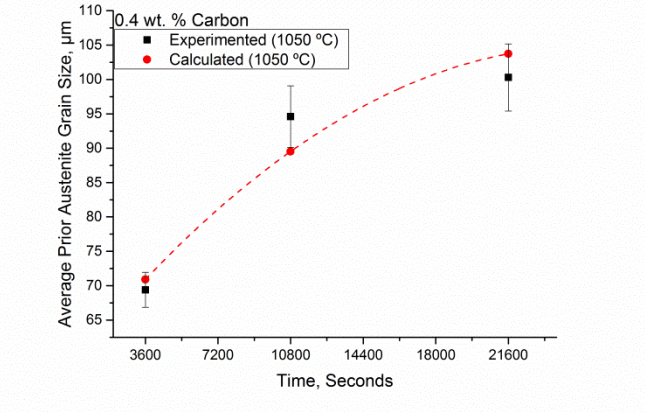

(d) Equation (E-12)

Figure E-4: Comparison of calculated austenite average grain size and the experimental measurements of the austenite grain size at a temperature of 1050°C.

$$D_{Plain\ C-Mn,1150°C} = 26.69 \cdot t^{0.21369} \quad \text{(E-13)}$$

$$D_{0.005\ wt.\%\ Nb,1150°C} = 24.82 \cdot t^{0.20448} \quad \text{(E-14)}$$

$$D_{0.01\ wt.\%\ Nb,1150°C} = 22.02 \cdot t^{0.20009} \quad \text{(E-15)}$$

$$D_{0.02\ wt.\%\ Nb,1150°C} = 20.87 \cdot t^{0.19024} \quad \text{(E-16)}$$

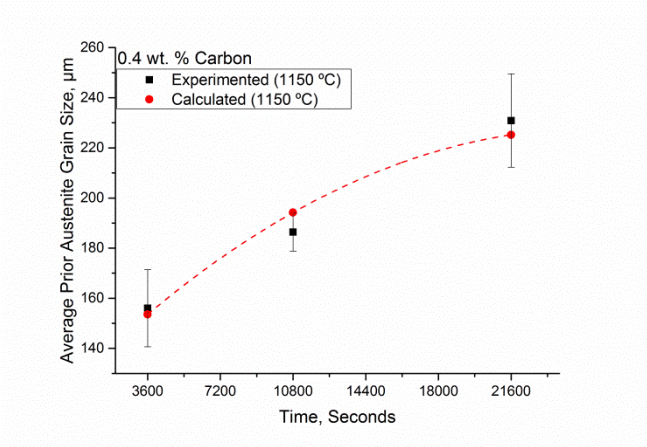

(a) Equation (E-13)

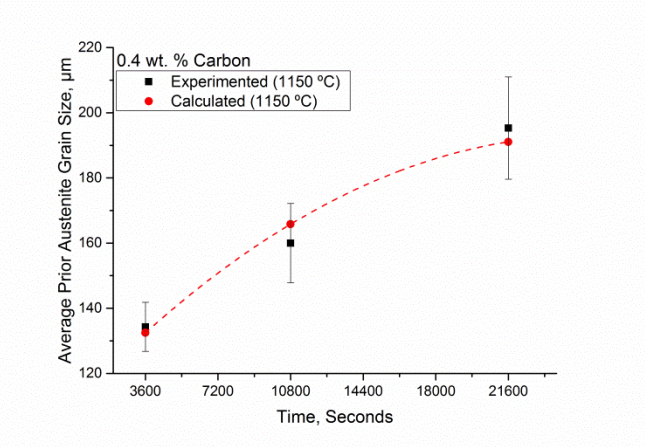

(b) Equation (E-14)

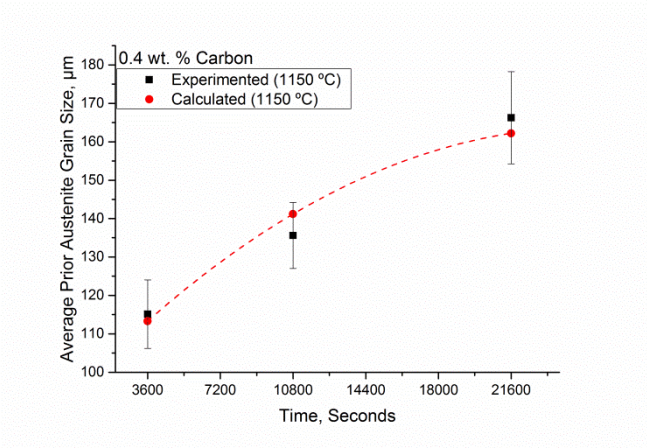

(c) Equation (E-15)

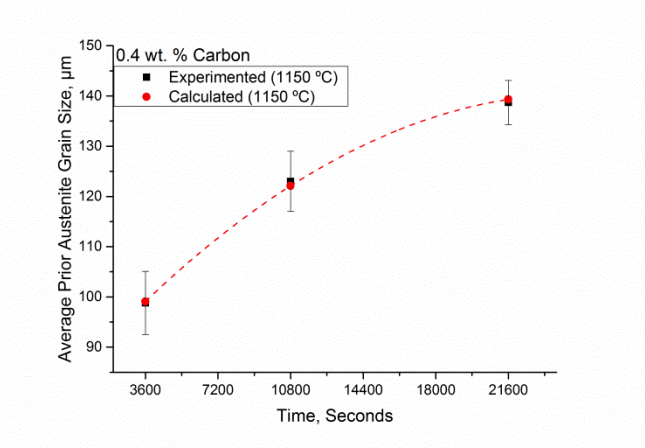

(d) Equation (E-16)

Figure E-5: Comparison of calculated austenite average grain size and the experimental measurements of the austenite grain size at a temperature of 1150°C.

High carbon, (0.8 wt. % C)

$$D_{Plain\ C-Mn,1050°C} = 35.11 \cdot t^{0.11015} \quad \text{(E-17)}$$

$$D_{0.005\ wt.\%\ Nb,1050°C} = 29.08 \cdot t^{0.12039} \quad \text{(E-18)}$$

$$D_{0.01\ wt.\%\ Nb,1050°C} = 19.04 \cdot t^{0.1159} \quad \text{(E-19)}$$

$$D_{0.02\ wt.\%\ Nb,1050°C} = 25.46 \cdot t^{0.0384} \quad \text{(E-20)}$$

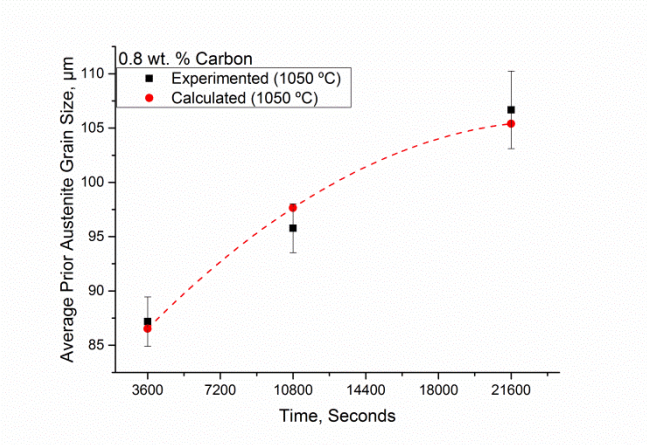

(a) Equation (E-17)

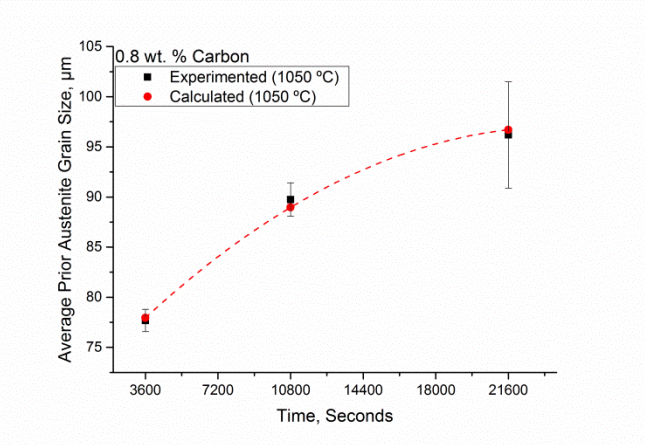

(b) Equation (E-18)

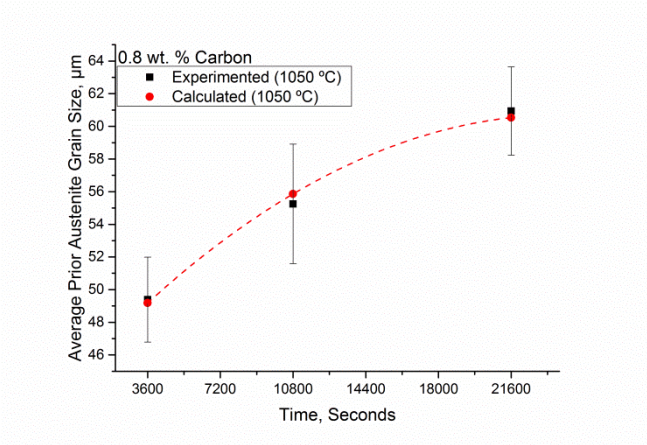

(c) Equation (E-19)

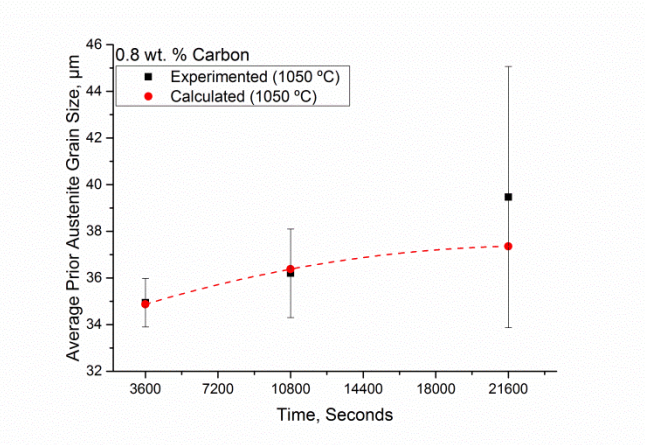

(d) Equation (E-20)

Figure E-6: Comparison of calculated austenite average grain size and the experimental measurements of the austenite grain size at a temperature of 1050°C.

$$D_{Plain\ C-Mn,1150°C} = 23.35 \cdot t^{0.21324} \quad \text{(E-21)}$$

$$D_{0.005\ wt.\%\ Nb,1150°C} = 23.33 \cdot t^{0.20469} \quad \text{(E-22)}$$

$$D_{0.01\ wt.\%\ Nb,1150°C} = 32.99 \cdot t^{0.14068} \quad \text{(E-23)}$$

$$D_{0.02\ wt.\%\ Nb,1150°C} = 30.34 \cdot t^{0.12736} \quad \text{(E-24)}$$

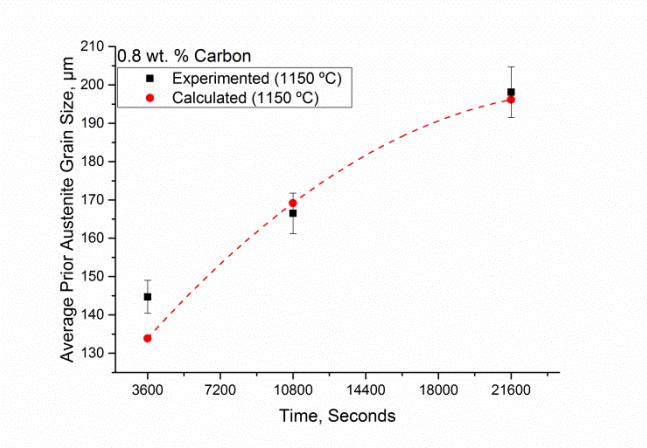

(a) Equation (E-21)

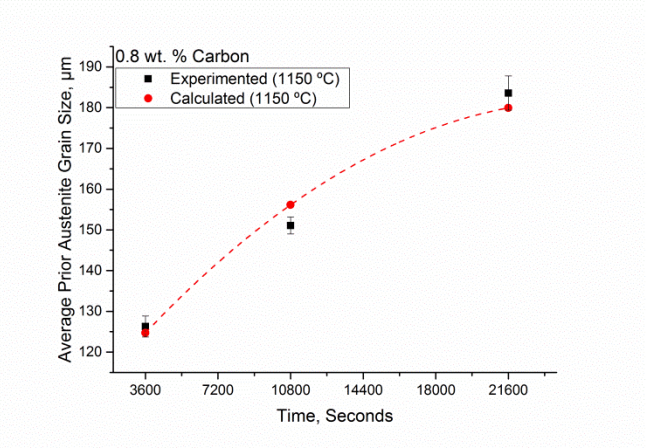

(b) Equation (E-22)

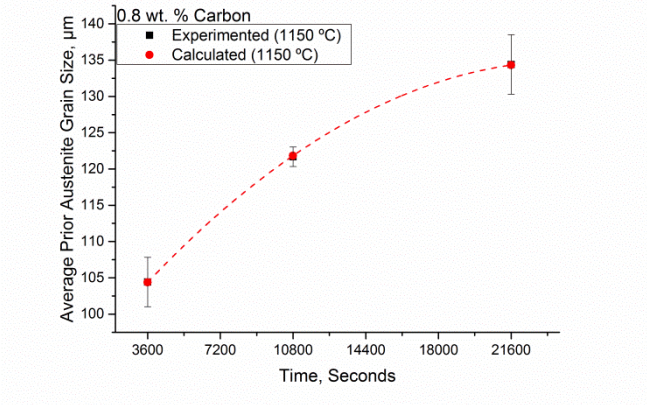

(c) Equation (E-23)

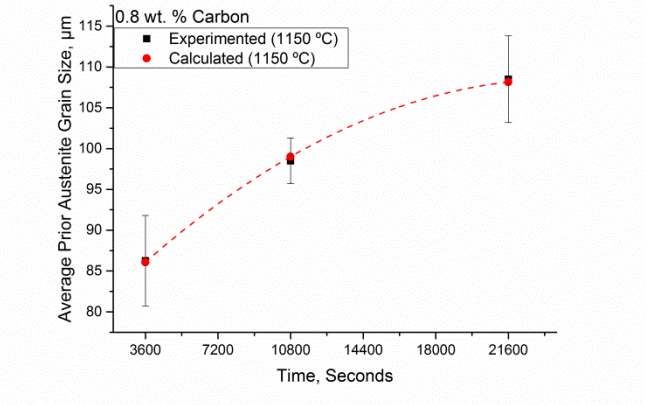

(d) Equation (E-24)

Figure E-7: Comparison of calculated austenite average grain size and the experimental measurements of the austenite grain size at a temperature of 1150°C.

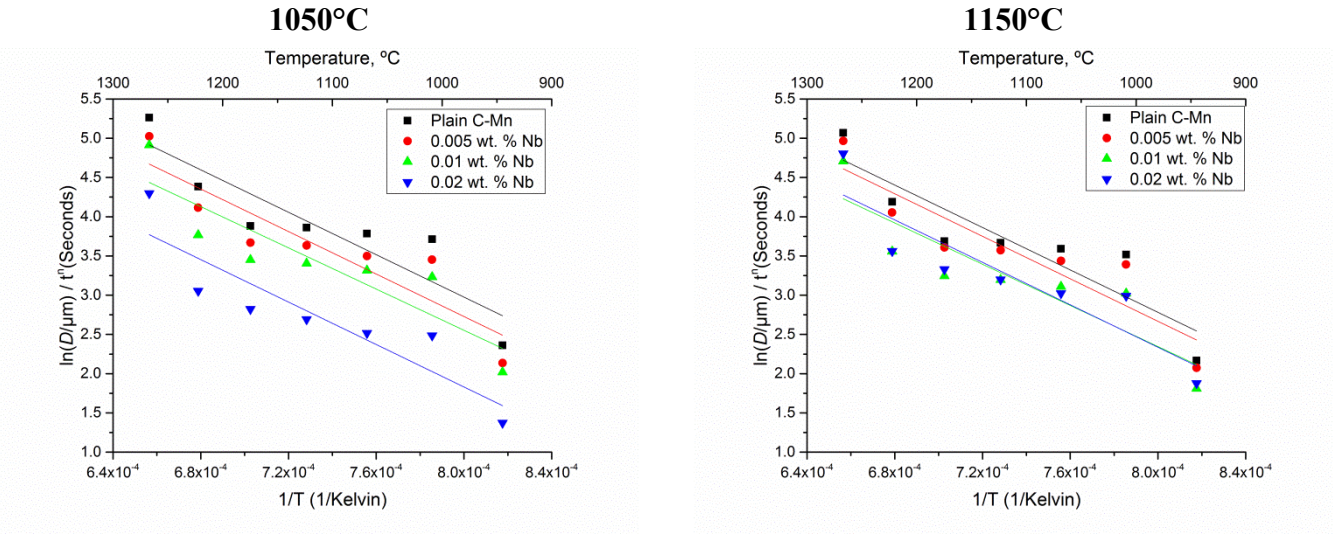

(a) 0.08 Carbon wt. %

Figure E-8: Presented above are the plots of $[ln\left(\frac{D}{t^n}\right)]$ versus $[\frac{1}{T}]$ of austenite grain growth for the data for both 1050°C and 1150°C, for Plain C-Mn and Nb microalloyed steels.

Table E-2: The calculated values for activation energy and the material constant for all the different compositions at the two different temperatures

		Activation Energy $[Q]$ kJ mol^{-1}	Material Constant $[A_3]$
0.08 wt. % C			
1050°C	Plain C-Mn	112.4	9.73E+05
	0.005 wt. % Nb	112.6	7.76E+05
	0.01 wt. % Nb	109.2	4.69E+05
	0.02 wt. % Nb	112.5	3.13E+05
1150°C	Plain C-Mn	112.4	8.02E+05
	0.005 wt. % Nb	112.6	7.30E+05
	0.01 wt. % Nb	109.2	3.81E+05
	0.02 wt. % Nb	112.5	5.19E+05
0.4wt. % C			
1050°C	Plain C-Mn	95.3	2.15E+05
	0.005 wt. % Nb	95.6	1.95E+05
	0.01 wt. % Nb	106.7	2.95E+05
	0.02 wt. % Nb	108.2	1.83E+05

1150°C	Plain C-Mn	95.3	9.67E+04
	0.005 wt. % Nb	95.6	1.02E+05
	0.01 wt. % Nb	106.7	2.09E+05
	0.02 wt. % Nb	108.2	2.20E+05
0.8 wt. % C			
1050°C	Plain C-Mn	102.9	3.19E+05
	0.005 wt. % Nb	100.7	2.19E+05
	0.01 wt. % Nb	109.7	4.13E+05
	0.02 wt. % Nb	110.7	7.16E+05
1150°C	Plain C-Mn	102.9	1.37E+05
	0.005 wt. % Nb	100.7	1.10E+05
	0.01 wt. % Nb	109.7	3.37E+05
	0.02 wt. % Nb	110.7	3.46E+05

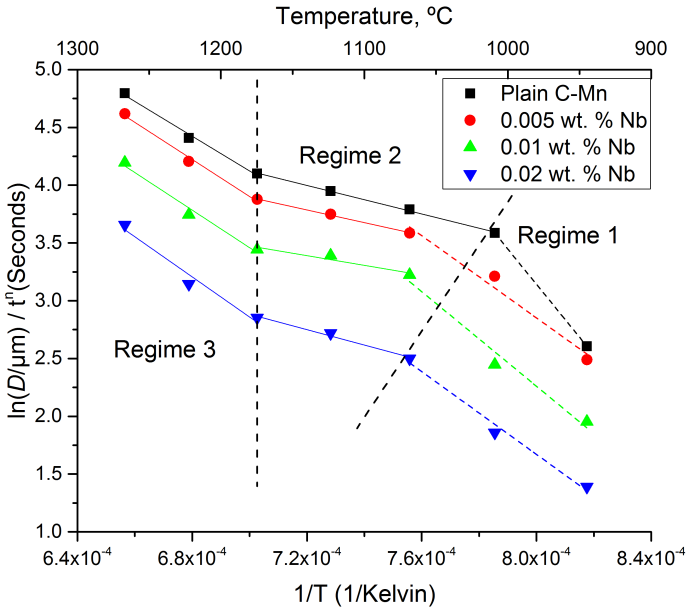

Figure E-9: The Arrhenius plot showing 3 different regimes of activation energy for grain growth in Plain C-Mn and Microalloyed steels for medium carbon steel.

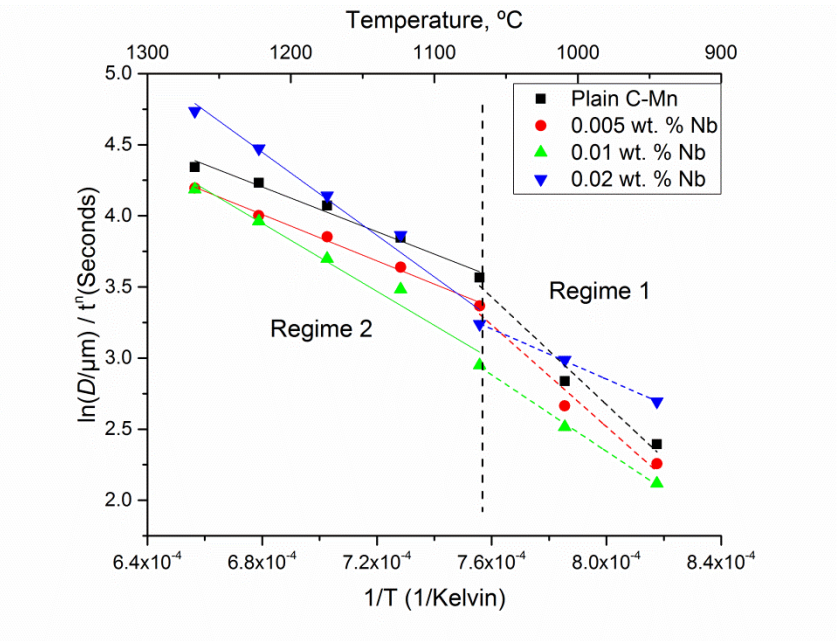

Figure E-10: The Arrhenius plot showing 2 different regimes of activation energy for grain growth for the plain C-Mn and microalloyed steels in high carbon steel.

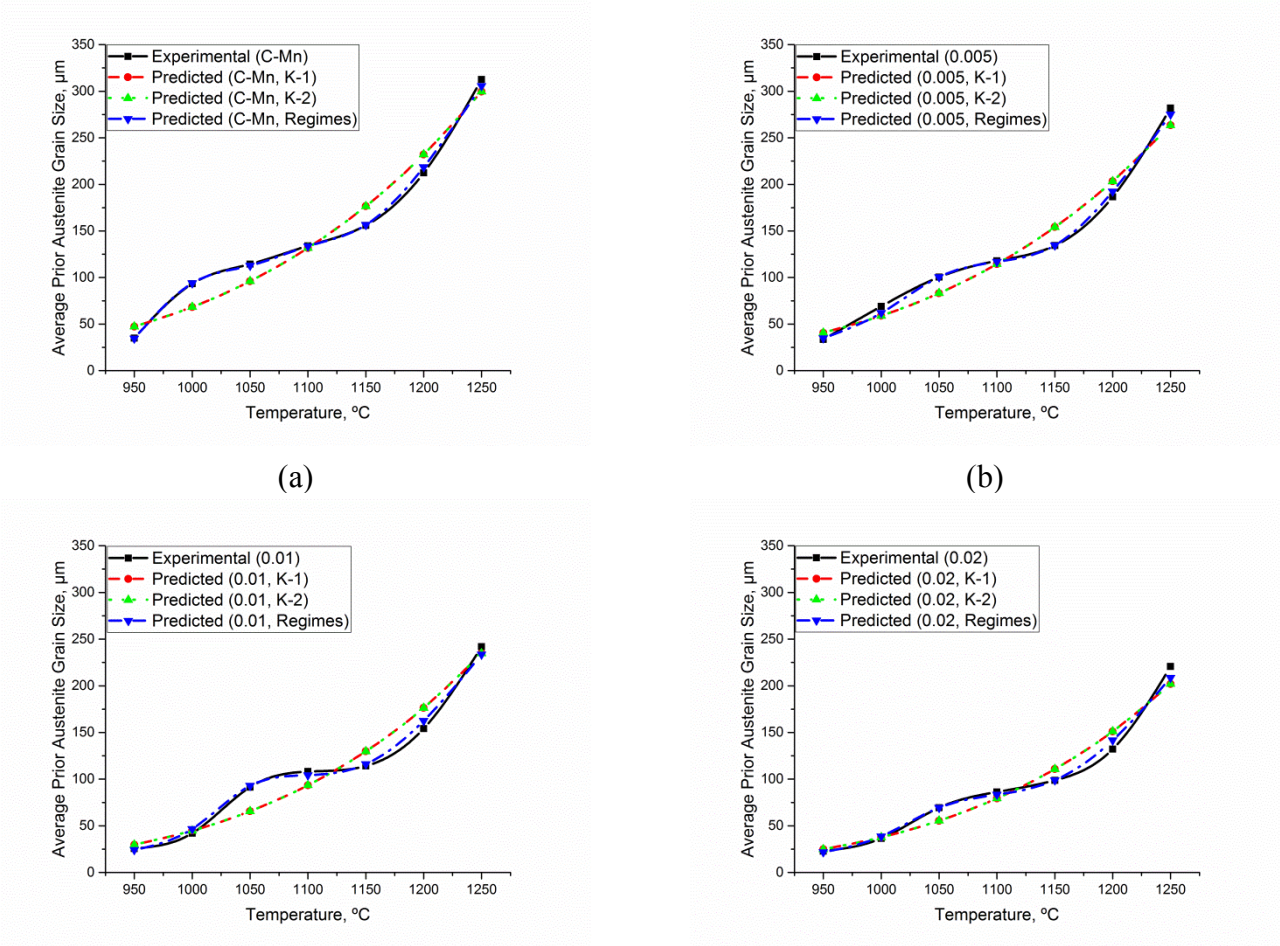

Figure E-11: Comparison of the Calculated with the experimental austenite grain size for medium carbon steel.

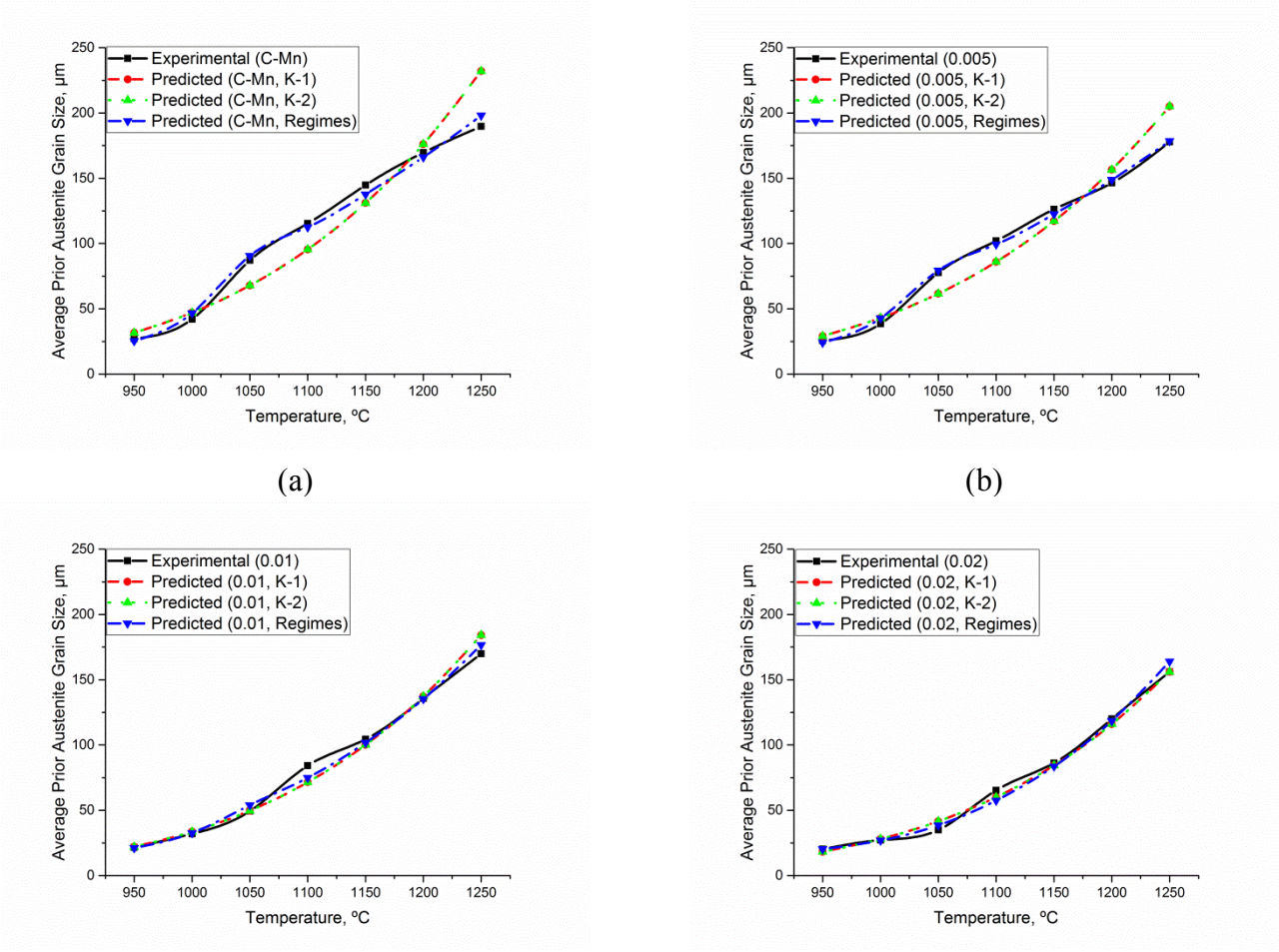

Figure E-12: Comparison of the Calculated with the experimental austenite grain size for high carbon steel.